EXPLORATIONS IN QUANTUM GRAVITY AND CONFORMAL BOOTSTRAP

A Dissertation

Presented to the Faculty of the Graduate School

of Cornell University

in Partial Fulfillment of the Requirements for the Degree of

Doctor of Philosophy

by

Amirhossein Tajdini

August 2020

EXPLORATIONS IN QUANTUM GRAVITY AND CONFORMAL BOOTSTRAP

Amirhossein Tajdini, Ph.D.
Cornell University 2020

In this thesis, I apply numerical and analytical bootstrap techniques for a better understanding of quantum gravity. Each chapter is separated by subject. Chapter two is about a proof of the averaged null energy condition (ANEC) in flat spacetime for relativistic quantum field theories in more than two dimensions. The proof is based on microcausality and isolation of the ANEC in the OPE of primary operators in the lightcone limit. I discuss a no-go theorem for massive higher spin particles in chapter three. The no-go theorem is established on analytic properties of the S-matrix in the Eikonal limit. In chapter four, I explore connections between two-dimensional CFTs and three-dimensional pure gravity using the numerical bootstrap. My collaborators and I developed a fast algorithm for bootstrapping two dimensional CFTs using the modular bootstrap. By bootstrapping theories with large central charge, we found a new bound on the scaling dimension of the spectral gap. Chapter five is about the black hole information paradox. Using the replica trick for computing the entropy of Hawking radiation, we found a new saddle-point in the gravitational path integral. This saddle-point corresponds to a wormhole solution connecting different replica sheets. By including this saddle, we showed that the entropy computation is consistent with unitarity.

BIOGRAPHICAL SKETCH

Amirhossein Tajdini was born in Tehran, Iran on March 12 1991. At the end of high school, he attended the International Physics Olympiad in Merida, Mexico. He then started his undergraduate studies in physics and mathematics at Sharif University of Technology. During his undergraduate studies, he taught physics to high school students who participated in Physics Olympiad. In 2014, he moved to Cornell University for his PhD and joined Professor Hartman's group from 2015 to the date this draft is being written. He will continue his research as a postdoctoral researcher at the University of Santa Barbara, California.

Dedicated to Martha and my family.

ACKNOWLEDGMENTS

First and foremost I would like to thank my advisor Tom Hartman for guiding me and supporting me in the past six years. His depth of knowledge, his originality, and his patience were a real inspiration. He was always very generous with his ideas and his time. I am extremely fortunate to have the chance to do research under his supervision during my PhD.

Many thanks to Liam McAllister for his guidance through these years and discussions in group meetings and in person about String theory and Cosmology. I am also grateful for other wonderful teachers I had at Cornell including Eanna Flanagan, Peter Lepage, and Csaba Csaki.

I am greatly indebted to my excellent collaborators whom I had the previlege to work with and learn from. I would like to especially thank Nima Afkhami-Jeddi and Sandipan Kundu who have been my collaborators on most of the projects. I would also like to thank Juan Maldacena, Edgar Shaghoulian, Ahmed Almheiri, Jorrit Kruthoff, Venkatesa Chandrasekaran, Kanato Goto, Henry Cohn, and Yikun Jiang with whom I collaborated on other projects.

I benefited greatly from conversations and dicussions with many people throughout my PhD, many of them now friends of mine. I would like to thank David Simmons-Duffin, Arvin Shahbazi-Moghaddam, David Meltzer, Eric Perlmutter, Mudassir Moosa, Sachin Jain, John Stout, Murat Kologlu, Ofri Telem, Mehmet Demirtas, Ibrahim Shehzad, Ryan Bilotta, Sungwoo Hong, Gowri Kurup, Naomi Gendler, Reza Javadi-Nezhad, Alex Grant, Pouya Asadi, Allic Sivaramakrishnan, Soner Albayrak, and Junkai Dong.

There is also life outside physics and graduate school. I am grateful for many friends who made my time in Ithaca so enjoyable. I would like to thank Najva, Saeed, Behrooz, Meraj, Hedyeh, Omid, Hamidreza, Saghar, Ali and Sajjad.

Thanks to my family for believing in me. Without your support and sacrifices throughout my life, I would not be where I am now. Despite being far away from each other, your constant love and support have been my main source of encouragement in the past six years.

Finally, I would like to thank my dearest Martha for your care, support and everything else. You changed the graduate school experience for me and you always make me so happy.

CONTENTS

LIST OF TABLES

LIST OF FIGURES

CHAPTER 1

INTRODUCTION

Quantum field theory (QFT) is a key formalism for understanding fundamental laws of nature. By combining classical fields, quantum mechanics, and symmetries, QFT provides a framework for describing all matter and forces in the standard model of particles. While originally developed for characterizing elementary particles, the formalism has been successfully applied to other areas of physics such as condensed matter physics, theories of inflation in cosmology, statistical mechanics, and even pure mathematics.

QFTs are traditionally defined with a set of fields in spacetime and a set of couplings for local interactions which respect the symmetries of the theory. In practice, calculations in QFTs often run into the difficulty of infinities due to high energy states at short distance. The problem was solved by regulating the theory by adding a cutoff scale and considering the QFT as an effective description for excitations with wavelengths below the cutoff scale. The couplings are not constant anymore and they flow with the change in the cutoff scale according to renormalization group (RG) equations. When couplings do not change with scale, the theory is in a fixed point and is called scale invariant. More generally, theories at fixed points have additional symmetry associated with spacetime inversion and are called conformally invariant. QFTs generically flow to a conformal field theory (CFT) at long distances. The modern way of understanding QFTs as effective field theories (EFTs) has led to the idea of universality classes where systems with different microscopics are described by the same QFT in long distances.

The effective theory of gravity is well described in long distances by general relativity (GR). The recent detection of gravitational waves has demonstrated how

well GR is consistent with experiments. These findings have resulted in stringent bounds on deviations from GR such as mass of gravitons and Lorentz invariance violation. As an example, the GW170817 neutron star merger [2] has placed a new bound on the difference between the speed of light (c_{EM}) and the speed of gravity (c_{GW}) with precision $-3\times10^{-15} \leq \frac{c_{GW}-c_{EM}}{c_{EM}} \leq +7\times10^{-16}$. Despite GR's enormous success in describing large objects in the universe, the theory does not incorporate quantum mechanics (QM). Therefore, GR is only a valid description for length scales below its natural cutoff which is the Plank scale $M_P = \sqrt{\frac{\hbar c}{G}} \sim 10^{19}$GeV. Quantum gravity (QG) attempts to find the microscopic theory of gravity by combining QM and GR. The consistency of any candidate theory requires to reproduction of GR and the standard model of particles in the low energy limit.

String theory has been the best candidate theory of QG. String theory has a rich spectrum of particles, including gravitons, and it yields Einstein's gravity at long distances. The theory has a vast set of vacua, which leads to a large number of EFTs in the IR description. Various recent developments in string theory have been focused on characterizing solutions that are consistent with the standard model of particles and early universe cosmology.

In the absence of direct experiments, studying black holes has been the main thought experiment for understanding various aspects of QG. Specifically, black holes thermodynamics have indicated basic differences between gravity and quantum fields. Classical dynamics of GR showed that black holes are subjected to the laws of thermodynamics [3–6]. In particular, a black hole has a temperature and an entropy. The Bekenstein-Hawking formula gave a remarkable and universal formula for the black-hole entropy S as

$$S = \frac{A}{4G}, \tag{1.1}$$

where A is the area of black-hole event horizon. This formula reveals that black hole degrees of freedom are encoded in one lower dimension than the volume of space. This *holographic* nature of gravity is in contrast with the entropy of QFTs in finite temperature, which are extensive in volume. Unlike QFTs, which are defined on a fixed spacetime, QG is the theory of spacetime itself. As a result, spacetime is expected to emerge from other fundamental degrees of freedom, as indicated by connections between string theory and large N matrix models.

The AdS/CFT correspondence [7] made the idea of holography [8, 9] concrete by proposing an exact duality between the partition functions of quantum gravity in an asymptotically Anti-de Sitter (AdS) spacetime and certain classes of CFTs in one lower dimensions. In its most famous form, the duality exists between type IIB string theory on $AdS^5 \times S^5$ and $\mathcal{N} = 4$ super Yang-Mills (SYM) in four dimensions. $\mathcal{N} = 4$ SYM is a supersymmetric version of QCD with a maximum number of supersymmetries. The theory is conformally invariant for any number of colors N and the gauge coupling $g_{\rm YM}$, which are the only free parameters of the theory. The duality has passed numerous non-trivial tests, especially in the planer limit $N \to \infty$ [10–14]. Even in this limit, both side of the duality are extremely complicated, and each description in AdS/CFT is useful in certain limits. When perturbative computations are possible in the CFT side, gravity is not simply described by a classical action. Conversely, when the quantum gravity side has a semi-classical description, the CFT side becomes strongly-coupled. The latter case has made AdS/CFT very applicable for understanding strongly-interacting quantum systems [15–18, 18–27] .

The AdS/CFT correspondence connects two very distant problems together, and as a result, each perspective opens a new pathway for understanding the other

side of duality. On the gravity side, some of the important developments center on the links between geometry and entanglement. Thanks to the Ryu-Takayanagi (RT) formula [28], entanglement entropy delivers a new way of understanding bulk locality and the emergent radial direction in AdS. In particular, progress has been made to find information-theoretic maps, such as the entanglement wedge reconstruction between operators in the bulk and the boundary [29–34]. In the context of black holes, similar ideas led to the firewall paradox [35, 36] and later the ER=EPR conjecture [37]. The latter proposes that if two distant black holes are entangled enough, a non-traversable wormholes could be created, and joining the two black holes. These new findings are crucial for recent progress on the information paradox.

From the CFT perspective, the conjecture suggests that unlike most understood CFTs in critical phenomena, there exists a class of CFTs which exhibits gravity-like features [38–50]. In particular, the black hole dynamics are encoded in the high energy states of these CFTs. Understanding properties of these CFTs, such as their symmetries, and ultimately solving them is an open question for understanding the landscape of UV-complete theories of gravity.

1.1 Conformal Bootstrap

How do we search for CFTs? Unlike effective field theories that are easy to construct using the Lagrangian and a set of interactions, constructing CFTs is non-trivial. In particular, modes with different scales do not decouple in a CFT and there is a strong connection between light and heavy operators. A well-known example of this phenomenon is the Cardy formula in 2d [51]. A thermal partition function of a 2d CFT on a spatial circle with unit radius and a thermal circle with length β

satisfies modular invariance

$$Z(\beta) = Z(4\pi^2/\beta), \tag{1.2}$$

$$Z(\beta) = \sum_{\text{eigenstates}} \rho_E \, e^{-\beta E}, \tag{1.3}$$

where ρ_E's are degeneracies of energy eigenstates. This is a highly non-trivial equation that the spectrum of CFTs has to satisfy. Taking $\beta \to \infty$, the left-hand side of 1.2 is dominated by the vacuum state with Casimir energy $E_{\text{vac}} = -\frac{c}{12}$, where c is the central charge. Cardy showed that in order to match the right-hand side of 1.2, the asymptotic degeneracies of states to leading order must be given by

$$\lim_{E\to\infty} \rho_E \sim \exp\left(2\pi\sqrt{\frac{cE}{3}}\right). \tag{1.4}$$

Interpreting light states, such as the vacuum, as IR and high energy states as UV, the Cardy formula manifestly shows that the IR and the UV are not independent in CFT and they constrain each other.

The modular invariance 1.2 is an example of bootstrap constraints, which have to be true for all CFTs. Traditionally, CFTs were found by tuning relevant parameters and RG flow from a lattice or a QFT model as a UV description. Various interesting cases such as the 3d Ising model have no controlled perturbative expansion, and only numerical methods are available to find the critical exponents. However, in the conformal bootstrap approach, an abstract space for the CFT spectrum is assumed as an starting point. The space of consistent CFTs then is carved out by imposing the consequences of modular invariance, unitarity, and crossing symmetry. The bootstrap program has made enormous progress in understanding CFTs by putting powerful analytical and numerical bounds on the spectrum of CFTs [52, 53]. As

we increase the number of bounds on CFTs, we hope to find more patterns and emergent principles for classifying CFTs.

1.1.1 Bootstrap in Lorentzian Signature

Alongside of the numerical bootstrap, many recent developments for understanding CFTs have focused on analytical bootstrap in the Lorentzian signature. Studying constraints of this type are the topics of chapters two and three. Generally speaking, Lorentzian manifolds have structures that are not easily visible in the Euclidean formulation. For instance, in GR, the horizon of a black hole is a codimension-one surface, whereas in Euclidean space, it corresponds to a codimension-two surface. More generally, null lines would collapse to a single point in Euclidean space.

For QFTs, there are bounds that are more naturally expressed in Lorentzian signature. More than a decade ago, in the theory of a massless field with higher derivative interactions $\mathcal{L} = -(\partial\phi)^2 + \lambda(\partial\phi)^4 + \cdots$, it was shown that λ has to be non-negative. Otherwise, in a non-trivial background, there are superluminal propagations which violate causality [54]. Causality itself is a Lorentzian notion, and as expected, bounds from causality are tied to Lorentzian signature.

Energy conditions are another set of Lorentzian inequalities which have consequences for both GR and quantum fields. In GR, they are reasonable assumptions on the stress-energy tensor in order to avoid pathological features in spacetime, such as a closed timelike curve. These constraints have been extensively used for proving theorems in GR, such as the singularity theorem and positive mass theorems [55]. When quantum mechanics is considered, the dominant, strong, weak, and null energy conditions fail. The exception is the achronal averaged null energy

condition, which is given by

$$\int_{-\infty}^{+\infty} \langle T_{uu} \rangle du \geq 0, \tag{1.5}$$

where T_{uu} is a null component of the stress tensor. This condition is shown to be sufficient for all of the major theorems in GR and avoid time machines.

Despite the importance of energy conditions in GR, their usefulness for quantum fields has been only recently appreciated. Hoffman and Maldacena showed that the ANEC puts strong bounds on interacting CFTs [56]. By applying the ANEC to states created by an energy-momentum wavepacket, they found a universal constraint on the scale anomaly coefficients in 4d

$$\frac{1}{3} \leq \frac{a}{c} \leq \frac{31}{18}, \tag{1.6}$$

where a, c are known as coefficients of the Euler term and the Weyl term in the anomaly equation.

For interacting QFTs in flat spacetime, the ANEC was first proved in [57] using information-theoretic techniques. Another proof of the ANEC from causality is the subject of chapter 2 of this thesis. The proof is based on an inequality developed in [58] and showing that the operator product expansion between two scalar operators reduces to ANEC when two operators are almost light-like separated. The proof is independent of holography even though holography provides an insight for the proof [59].

1.1.2 Bootstrapping 3d Gravity

In chapter four, I discuss the AdS/CFT correspondence in the context of AdS_3/CFT_2. This has been a rich arena for exploring both sides of the duality [60–63] because both sides are simpler than their higher-dimensional analogs.

In 2d, the conformal algebra is enhanced to a an infinite dimensional Virasoro algebra. As a result, 2d CFTs are greatly constrained due to additional symmetries. In fact, using only consistency conditions, a class of 2d CFTs called rational CFTs have been found and classified.

On the AdS side, Einstein gravity without any matter in 3d is a topological theory and does not have local degrees of freedom. The theory is still non-trivial, has boundary gravitons, and admits solutions such as BTZ black holes [64]. Brown and Henneaux [65] showed the asymptotic symmetries of 3d gravity matches the conformal symmetry of a 2d CFT with a central charge

$$c = \frac{3}{2}\left(\frac{l_{\text{AdS}}}{l_{\text{Planck}}}\right). \tag{1.7}$$

In particular, the semi-classical limit corresponds to $c \gg 1$. Black-holes are non-trivial excitations of the theory, and there is a energy gap of $\frac{c}{12}$ in AdS units between the vacuum AdS_3 solution and the lightest black hole solution. There has been an extensive literature on whether there are CFTs corresponding to the theory of pure gravity [49, 60–63, 66–70]. Here pure gravity means that there is no matter in the low energy sector, and all non-trivial excitations are black holes[1].

Constructing CFTs that have both a large central charge and a large gap in

[1] In the literature, pure gravity sometimes refers to a theory which has the gap of energy $\Delta_{min} \gtrsim \frac{c}{12}$, and sometimes to a theory that has Plankian energy gap $\Delta_{min} \sim \mathcal{O}(c)$.

the spectrum is a challenging task. Known examples of this class of theories are the deformations of symmetric orbifold in certain supersymmetric CFTs [71]. More generally, for the question of having a large gap, it was shown that any unitary CFT with central charge $c > 1$ has to have at least one primary operator with scaling dimension $\Delta \leq \frac{c}{6}$ [72]. This differs from the black hole bound $c/12$ by a factor of two. Via improving bootstrap bounds, the hope is to either find or rule out the theory of pure gravity.

The improvement of the scaling gap in the context of 2d CFTs is given in chapter 4 of this thesis [73]. By imposing spinless modular invariance and using a new numerical algorithm, we found an upper bound $c/9.1$ by bootstrapping CFTs with $c \lesssim 2000$. So far, this has been the lowest upper bound in scaling dimension, surpassing other numerical and analytical bounds.

1.2 Information loss in Quantum Gravity

Finally in chapter five, I study aspects of the black hole information paradox. As Hawking originally noted, the second law of thermodynamics would be violated if a black hole only absorbs and does not emit any energy. He famously showed that the vacuum state for an infalling observer of QFT in a black hole background leads to a thermal density matrix for the radiation measured by far away observers. This thermal radiation would lead to the evaporation of a black hole. Hawking advocated that information would be lost in black holes because an object thrown into a black hole, no matter its details, always ends up in a final thermal radiation state of quantum fields. In other words, a pure quantum state would collapse due to gravity, form a black hole, and end up in a thermal density matrix after the

black hole completely evaporates. One may compute the von Neumann entropy (fine-grained entropy) $S = -\mathrm{Tr}(\rho \log \rho)$ of initial versus final state to sharpen this argument as opposed to thermodynamic entropy, which is subjected to arbitrary coarse-graining procedures. Although the Hawking paradox is phrased originally for evaporating black holes in flat spacetime, there are also versions of information loss for other spacetimes, like AdS.

The AdS/CFT correspondence strongly advocates for a whole process of evaporation that is unitary, based on the precept that the CFT dual is unitary. There has been a large body of literature on formulating the Hawking paradox in AdS and resolving versions of the paradox for CFT observables [74–77]. These works indicated that, similar to the gravity computation, holographic CFTs naively loose information. However, when the non-perturbative corrections are included, the CFT final answer is unitary, as expected. This is only a hint for the information paradox, and it does not resolve the original paradox, which was stated for black holes and not CFTs.

A candidate for a missed contribution to the original Hawking calculation for the entropy is the subject of chapter [78] of this thesis. The proposal is that, using the replica trick, there is a new saddle-point, which includes wormholes, in the path integral calculation of the entropy. The proposal does not rely on any new physics or microscopic details and instead relies on the saddle point analysis of gravitational path integral. Analogous to the ER=EPR conjecture, the wormhole, which exists for these saddles, would entangle the regions inside the black hole to the radiation outside the black hole. As a result, the late time and early time modes are entangled with each other, which results in a unitary Page curve for the radiation.

CHAPTER 2

AVERAGED NULL ENERGY CONDITION

Abstract[1]

Unitary, Lorentz-invariant quantum field theories in flat spacetime obey microcausality: commutators vanish at spacelike separation. For interacting theories in more than two dimensions, we show that this implies that the averaged null energy, $\int du T_{uu}$, must be non-negative. This non-local operator appears in the operator product expansion of local operators in the lightcone limit, and therefore contributes to n-point functions. We derive a sum rule that isolates this contribution and is manifestly positive. The argument also applies to certain higher spin operators other than the stress tensor, generating an infinite family of new constraints of the form $\int du X_{uuu\cdots u} \geq 0$. These lead to new inequalities for the coupling constants of spinning operators in conformal field theory, which include as special cases (but are generally stronger than) the existing constraints from the lightcone bootstrap, deep inelastic scattering, conformal collider methods, and relative entropy. We also comment on the relation to the recent derivation of the averaged null energy condition from relative entropy, and suggest a more general connection between causality and information-theoretic inequalities in QFT.

[1]This chapter is based on the paper [79].

2.1 Introduction

The average null energy condition (ANEC) states that

$$\int_{-\infty}^{\infty} d\lambda \, \langle T_{\alpha\beta} \rangle u^\alpha u^\beta \geq 0 \ , \tag{2.1}$$

where the integral is over a complete null geodesic, and u is the tangent null vector. This inequality plays a central role in many of the classic theorems of general relativity [80–83]. Matter violating the ANEC, if it existed, could be used to build time machines [84, 85] and violate the second law of thermodynamics [86]. And, unlike most of the other energy conditions discussed in relativity (dominant, strong, weak, null, etc.), the ANEC has no known counterexamples in consistent quantum field theories (assuming also that the null geodesic is achronal [55]).

Though often discussed in the gravitational setting, the ANEC is a statement about QFT that is nontrivial even in Minkowski spacetime without gravity. In this context, the first general argument for the ANEC in QFT was found just recently by Faulkner, Leigh, Parrikar, and Wang [57]. (Earlier derivations [87–91], were restricted to free or superrenormalizable theories, or to two dimensions.) The crucial tool in the derivation of Faulkner *et al.* is monotonicity of relative entropy. Assuming all of the relevant quantities are well defined in the continuum limit, the argument applies to a large (and perhaps dense) set of states in any unitary, Lorentz-invariant QFT.

Separately, the ANEC for a special class of states in conformal field theory was derived recently using techniques from the conformal bootstrap developed in [27, 58]. These special cases of the ANEC, known as the Hofman-Maldacena conformal collider bounds [56], were derived in [92, 93]. The derivation relied on causality of the CFT, in the microscopic sense that commutators must vanish outside the

lightcone, applied to the 4-point correlator $\langle\phi[T,T]\phi\rangle$ where T is the stress tensor and ϕ is a scalar. However, it was not clear from the derivation why the bootstrap agreed with the ANEC as applied by Hofman and Maldacena, or whether there was a more general connection between causality and the ANEC in QFT.

In this paper, we simplify and extend the causality argument and show that it implies the ANEC more generally. We conclude that any unitary, Lorentz-invariant QFT with an interacting conformal fixed point in the UV must obey the ANEC, in agreement with the information-theoretic derivation of Faulkner *et al.* The argument assumes no higher spin symmetries at the UV fixed point, so it requires $d > 2$ spacetime dimensions and does not immediately apply to free (or asymptotically free) theories. A byproduct of the analysis is a sum rule for the integrated null energy in terms of a manifestly positive 4-point function. Furthermore, we argue that the ANEC is just one of an infinite class of positivity constraints of the form

$$\int du X_{uu\cdots u} \geq 0 \tag{2.2}$$

where X is an even-spin operator on the leading Regge trajectory (normalized appropriately) — *i.e.,* it is the lowest-dimension operator of spin $s \geq 2$. This implies new constraints on 3-point couplings in CFT; we work out the example of spin-1/spin-1/spin-4 couplings. Another interesting corollary is that, like the stress tensor, the minimal-dimension operator of each even spin must couple with the same sign to all other operators in the theory. (There may be exceptions under certain conditions; see section 2.6 for a discussion of the subtleties.) In analogy with the Hofman-Maldacena conditions on stress tensor couplings, we conjecture that (2.2) evaluated in a momentum basis is optimal, meaning that the resulting constraints on 3-point couplings can be saturated in consistent theories. This remains to be proven.[2]

[2]In free field theory our methods do not apply directly, but a simple mode calculation in

The connection between causality and null energy is well known in the gravitational context (see for example [94, 95] and the references above) and in AdS/CFT (see for example [59, 96]). In a gravitational theory, null energy can backreact on the geometry in a way that leads to superluminal propagation in a curved background. Our approach is quite different, since we work entirely in quantum field theory, without gravity, and invoke microcausality rather than superluminal propagation in curved spacetime. On the other hand, in holographic theories, the derivation of the ANEC in [59] only relies on physics close to the boundary, so it is natural to guess that it can be rephrased as a general derivation using the OPE.

Causality vs. Quantum Information

Our derivation bears no obvious resemblance to the relative entropy derivation of Faulkner *et al.*, except that both seem to rely on Lorentzian signature. (Our starting point is Euclidean, and we do not make any assumptions about the QFT beyond the usual Euclidean axioms, but we do analytically continue to Lorentzian.) It is intriguing that causality and information-theoretic inequalities lead to overlapping constraints in this context.

There are significant hints that this connection between entanglement and causality is more general. This is certainly true in 2d CFT; see for example [97]. It is also clear in general relativity; for example, both the second law and strong subadditivity of the holographic entanglement entropy require the NEC [86, 98, 99]. But there are also hints in higher-dimensional QFT for a deeper connection between

an appendix demonstrates that the inequality (2.2) holds also for free scalars. This appears to have escaped notice. It may have interesting implications for coupling quantum fields to stringy background geometry, just as the ANEC plays an important role in constraining physical spacetime backgrounds. The operators X generalize the stress tensor to the full leading Regge trajectory of the closed string. A first step would be to confirm that (2.2) holds for other types of free fields.

entanglement and causality constraints. Recent work on the quantum null energy condition [91, 100, 101] is one example, and they are also linked by c-theorems for renormalization group flows in various dimensions. The F-theorem, which governs the renormalization group in three dimensions [102–104], was derived from strong subadditivity of entanglement entropy but has resisted any attempt at a derivation using more traditional tools. On the other hand, its higher-dimensional cousin, the a-theorem in four dimensions, was derived by invoking a causality constraint [105] (and in this case, attempts to construct an entanglement proof have been unsuccessful). So causality and entanglement constraints both tie deeply to properties of the renormalization group, albeit in different spacetime dimensions. Another tantalizing hint is that in holographic theories, RG monotonicity theorems in general dimensions are equivalent to causality in the emergent radial direction [102].

These clues suggest that the two types of Lorentzian constraints — from causality and from quantum information — are two windows on the same phenomena in quantum field theory. It would be very interesting to explore this further. For instance, perhaps the F-theorem can be understood from causality; after all, a holographic violation of the F-theorem would very likely violate causality, too. It also suggests that the higher-spin causality constraints (2.2) on the leading Regge trajectory could have an information-theoretic origin, presumably involving non-geometric deformations of the operator algebra.

Comparison to previous methods

Both conceptually and technically, the argument presented here has several advantages over previous bootstrap methods in [58, 92, 93]. First, it makes manifest the connection between causality constraints and integrated null energy. Second, it

produces optimal constraints (for example the full Hofman-Maldacena bounds on $\langle TTT\rangle$) without the need to decompose the correlator into a sum over composite operators in the dual channel. This decomposition, accomplished in [93], was technically challenging for spinning probes, and becomes much more unweildy with increasing spins (say, for $\langle TTTT\rangle$). The simplification here comes from the fact that the new approach allows for smeared operator insertions, and these can be used to naturally project out an optimal set of positive quantities. Finally, the new method produces stronger constraints on the 3-point functions of non-conserved spinning operators. On the other hand, this approach does not give us the solution of the crossing equation in the lightcone limit or the anomalous dimensions of high-spin composite operators as in [93].

Outline

The main argument is given first, in section 2.2. The essential new ingredient that it relies on is the fact that the null energy operator appears in the lightcone OPE; this is derived in section 2.3. For readers already familiar with the chaos bound [27] and/or earlier causality constraints [58], sections 2.2 - 2.3 give a complete derivation of $\int du T_{uu} \geq 0$. The sum rule is derived in section 2.4, where we also review the methods of [27, 58]. In section 2.5, we show how to smear operators to produce directly the conformal collider bounds in the new approach — this section is in a sense superfluous because conformal collider bounds follow from the ANEC, but it is useful to see directly how the two methods compare. In all cases we are aware of, this particular smearing produces the optimal set of constraints on CFT 3-point couplings. Finally, in section 2.6, we generalize the argument to the ANEC in any dimension $d > 2$, as well as to an infinite class of higher spin operators X.

2.2 Derivation of the ANEC

In this section we outline the main argument. Various intermediate steps are elaborated upon in later sections. Our conventions for points $x \in R^{1,d-1}$ are

$$x = (t, y, \vec{x}) \quad \text{or} \quad (u, v, \vec{x}), \quad u = t - y, \quad v = t + y \ . \tag{2.3}$$

In expressions where some arguments are dropped, those coordinates are set to zero. ψ is always a real scalar primary operator. Hermitian conjugates written as $O^\dagger(x)$ act only on the operator, not the coordinates, so $[O(t, \dots)]^\dagger = O^\dagger(t^*, \dots)$. To simplify the formulas we set $d = 4$ in the first few sections, leaving the general case ($d > 2$) for section 2.6.

Define the average null energy operator

$$\mathcal{E} = \int_{-\infty}^{\infty} du T_{uu}(u, v = 0, \vec{x} = 0) \ . \tag{2.4}$$

The goal is to show that this is positive in any state, $\langle \Psi | \mathcal{E} | \Psi \rangle \geq 0$. We first discuss conformal field theories. In CFT, it is sufficient to show that

$$\langle O^\dagger(t = i\delta, y = 0)\, \mathcal{E}\, O(t = -i\delta, y = 0) \rangle \geq 0 \tag{2.5}$$

for an arbitrary local operator O (not necessarily primary). The insertion of O in imaginary time creates a state on the $t = 0$ plane so that this 3-point function can be interpreted as an expectation value $\langle O | \mathcal{E} | O \rangle$. And, in a conformal field theory, a dense subset of normalizable states can be created this way.[3]

In section 2.3, we show that the non-local operator $\mathcal{E}$ makes a universal contribution to correlation functions in the lightcone limit. The key observation is that

[3] On the sphere, these states are complete by the state-operator correspondence. On the plane, therefore, any state the consists of local operators smeared over some finite region can be created this way, and by the Reeh-Schlieder theorem, such states are dense in the Hilbert space [106].

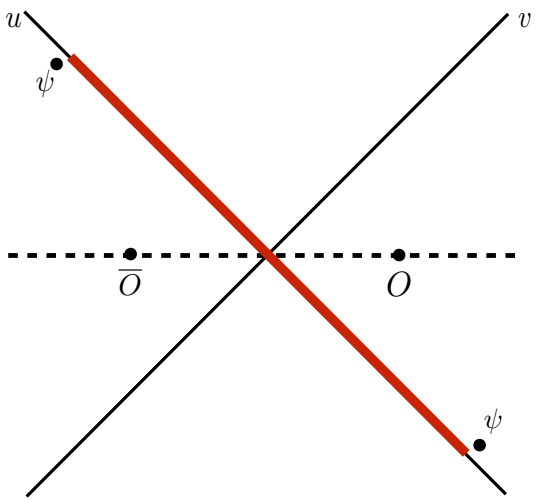

Figure 2.1: Kinematics for the derivation of the ANEC. The leading correction to the $\psi\psi$ OPE is the null energy integrated over the red line, which in the limit of large u takes the form $\langle \overline{O} \int du T_{uu} O \rangle$. This is then related to an expectation value by a Euclidean rotation.

the operator product expansion of two scalars in the lightcone limit can be recast as

$$\psi(u,v)\psi(-u,-v) \approx \langle \psi(u,v)\psi(-u,-v)\rangle (1 + \lambda_T v u^2 \mathcal{E}) \ , \tag{2.6}$$

where $\lambda_T = \frac{10\Delta_\psi}{c_T \pi^2}$ (c_T is the coefficient of the TT two-point function). This is the leading term in the regime

$$|v| \ll \frac{1}{|u|} \ll 1 \qquad (\text{with } uv < 0) \ . \tag{2.7}$$

The result (2.6) is an operator equation that can be used inside correlation functions (subtleties are discussed below). It sums the usual lightcone OPE (studied for example in [43, 107]) including the contributions of all minimal-twist operators, $(\phi_u)^n T_{uu}$ for $n \geq 0$. We have assumed that the theory is interacting, so there are no conserved currents of spin > 2 [108], and that there are no very low-dimensions scalars in this OPE. (The second assumption is not necessary for the derivation of the sign constraints since we can project onto stress tensor exchange; see section

2.6.)

Now consider the normalized 4-point function

$$G = \frac{\langle \overline{O(y=\delta)}\psi(u,v)\psi(-u,-v)O(y=\delta)\rangle}{\langle \overline{O(y=\delta)}O(y=\delta)\rangle\langle\psi(u,v)\psi(-u,-v)\rangle} , \tag{2.8}$$

in the regime (2.7), as illustrated in figure 2.1. $\overline{O}$ denotes the Rindler reflection of the operator O. For scalars, $\overline{O(t,y,\vec{x})} \equiv O^\dagger(-t,-y,\vec{x})$; see section 2.4.2 for the action on spinning operators. The OPE (2.6) gives

$$G = 1 + \frac{\lambda_T}{N_\delta} v u^2 \langle \overline{O(y=\delta)}\, \mathcal{E}\, O(y=\delta)\rangle \tag{2.9}$$

with $N_\delta = \langle \overline{O(y=\delta)}O(y=\delta)\rangle > 0$. The correction term, $\langle \overline{O(y=\delta)}\, \mathcal{E}\, O(y=\delta)\rangle$, is computed by a residue of the null line integral, and is purely imaginary.

Although the correction in (2.9) is small, it is growing with u. Corrections of this form were studied by Maldacena, Shenker, and Stanford in [27], and in the CFT context in [58, 92], where it was shown that if such a term appears, it must have a negative imaginary part.[4] Therefore

$$i\langle \overline{O(y=\delta)}\, \mathcal{E}\, O(y=\delta)\rangle \geq 0 . \tag{2.10}$$

This conclusion relies on a number of analyticity and positivity conditions that the correlator must satisfy; we check these conditions and review the argument in detail below. It can be understood as a causality constraint. If the correction has the wrong sign, then it requires the correlator to have singularities in a disallowed regime, and these singularities lead to non-vanishing commutators at spacelike separation.

[4]The chaos bound of MSS refers to large-N theories, and the interest in [27] was in a different regime of the correlator (the Regge regime). Here, as in [58], we are applying similar methods to the lightcone regime of a small-N theory. In the Regge/chaos regime, the small parameter that controls the OPE is $1/N$, whereas here it is the expansion in v as we approach the lightcone. These limits do not, in general, commute, even in large N theories, so the physics of the two classes of constraints is different.

This is not yet (2.5), since in one case the operators are inserted in Minkowski space and in the other case offset in imaginary time. In fact, these are equivalent, by acting with a rotation R that rotates by $\frac{\pi}{2}$ in the Euclidean $y\tau$-plane (with $\tau = it$):

$$i\langle\overline{O(y=\delta)}\,\mathcal{E}\,O(y=\delta)\rangle = \langle(R{\cdot}O)^\dagger(t=i\delta)\;\mathcal{E}\;R{\cdot}O(t=-i\delta)\rangle\ . \tag{2.11}$$

(The null contour defining $\mathcal{E}$ is also trivially rotated in relating these two expressions.) The ANEC, in an arbitrary state in CFT, then immediately follows from (2.10).

For comparison to previous work, we note that the arguments in [27,58,92] were phrased in terms of conformal cross ratios, and it was important that the correlator was evaluated on the '2nd sheet', *i.e.,* after a particular analytic continuation in the cross ratios. The current approach is equivalent. The analytic continuation is entirely captured by the choice of contour that defines $\mathcal{E}$ in the formulas above, implicit in the way we have ordered the operators, as we will discuss in detail in section 2.3.

It was previously noted in [109] that the ANEC would follow if $\mathcal{E}$ appears as the leading term in a reflection-positive OPE. This is similar in some ways to our argument, but the details are different. The lightcone OPE invoked in the first step actually produces not $\langle\mathcal{E}\rangle$ but $\sim 1 + i\langle\mathcal{E}\rangle$, and because of the crucial factor of i, the argument for positivity is more intricate.

Conformal invariance was used several times in the derivation above, but under mild assumptions the conclusions apply also to non-conformal QFTs with an interacting fixed point in the UV. The approach to the lightcone is controlled by the UV fixed point, so if the fixed point is an interacting CFT, then the OPE formula (2.6) still applies. (This would not be true if the UV fixed point were free, since then an infinite tower of higher spin currents would contribute to the lightcone

OPE at leading order.) One might worry that in the limit $u \gg 1$, some pairs of operators in the 4-point function are at large timelike separation, so perhaps there are significant infrared effects. We do not have a complete argument that it is impossible, so leave this as an open question. A similar OPE argument was used in [110] to derive Bousso's covariant entropy bound, and it was argued that such effects should be absent — the same arguments apply here, so we consider this a mild assumption. See section 2.4.6 for further discussion.

2.3 Average null energy in the lightcone OPE

In this section, we will derive the universal contribution of the null energy operator $\mathcal{E}$, defined in (2.4), to n-point correlation functions in $(3+1)-$dimensions. The general case ($d \neq 4$ and/or spin > 2) is in section 2.6.

2.3.1 Lightcone OPE

Consider a scalar primary ψ. In general, two nearby operators can be replaced by their operator product expansion,

$$\psi(x_2)\psi(x_1) = \sum_i C_i^{\mu\nu\cdots}(x_1 - x_2) O^i_{\mu\nu\ldots}(x_2) \ . \tag{2.12}$$

In the limit that $x_2 - x_1$ becomes null, the OPE is organized as an expansion in twist, $\Delta_i - J_i$, where Δ is scaling dimension and J is spin. For now we will assume that the stress tensor $T_{\mu\nu}$ is the unique operator of minimal twist. (This assumption is not necessary for the ANEC, as long as the theory is interacting and the stress tensor is the only spin-2 conserved current; see section 2.6.) Then the

leading contributions to the OPE in the lightcone limit $v \to 0$ are

$$\psi(u,v)\psi(-u,-v) = \langle\psi(u,v)\psi(-u,-v)\rangle \left[1 + vu^3 \sum_{n=0}^{\infty} c_n (u\partial_u)^n T_{uu}(0) + \cdots\right], \tag{2.13}$$

with corrections suppressed by powers of v. We have inserted the operators symmetrically in the uv-plane with $\vec{x} = 0$, and expanded about the midpoint. Other descendants of T are subleading because they must come with powers of v in order to contract indices.

The constants c_n can be determined by plugging (2.13) into the 3-point function $\langle\psi\psi T_{\mu\nu}\rangle$ and comparing to the known answer, which can be found in [111]. However it is more elucidating to rewrite the lightcone OPE as an integral, rather than a sum. In fact (2.13) is exactly equivalent to

$$\frac{\psi(u,v)\psi(-u,-v)}{\langle\psi(u,v)\psi(-u,-v)\rangle} = \left[1 - \frac{15c_{\psi\psi T}}{c_T} vu^2 \int_{-u}^{u} du' \left(1 - \frac{u'^2}{u^2}\right)^2 T_{uu}(u', v=0) + \cdots\right]. \tag{2.14}$$

This is derived by assuming an ansatz with an arbitrary kernel inside the integral, plugging into $\langle\psi\psi T_{\mu\nu}\rangle$, and designing the kernel to reproduce the known answer. Alternatively, we can expand the integrand as $T_{uu}(u') = T_{uu}(0) + u'\phi_u T_{uu}(0) + \cdots$, do the integral, and check that (2.14) reproduces (2.13) with the correct c_n's. The OPE coefficient $c_{\psi\psi T}$ is fixed by the conformal Ward identity to $c_{\psi\psi T} = -\frac{2\Delta_\psi}{3\pi^2}$.

In (2.14), the lightcone OPE is expressed as an integral of T_{uu} over the null ray connecting the two ψ's. It is an operator equation, meaning it can be used inside correlation functions, though we must be careful about convergence (or, equivalently, coincident point singularities).[5]

[5]See [112] for recent progress in writing general OPEs by integrating over causal diamonds. The OPE (2.13) can also be derived using shadow operators, as described in appendix B of that paper. It is interesting to note the similarity to the formula for the vacuum modular Hamiltonian of an interval in 1+1 dimensions, $H \sim \int_{-L}^{L}(1 - x^2/L^2)T_{tt}$, and also to the recent derivation of

In the limit $u \to \infty$, the integration kernel is trivial, so the lightcone OPE produces the integrated null energy operator:

$$\psi(u,v)\psi(-u,-v) \approx \langle \psi(u,v)\psi(-u,-v)\rangle(1 + \lambda_T v u^2 \mathcal{E}) \ , \tag{2.15}$$

where $\lambda_T = \frac{10\Delta_\psi}{c_T \pi^2}$. This equation holds in the limit where we first take $v \to 0$, then $u \to \infty$, assuming that all other operator insertions are confined to some finite region. Corrections are subleading in $1/u$ or v.

2.3.2 Contribution to correlators

Now consider the correlator

$$\langle \psi(x_1)\psi(x_2)O(x_3)\cdots O(x_n)\rangle \ . \tag{2.16}$$

(O may have spin; its indices are suppressed.)

If all points are spacelike separated, then the $\psi\psi$ OPE is convergent. If, on the other hand, for instance $x_1 - x_3$ is spacelike but $x_2 - x_3$ is timelike, then the full $\psi\psi$ OPE may diverge. Still, we expect that any finite number of terms in the lightcone OPE produce a reliable asymptotic expansion in the limit $v_2 \to v_1$. This is argued in detail for 4-point functions in section 4.5 of [58] by comparing to a different, convergent OPE channel. (More heuristically, it is reasonable to trust a divergent expansion in v as $v \to 0$ so long as subsequent terms are highly suppressed, just as in ordinary perturbation theory.) For n-point functions, a similar argument holds. The conclusion is that (2.15) can be used inside arbitrary correlation functions, as long as we take the limits with all other quantities held fixed.

the Bousso bound [110], which relied on an integral expression for the null OPE of twist line operators.

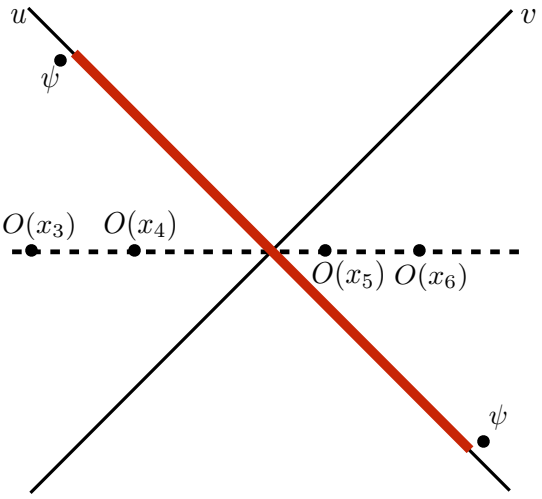

Figure 2.2: Operator insertions in Minkowski spacetime. In the limit where the two ψ's become null, but are widely separated in u, the leading non-identity term in the $\psi\psi$ OPE is $\int du T_{uu}$, integrated over the red null line.

Operators are ordered by the standard prescription (reviewed in detail in [58]): To compute

$$\langle O_1(x_1)O_2(x_2)\cdots O_n(x_n)\rangle \ , \tag{2.17}$$

shift $t_i \to t_i - i\epsilon_i$ with $\epsilon_1 > \epsilon_2 > \cdots > \epsilon_n$, and define the correlator by analytic continuation from the Euclidean. In the domain with a fixed imaginary time ordering, the function is analytic, and sending $\epsilon_i \to 0$, it produces the Lorentzian correlator with operators ordered as written in (2.17). When we apply the lightcone OPE (2.15), this translates into a choice of contour for the u-integral. For concreteness, set $n = 6$ and suppose the O's are all at $t = \vec{x} = 0$, with two O's in each Rindler wedge, as in figure 2.2. (Generalizing to arbitrary Minkowski insertions $x_{3,\ldots,n} \in R^{1,d-1}$ with $x_i^2 > 0$ is straightforward.) Suppressing coordinates set to zero, first consider the ordering

$$\langle \psi(u_1, v_1)\psi(-u_1, -v_1)O(y_3)O(y_4)O(y_5)O(y_6)\rangle \tag{2.18}$$

with $v_1 < 0 < u_1$. In the limit $|v_1| \ll \frac{1}{|u_1|} \ll 1$, the OPE gives the leading terms

$$\langle \psi(u_1, v_1)\psi(-u_1, -v_1)\rangle \langle \left[1 + \lambda_T v_1 u_1^2 \int_{-\infty}^{\infty} du T_{uu}(u, v = 0)\right] O(y_3)O(y_4)O(y_5)O(y_6)\rangle \ . \tag{2.19}$$

The integral has singularities at $-u = y_3, \ldots, y_6$. The $i\epsilon$ prescription says that to compute the correlator ordered as in (2.18), the contour in the complex u-plane goes below the poles:

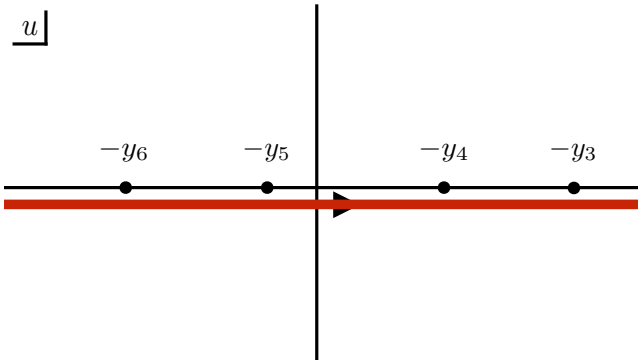

(2.20)

As $|u| \to \infty$, applying the OPE to all the O's implies that the integrand falls off the same as (or faster than) $\langle T_{uu}(u)T_{\alpha\beta}(x)\rangle \sim u^{-6}$, so we can deform the contour and the integral vanishes. (This does not mean that the stress tensor contribution to the lightcone OPE vanishes, only that it has no terms $\sim v_1 u_1^2$. The first non-zero contribution is actually $\sim v_1/u_1^3$, using (2.14).) Other orderings are obtained by deforming the contour across poles. For example, the time-ordered correlator

$$\langle \psi(u_1, v_1)O(y_3)O(y_4)O(y_5)O(y_6)\psi(-u_1, -v_1)\rangle \tag{2.21}$$

is again computed by (2.19), but now integrating on the following contour:

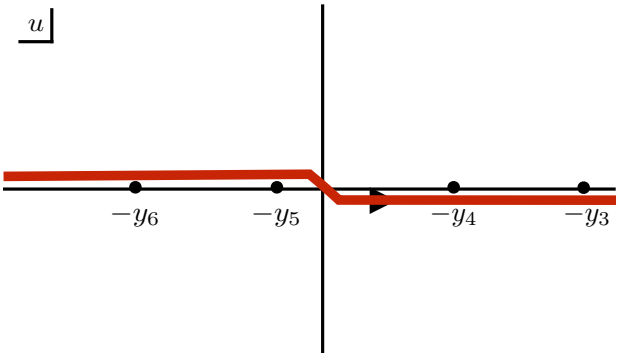

(2.22)

The integral is equal to the sum of residues at $u = -y_5, -y_6$ or at $u = -y_4, -y_3$, so this ordering does have terms $\sim v_1 u_1^2$.

2.3.3 Scalar example

In the language of [27, 58], the trivial contour (2.20) is the 1st sheet (or Euclidean) correlator, while the non-trivial contour (2.22) produces the correlator on the 2nd sheet.

As a simple application, let us reproduce the well known hypergeometric formula for the four-point conformal block in the lightcone limit. Consider the four-point function of identical scalars,

$$G_{scalar}(z, \bar{z}) = \langle \phi(0)\phi(z, \bar{z})\phi(1)\phi(\infty) \rangle \ . \tag{2.23}$$

With these kinematics, the cross ratios are simply the lightcone coordinates of the second insertion. For $z, \bar{z} \in (0, 1)$, all points are spacelike. Plugging in the lightcone OPE (2.14) gives an integral that is easily recognized as a hypergeometric function, and we reproduce the well known formula for the stress tensor lightcone block (see [43, 107]):

$$\bar{z} z^3 \, {}_2F_1(3, 3, 6, z) = -\frac{30\bar{z}}{z^2} \left[-3(-2+z)z + (6 - 6z + z^2) \log(1-z) \right] \ . \tag{2.24}$$

This is regular as $z \to 0$. But after going to the second sheet, *i.e.,* sending $\log(1-z) \to \log(1-z) - 2\pi i$, the behavior near the origin is $\sim i\bar{z}/z^2$. This growing term, with the correct coefficient, is what is captured by the approximation where we replace the full lightcone OPE by just the null energy operator, as in (2.15). So what we have shown is that these growing terms, responsible for all the results in [58, 92, 93], are precisely the contributions of the null energy operator $\mathcal{E}$.

2.4 Sum rule for average null energy

Now we will fill in the details of the ANEC derivation in section 2.2. Most of this discussion is a review of [27] and [58], some of it from a different perspective. First, we will collect some facts about position-space correlation functions, which hold in any unitary, Lorentz-invariant QFT. Then we put them together to derive the sum rule and positivity condition.

2.4.1 Analyticity in position space

The point of view taken throughout the paper is that a QFT can be defined by its Euclidean n-point correlation functions [106]. These are single-valued, permutation invariant functions of $x_{1,\ldots,n} \in R^d$, *i.e.,* there are no branch cuts in Euclidean signature. This ensures that in the Lorentzian theory, non-coincident local fields at $t = 0$ commute with each other.

The Euclidean correlators can be analytically continued to complex x_i. However, there are branch points when one operator hits the lightcone of another. (See [106] for details or section 3 of [58] for a review.) When we encounter one of these branch points, we must choose whether to go around it by deforming $t \to t+i\epsilon$ or $t \to t-i\epsilon$, and this selects whether the two operators are time-ordered or anti-time-ordered. Thus the $i\epsilon$ prescription to compute a Minkowski correlator ordered as

$$\langle \phi_1(x_1)\phi_2(x_2)\phi_3(x_3)\cdots \rangle \tag{2.25}$$

is to gives each t_i a small imaginary part, with

$$\text{Im } t_1 < \text{Im } t_2 < \text{Im } t_3 < \cdots \ . \tag{2.26}$$

The resulting function is analytic as long as we maintain (2.26), so once we've specified the $i\epsilon$ prescription, the analytic continuation from Euclidean is unambiguous.

In fact, the domain of analyticity of the n-point correlator $G(x_i)$, viewed as a function on (a subdomain of a cover of) n copies of complexified Minkowski space, is larger than indicated by (2.26). It is also analytic on the domain defined by the covariant version of (2.26):

$$\text{Im } x_1 \lhd \text{Im } x_2 \lhd \text{Im } x_3 \lhd \cdots , \tag{2.27}$$

where $x \lhd y$ means 'x is in the past lightcone of y'.[6] (Actually, it is analytic on an even larger domain, but (2.27) is all we need.[7])

2.4.2 Rindler positivity

Correlation functions in Minkowski space restricted to the left and right Rindler wedges obey a positivity property analogous to reflection positivity in Euclidean signature. This is derived in [113][8] and also in [27].

Define the Rindler reflection

$$\overline{x} = \overline{(t, y, \vec{x})} = (-t^*, -y^*, \vec{x}) \ . \tag{2.28}$$

[6]We define the imaginary part of a complexified point by the convention that a point in Minkowski space $R^{1,d-1}$ has $x_i = \text{Re } x_i$. Thus the real and imaginary parts each live in a copy of Minkowski space, not Euclidean space.

[7]The full domain is described as follows [106]. First act on the domain (2.27) by all possible complex Lorentz transformations; this defines the *extended tube*. Then, permute the n points and a repeat this procedure, to define the *permuted extended tube*. In the theory of multiple complex variables, the domain of analyticity cannot be an arbitrary shape — once we know a function is analytic on some domain, it must actually be analytic on a (generally larger) domain called the *envelope of holomorphy*. The domain of analyticity of the correlator $G(x_i)$ is the envelope of holomorphy of the union of permuted extended tubes.

[8]What we call Rindler positivity is not, however, quite the same as 'wedge reflection positivity' referred to in the title of the paper [113]. The difference is discussed in section 3 of [113].

The transverse coordinate $\vec{x}$ is taken to be real. For real (t, y), this reflects a point in the right Rindler wedge to the left Rindler wedge. Acting on a spinning operator O,

$$\overline{O_{\mu\nu\cdots}(t, y, \vec{x})} = (-1)^P O^\dagger_{\mu\nu\cdots}(-t^*, -y^*, \vec{x}) \tag{2.29}$$

where P is the number of t-indices plus y-indices. (The Hermitian conjugate on the right-hand side acts only on the operator, not the coordinates.) This operation is CPT together with a rotation by π around the y-axis: $\overline{O} = JOJ$ with $J = U(R(y, \pi))CPT$ [113].

We will insert points in a complexified version of the left and right Rindler wedges. The complexified right wedge is defined as

$$R_C = \{(u, v, \vec{x}) : uv < 0,\ \arg v \in (-\frac{\pi}{2}, \frac{\pi}{2}),\ \vec{x} \in R^{d-2}\}\ , \tag{2.30}$$

and the complexified left wedge is

$$L_C = \overline{R_C} = \{(u, v, \vec{x}) : uv < 0,\ \arg v \in (\frac{\pi}{2}, \frac{3\pi}{2}),\ \vec{x} \in R^{d-2}\}\ . \tag{2.31}$$

The positivity condition for $2n$-point correlators is

$$\langle \overline{O_1(x_1)}\, \overline{O_2(x_2)}\, \cdots \overline{O_n(x_n)} O_1(x_1) O_2(x_2) \cdots O_n(x_n) \rangle > 0\ , \tag{2.32}$$

for $x_{1,\ldots,n} \in R_C$ and

$$\text{Im } t_1 \leq \text{Im } t_2 \leq \cdots \leq \text{Im } t_n\ . \tag{2.33}$$

Note that for product operators, the order does not reverse under reflection:

$$\overline{O_1 O_2} = \overline{O_1}\ \overline{O_2}\ . \tag{2.34}$$

For real insertions, Im $t_i = 0$, the operators in (2.32) are ordered as written, which we will refer to as 'positive ordering'. They are not time ordered. For complex

insertions, the correlator is defined by analytic continuation from Euclidean within the domain (2.26). The reflected operators have

$$\text{Im } -t_1^* \leq \text{Im } -t_2^* \leq \cdots \leq \text{Im } -t_n^* \ , \tag{2.35}$$

which explains why they must be ordered as in (2.32).

Positivity applies also to smeared operators, and products of smeared operators, with support in a single complexified Rindler wedge. That is,

$$\langle \overline{\Theta}\Theta \rangle > 0 \ , \tag{2.36}$$

for

$$\Theta = \int f^{(1)}(x_1) O_1(x_1) + \int\int f^{(2)}(x_1, x_2) O_1(x_1) O_2(x_2) + \cdots \ , \tag{2.37}$$

where the smearing functions f have support in some localized region of R_C, and the operator ordering in $\overline{\Theta}$ is the same as in Θ.

These positivity conditions hold in any unitary, Lorentz-invariant QFT [27, 113]. We will not repeat the derivation, but an intuitive way to understand this is as follows. To be concrete, consider a case of particular interest for the ANEC and the Hofman-Maldacena constraints that will be used below:

$$\Theta_0 = \psi(t_0, y_0) \int_0^\infty d\tau \int_0^\infty dy \int d^{d-2}\vec{x} f(\tau, y, \vec{x}) O(t = -i\tau, y, \vec{x}) \tag{2.38}$$

with $t_0, y_0 > 0$, and assume f is non-zero in some finite region. ψ and O may be timelike separated, in the sense that Re $(x_0 - x) \in R^{1,d-1}$ lies in the forward lightcone for points of the integral. We want to understand why $\langle \overline{\Theta}_0 \Theta_0 \rangle > 0$. First, we can evolve $\psi(t_0, y_0)$ back to the $t = 0$ slice; it becomes non-local, but with support only in the right Rindler wedge. The same can be done in $\overline{\Theta}_0$, evolving $\psi(-t_0, -y_0)$ forward to the $t = 0$ slice. Then in the τy-plane, the 4-point function $\langle \overline{\Theta}_0 \Theta_0 \rangle$ is smeared over the regions shown in figure 2.3. These insertions are symmetric

under $y \to -y$ together with complex conjugation; therefore, reflection positivity of the Euclidean theory guarantees that this correlator is positive. Keeping track of Lorentz indices on O leads to the same conclusion. For a more precise derivation we refer to [113] for real insertions, and [27] for insertions in the complexified wedge R_C.

To recap, although $\langle\overline{\Theta}\Theta\rangle$ does not look like a norm in the theory quantized on the $\tau = 0$ plane — since $\Theta|0\rangle$ is not normalizable, and $\overline{\Theta} \neq \Theta^\dagger$ — it is a norm in the theory quantized on the $y = 0$ plane. These two different quantizations correspond to two different ways of analytically continuing a Euclidean theory to Minkowski space as shown in figure 2.4.

In conformal field theory, the positivity properties discussed here follow from the fact that the conformal block expansion has positive coefficients (in the appropriate channel), as described in [58,92]. We have chosen a different but conformally related kinematics in the present paper because (i) it makes the positivity conditions more manifest, (ii) positivity in the new kinematics does not require conformal invariance, and (iii) it allows us to smear operators while easily maintaining positivity properties needed to derive the constraints.

2.4.3 Bound on the real part

With operators inserted symmetrically across the Rindler horizon, the positive-ordered correlator is real and positive. The time-ordered correlator is generally complex, but it inherits from (2.32) bounds on its magnitude and real part. This was derived in [27] by interpreting the correlator as a Rindler trace and applying

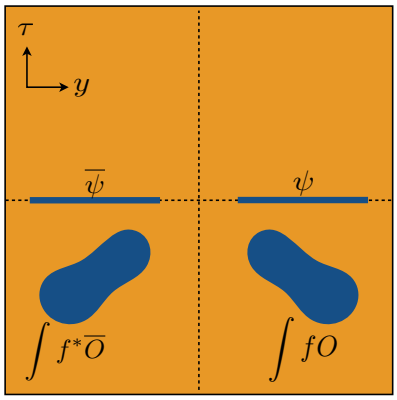

Figure 2.3: Operator insertions on the τy-plane defining the smeared 4-point function $\langle\overline{\Theta}_0\Theta_0\rangle$.

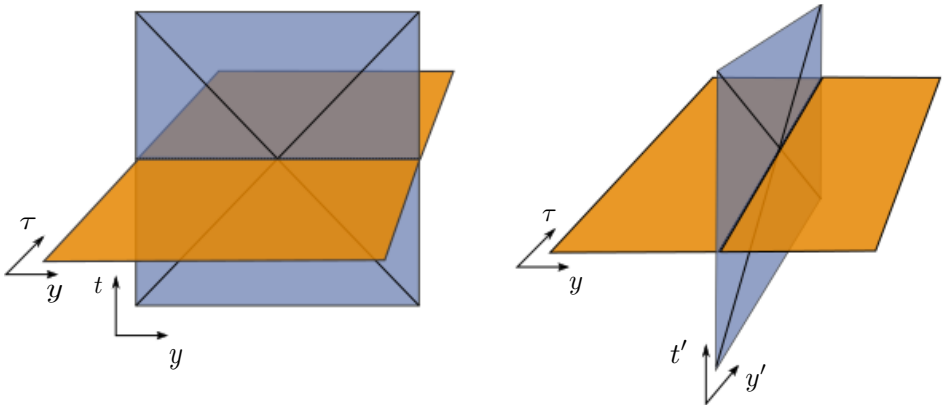

Figure 2.4: Two different ways to interpret the same Euclidean theory. The Euclidean R^d (horizontal orange plane, parameterized by $(\tau, y, \vec{x})$) is the same in both pictures, but the definition of states and corresponding notion of Minkowski spacetime (vertical blue planes) is different in the two cases. On the left, the continuation to Lorentzian is $\tau \to it$, states of the theory are defined on the plane $\tau = 0$, and y is a space direction. On the right, the continuation to Lorentzian is $y \to it'$, states are defined at $y = 0$, and $\tau = y'$ is a space direction. The two theories are identical, since they are determined by the same set of Euclidean correlators, but the map of observables and matrix elements from one description to the other is nontrivial.

Cauchy-Schwarz inequalities. The positivity condition for CFT shockwaves derived in [58,92] using the decomposition into conformal partial waves can also be restated in this way.

Here we repeat the Cauchy-Schwarz derivation, but in Minkowski language. Let A, B be operators (possibly nonlocal) with support in the right wedge R_C. The positive-ordered correlator defines a positive inner product $(A, B) \equiv \langle \overline{A} B \rangle$. Therefore the Cauchy-Schwarz inequality applies,

$$|\langle \overline{A} B \rangle|^2 \leq \langle \overline{A} A \rangle \langle \overline{B} B \rangle \ . \tag{2.39}$$

In the derivation of the ANEC in section 2.2 we considered

$$G_{anec} = \langle \overline{O} \psi(u, v) \psi(-u, -v) O \rangle \ . \tag{2.40}$$

(There O was local, but for the present purposes it can also be smeared.) Applying Cauchy-Schwarz with $A = O\psi(-u, -v)$, $B = \psi(-u, -v)O$,

$$\text{Re } G_{anec} \leq |G_{anec}| \leq \left(\langle \overline{\mathcal{O}\psi} O\psi \rangle \langle \overline{\psi \mathcal{O}} \psi O \rangle \right)^{1/2} \tag{2.41}$$

where $\psi \equiv \psi(-u, -v), \overline{\psi} \equiv \psi(u, v)$. Note that both of the correlators on the right-hand side are positive-ordered.

2.4.4 Factorization

In the limit $u \to \infty$ (with everything else held fixed or $v \sim 1/u$), positive-ordered correlators factorize into products of two-point functions. In a CFT, this follows from the OPE. In this limit, we can replace O by a local operator, and the conformal cross ratios of the 4-point function $\langle \overline{\mathcal{O}\psi} O\psi \rangle$ are $z, \bar{z} \sim 0$. Positive ordering means that we do not cross any branch cuts to reach this regime [27,58], so the correlator

can be computed by the usual Euclidean OPE and is dominated by the identity term. Thus

$$\langle\overline{\mathcal{O}\psi}O\psi\rangle \sim \langle\overline{\psi\mathcal{O}}\psi O\rangle \sim \langle\overline{\mathcal{O}}O\rangle\langle\overline{\psi}\psi\rangle \tag{2.42}$$

and (2.41) becomes

$$\text{Re } G_{anec} \leq |G_{anec}| \leq \langle\overline{\mathcal{O}}O\rangle\langle\psi(u,v)\psi(-u,-v)\rangle + \varepsilon \ . \tag{2.43}$$

The correction term ε on the right is necessary because the positive-ordered correlator does not exactly factorize. It has corrections from subleading operator exchange. But ε is suppressed by positive powers of v and $1/u$, so it can be neglected everywhere in the derivation.

This argument relied on conformal invariance, but factorization is expected to hold in a general interacting theory (possibly excluding integrable theories). This is motivated on physical grounds in [27] by relating it to thermalization of finite temperature Rindler correlators.

2.4.5 Sum rule

Now we use the method of [58] to derive a manifestly positive sum rule for averaged null energy, $\langle O|\mathcal{E}|O\rangle$. Let

$$v = -\eta\sigma, \quad u = 1/\sigma \ , \tag{2.44}$$

with $0 < \eta \ll 1$ and consider the function G defined in (2.8) as a function of complex σ, with all other coordinates fixed. The function $G(\sigma)$ obeys two important properties:

(i) $G(\sigma)$ is analytic on the lower-half σ plane in a region around $\sigma \sim 0$. This

follows from (2.27) with complexified points labeled as $x_1 = (-u, -v)$, $x_2 = (y = \delta)$, $x_3 = (y = -\delta)$, $x_4 = (u, v)$.

(ii) For real σ with $|\sigma| < 1$,

$$\text{Re } G \leq 1 + \varepsilon \ , \tag{2.45}$$

where the correction ε is suppressed by positive powers of both η and σ. This follows directly from (2.43).

Equipped with these facts, the sum rule is derived by integrating $G(\sigma)$ over the boundary of a half-disk, just below $\sigma = 0$:

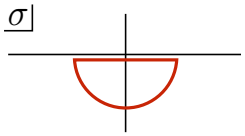

(2.46)

The radius R of the semicircle does not matter, as long as it is in the regime (2.7), *i.e.*, $\eta \ll R \ll 1$. The integral over a closed contour vanishes,

$$\text{Re} \oint d\sigma (1 - G(\sigma)) = 0 \ . \tag{2.47}$$

We split this into the contribution from the semicircle and from the real line, then use the OPE (2.9) to evaluate the correlator on the semicircle and do the integral. The result is

$$i\overline{\langle O(y=\delta)}\, \mathcal{E}\, O(y=\delta) = \frac{N_\delta}{\pi \eta \lambda_T} \int_{-R}^{R} d\sigma \text{Re } (1 - G(\sigma)) \ . \tag{2.48}$$

The right-hand side is positive by property (ii) above. Using (2.11), the sum rule can be written as a manifestly positive integral for the expectation value of average null energy:

$$\langle O|\mathcal{E}|O\rangle = \frac{1}{\pi \eta \lambda_T} \int_{-R}^{R} \text{Re } (1 - G(u = \frac{1}{\sigma}, v = -\eta\sigma)) \tag{2.49}$$

where $|O\rangle \equiv \frac{1}{\sqrt{N_\delta}} O(t = -i\delta)|0\rangle$ (and if O is not a scalar, the operator is rotated by $\pi/2$ in the Euclidean τy-plane).

Note that two distinct positivity conditions came into play. First, there was Rindler positivity, property (ii). Applied to the correlator G in the lightcone regime, this would imply Re $\langle \overline{O(y = \delta)} \mathcal{E} O(y = \delta) \rangle \geq 0$. However, this 3-point function is purely imaginary, so this constraint is trivial. Rindler positivity is nontrivial only near the origin of the σ-plane (the Regge-like limit), where the OPE is not dominated by the low-dimension (or low-twist) operators. Second, there is the positivity condition on the imaginary part of the OPE correction, coming from the sum rule. It is this second, less direct consequence of reflection positivity that leads to the ANEC. This is similar to the use of dispersion relations for scattering amplitudes in momentum space – the optical theorem gives a positivity condition on the forward amplitude, and sum rules relate this positive quantity to the amplitude in other regimes (see for example [114]).

2.4.6 Non-conformal QFTs

As mentioned in section 2.2, we expect the main conclusions and the sum rule to hold even in non-conformal QFTs as long as there is an interacting UV fixed point. This is essentially because it is a UV argument. The applicability of the lightcone OPE was discussed at the end of section 2.2. Conformal symmetry was used again when we invoked the state-operator correspondence to claim that any normalizable state can be created by inserting a local operator at $t = -i\delta$. This made the derivation simpler, since we could restrict to local operator insertions $O(y = \delta, t = 0, \vec{x} = 0)$. But in fact this restriction was not necessary. The ingredients that go into the sum rule — positivity, etc — still apply if O is a non-local operator defined by

smearing local operators (and their products) over a complexified version of the Rindler wedge. In any QFT a dense set of states can be created in this way [106].

2.5 Hofman-Maldacena bounds

The conformal collider bounds of Hofman and Maldacena [56] are constraints on CFT 3-point functions that come from imposing

$$\lim_{v\to\infty} v^2 \langle \varepsilon^* \cdot O(P)^\dagger \int_{-\infty}^{\infty} du T_{uu}(u,v) \varepsilon \cdot O(P) \rangle \geq 0 \ . \tag{2.50}$$

Here $O(P)$ is a wave packet with timelike momentum $P = \omega \hat{t}$, created by inserting a spinning operator near the origin:

$$\varepsilon O(P) = \int dt dy d^{d-2}\vec{x}\, e^{-(t^2+y^2+\vec{x}^2)/D^2} e^{-i\omega t} \varepsilon^{\mu\nu\cdots} O_{\mu\nu\cdots}(t,y,\vec{x}) \ , \qquad \omega D \gg 1 \ . \tag{2.51}$$

The positivity condition (2.50) was an assumption in [56], motivated by the fact that this computes the energy measured in a far-away calorimeter if we prepare a CFT in the state $\varepsilon \cdot O(P)|0\rangle$. It leads to constraints on the 3-coupling constants that appear in $\langle OTO \rangle$.

Since we have shown that $\mathcal{E}$ is a positive operator, the inequality (2.50) follows from the above analysis. But it is instructive to see how constraints in this particular state are related to our discussion of Minkowski scattering and the ANEC sum rule. That is the goal of this section. In particular, we will show exactly how to smear the probe operators in the previous analyses [58, 92, 93] to produce the Hofman-Maldacena inequalities. This avoids the step of decomposing the correlator into the crossed channel, used in [93] in order to improve upon the bounds derived in [92].

2.5.1 Conformal collider redux

First we will restate the Hofman-Maldacena condition in a way that makes all of the integrals trivial. We perform the Fourier transform over t first. In the regime $\omega D \gg 1$ it is dominated by a saddlepoint at $t = -\frac{i}{2}\omega D^2$. Therefore, instead of viewing this as a wavepacket with frequency ω, we can replace it by an operator inserted at a fixed, imaginary value of t:

$$\varepsilon \cdot O(P) \approx \int dy d^{d-2}\vec{x}\, e^{-(y^2+\vec{x}^2)/D^2} \varepsilon^{\mu\nu\cdots} O_{\mu\nu\ldots}(t = -i\delta, y, \vec{x}) \tag{2.52}$$

with $\delta > 0$. Also, in this limit, we only need to integrate over the position of one of the O insertions, since the other integral gives an overall factor. The remaining gaussian can be dropped, and the final $d-1$ integrals are done by residues.[9]

In (2.50), the state is created near the origin of Minkowski space, and the average null energy is evaluated near future null infinity. For comparison to the rest of the paper, it is more convenient to shift coordinates so that the null energy is integrated over a ray at $v = 0$, and O is inserted near spatial infinity. That is, (2.50) is equivalent to

$$\lim_{\lambda\to\infty} \lambda^2 \langle \varepsilon \cdot O_\lambda | \, \mathcal{E} \, | \varepsilon \cdot O_\lambda \rangle \geq 0 \tag{2.53}$$

where $\mathcal{E}$ is integrated over $v = 0$ as in (2.4), and

$$|\varepsilon \cdot O_\lambda\rangle \equiv \int d\tilde{y} d^{d-2}\vec{x}\, \varepsilon \cdot O(t = -i\delta, y = \lambda\tilde{y}, \vec{x})|0\rangle \ . \tag{2.54}$$

In (2.53), the wavepacket is implemented by the order of limits: first we do the u-integral (by residues) to compute $\mathcal{E}$, then take $\lambda \to \infty$, then perform the integrals over $\vec{x}, \tilde{y}$.

[9] Dropping the gaussian can lead to unphysical divergences in the remaining integrals, depending on the dimensions of the operators. These are dealt with by dimensional regularization in the transverse directions, $d-2 \to d-2+\epsilon$ with $\epsilon \to 0$ at the end [115].

To recap, the Hofman-Maldacena constraints are restated as:

$$\int d\tilde{y} d^{d-2}\vec{x} \lim_{\lambda\to\infty} \lambda^2 \langle \varepsilon^* \cdot O(t = i\delta, y = \lambda, \vec{0})\, \mathcal{E}\, \varepsilon \cdot O(t = -i\delta, y = \lambda\tilde{y}, \vec{x})\rangle \geq 0 \ . \quad (2.55)$$

This expression is a convenient way to compute the explicit constraints in terms of the 3-point coupling constants.

2.5.2 Relation to scattering with smeared insertions

The state (2.54) is most naturally created by smearing an operator near spatial infinity, but like any localized state in a CFT, it can also be created by inserting a single, non-primary operator at $t = -i\delta, y = \vec{x} = 0$.[10] It is straightforward to find the operator explicitly by a series expansion of the wavepacket integral, $\int dy d^{d-2}\vec{x}\, O(t = -i\delta, y, \vec{x}) e^{-((y-\lambda)^2+\vec{x}^2)/D^2}$. Applying section 2.2 to this particular operator is one way to derive the Hofman-Maldacena inequalities directly from the causality of the 4-point function. However, we would need to be more careful about the order of limits in the series defining the operator and various other steps of the calculation, especially since we are expanding a wavepacket about a point very far from its center.

This problem is avoided if we instead apply the causality argument directly to a correlator with smeared operator insertions, corresponding to wavepackets offset far into imaginary time. As explained around figure 2.4, the interpretation of the ANEC as an expectation value and the interpretation of the ANEC as it appears in the lightcone OPE differ by a $\pi/2$ rotation in the Euclidean τy-plane. Therefore,

[10] Everywhere in this section, the limit $\lambda \to \infty$ should be interpreted as large but finite λ, with $|v| \ll \frac{1}{|u|} \ll \frac{1}{\lambda} \ll 1$ and $\delta \sim 1$. As we move the wavepacket further, the constraints obtained this way approach arbitrarily close to the Hofman-Maldacena type constraints. (And, in the version of the argument with smeared insertions, we put a hard cutoff on the wavepacket at some distance where it is exponentially suppressed, in order to avoid coincident point singularities.)

after the rotation, in order to make contact with section 2.2 we are led to study the correlator

$$G_{HM} = \frac{\langle \overline{O_{HM}} \psi(u,v)\psi(-u,-v) O_{HM}\rangle}{\langle \overline{O_{HM}} O_{HM}\rangle \langle \psi(u,v)\psi(-u,-v)\rangle} \tag{2.56}$$

where

$$O_{HM} = \lim_{\lambda\to\infty} \int d\tau d^{d-2}\vec{x}\ \varepsilon\cdot O(t = i\tau, y = \delta, \vec{x}) e^{-((\tau-\lambda)^2+\vec{x}^2)/D^2} \tag{2.57}$$

The insertions are now symmetric under Rindler reflection, and the wavepacket is centered at large imaginary time. We could of course map the centers to real points in Minkowski, but the smearing procedure in this frame would be more complicated.

As in the discussion of the Hofman-Maldacena calculation above, the wavepacket can be implemented by instead taking

$$O_{HM} = \int d\tau d^{d-2}\vec{x}\ \varepsilon\cdot O(t = -i\lambda + i\tau, y = \delta, \vec{x})\ , \tag{2.58}$$

$$\overline{O_{HM}} = \int d\tau' d^{d-2}\vec{x}'\ \bar{\varepsilon}\cdot O^\dagger(t = -i\lambda + i\tau', y = -\delta, \vec{x}')\ , \tag{2.59}$$

where $\bar{\varepsilon}^{\mu\nu} = (-1)^P (\varepsilon^{\mu\nu})^*$ and P is the number of t-indices plus y-indices; the integral in $\mathcal{E}$ is done first, then the limit $\lambda \to \infty$, then the remaining integrals.

The leading correction to (2.56) in the lightcone limit comes, as usual, from the integrated null energy:

$$\delta G \sim \langle \overline{O_{HM}}\, \mathcal{E}\, O_{HM}\rangle\ . \tag{2.60}$$

The operator ordering here and in (2.56) is subtle: we do *not* follow the usual prescription of analytic continuation (2.26) which orders operators by imaginary time. If we did, then the u-contour (in the integral defining $\mathcal{E}$) would not circle any poles, and the constrained term would vanish as in (2.20). Instead we define

the correlator in (2.56) with the u-contour as follows:

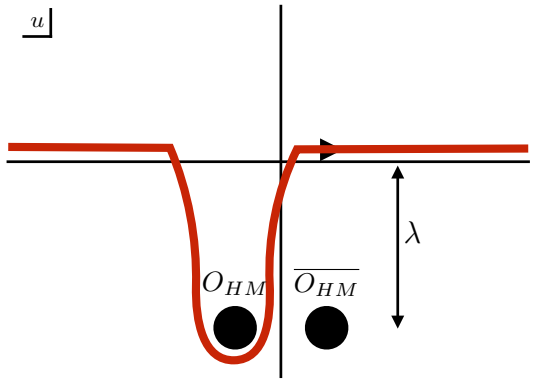

(2.61)

The black circles indicate the wavepacket insertions. This picture can be interpreted two ways: First, it shows the path of analytic continuation that defines G_{HM}, ie the route taken by the ψ's as we push $\psi(u, v)$ forward in time starting from the Euclidean correlator. Second, it is the contour of integration used when $\mathcal{E}$ appears in the OPE. [11] The correlator defined in this way has the same properties as G_{anec} in section 2.2, so the sum rule (2.49) still applies; thus the correction (2.60) has a positive imaginary part, and this inequality is identical to the conformal collider constraints.

2.5.3 Relation to the shockwave kinematics

In earlier work [58,92,93] a different kinematics was used for the four-point function in order to derive causality constraints. There, the kinematics corresponded to expectation values of OO in a shockwave state created by ψ inserted near the origin. Although the conformal cross ratios are the same in the two setups, the advantage of the scattering kinematics used here is that positivity conditions are now manifest,

[11] An equivalent prescription is to define the correlator by first expanding each wavepacket in a series expansion around $t = 0$, then compute the usual time-ordered correlator. Yet another equivalent prescription is to first compute the time-ordered correlator at $\lambda \sim 0$ as we did in previous sections, then analytically continue to finite λ.

using Rindler reflections as in [27]. This makes it easy to generalize the argument to non-primary, smeared insertions, which does not appear to be straightforward using the kinematics of [58, 92, 93].

2.6 New constraints on higher spin operators

So far we have discussed constraints on the integrated stress tensor. As in many other contexts (for example [58, 92, 93, 107, 114, 116], the positive sum rules for spin-2 exchange readily generalize to the exchange of higher spin operators. Let X be the lowest-dimension operator of spin s, where $s > 2$ is even. This operator is the dominant spin-s exchange in the lightcone limit [107]. We will argue that

$$\mathcal{E}_s = \int_{-\infty}^{\infty} du X_{uuu\cdots u}(u, v = 0, \vec{x} = 0) \tag{2.62}$$

is positive in any state. The resulting constraints agree in many cases with other methods, but are generally stronger for non-conserved operators. It would be interesting to check them in known conformal field theories, for example by numerical bootstrap or other methods. Although our OPE method does not apply to free theories, it is shown by direct calculation in appendix A.3 that (2.62) holds for free scalars.

The formulas in this section also hold for $s = 2$, so this generalizes the discussion in the rest of the paper to the ANEC in any spacetime dimension $d > 2$.

2.6.1 $\mathcal{E}_s$ in the lightcone OPE

First let us derive the contribution of the operator X and its descendants to the operator product expansion of two scalars in the lightcone limit. Repeating the steps in section 2.3, we find the lightcone OPE can be written as the integral

$$\psi(u,v)\psi(-u,-v)|_X = \langle\psi(u,v)\psi(-u,-v)\rangle \frac{2^{\Delta_X} c_{\psi\psi X}\Gamma\left(\frac{\Delta_X+s+1}{2}\right)}{\sqrt{\pi}c_X\Gamma\left(\frac{\Delta_X+s}{2}\right)} \frac{(-v)^{\tau_X/2}}{u^{\frac{\Delta_X+s}{2}-1}} \times \int_{-u}^{u} du' \left(u^2-u'^2\right)^{\frac{\Delta_X+s}{2}-1} X_{uu\cdots u}(u',0) \tag{2.63}$$

where $c_{\psi\psi X}$ is the OPE coefficient, $c_X > 0$ is the coefficient of the XX two-point function, and $\tau_X = \Delta_X - s$ is the twist. (Conventions for the constants follow [117]). The notation $(\cdots)|_X$ means the contribution of the operator X, and the expression in (2.63) is the full contribution of the operators $(\phi_u)^n X_{uu\cdots u}(0)$ for $n \geq 0$. Other descendants are subleading in the lightcone limit.

The OPE in the regime relevant to the ANEC is a divergent asymptotic series, organized by twist τ schematically as

$$\psi\psi \sim 1 + \eta^{\tau_1/2}\sigma^{1-s_1}(1+O(\sigma)) + \eta^{\tau_2/2}\sigma^{1-s_2}(1+O(\sigma)) + \cdots \tag{2.64}$$

where $v = -\eta\sigma$, $u = 1/\sigma$. Let us focus on a particular power σ^{1-s}. Contributions of this form come from operators with spin $s' \geq s$, so in the lightcone limit $\eta \to 0$, the dominant contribution is the lowest-twist operator satisfying $s' \geq s$. Denote by τ_s^* the twist of the spin-s operator with smallest dimension. It was argued in [107] that τ_s^* is a monotonically increasing, convex function of spin, with $\tau_s^* \leq 2(d-2)$.[12] This guarantees that at the order $1/\sigma^{s-1}$, the leading contribution to the OPE

[12] There, the argument held only above some unknown minimum spin, $s \geq s_{min}$. An identical argument can be made using the position-space sum rules, following the same logic. In this case we know that the sum rule is convergent for spin-2, so this establishes monotonicity and convexity for $s \geq 2$.

indeed comes from X, which we defined to be the lowest dimension operator with spin s.

If $\Delta_\psi < d-2$, an additional subtlety arises because there is an accumulation point in the twist spectrum at $\tau \sim 2\Delta_\psi$ [43, 107]. It is unclear whether the asymptotic lightcone OPE can be applied at orders in η beyond the accumulation point. Therefore in what follows we assume the probe satisfies $\Delta_\psi > \tau_X/2$ (and that any other light scalars in the OPE that would lead to accumulation points are absent). Note that this restriction was not necessary for the ANEC, since it is already enforced by the unitarity bound when X is a conserved operator.

2.6.2 Sum rule and positivity

We can now simply repeat the argument of section 2.4, inserting a factor of σ^{s-2} into the sum rule integral to project onto the spin-s contribution: $\oint d\sigma(1-G) \to \oint d\sigma \sigma^{s-2}(1-G)$.[13] The other steps are identical, leading to

$$-i\, c_{\psi\psi X}\langle\overline{O(y=\delta)}\,\mathcal{E}_s\, O(y=\delta)\rangle = \frac{N_\delta}{\pi\lambda_X \eta^{\tau_s/2}} \lim_{R\to 0}\lim_{\eta\to 0} \mathrm{Re}\int_{-R}^{R} d\sigma\ \sigma^{s-2}(1-G(\sigma)) \tag{2.65}$$

for any $s \geq 2$ where $\lambda_X = \frac{2^{\Delta_X}\Gamma\left(\frac{\Delta_X+s+1}{2}\right)}{\sqrt{\pi}c_X\Gamma\left(\frac{\Delta_X+s}{2}\right)}$. When s is an even integer, Rindler positivity ensures that the right hand side of the above sum rule is non-negative. Finally by acting with a rotation R that rotates by $\frac{\pi}{2}$ in the Euclidean $y\tau$-plane, we can generalize (2.11) for arbitrary spinning operators:

$$\langle\overline{O(y=\delta)}\,\mathcal{E}_s\, O(y=\delta)\rangle = i^{s+1}\langle (R\cdot O)^\dagger(t=i\delta)\mathcal{E}_s(R\cdot O)(t=-i\delta)\rangle\ . \tag{2.66}$$

[13] Here we have followed [93] to project onto a given spin. This method assumes that lower spin operators have integer dimensions, to avoid additional non-analytic contributions to the OPE which are subleading in σ but leading in η, so can spoil the projection. However the method can be generalized by subtracting these terms as well [118].

This is derived in appendix A.1. Therefore, there is a constraint on the lowest dimensional operator at each even spin:

$$(-1)^{\frac{s}{2}} c_{\psi\psi X} \mathcal{E}_s \geq 0 \ . \tag{2.67}$$

Note that by taking $X \to -X$ it is always possible to choose $(-1)^{\frac{s}{2}} c_{\psi\psi X} > 0$, and in that case we have a positivity condition similar to the ANEC. However, once this choice has been made for some coupling $\langle \psi\psi X \rangle$ we do not have the freedom to flip the sign for a different probe, $\langle \psi'\psi' X \rangle$. This means that, like the stress tensor, the lowest-dimension operator of each spin must couple with the same sign to all possible probes.

In fact these conclusions apply to the tower of operators appearing in any given $\psi\psi$ OPE. In theories with global symmetries, different probes may lead to different infinite families of constraints.

2.6.3 Comparison to other constraints and spin-1-1-4 example

In many cases, this sum rule implies the same sign constraints on CFT 3-point couplings that have already been deduced by other methods:

- For $s = 2$, the same results can be obtained from the ANEC using conformal collider methods [56]. Therefore these constraints follow from monotonicity of relative entropy [57].
- For $s > 2$ with transverse polarizations $\varepsilon \cdot n = 0$, where n is the null direction separating the wavepacket insertion from the insertion of $\mathcal{E}$, the results

agree with deep inelastic scattering [116]. In examples where the results are available, these also agree with the lightcone bootstrap [92, 93]. If O is a conserved current, then we can always choose a gauge where the polarizations are transverse.

For $s = 2$ and $\varepsilon \cdot n \neq 0$ — assuming O is not a conserved current — it was shown in [116] that the ANEC is stronger than deep inelastic scattering and the lightcone bootstrap. Therefore, analogously at higher spin, we expect the condition $\mathcal{E}_s \geq 0$ to produce new constraints, stronger than any of these other methods, when $s > 2$ and O is not conserved.

The simplest such case is $s = 4$ with O taken to be a spin-1, nonconserved operator J of dimension $\Delta_J > d - 1$. We will work out this example in detail and confirm that the sign constraints are indeed new.

The most general 3-point function $\langle JXJ \rangle$ consistent with conformal symmetry is written in appendix A.2, following [117]. It has four free numerical constants, $\alpha_{1,2,3,4}$. To derive the constraints, we apply the Hofman-Maldacena analysis to this 3-point function. In practice, this amounts to computing the integral (2.55), with $O \to J$ and $T_{uu} \to X_{uuuu}$. Requiring this to be positive gives a constraint of the form

$$\varepsilon^\dagger \mathbf{A} \varepsilon \geq 0 \ , \tag{2.68}$$

where $\varepsilon = (\varepsilon^+, \varepsilon^-, \vec{\varepsilon}^\perp)$ and $\mathbf{A}$ is a block diagonal matrix which depends on Δ_X, Δ_J and the α_i. The explicit formula can be found in (A.9). It follows that $\mathbf{A}$ must be a positive semi-definite matrix. Requiring the eigenvalues to be non-negative gives quadratic inequalities on the α_i; the explicit form is unilluminating, so we will not write it explicitly, but it is easily found from (A.9).

Now let us compare to deep inelastic scattering [116]. Repeating their calculation for the present example, we find that the DIS constraints are

$$c_{\psi\psi X}(2\alpha_4 - \alpha_1) \geq 0 \tag{2.69}$$
$$c_{\psi\psi X}(\alpha_1 + (2 + 2\Delta_J - \Delta_X)\alpha_4) \geq 0 \ .$$

The constraints (2.69) are identical to the constraint (2.68) only if we set $\varepsilon^- = 0$. The constraints from the $\varepsilon^- \neq 0$ polarizations in (2.68) are stronger, so these are new — they do not follow from any of the known methods based on conformal collider bounds, the ANEC, relative entropy, DIS, or the lightcone bootstrap. The special role played by ε^- polarizations is analogous to the situation for the integrated null energy as described in [116].

Acknowledgments We are grateful to Nima Afkhami-Jeddi, John Cardy, Ven Chandrasekaran, Netta Engelhardt, Eanna Flanagan, Diego Hofman, Sachin Jain, Juan Maldacena, Samuel McCandlish, Eric Perlmutter, David Poland, Andy Strominger, John Stout, and Aron Wall for useful discussions. The work of TH and AT is supported by DOE grant DE-SC0014123, and the work of SK is supported by NSF grant PHY-1316222. We also thank the Galileo Galilei Institute for Theoretical Physics and the organizers of the workshop Conformal Field Theories and Renormalization Group Flows in Dimensions $d > 2$, as well as the Perimeter Institute for Theoretical Physics and the organizers of the It from Qubit workshop, which provided additional travel support and where some of this work was done.

CHAPTER 3

A NO-GO THEOREM FOR MASSIVE HIGHER SPIN PARTICLES

Abstract[1]

According to common lore, massive elementary higher spin particles lead to inconsistencies when coupled to gravity. However, this scenario was not completely ruled out by previous arguments. In this paper, we show that in a theory where the low energy dynamics of the gravitons are governed by the Einstein-Hilbert action, any finite number of massive elementary particles with spin more than two cannot interact with gravitons, even classically, in a way that preserves causality. This is achieved in flat spacetime by studying eikonal scattering of higher spin particles in more than three spacetime dimensions. Our argument is insensitive to the physics above the effective cut-off scale and closes certain loopholes in previous arguments. Furthermore, it applies to higher spin particles even if they do not contribute to tree-level graviton scattering as a consequence of being charged under a global symmetry such as $\mathbb{Z}_2$. We derive analogous bounds in anti-de Sitter spacetime from analyticity properties of correlators of the dual CFT in the Regge limit. We also argue that an infinite tower of fine-tuned higher spin particles can still be consistent with causality. However, they necessarily affect the dynamics of gravitons at an energy scale comparable to the mass of the lightest higher spin particle. Finally, we apply the bound in de Sitter to impose restrictions on the structure of three-point functions in the squeezed limit of the scalar curvature perturbation produced during inflation.

[1]This chapter is based on the paper [119].

3.1 Introduction

Weinberg in one of his seminal papers [120] showed that general properties of the S-matrix allow for the presence of the graviton. Not only that, the soft-theorem dictates that at low energies gravitons must interact universally with all particles – which is the manifestation of the equivalence principle in QFT. This remarkable fact has many far-reaching consequences for theories with higher spin particles.

Even in the early days of quantum field theory (QFT), it was known that there are restrictions on particles with spin $J > 2$ in flat spacetime. For example, Lorentz invariance of the S-matrix requires that massless particles interacting with gravity in flat spacetime cannot have spin more than two [120–122]. Moreover, folklore has it that any finite number of massive elementary higher spin particles, however fine-tuned, cannot interact with gravity in a consistent way. There is ample evidence suggestive of a strict bound on massive higher spin particles at least in flat spacetime in dimensions $D \geq 4$ from tree-level unitarity and asymptotic causality [46, 123–127],[2] however, to our knowledge there is no concrete argument which completely rules out a finite number of massive particles with spin $J > 2$.

Most notably, it was argued in [46] that in a theory with finite number of massive particles with spin $J > 2$, unless each higher spin particle is charged under a global symmetry such as $\mathbb{Z}_2$, they will contribute to eikonal scattering of particles, even with low spin ($J \leq 2$), in a way that violates asymptotic causality in flat spacetime. The same statement is true even in anti-de Sitter (AdS) spacetime where the global symmetries of higher spin particles are required by the chaos growth bound of the dual CFT [27]. In addition, there is no known string compactification which

[2] See comments in section 3.2.6 for comparison between arguments in the literature and the argument presented in this paper.

leads to particles with spin $J > 2$ and masses $M \ll M_s$ in flat spacetime, where M_s is the string scale. Of course, it is well known that higher spin particles do exist in AdS, but they always come in an infinite tower and these theories become strongly interacting at low energies [128, 129]. All of these observations indicate that there are universal bounds on theories with higher spin massive particles. In this paper, we will prove such a bound from causality. We will show that any finite number of massive elementary particles with spin $J > 2$, however fine tuned, cannot interact with gravitons in flat or AdS spacetimes (in $D \geq 4$ dimensions) in a way that is consistent with the QFT equivalence principle and preserves causality. In particular, we will demonstrate that the three-point interaction J-J-graviton must vanish for $J > 2$. However, this is one interaction that no particle can avoid due to the equivalence principle, implying that elementary particles with spin $J > 2$ cannot exist.

For massless higher spin particles, the inconsistencies are even more apparent. The tension between Lorentz invariance of the S-matrix and the existence of massless particles with spin $J > 2$ was already visible in [120]. Subsequently, the same tension was shown to exist for massless fermions with spin $J > 3/2$ [130, 131]. A concrete manifestation of this tension is an elegant theorem due to Weinberg and Witten which states that any massless particle with spin $J > 1$ cannot possess a Lorentz covariant and gauge invariant energy-momentum tensor [121].[3] Of course, this theorem does not prohibit the existence of gravitons, rather it implies that the graviton must be fundamental. More recently, a generalization of the Weinberg-Witten theorem has been presented by Porrati which states that massless particles with spin $J > 2$ cannot be minimally coupled to the graviton in flat spacetime [122]. Both of these theorems are completely consistent

[3] See [132] for a nice review.

with various other observations made about interactions of massless higher spin particles in flat spacetime (see [133–138] and references therein). Furthermore, the generalized Weinberg-Witten theorem and the QFT equivalence principle are sufficient to completely rule out massless particles with spin $J > 2$ in flat spacetime [121, 122]. The basic argument is rather simple. The Weinberg-Witten theorem and its generalization by Porrati only allow non-minimal coupling between massless particles with spin $J > 2$ and the graviton. Whereas, it is well known that particles with low spin can couple minimally with the graviton. Therefore, the QFT equivalence principle requires that massless higher spin particles, if they exist, must couple minimally with the graviton at low energies – which directly contradicts the Weinberg-Witten/Porrati theorem.

Any well behaved Lorentzian QFT must also be unitary and causal.[4] Lorentz invariance alone was sufficient to rule out massless higher spin particles in flat spacetime. Whereas, massive elementary particles with spin $J > 2$ do not lead to any apparent contradiction with Lorentz invariance in flat spacetime. However, any such particle if present, must interact with gravitons. The argument presented in [46] implies that finite number of higher spin particles cannot be exchanged in any tree-level scattering. However, this restriction is not sufficient to rule out massive higher spin particles, rather it implies that each massive higher spin particle must be charged under $\mathbb{Z}_2$ or some other global symmetry. On the other hand, the equivalence principle requires the coupling between a single graviton and two spin-J particles to be non-vanishing. By considering an eikonal scattering experiment between scalars and elementary higher spin particles with spin J and mass m in the regime $|s| \gg |t| \gg m$, where s and t are the Mandelstam variables, we will show that any such coupling between the higher spin particle and the graviton

[4] Unitarity and causality, as demonstrated in [114], are not completely unrelated in relativistic QFT.

in flat spacetime leads to violation of asymptotic causality. This is accomplished by extending the argument of [46] to the scattering of higher spin particles which requires the phase shift to be non-negative for all choices of polarization of external particles.

A similar high energy scattering experiment can be designed in AdS to rule out elementary massive higher spin particles. However, we will take a holographic route which has several advantages. We consider a class of large-N CFTs in $d \geq 3$ dimensions with a sparse spectrum. The sparse spectrum condition, to be more precise, implies that the lightest single trace primary operator with spin $J > 2$ has dimension $\Delta_{\text{gap}} \gg 1$. It was first conjectured in [42] that this class of CFTs admit a universal holographic dual description with a low energy description in terms of Einstein gravity coupled to matter fields. The conjecture was based on the observation that there is a one-to-one correspondence between scalar effective field theories in AdS and perturbative solutions of CFT crossing equations in the $1/N$ expansion. The scalar version of this conjecture was further substantiated in [41, 43, 45, 48, 107, 139–151] by using the conformal bootstrap. More recently, the conjecture has been completely proven at the linearized level even for spinning operators including the stress tensor [152–157]. In the second half of the paper, we will exploit this connection to constrain massive higher spin particles in AdS by studying large-N CFTs with a sparse spectrum. To this end, we introduced a new non-local operator, capturing the contributions to the Regge limit of the OPE of local operators. This operator is expressed as an integral of a local operator over a ball times a null-ray. It is obtained by generalizing the Regge OPE introduced in [157] to non-integer spins, resulting in an operator that is more naturally suited for parametrizing the contribution of Regge trajectories which require analytic continuation in both spin and scaling dimension.

In the holographic CFT side we will ask the dual question: is it possible to add an extra higher spin single trace primary operator with $J > 2$ and scaling dimension $\Delta \ll \Delta_{\text{gap}}$ and still get a consistent CFT? A version of this question has already been answered by a theorem in CFT that rules out any finite number of higher spin conserved currents [58, 108, 158, 159]– which is the analog of the Weinberg-Witten theorem in AdS. However, ruling out massive higher spin particles in AdS requires a generalization of this theorem for non-conserved single trace primary operators of holographic CFTs. The chaos (growth) bound of Maldacena, Shenker, and Stanford [27] partially achieves this by not allowing any finite number of higher spin single trace primary operators to contribute as exchange operators in CFT four-point functions in the Regge limit. However, this restriction does not rule out the existence of such operators rather it prohibits these higher spin operators to appear in the operator product expansion (OPE) of certain operators. On the other hand, causality (chaos sign bound) imposes stronger constraints on non-conserved single trace primary operators. In particular, by using the holographic null energy condition (HNEC) [155, 157] applied to correlators with external higher spin operators, we will show that massive higher spin fields in AdS (in $D \geq 4$ dimensions) lead to causality violation in the dual CFT. This implies that any finite number of massive elementary particles with spin $J > 2$ in AdS cannot be embedded in a well behaved UV theory in which the dynamics of gravitons at low energies is described by the Einstein-Hilbert action.

One advantage of the holographic approach is that it also provides a possible solution to the causality problem. From the dual CFT side, we will argue that in a theory where the dynamics of gravitons is described by the Einstein-Hilbert action at energy scales $E \ll \Lambda$ (Λ can be the string scale M_s), a single elementary

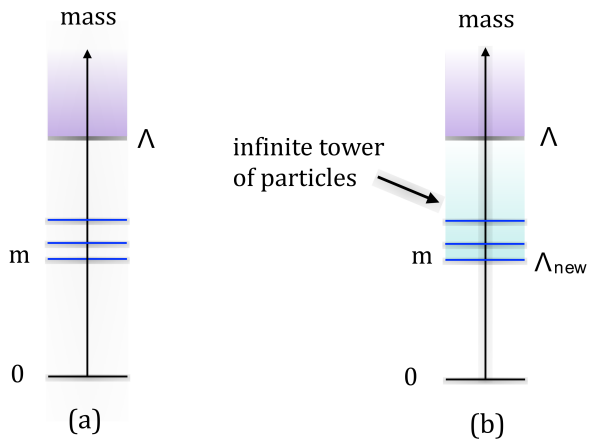

Figure 3.1: Spectrum of elementary particles with spin $J > 2$ in a theory where the dynamics of gravitons is described by the Einstein-Hilbert action at energy scales $E \ll \Lambda$. The cut-off scale Λ can be the string scale and hence there can be an infinite tower of higher spin particles above Λ. Figure (a) represents a scenario that also contains a finite number of higher spin particles below the cut-off and hence violates causality. Causality can only be restored if these particles are accompanied by an infinite tower of higher spin particles with comparable masses which is shown in figure (b). This necessarily brings down the cut-off scale to $\Lambda_{\text{new}} = m$, where m is the mass of the lightest higher spin particle.

particle with spin $J > 2$ and mass $m \ll \Lambda$ violates causality unless the particle is accompanied by an infinite tower of (finely tuned) higher spin elementary particles with mass $\sim m$. Furthermore, causality also requires that these new higher spin particles (or at least an infinite subset of them) must be able to decay into two gravitons and hence modify the dynamics of gravitons at energy scales $E \sim m$. So, one can have a causal theory without altering the low energy behavior of gravity only if all the higher spin particles are heavier than the cut-off scale Λ.

Causality of CFT four-point functions in the lightcone limit also places nontrivial constraints on higher spin primary operators. In particular, it generalizes the Maldacena-Zhiboedov theorem of $d = 3$ [108] to higher dimensions by ruling out

a finite number of higher spin conserved currents [58]. The advantage of the lightcone limit is that the constraints are valid for all CFTs – both holographic and non-holographic. However, the argument of [58] is not applicable when higher spin conserved currents do not contribute to generic CFT four-point functions as exchange operators. We will present an argument in the lightcone limit that closes this loophole by ruling out higher spin conserved currents even when none of the operators are charged under it.[5] For holographic CFTs, this completely rules out a finite number of massless higher spin particles in AdS in $D \geq 4$ dimensions.

The bound on higher spin particles has a natural application in inflation. If higher spin particles are present during inflation, they produce distinct signatures on the late time three-point function of the scalar curvature perturbation in the squeezed limit [160]. The bounds on higher spin particles in flat space and in AdS were obtained by studying local high energy scattering which is insensitive to the spacetime curvature. This strongly suggests that the same bound should hold even in de Sitter space.[6] Our bound, when applied in de Sitter, immediately implies that contributions of higher spins to the three-point function of the scalar curvature perturbation in the squeezed limit must be Boltzmann suppressed $\sim e^{-2\pi\Lambda/H}$, where H is the Hubble scale. Therefore, if the higher spin contributions are detected in future experiments, then the scale of new physics must be $\Lambda \sim H$. This necessarily requires the presence of not one but an infinite tower of higher spin particles with spins $J > 2$ and masses comparable to the Hubble scale. Any such detection can be interpreted as evidence in favor of string theory with the string scale comparable to the Hubble scale.

[5] We should note that we have not ruled out an unlikely scenario in which the OPE coefficients conspire in a non-trivial way to cancel the causality violating contributions. Three-point functions of conserved currents are heavily constrained by conformal invariance and hence this scenario is rather improbable.

[6] This argument parallels the argument made by Cordova, Maldacena, and Turiaci in [161]. The same point of view was also adopted in our previous paper [157].

The rest of the paper is organized as follows. In section 3.2, we present an S-matrix based argument to show that massive elementary particles with spin $J > 2$ cannot interact with gravitons in a way that preserves asymptotic causality. We derive the same bounds in AdS from analyticity properties of correlators of the dual CFT in section 3.3. In section 3.4, we argue that the only way one can restore causality is by adding an infinite tower of massive higher spin particles. In addition, we also discuss why stringy states in classical string theory are consistent with causality. Finally, in section 3.5, we apply our bound in de Sitter to constrain the squeezed limit three-point functions of scalar curvature perturbations produced during inflation.

3.2 Higher Spin Fields in Flat Spacetime

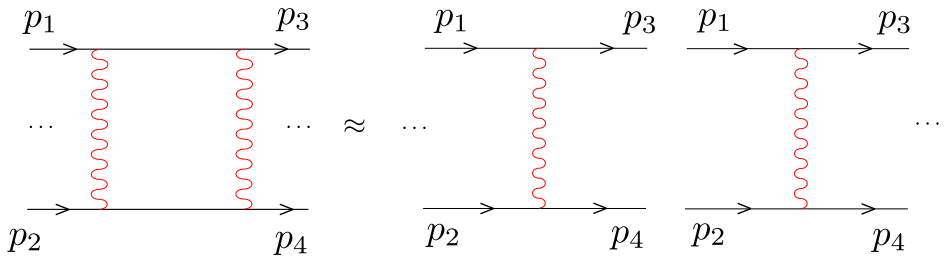

Figure 3.2: Tree-level exchange diagrams are the building blocks of ladder diagrams.

In this section, we explicitly show that interactions of higher spin particles with gravity lead to causality violation. Eikonal scattering has been used in the literature [46, 162–166] to impose constraints on interactions of particles with spin. When the center of mass energy is large and transfer momentum is small, the scattering amplitude is captured by the eikonal approximation. Focusing on a specific exchange particle for now, the scattering amplitude is given by a sum

of ladder diagrams. These diagrams can be resumed (see figure 3.2) and as a result introduce a phase shift in the scattering amplitude [167].[7] This phase shift produces a Shapiro time delay [168] that particles experience [46]. Asymptotic causality in flat spacetime requires the time delay and hence the phase shift to be non-negative [46,94]. Moreover, positivity of the phase shift imposes restrictions on the tree-level exchange diagrams –which are the building blocks of ladder diagrams– constraining three-point couplings between particles. This method has been utilized to constrain three-point interactions between gravitons, massive spin-2 particles, and massless higher spin particles [46,162,163]. Here we apply the eikonal scattering method to external massive and massless elementary particles with spin $J > 2$.

We will briefly review eikonal scattering in order to explicitly relate the phase shift to the three-point interactions between elementary particles. We will take two of the external particles to be massive or massless higher spin particles ($J > 2$) and the other two particles to be scalars. The setup is shown in figure 3.3 where particles 1 and 3 are the higher spin particles, whereas particles 2 and 4 are scalars. We will then use on-shell methods to write down the general three-point interaction between higher spin elementary particles and gravitons [117]. This allows us to derive the most general form of the amplitude in the eikonal limit. Positivity of the phase shift for all choices of polarization tensors of external particles, constrains the coefficients of three-point vertices. In particular, for both massive and massless particles with spin $J > 2$ in space-time dimensions $D \geq 4$, we find that the three-point interaction J-J-graviton must be zero. However, this is one interaction that no particle can avoid due to the equivalence principle, implying that elementary particles with spin $J > 2$ cannot exist.

[7] We will comment more about the resummation later in the section.

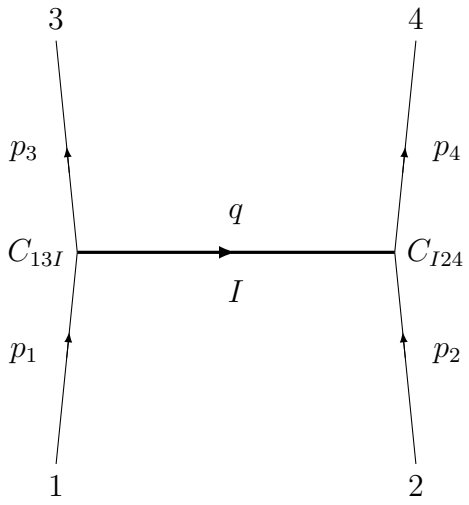

Figure 3.3: Eikonal scattering of particles. In this highly boosted kinematics, particles are moving almost in the null directions such that the center of mass energy is large.

3.2.1 Eikonal Scattering

Let us consider $2 \to 2$ scattering of particles in space-time dimensions $D \geq 4$ as shown in figure 3.3. Coordinates are written in $\mathbb{R}^{1,D-1}$ with the metric

$$ds^2 = -dudv + d\vec{x}_\perp^2. \tag{3.1}$$

Denoting the momentum of particles by p_i, with i labeling particles 1 through 4, the Mandelstam variables are given by

$$s = -(p_1 + p_2)^2, \qquad t = -(p_1 - p_3)^2 = -q^2, \tag{3.2}$$

where q is the momentum of the particle exchanged which in the eikonal limit has the property $q^2 = \vec{q}^2$, where $\vec{q}$ has components in directions transverse to the propagation of the external particles.[8] The tree level amplitude consists of the

[8]See section 3.2.3 for the details of the kinematics.

products of three-point functions[9]

$$M_{\text{tree}}(s,\vec{q}) = \sum_I \frac{C_{13I}(\vec{q})C_{I24}(\vec{q})}{\vec{q}^{\,2}+m_I^2} \ , \tag{3.3}$$

where the sum is over all of the states of the exchanged particles with mass m_I. In the above expression, C_{13I} and C_{24I} are on-shell three-point amplitudes which are generally functions of the transferred momentum $\vec{q}$, as well as the polarization tensors and the center of mass variables.

In highly boosted kinematics, particles are moving almost in the null directions u and v with momenta P^u and P^v respectively. The center of mass energy s is large with respect to other dimensionful quantities such as the particle masses. In particular, we have $s \gg |t| = \vec{q}^{\,2}$. The total scattering amplitude is given by the sum of all ladder diagrams in t-channel which exponentiates when it is expressed in terms of the impact parameter $\vec{b}$ which has components only along the transverse plane,

$$iM_{\text{eik}}(s,-\vec{q}^{\,2}) = 2s\int d^{D-2}\vec{b}e^{-i\vec{q}\cdot\vec{b}}\left(e^{i\delta(s,\vec{b})}-1\right) \ , \tag{3.4}$$

where,

$$\delta(s,\vec{b}) = \frac{1}{2s}\int \frac{d^{D-2}\vec{q}}{(2\pi)^{D-2}}\, e^{i\vec{q}\cdot\vec{b}} M_{\text{tree}}(s,\vec{q}\,) \ . \tag{3.5}$$

Before we proceed, let us comment more on the exponentiation since it plays a central role in the positivity argument. We can interpret the phase shift as the Shapiro time-delay only when it exponentiates in the eikonal limit. However, it is known that the eikonal exponentiation fails for the exchange of particles with spin $J < 2$ [169–171]. It is also not obvious that the tree level amplitude must exponentiate in the eikonal limit for the exchange of particles with spin $J \geq 2$. A physical argument was presented in [46] which suggests that for higher spin

[9]For a detail discussion about the iϵ see [46].

exchanges it is possible to get a final amplitude that is exponential of the tree level exchange diagram. First, let us think of particle 2 as the source of a shockwave and particle 1 to be a probe particle traveling in that background. At tree-level, the amplitude is given by $1 + i\delta$, where we ensure that $\delta \ll 1$ by staying in a weakly coupled regime. Let us then send N such shockwaves so that we can treat them as individual shocks and hence the final amplitude, in the limit $\delta \to 0, N \to \infty$ with $N\delta$ =fixed, is approximately given by $(1 + i\delta)^N \approx e^{iN\delta}$. This approximation is valid only if we can view N scattering processes as independent events. Moreover, we want to be in the weakly coupled regime. Both of these conditions can only be satisfied if δ grows with s – which is true for the exchange of particles with spin $J \geq 2$ [46]. Therefore, for higher-spin exchanges, we can interpret δ (or rather N times δ) as the Shapiro time delay of particle 1.

There is one more caveat. The exponentiation also depends on the assumption that δ is the same for each of the N-processes – in other words, the polarization of particle 3 is the complex conjugate of that of particle 1. In general, particle 3 can have any polarization, however, we can fix the polarization of particle 3 by replacing particle 1 by a coherent state of particles with a fixed polarization. Since we are in the weakly coupled regime, we can make the mean occupation number large without making δ large. This allows us to fix the polarization of particle 3 to be complex conjugate of that of particle 1 because of Bose enhancement (see [46] for a detail discussion).

Let us end this discussion by noting that the N-shock interpretation of the eikonal process is also consistent with classical gravity calculations. For example, the Shapiro time delay as obtained in GR from shockwave geometries is the same as the time delay obtained from the sum of all ladder diagrams for graviton exchanges

– which indicates that these are the only important diagrams in the eikonal limit. Thus, it is reasonable to expect that the exponentiation of the tree-level diagram correctly captures the eikonal process.

Positivity:

When $\delta(s,\vec{b})$ grows with s, we can trust the eikonal exponentiation which allows us to relate the phase shift to time delay. In particular, for a particle moving in u direction with momentum $P^u > 0$, the phase shift $\delta(s,\vec{b})$ is related to the time delay of the particle by

$$\delta\left(s,\vec{b}\right) = P^u \Delta v \ . \tag{3.6}$$

Asymptotic causality in flat space requires that particles do not experience a time advance even when they are interacting [94]. Therefore, $\Delta v \geq 0$, implying that the phase shift must be non-negative as well.

So far our discussion is very general and it is applicable even when multiple exchanges contribute to the tree level scattering amplitude. From now on, let us restrict to the special case of massless exchanges.[10] Using the tree-level amplitude (3.3), we can write

$$\begin{aligned}\delta(s,\vec{b}) &= \frac{1}{2s}\sum_I \int \frac{d^{D-2}\vec{q}}{(2\pi)^{D-2}}\, e^{i\vec{q}\cdot\vec{b}} \frac{C_{13I}(\vec{q})C_{I24}(\vec{q})}{q^2} \\ &= \frac{\Gamma(\frac{D-4}{2})}{4\pi^{\frac{D-2}{2}}}\sum_I \frac{C_{I24}(-i\vec{\partial}_b)C_{13I}(-i\vec{\partial}_b)}{2s}\frac{1}{|\vec{b}|^{D-4}}\end{aligned} \tag{3.7}$$

which must be non-negative. Note that $\vec{\partial}_b^2$ annihilates $1/|\vec{b}|^{D-4}$, which is why we can consider the exchange particle to be on-shell.[11]

[10] For non-zero m_I, the $\vec{q}$ integral yields $(2\pi)^{\frac{2-D}{2}}(\frac{m_I}{b})^{\frac{D-4}{2}}K_{\frac{D-4}{2}}(m_I b)$, where K is the Bessel-K function.

[11] The same can be seen from the choice of the integration contour, as described in more detail

3.2.2 Higher Spin-graviton Couplings

There are Lagrangian formulations of massive higher spin fields in flat spacetime, as well as in AdS [172–174]. However, in this section, we present a more general approach that does not require the knowledge of the Lagrangian. We write down all possible local three-point interactions between two higher spin elementary particles with spin J and a graviton. This three-point interaction is of importance for several reasons. First, this is one interaction that no particle can avoid because of the equivalence principle. Therefore the vanishing of this three-point interaction is sufficient to rule out existence of such higher spin particles. Moreover, as we will discuss later, this three-point interaction is sufficient to compute the full eikonal scattering amplitude between a scalar and a higher spin particle.

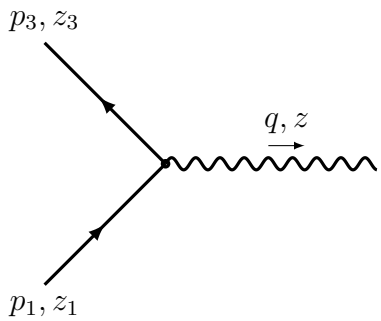

Figure 3.4: The three-point interaction between two elementary particles with spin J and a graviton.

We start with the massive case and consider the massless case later on. Here we use the same method used in [117, 162] for deriving the most general $J - J - 2$ interaction. The momenta of higher spin particles are p_1, p_3 and the graviton has

in [46]. By rotating the contour of integration in $\vec{q}$, we cross the pole at $\vec{q}^{\,2} = 0$ and hence it is sufficient to consider only three-point functions on-shell.

momentum q (see figure 3.4). The conservation and the on-shell conditions imply

$$p_1 = p_3 + q \ , \qquad p_1^2 = p_3^2 = -m^2 \ , \qquad q^2 = 0 \ , \tag{3.8}$$

where m is the mass of the higher spin particle. It is sufficient for us to consider polarization tensors which are made out of null and transverse polarization vectors z_1, z_3, z satisfying

$$z_1^2 = z_3^2 = z^2 = 0, \qquad z_1 \cdot p_1 = z_3 \cdot p_3 = z \cdot q = 0 \ . \tag{3.9}$$

Transverse symmetric polarization tensors can be constructed from null and transverse polarization vectors by substituting $z_i^{\mu_1} z_i^{\mu_2} \cdots z_i^{\mu_s} \to \mathcal{E}_i^{\mu_1 \mu_2 \cdots \mu_s}$ – traces. In addition, we need to impose gauge invariance for the graviton. This means that each on-shell vertex should be invariant under $z \to z + \alpha q$, where α is an arbitrary number. Using (3.8) and (3.9), we can write down all vertices in terms of only five independent building blocks[12]

$$\begin{aligned} &z_1 \cdot z_3 \ , \qquad z_1 \cdot q \ , \qquad z_3 \cdot q \ , \\ &z \cdot p_3 \ , \qquad (z \cdot z_3)(z_1 \cdot q) - (z \cdot z_1)(z_3 \cdot q) \ . \end{aligned} \tag{3.10}$$

In order to list all possible vertices for the interaction $J - J - 2$, we must symmetrize the on-shell amplitudes under $1 \leftrightarrow 3$. We can then construct the most general form of on-shell three-point amplitude from these building blocks. In particular, for $J \geq 2$, we can write three distinct sets of vertices. The first set contains $J + 1$ independent structures all of which are proportional to $(z \cdot p_3)^2$:

$$\begin{aligned} \mathcal{A}_1 &= (z \cdot p_3)^2 (z_1 \cdot z_3)^J \ , \\ \mathcal{A}_2 &= (z \cdot p_3)^2 (z_1 \cdot z_3)^{J-1} (z_3 \cdot q)(z_1 \cdot q) \ , \\ &\vdots \\ \mathcal{A}_{J+1} &= (z \cdot p_3)^2 (z_3 \cdot q)^J (z_1 \cdot q)^J \ . \end{aligned} \tag{3.11}$$

[12] In $D = 4$, the collection of momentum and polarization vectors $p_1, p_2, z_j \ i, j = 1, 2, 3$ are not linearly independent and there are additional relations between the building blocks.

The second set contains J-independent structures which are proportional to $(z \cdot p_3)$:

$$\begin{aligned}
&\mathcal{A}_{J+2} = (z \cdot p_3)((z \cdot z_3)(z_1 \cdot q) - (z \cdot z_1)(z_3 \cdot q))(z_1 \cdot z_3)^{J-1}, \\
&\mathcal{A}_{J+3} = (z \cdot p_3)((z \cdot z_3)(z_1 \cdot q) - (z \cdot z_1)(z_3 \cdot q))(z_1 \cdot z_3)^{J-2}(z_3 \cdot q)(z_1 \cdot q), \\
&\vdots \\
&\mathcal{A}_{2J+1} = (z \cdot p_3)((z \cdot z_3)(z_1 \cdot q) - (z \cdot z_1)(z_3 \cdot q))(z_3 \cdot q)^{J-1}(z_1 \cdot q)^{J-1} \ . \qquad (3.12)
\end{aligned}$$

Finally the third set consists of $J-1$ independent structures which do not contain $(z \cdot p_3)$:

$$\begin{aligned}
&\mathcal{A}_{2J+2} = ((z \cdot z_3)(z_1 \cdot q) - (z \cdot z_1)(z_3 \cdot q))^2(z_3 \cdot z_1)^{J-2}, \\
&\mathcal{A}_{2J+3} = ((z \cdot z_3)(z_1 \cdot q) - (z \cdot z_1)(z_3 \cdot q))^2(z_3 \cdot z_1)^{J-3}(z_3 \cdot q)(z_1 \cdot q), \\
&\vdots \\
&\mathcal{A}_{3J} = ((z \cdot z_3)(z_1 \cdot q) - (z \cdot z_1)(z_3 \cdot q))^2(z_3 \cdot q)^{J-2}(z_1 \cdot q)^{J-2} \ . \qquad (3.13)
\end{aligned}$$

In total there are $3J$ independent structures that contribute to the on-shell three-point amplitude of two higher spin particles with mass m and spin J and a single graviton. Therefore the most general form of the three-point amplitude for $J \geq 1$, is given by[13]

$$C_{JJ2} = \sqrt{32\pi G_N} \sum_{n=1}^{3J} a_n \mathcal{A}_n. \qquad (3.14)$$

Note that $3J$ is also the number of independent structures in the three point functions in the CFT side after imposing permutation symmetry between operators $1, 3$ and taking conservation of stress-tensor into account.

[13]Here the propagators of the gravitons are canonically normalized to 1. Therefore we need explicit G_N dependence in (3.14) since it couples to the graviton.

3.2.3 Eikonal Kinematics

We now study the eikonal scattering of higher spin particles: $1,2 \to 3,4$, where, 1 and 3 label the massive higher spin particles with mass m and spin J and 2, 4 label scalars of mass m_s (see figure 3.3). Let us specify the details of the momentum and polarization tensors. In the eikonal limit, the momentum of particles are parametrized as follows[14]

$$\begin{aligned} p_1^\mu &= \left(P^u, \frac{1}{P^u}\left(\frac{\vec{q}^{\,2}}{4}+m_1^2\right), \frac{\vec{q}}{2}\right) \ , \qquad p_3^\mu = \left(\bar{P}^u, \frac{1}{\bar{P}^u}\left(\frac{\vec{q}^{\,2}}{4}+m_3^2\right), -\frac{\vec{q}}{2}\right) \ , \\ p_2^\mu &= \left(\frac{1}{P^v}\left(\frac{\vec{q}^{\,2}}{4}+m_2^2\right), P^v, -\frac{\vec{q}}{2}\right) \ , \qquad p_4^\mu = \left(\frac{1}{\bar{P}^v}\left(\frac{\vec{q}^{\,2}}{4}+m_4^2\right), \bar{P}^v, \frac{\vec{q}}{2}\right) \ , \end{aligned} \tag{3.15}$$

where, $P^u, \bar{P}^u, P^v, \bar{P}^v > 0$ and $p_1^\mu - p_3^\mu \equiv q$ is the transferred momentum of the exchange particle which is spacelike. The eikonal limit is defined as $P^u, P^v \gg |q|, m_i$. In this limit $P^u \approx \bar{P}^u, P^v \approx \bar{P}^v$ and the Mandelstam variable s is given by $s = -(p_1+p_2)^2 \approx P^u P^v$. Moreover, for our setup we have $m_1 = m_3 = m$ and $m_2 = m_4 = m_s$.

Massless particles have only transverse polarizations but massive higher spin particles can have both transverse and longitudinal polarizations. General polarization tensors can be constructed using the following polarization vectors

$$\begin{aligned} \epsilon^\mu_{T,\lambda}(p_1) &= \left(0, \frac{\vec{q}\cdot\vec{e}^{\,(1)}_\lambda}{P^u}, \vec{e}^{\,(1)}_\lambda\right) \ , \qquad \epsilon^\mu_L(p_1) = \left(\frac{P^u}{m}, \frac{1}{mP^u}\left(\frac{\vec{q}^{\,2}}{4}-m^2\right), \frac{\vec{q}}{2m}\right) \ , \\ \epsilon^\mu_{T,\lambda}(p_3) &= \left(0, -\frac{\vec{q}\cdot\vec{e}^{\,(3)}_\lambda}{P^u}, \vec{e}^{\,(3)}_\lambda\right) \ , \quad \epsilon^\mu_L(p_3) = \left(\frac{P^u}{m}, \frac{1}{mP^u}\left(\frac{\vec{q}^{\,2}}{4}-m^2\right), -\frac{\vec{q}}{2m}\right) \ , \end{aligned} \tag{3.16}$$

where vectors $e^\mu_\lambda \equiv (0,0,\vec{e}_\lambda)$ are complete orthonormal basis in the transverse direction $\vec{x}_\perp$. The longitudinal vectors do not satisfy (3.9) because $\varepsilon_L \cdot \varepsilon_L \neq 0$.

[14] Our convention is $p^\mu = (p^u, p^v, \vec{p})$.

However, they still form a basis for constructing symmetric traceless polarization tensors which are orthogonal to the corresponding momentum.

The polarization tensors constructed from (3.16) are further distinguished by their spin under an $SO(D-2)$ rotation group which preserves the longitudinal polarization ε_L for each particle. We denote this basis of polarization tensors as $\mathcal{E}_j^{\mu_1\mu_2\cdots\mu_J}(p_i)$ where j labels the spin under $SO(D-2)$. These tensors are basically organized by the number of transverse polarization vectors they contain. The most general polarization tensor for a particle with spin J can now be decomposed as

$$\boldsymbol{\mathcal{E}}^{\mu_1\cdots\mu_J}(p) = \sum_{j=0}^{J} r_j \mathcal{E}_j^{\mu_1\cdots\mu_J}(p), \tag{3.17}$$

where r_j's are arbitrary complex numbers. However, in order to show that the higher spin particles cannot interact with gravity in a consistent way, we need only to consider a subspace spanned by

$$\mathcal{E}_J^{\mu_1\mu_2\cdots\mu_J} = \varepsilon_{T,\lambda_1}^{\mu_1}\varepsilon_{T,\lambda_2}^{\mu_2}\cdots\varepsilon_{T,\lambda_J}^{\mu_J}, \tag{3.18}$$

$$\mathcal{E}_{J-1}^{\mu_1\mu_2\cdots\mu_J} = \sqrt{J}\varepsilon_L^{(\mu_1}\varepsilon_{T,\lambda_2}^{\mu_2}\varepsilon_{T,\lambda_3}^{\mu_3}\cdots\varepsilon_{T,\lambda_J}^{\mu_J)}, \tag{3.19}$$

$$\mathcal{E}_{J-2}^{\mu_1\mu_2\cdots\mu_J} = \sqrt{\frac{D-1}{D-2}}\left(\varepsilon_L^{(\mu_1}\varepsilon_L^{\mu_2} - \frac{\mathcal{P}^{\mu_1\mu_2}}{D+2J-5}\right)\varepsilon_{T,\lambda_3}^{\mu_3}\varepsilon_{T,\lambda_4}^{\mu_4}\cdots\varepsilon_{T,\lambda_J}^{\mu_J)}, \quad \mathcal{P}^{\mu\nu} \equiv \eta^{\mu\nu} + \frac{p^\mu p^\nu}{m^2}, \tag{3.20}$$

where, after contractions with other tensors we perform the following substitution: $e_{\lambda_1}^{i_1}e_{\lambda_2}^{i_2}\cdots e_{\lambda_j}^{i_j} \to e^{i_1\cdots i_j}$ in which $e^{i_1\cdots i_j}$ is a transverse symmetric traceless tensor.[15] One can easily continue this construction to generate the remaining polarization tensors. One should add more longitudinal polarization vectors and subtract traces in order to make them traceless.

[15] In other words, whenever we see a combination of transverse polarization vectors: $\varepsilon_{T,\lambda_1}^{\mu_1}\varepsilon_{T,\lambda_2}^{\mu_2}\cdots\varepsilon_{T,\lambda_S}^{\mu_S}$, we will replace that by either of $\varepsilon_{T,+}^{\mu_1}\varepsilon_{T,+}^{\mu_2}\cdots\varepsilon_{T,+}^{\mu_S} \pm \varepsilon_{T,-}^{\mu_1}\varepsilon_{T,-}^{\mu_2}\cdots\varepsilon_{T,-}^{\mu_S}$, where $e_+^\mu \equiv (0,0,1,i,\vec{0})$ and $e_-^\mu \equiv (0,0,1,-i,\vec{0})$. For us, it is sufficient to restrict to these set of polarization tensors.

3.2.4 Bounds on Coefficients

We now have all the tools we need to utilize the positivity condition (3.7) in the eikonal scattering of a massive higher spin particle and a scalar. The expression (3.7) requires knowledge of the contributions of all the particles that can be exchanged. However as we explain next, in the eikonal limit the leading contribution is always due to the graviton exchange. Let us explain this by discussing all possible exchanges:

- Graviton exchange: Since, gravitons couple to all particles, the scattering amplitude in the eikonal limit will always receive contributions from graviton exchanges. In particular, in the eikonal limit, the contribution of graviton exchange to the phase shift goes as $\delta(s,b) \sim s$.
- Exchange of particles with spin $J < 2$: These exchanges are always subleading in the eikonal limit and hence can be ignored.[16]
- Exchange of higher spin particles $J > 2$: In the eikonal limit, the exchange of a particle with spin J can produce a phase shift $\delta(s,b) \sim s^{J-1}$. However, it was shown in [46] that a phase shift that grows faster than s leads to additional causality violation. Therefore if higher spin particles are present, their interactions must be tuned in such a way that they cannot be exchanged in eikonal scattering. This happens naturally when each higher spin particle is individually charged under a global symmetry such as $\mathbb{Z}_2$. We should note that it is possible to have a scenario in which an infinite tower of higher spin particles can be exchanged without violating causality. However, we will

[16] We have mentioned before that the eikonal exponentiation fails for the exchange of particles with spin $J < 2$. However, we can still ignore them because the exchange of lower spin particles cannot compete with the graviton exchange in the eikonal limit.

restrict to the case where only a finite number of higher spin particles are present. At this point, let us also note that in AdS, the exchange of a finite number of higher spin particles are ruled out by the chaos growth bound of the dual CFT.

- Exchange of massive spin-2 particles: Massive spin-2 particles can be present in nature. However, the exchange of these particles, as explained in [46], cannot fix the causality violation caused by the graviton exchange. Therefore, without any loss of generality, we can assume that the scalar particles do not interact with any massive spin-2 particle. For now this will allow us to ignore massive spin-2 exchanges. Let us note that it is not obvious that the argument of [46] about massive spin-2 exchanges necessarily holds for scattering of higher spin particles. So, at the end of this section, we will present an interference based argument to explain the reason for why even an infinite tower of massive spin-2 exchanges cannot restore causality.

In summary, in the eikonal limit, it is sufficient to consider only the graviton exchange. In fact, we can safely assume that the scalar interacts with everything, even with itself, only via gravity. Let us also note that we are studying eikonal scattering of higher spin particles with scalars only for simplicity. The calculations as well as the rest of the arguments are almost identical even if we replace the scalar by a graviton. In the graviton case, the argument of [46] about massive spin-2 exchanges holds – this implies that the presence of massive spin-2 particles will not change our final bounds.

We now use (3.7) to calculate the phase shift where C_{13I} is given by equation (3.14). For scalar-scalar-graviton there is only one vertex, written as

$$C_{I24} \equiv C_{002} = \sqrt{32\pi G}(z \cdot p_2)^2 \ . \tag{3.21}$$

Consequently, the sum in (3.7) is over the polarization of the exchanged graviton. In the eikonal limit, this sum receives a large contribution from only one specific intermediate state corresponding to the polarization tensor of the exchanged graviton appearing in C_{13I} of the form $z^v z^v$ and the polarization tensor appearing in C_{I24} of the form $z^u z^u$.[17]

As discussed earlier, if $\delta(s,\vec{b})$ grows with s, causality requires $\delta(s,\vec{b}) \geq 0$ as a condition which must be true independent of polarization tensors we choose for our external particles. In particular, in the basis $\boldsymbol{\mathcal{E}}$, $\delta(s,\vec{b})$ can be written as

$$\delta(s,\vec{b}) = \boldsymbol{\mathcal{E}}_1^\dagger \mathcal{K}(\vec{b}) \boldsymbol{\mathcal{E}}_3, \tag{3.23}$$

where $\mathcal{K}$ is a Hermitian matrix which is encoding the eikonal amplitude in terms of the structures written in (3.14).[18] Causality then requires $\mathcal{K}$ to be a positive semi-definite matrix for any $\vec{b}$. We sketch the argument for constraining three-point interactions here and leave the details to appendices B.1 and B.2.

First, let us discuss $D > 4$.[19] We start with the general expressions for on-shell three point amplitudes. The polarization tensors for both particles 1 and 3 are chosen to be in the subspace spanned by $\mathcal{E}_J, \mathcal{E}_{J-1}$ and $\mathcal{E}_{J-2}$:

$$\boldsymbol{\mathcal{E}} = r_J \mathcal{E}_J + r_{J-1}\mathcal{E}_{J-1} + r_{J-2}\mathcal{E}_{J-2} \ , \tag{3.24}$$

where, r_J, r_{J-1} and r_{J-2} are real numbers. Using eikonal scattering we organize the phase shift in the small b limit in terms of the highest negative powers of the

[17] In the eikonal limit, the sum over the polarization of the graviton, in general, is given by [46]

$$\sum_I \epsilon^I_{\mu\nu}(q)(\epsilon^I_{\rho\sigma}(q))^* \sim \frac{1}{2}\left(\eta_{\mu\rho}\eta_{\nu\sigma} + \eta_{\nu\rho}\eta_{\mu\sigma}\right) \ . \tag{3.22}$$

[18] This assumes polarization tensors being properly normalized, i.e. $\boldsymbol{\mathcal{E}}_i^\dagger \boldsymbol{\mathcal{E}}_i = 1$, otherwise (3.23) should be divided by $\boldsymbol{\mathcal{E}}_1^\dagger \boldsymbol{\mathcal{E}}_3$.

[19] $D = 4$ is more subtle for various reasons and we will discuss it separately.

impact parameter b. We start by setting $r_{J-2} = 0$. We then demand $\mathcal{K}(\vec{b})$ to have non-negative eigenvalues order by order in $1/b$ for transverse polarization $e^{\oplus}$ (or $e^{\otimes}$) for all directions of the impact parameter $\vec{b}$.[20] This imposes the following constraints on the coefficients

$$a_i = 0 \ , \qquad i \in \{2, 3, \cdots 3J\} \setminus \{J+2, 2J+2\} \ , \tag{3.25}$$

where, a_i is defined in (3.14). In other words, we find that all vertices with more than two derivatives must vanish. Moreover, the coefficients a_1, a_{J+2}, a_{2J+2} are related and the interaction C_{JJ2} can be reduced to the following vertex

$$\begin{aligned} C_{JJ2} =& a_1 (z_1 \cdot z_3)^{J-2} \Big((z_1 \cdot z_3)^2 (z \cdot p_3)^2 + J \Big((z \cdot z_3)(z_1 \cdot q) - (z \cdot z_1)(z_3 \cdot q) \Big) (z_1 \cdot z_3)(z \cdot p_3) \\ &+ \frac{J(J-1)}{2} \Big((z \cdot z_3)(z_1 \cdot q) - (z \cdot z_1)(z_3 \cdot q) \Big)^2 \Big) \ . \end{aligned} \tag{3.26}$$

When $J = 2$, no further constraints can be obtained using any other choice of polarization tensors. On the other hand, for $J > 2$ we can use the polarization tensor $\mathcal{E}_{J-2}$ (which always exists for $J \geq 2$) yielding

$$a_1 = 0 \ , \tag{3.27}$$

implying that $C_{JJ2} = 0$. Therefore, there is no consistent way of coupling higher spin elementary particles with gravity in flat spacetime in $D > 4$ dimensions.[21]

3.2.5 $D = 4$

The $D = 4$ case is special for several reasons. First of all, the $3J$ structures of on-shell three-point amplitude of two higher spin particles with mass m and spin J

[20] Transverse polarizations $e^{\otimes}, e^{\oplus}$ are given explicitly in appendix B.1.

[21] There are parity odd structures in $D = 5$ for massive particles of any spin. As we show in appendix B.3, These interactions also violate causality for $J > 2$ as well as $J \leq 2$.

and a single graviton are not independent in $D = 4$. These structures are built out of 5 vectors, however, in $D = 4$, any 5 vectors are necessarily linearly dependent. In particular, one can show that

$$m^2B^2 + 2AB(q \cdot z_3)(q \cdot z_1) + 2A^2(q \cdot z_3)(q \cdot z_1)(z_1 \cdot z_3) = 0 \ , \tag{3.28}$$

where, $A = (z \cdot p_3)$ and $B = (z \cdot z_3)(z_1 \cdot q) - (z \cdot z_1)(z_3 \cdot q)$ are two of the building blocks of on-shell three-point amplitudes. The above relation implies that structures in the set (3.13) in $D = 4$ are not independent since they can be written as structures from set (3.11) and (3.12). Therefore, for spin J in $D = 4$, there are $2J + 1$ independent structures which is in agreement with the number of independent structures in the CFT three point function of the stress tensor and two spin-J non-conserved primary operators. The $D = 4$ case is special for one more reason – there are parity odd structures for any spin J. In order to list all possible parity odd vertices for the interaction $J - J - 2$, we introduce the following building block that does not preserve parity :

$$\mathcal{B} = \epsilon^{\mu_1\mu_2\mu_3\mu_4} z_{1\mu_1} z_{3\mu_2} z_{\mu_3} q_{\mu_4} \ . \tag{3.29}$$

The parity odd on-shell three-point amplitude can be constructed using this building block. In particular, we can write two distinct sets of vertices with $\mathcal{B}$. The first set contains J independent structures:

$$\begin{aligned}
&\mathcal{A}_1^{odd} = \mathcal{B}(z \cdot p_3)(z_1 \cdot z_3)^{J-1} \ , \\
&\mathcal{A}_2^{odd} = \mathcal{B}(z \cdot p_3)(z_1 \cdot z_3)^{J-2}(z_3 \cdot q)(z_1 \cdot q) \ , \\
&\vdots \\
&\mathcal{A}_J^{odd} = \mathcal{B}(z \cdot p_3)(z_3 \cdot q)^{J-1}(z_1 \cdot q)^{J-1} \ .
\end{aligned} \tag{3.30}$$

The second set contains $J-1$ independent structures:

$$\begin{aligned}
\mathcal{A}_{J+1}^{odd} &= \mathcal{B}((z\cdot z_3)(z_1\cdot q)-(z\cdot z_1)(z_3\cdot q))(z_1\cdot z_3)^{J-2},\\
\mathcal{A}_{J+2}^{odd} &= \mathcal{B}((z\cdot z_3)(z_1\cdot q)-(z\cdot z_1)(z_3\cdot q))(z_1\cdot z_3)^{J-3}(z_3\cdot q)(z_1\cdot q),\\
&\vdots\\
\mathcal{A}_{2J-1}^{odd} &= \mathcal{B}((z\cdot z_3)(z_1\cdot q)-(z\cdot z_1)(z_3\cdot q))(z_3\cdot q)^{J-2}(z_1\cdot q)^{J-2}\ .
\end{aligned} \tag{3.31}$$

In $d=4$, there is another parity odd structure which is not related to the above structures and hence should be considered independent[22]

$$\mathcal{A}_{2J}^{odd} = \epsilon^{\mu_1\mu_2\mu_3\mu_4} z_{1\mu_1} p_{1\mu_3} z_{3\mu_3} p_{3\mu_4} (z\cdot p_3)^2 (z_3\cdot q)^{J-1}(z_1\cdot q)^{J-1}\ . \tag{3.32}$$

Therefore, the most general form of the three-point amplitude for $J\geq 1$ is given by

$$C_{JJ2} = \sqrt{32\pi G_N}\left(\sum_{n=1}^{2J+1} a_n \mathcal{A}_n + \sum_{n=1}^{2J} \bar{a}_n \mathcal{A}_n^{odd}\right)\ . \tag{3.33}$$

We can again use the polarization tensors (3.18) to derive constraints. However, for $D=4$ the setup of this section is not adequate to completely rule out particles with $J>2$. In $D=4$, the transverse space is only two-dimensional and therefore does not provide enough freedom to derive optimal bounds. In particular, we find that a specific non-minimal coupling is consistent with the positivity of the phase shift. We eliminate this remaining non-minimal coupling by considering interference between the graviton and the higher spin particle.

In $D=4$, the use of the polarization tensors (3.18) leads to the following bounds: $\bar{a}_n = 0$ and $a_2, \cdots, a_{2J+1}$ are fixed by a_1 (see (B.20)). The same set of bounds can also be obtained by using a simple null polarization vector

$$\epsilon^\mu(p_1) = i\epsilon_L^\mu(p_1) + \epsilon_{T,\hat{x}}^\mu(p_1)\ , \qquad \epsilon^\mu(p_3) = -i\epsilon_L^\mu(p_3) + \epsilon_{T,\hat{x}}^\mu(p_3)\ , \tag{3.34}$$

[22]We would like to thank J. Bonifacio for pointing this out.

where the transverse and longitudinal vectors are defined in (3.16) and the vector $\hat{x}$ is given by $\hat{x} = (0, 0, 1, 0)$. The phase-shift in $D = 4$ is

$$\delta(s, \vec{b}) = \frac{1}{4\pi s} \sum_I C_{I24}(-i\vec{\partial}_b) C_{13I}(-i\vec{\partial}_b) \ln\left(\frac{L}{b}\right) \ , \tag{3.35}$$

where, L is the IR regulator. Introduction of the IR regulator is necessary because of the presence of IR divergences in $D = 4$. Using the polarization (3.34) we obtain

$$\delta(s, \vec{b}) \sim s a_1 \ln\left(\frac{L}{b}\right) + s \sum_{n=0}^{2J-1} \frac{1}{b^{2J-n}} \left(f_n \cos((2J-n)\theta) + \bar{f}_n \sin((2J-n)\theta) \right) \ , \tag{3.36}$$

where, $\cos\theta = \hat{b} \cdot \hat{x}$. Coefficients f_n and $\bar{f}_n$ are linear combinations of parity even and parity odd coupling constants respectively. Requiring the phase shift to be positive order by order in $1/b$ in the limit $b \ll 1/m$ imposes the condition $f_n = \bar{f}_n = 0$. This implies that all the parity odd couplings must vanish and all the parity even couplings are completely fixed once we specify a_1 (full set of constraints for spin J are shown in (B.20).) Therefore, positivity of the phase shift (3.36) is consistent with a specific non-minimal coupling of higher spin particles in $D = 4$. In order to rule out this specific interaction, we now consider interference between the graviton and the higher spin particle.

Bound from Interference

We now consider eikonal scattering of gravitons and massive higher spin particles: $1, 2 \to 3, 4$. In this setup, 1 and 3 are linear combinations of massive higher spin particle X and the graviton: $\alpha h + \beta X$ and $\alpha' h + \beta' X$ respectively, where $\alpha, \alpha', \beta, \beta'$ are arbitrary real coefficients. While 2 and 4 are a fixed combination of X and the graviton: $h + X$. We will treat 2 as the source and 1 as the probe (see figure 3.5). This setup is very similar to the setup of [175].

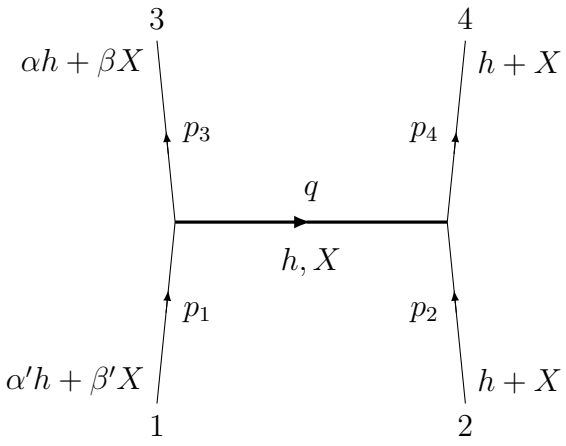

Figure 3.5: Bounds from interference in $D = 4$. In-states are linear combinations of massive higher spin particle X and the graviton h.

Positivity of the phase-shift can now be expressed as semi-definiteness of the following matrix

$$\begin{pmatrix} \delta_{hh} & \delta_{hX} \\ \delta_{Xh} & \delta_{XX} \end{pmatrix} \succeq 0 \ , \tag{3.37}$$

where, δ_{Xh} represents phase-shift when particle 1 is a higher spin particle of mass m and spin J and particle 3 is a graviton.[23] The above condition can also be restated as an interference bound

$$|\delta_{Xh}|^2 \leq \delta_{hh}\delta_{XX} \ , \tag{3.38}$$

where we have used the fact that $\delta_{Xh} = \delta^*_{hX}$. In the eikonal limit, the dominant contribution to both δ_{hh} and δ_{XX} comes from the graviton exchange and hence $\delta_{hh}, \delta_{XX} \sim s$, where s is the Mandelstam variable. Therefore, asymptotic causality requires that δ_{Xh} should not grow faster than s.

Let us now compute δ_{Xh} for a specific configuration. Momenta of the particles are again given by (3.15) with appropriate masses. Moreover, we will use the

[23] similar notation is used for other elements of the phase-shift matrix.

following null polarization vectors for various particles:

$$\begin{aligned}
\epsilon_X^\mu(p_1) &= i\epsilon_L^\mu(p_1) + \epsilon_{T,\hat{x}}^\mu(p_1) \ , \qquad & \epsilon_h^\mu(p_3) &= \epsilon_{T,\hat{x}}^\mu(p_3) + i\epsilon_{T,\hat{y}}^\mu(p_3) \ , \\
\epsilon_X^\mu(p_2) &= i\epsilon_L^\mu(p_2) + \epsilon_{T,\hat{x}}^\mu(p_2) \ , \qquad & \epsilon_h^\mu(p_2) &= \epsilon_{T,\hat{x}}^\mu(p_2) - i\epsilon_{T,\hat{y}}^\mu(p_2) \ , \\
\epsilon_X^\mu(p_4) &= -i\epsilon_L^\mu(p_4) + \epsilon_{T,\hat{x}}^\mu(p_4) \ , \qquad & \epsilon_h^\mu(p_4) &= \epsilon_{T,\hat{x}}^\mu(p_4) + i\epsilon_{T,\hat{y}}^\mu(p_4) \ ,
\end{aligned} \tag{3.39}$$

where $\hat{x} = (0,0,1,0)$ and $\hat{y} = (0,0,0,1)$. In the eikonal limit the dominant contribution to δ_{Xh} comes from X-exchange. In particular, after imposing constraints (B.20), we find that

$$\delta_{Xh} \sim a_1 s^{J-1} \frac{e^{-2i(J-2)\theta}}{b^{2(J-2)} m^{4(J-2)}} \ , \tag{3.40}$$

where $\cos\theta = \hat{b}\cdot\hat{x}$. The above phase-shift violates causality for $J > 2$ implying

$$a_1 = 0 \qquad \text{for} \qquad J > 2 \ . \tag{3.41}$$

Therefore there is no consistent way of coupling higher spin elementary particles with gravity even in four dimensional flat spacetime.

3.2.6 Comments

Comparison with other arguments

As mentioned in the introduction, there are qualitative arguments in the literature in $D = 4$ suggesting that elementary massive higher spin particles cannot exist. The idea originally advocated by Weinberg, is to require physical theories for elementary particles to have a well behaved high energy limit or equivalently to demand a smooth limit for the amplitude as $m_X \to 0$ [124, 125]. However, for minimal coupling with spin $J > 2$ particles, the amplitude grows with powers of $\left(\frac{s}{m_X^2}\right)$ as $m_X \to 0$ [123]. Therefore, given a fixed and finite cutoff scale Λ and a

mass m_X, the amplitude can become $\mathcal{O}(1)$ for $m_X \ll \sqrt{s} \ll \Lambda$. For instance, it was shown in [126] by considering only the minimal coupling of spin $\frac{5}{2}$ to gravity, that tree-level unitarity breaks down at the energy $\sqrt{s} \sim \sqrt{m_X M_{pl}} \ll M_{pl}$. Moreover, the break-down scale for a particle of spin J was conjectured to be even lower $\sim \left(m_X^{2J-2} M_{pl}\right)^{\frac{1}{2J-1}}$ [176]. This was shown to be true for massive spin $J = 2$ particles [175]. The existence of this scale implies that this particle cannot exist if tree-level unitarity is required to persist for scales up to M_{pl}. This seems natural if we require the theory of higher spin fields to be renormalizable. However, from an effective field theory point of view, the smooth $m_X \to 0$ requirement, determines only the range of masses and cut-off scales over which the low energy tree level amplitude is a good description of this massive higher spin scattering experiment. Note that even within the tree level unitarity arguments, one still needs to consider all possible non-minimal couplings as well as all contact interactions in order to ensure that they do not conspire to change the singular behavior of the amplitude in the $m_X \to 0$ limit. In fact, [126,127] demonstrates examples in which adding non-minimal couplings can change the high energy singular behavior of the amplitude for longitudinal part of polarizations.

By contrast, the causality arguments used here, require only the cut-off to be parametrically larger than the mass of the higher spin particle, $\Lambda \gg m_X$. Then, given an impact parameter $b \ll m_X^{-1}$, the desired bounds are obtained even if the amplitude or phase shift $M(s,t)$, $\delta(s,b) \ll 1$ (unlike the violation of tree-level unitarity requiring the amplitude to be $\mathcal{O}(1)$) since even the slightest time advance is forbidden by causality. Moreover, in the eikonal experiment, the two incoming particles do not overlap and hence contributions from the other channel and contact diagrams can be ignored [46].

An Interference Argument for $D > 4$

A generalization of the interference argument of $D = 4$ to higher dimensions also suggests that there is tension between massive higher spin particles and asymptotic causality. In fact, it might be possible to derive the bounds of this section by demanding that the phase shift δ_{Xh} does not grow faster than s, however, we have not checked this explicitly. This argument has one immediate advantage. For a particle with spin J, $\delta_{Xh} \sim s^{J-1}$ and therefore it is obvious that even an infinite tower of massive spin-2 exchanges cannot restore causality. The only way causality can be restored is if we add an infinite tower of massive higher spin particles. We should note that this arguments rely on the additional assumption that the eikonal approximation is valid for spin-J exchange with $J > 2$. The N-shocks argument of [46] is also applicable here which strongly suggests that the eikonal exponentiation holds even for $J > 2$, however, a rigorous proof is still absent.

Massless Case

Higher spin massless particles are already ruled out by the Weinberg-Witten theorem. Nonetheless, we can rederive this fact using the eikonal scattering setup. If the higher spin particles are massless, then gauge invariance requires that each vertex is invariant under the shift $z_i \to z_i + \alpha_i\, p_i$, where α_i's are arbitrary real numbers. In this case only the three following structures are allowed for $J \geq 2$

$$\mathcal{D}_1 = (z \cdot p_3)^2 (z_1 \cdot q)^J (z_3 \cdot q)^J, \tag{3.42}$$

$$\mathcal{D}_2 = ((z_3 \cdot q)(z_1 \cdot z) - (z \cdot z_3)(z_1 \cdot q) - (z \cdot p_3)(z_1 \cdot z_3))(z \cdot p_3)(z_1 \cdot q)^{J-1}(z_3 \cdot q)^{J-1},$$

$$\mathcal{D}_3 = ((z_3 \cdot q)(z_1 \cdot z) - (z \cdot z_3)(z_1 \cdot q) - (z \cdot p_3)(z_1 \cdot z_3))^2 (z_1 \cdot q)^{J-2}(z_3 \cdot q)^{J-2}\ .$$

This is again, as we will see in the next section, in agreement with the three structures appearing in the CFT three point function once we impose conservation constraints for all three operators. The general form of the three-point function for $J \geq 2$ is now given by

$$C_{JJ2} = \sqrt{32\pi G_N} \sum_{n=1}^{3} d_n \mathcal{D}_n \ . \tag{3.43}$$

For massless particles, $\mathcal{E}_J$ is the only polarization tensor. As before, by requiring asymptotic causality we find

$$d_n = 0 \qquad n = 1, 2, 3 \tag{3.44}$$

for $J > 2$.

Parity Violating Interactions of Massive Spin-2 in $D = 4$

The argument presented in this section can also be applied to $J = 2$ in $D \geq 4$. Of course, our argument does not rule out massive spin-2 particles. Rather it restricts the coupling between two massive spin-2 particles and a graviton to be minimal (3.26) which agrees with [163]. However, for $D = 4$ our argument does rule out parity violating interactions between massive spin-2 particles and the graviton. Moreover, the same conclusion about parity violating interactions holds even for massive spin-1.

Restoration of Causality

Let us now discuss the possible ways of bypassing the arguments presented in this section. Our arguments utilized the eikonal limit $m, q \ll \sqrt{s} \ll \Lambda$, where Λ is the

UV cut-off of the theory. Hence, our argument breaks down if the mass of the higher spin particle $m \sim \Lambda$.

There is another interesting possibility. One can have a massive higher spin particle with mass $m \ll \Lambda$ and causality is restored by adding one or more additional particles. The contribution to the phase shift for a tree level exchange of a particle of mass $M \gg m$, $\frac{1}{b}$ is exponentially suppressed $\sim e^{-bM}$. Hence, these additional contributions can be significant enough if the masses of these particles are not much larger than m. In addition, exchange of these additional particles can only restore causality if they have spin $J > 2$. However, exchange of any finite number of such particles will lead to additional causality violation. Hence, the only possible way causality can be restored is by adding an infinite tower of fine-tuned higher spin particles with masses comparable to m. Furthermore, causality for the scattering J+graviton$\rightarrow$ J+graviton also requires that an infinite subset of these new higher spin particles must be able to decay into two gravitons which implies that this infinite tower does affect the dynamics of gravitons at energies $\sim m$.[24] We will discuss this in more detail in section 3.4.

Composite Higher Spin Particles

The argument of this section is applicable to elementary massive higher spin particles. However, whether a particle is elementary or not must be understood from the perspective of effective field theory. Hence, the argument of this section is also applicable to composite higher spin particles as long as they look elementary enough at a certain energy scale. In particular, if the mass of a composite particle

[24]Note that we ignored loops of the higher spin tower. From the scattering J+graviton$\rightarrow$ J+graviton, it is clear that an infinite tower of higher spin particles with mass $M \gg m$ cannot restore causality even if we consider loops.

is m but it effectively behaves like an elementary particle up to some energy scale Λ which is parametrically higher than m, then the argument of this section is still applicable. More generally, argument of this section rules out any composite higher spin particle which is isolated enough such that it does not decay to other particles after interacting with high energy gravitons $q \gg m$.

Validity of the Causality Condition

Let us end this section by mentioning a possible caveat of our argument. In this section, we have shown that presence of massive higher spin particles is inconsistent with asymptotic causality which requires that particles do not experience a time advance even when they interact with each other. It is believed that any Lorentzian QFT must obey this requirement. However, there is no rigorous S-matrix based argument that shows that positivity of the time delay is a necessary requirement of any UV complete theory. A physical argument was presented in [46] which relates positivity of the phase shift to unitarity but it would be nice to have a more direct derivation. In the next section, we present a CFT-based derivation of the same bounds in anti-de Sitter spacetime which allows us to circumvent this technical loophole.

3.3 Higher Spin Fields in AdS$_D$

Let us now consider large-N CFTs in dimensions $d \geq 3$ with a sparse spectrum. CFTs in this class are special because at low energies they exhibit universal, gravity-like behavior. This duality allows us to pose a question in the CFT in d-dimensions which is dual to the question about higher spin fields in AdS in $D = d+1$ dimensions.

Is it possible to have additional higher spin single trace primary operators X_J with $J > 2$ and scaling dimension $\Delta \ll \Delta_{\text{gap}}$ in a holographic CFT?

In general, any such operator X_J will appear as an exchange operator in a four-point function of even low spin operators. In the Regge limit $\sigma \to 0$,[25] the contribution to the four-point function from the X_J-exchange goes as $\sim 1/\sigma^{J-1}$ which violates the chaos growth bound of [27] for $J > 2$ and hence all CFT three-point functions $\langle X_J O O \rangle$ must vanish for any low spin operator O. In the gravity side, this rules out all bulk couplings of the form $\mathcal{O}\mathcal{O}\mathcal{X}_J$ in AdS, where $\mathcal{X}_J$ is a higher spin bulk field (massive or massless) and $\mathcal{O}$ is any other bulk field with or without spin. For example, this immediately implies that in a theory of quantum gravity where the dynamics of gravitons at low energies is described by Einstein gravity, decay of a higher spin particle into two gravitons is not allowed.

The above condition is not sufficient to completely rule out the existence of higher spin operators. In particular, we can still have higher spin operators without violating the chaos growth bound if the higher spin operator X_J does not appear in the OPE of any two identical single trace primary operators. For example, if each higher spin operator has a $\mathbb{Z}_2$ symmetry, they will be prohibited from appearing in the OPE of identical operators. However, a priori we can still have non-vanishing $\langle X_J X_J O \rangle$. In fact, the Ward identity dictates that the three-point function $\langle X_J X_J T \rangle$ must be non-zero where T is the CFT stress tensor. In this section, we will utilize the holographic null energy condition to show that $\langle X_J X_J T \rangle$ must vanish for CFTs (in $d \geq 3$) with large N and a sparse spectrum, or else causality (the chaos sign bound) will be violated. The Ward identity then requires that the two-point function $\langle X_J X_J \rangle$ must vanish as well. However, the two-point

[25] In terms of the conformal cross-ratios, $z \sim \sigma$ and $\bar{z} \sim \eta\sigma$. The Regge limit is defined as $\sigma \to 0$ with $\eta =$ fixed after we analytically continue $\bar{z}$ around the singularity at 1 (see [152, 155, 157]).

function $\langle X_J X_J \rangle$ is a measure of the norm of a state created by acting X_J on the vacuum and therefore must be strictly positive in a unitary CFT. Vanishing of the norm necessarily requires that the operator X_J itself is zero.

In the gravity language, this forbids the bulk interaction $\mathcal{X}_J$-$\mathcal{X}_J$-graviton – which directly contradicts the equivalence principle. Therefore, a finite number of higher spin elementary particles, massless or massive, cannot interact with gravity in a consistent way even in AdS spacetime (in $D \geq 4$).

3.3.1 Causality and Conformal Regge Theory

We start with a general discussion about the Regge limit in generic CFTs and then review the holographic null energy condition (HNEC) in holographic CFTs which we will use to rule out higher spin single trace primary operators. The HNEC was derived in [155, 157], however, let us provide a more general discussion of the HNEC here. The advantage of the new approach is that it can be applied to more general CFTs. However, that makes this subsection more technical, so casual readers can safely skip this subsection.

As discussed in [41, 140, 157] the relevant kinematic regime of the CFT 4-point function for accessing the physics of deep inside the bulk interior is the Regge limit. In terms of the familiar cross-ratios, in our conventions this limit corresponds to analytically continuing $\bar{z}$ around the singularity at 1 followed by taking the limit $z, \bar{z} \to 0$ with $z/\bar{z}$ held fixed. Unlike the more familiar euclidean OPE limit, the contributions to the correlation function in this limit are not easily organized in terms of local CFT operators. In fact contributions of individual local operators become increasingly singular with increasing spin. Using conformal

Regge theory [177], these contributions may be resummed into finite contributions by rewriting the sum over spins as a contour integral using the Sommerfeld-Watson transform. This formalism relied on the fact that the coefficients in the conformal block expansion are well defined analytic functions of J away from integer values which was later justified in [151]. This allows one to rewrite the sum over spins in the conformal block expansion as a deformed contour integral over J, reorganizing the contributions to a sum over Regge trajectories. We will not discuss the derivation here as the details are well reviewed in [153–155, 177]. We will instead derive an expression for the contribution of a Regge trajectory directly to the OPE of two local operators in terms of a non-local operator $\mathbb{E}_{\Delta,J}$ described below.

We will first derive an expression for the contribution to the OPE of scalar operators $\psi\psi$ by an operator of spin J and scaling dimension Δ. To this end, we will utilize the methods introduced in [117] to encode primary symmetric traceless tensor operators into polynomials of degree J by contracting them with null polarization vectors z^μ :

$$\mathcal{O}(x;z) \equiv z^{\mu_1}...z^{\mu_J}\mathcal{O}(x)_{\mu_1...\mu_J}. \tag{3.45}$$

It was shown in [117] that the tensor may be recovered from this polynomial by using the Thomas/Todorov operator. We are however interested in the case where the spin J is not necessarily an integer. Therefore we will employ the procedure introduced in [178] to generalize this expression to continuous spin by dropping the requirement that $\mathcal{O}(x;z)$ be a polynomial in z. With this definition, the expression for the contribution to the OPE by a continuous spin operators is given by a simple generalization of the expression appearing in [155]. We will then use the shadow

representation [179–181] for the OPE in Lorentzian signature [112, 182]:

$$\frac{\psi(x_1)\psi(x_2)}{\langle\psi(x_1)\psi(x_2)\rangle}\bigg|_{\Delta,J} = \mathcal{N}\int_{\diamond_{12}} d^d x_3 \int D^{d-2}z D^{d-2}z' \times \frac{(-2z.z')^{2-d-J}\langle\psi(x_1)\psi(x_2)\tilde{\mathcal{O}}(x_3;z)\rangle}{\langle\psi(x_1)\psi(x_2)\rangle}\mathcal{O}(x_3,z'). \quad (3.46)$$

where we let points x_1 and x_2 to be time-like separated and the integration of x_3 is performed over the intersection of causal future of x_1 and the causal past of x_2, $\mathcal{N}$ is a normalization constant and

$$D^{d-2}z \equiv \frac{d^d z\delta(z^2)\theta(z_0)}{\text{vol }\mathbb{R}_+} \ . \quad (3.47)$$

The integrals over z and z' replace the contraction over tensor indices that would appear for integer J using the inner product for Lorentzian principal series introduced in [178]. These are manifestly conformal integrals and the integration can be performed using the methods described in [180].

In order to obtain the contribution to the Regge limit we will set $x_1 = -x_2 = (u, v, \vec{0})$ and analytically continue the points to space-like separations resulting in integration over a complexified Lorentzian diamond. We will then take the Regge limit by sending $v \to 0$ and $u \to \infty$ with uv held fixed. The resulting expression is an integral over a complexified ball times a null ray along the u direction:

$$\begin{aligned}\frac{\psi(u,v,\vec{0})\psi(-u,-v,\vec{0})}{\langle\psi(u,v,\vec{0})\psi(-u,-v,\vec{0})\rangle}\bigg|_{\Delta,J} &= (-1)^{\frac{\Delta-1}{2}}\pi^{\frac{1-d}{2}}2^{\Delta}\frac{\Gamma\left(\frac{\Delta+J+1}{2}\right)\Gamma(\Delta-d/2+1)}{\Gamma\left(\frac{\Delta+J}{2}\right)\Gamma(\Delta-d+2)}\frac{C_{\psi\psi\mathcal{O}_{\Delta,J}}}{C_{\mathcal{O}_{\Delta,J}}} \\ &\times \frac{(uv)^{\frac{d-\Delta-J}{2}}}{u^{1-J}}\int_{-\infty}^{\infty}d\tilde{u}\int_{\vec{x}^2\leq uv} d^{d-2}\vec{x}(uv-\vec{x}^2)^{\Delta-d+1}\mathcal{O}((\tilde{u},0,i\vec{x});(0,1,0)) \\ &\equiv u^{J-1}\mathbb{E}_{\Delta,J} \ , \end{aligned} \quad (3.48)$$

where $C_{\psi\psi\mathcal{O}_{\Delta,J}}$ is the OPE coefficient, $C_{\mathcal{O}_{\Delta,J}}$ is the normalization of $\langle\mathcal{O}\mathcal{O}\rangle$ and we have used $(u, v, \vec{x}_\perp)$ to express coordinates. This operator captures the contribution to OPE of $\psi\psi$ in the Regge limit. Therefore, analytically continued conformal blocks

can be computed by inserting $\mathbb{E}_{\Delta,J}$ inside a three-point function. For example, in the case of external scalars we find

$$\frac{\langle\phi(x_3)\phi(x_4)\mathbb{E}_{\Delta,J}\rangle}{\langle\phi(x_3)\phi(x_4)\rangle}u^{J-1} \sim \lim_{\substack{z,\bar{z}\to 0 \\ z/\bar{z} \text{ fixed}}} G^{\circlearrowleft}_{\Delta,J}(z,\bar{z})$$
$$= \frac{i(-1)^J 2^{2\Delta+3J-2}\Gamma\left(\frac{J+\Delta-1}{2}\right)\Gamma\left(\frac{J+\Delta+1}{2}\right)}{\Gamma\left(\frac{J+\Delta}{2}\right)^2} \frac{z^{\frac{\Delta-J}{2}}\bar{z}^{-\frac{\Delta}{2}-\frac{J}{2}+2}}{(z-\bar{z})} , \tag{3.49}$$

where $G^{\circlearrowleft}_{\Delta,J}(z,\bar{z})$ is obtained from the conformal block by taking $\bar{z}$ around 1 while holding z fixed. In (3.48) this analytic continuation corresponds to the choice of contour in performing the $\tilde{u}$ integral. The integrand encounters singularities in $\tilde{u}$ as the points become null separated from x_3 or x_4. Different analytic continuations of the conformal block can be obtained by choosing appropriate contours. The choice of contour in the $\tilde{u}$ plane was discussed in [157] in greater detail. By an identical Sommerfeld-Watson transform and contour deformation argument as in [177], the expression for the Regge OPE can now be used to capture the contribution of Regge trajectories

$$\left.\frac{\psi(u,v,\vec{0})\psi(-u,-v,\vec{0})}{\langle\psi(u,v,\vec{0})\psi(-u,-v,\vec{0})\rangle}\right|_{J(\nu)} = \int d\nu u^{J(\nu)-1}a(\nu)\mathbb{E}_{\Delta(J(\nu)),J(\nu)} , \tag{3.50}$$

where the coefficient $a(\nu)$ encodes the dynamical information about the spectrum of the CFT for the Regge trajectory parametrized by $J(\nu)$.

The operator $\mathbb{E}_{\Delta,J}$ can be contrasted with the light-ray operator $\mathbf{L}[\mathcal{O}]$ introduced in [178]. Although both correspond to non-local contributions to the OPE in the Regge limit, they do not compute the same quantity. As mentioned above $\mathbb{E}_{\Delta,J}$ computes the analytic continuation of the conformal block, whereas $\mathbf{L}[\mathcal{O}]$ computes the analytic continuation of conformal partial wave which is the sum of the block and its shadow which is proportional to $G_{1-J,1-\Delta}(z,\bar{z})$. However, because of the

symmetry of the coefficient $a(\nu)$ under $\nu \to -\nu$ using either operator in the Regge limit will yield the same results after integration.

Holographic CFT: Holographic Null Energy Condition

As described in more detail in [153–156, 177, 183] the leading Regge trajectory in a holographic theory with a large Δ_{gap} can be parametrized as

$$J(\nu) = 2 - \frac{1}{\Delta_{gap}^2}\left(\frac{d^2}{4} + \nu^2\right) + \mathcal{O}\left(\frac{1}{\Delta_{gap}^4}\right) \ . \tag{3.51}$$

Using this expression for the trajectory we find that at leading order in Δ_{gap} the coefficient $a(\nu)$ will have single poles corresponding to the stress-tensor exchange as well as an infinite set of double-trace operators. As shown in [155, 157], in the class of states in which we are interested, the dominant contribution to this OPE is given by the stress-tensor and the double-trace operators will not contribute. This contribution is captured by the holographic null energy operator

$$\mathcal{E}_r(\nu) = \int_{-\infty}^{+\infty} du' \int_{\vec{x}^2 \leq r^2} d^{d-2}\vec{x}\left(1 - \frac{\vec{x}^2}{r^2}\right) T_{uu}\left(u', \nu, i\vec{x}\right) \tag{3.52}$$

which is a generalization of the averaged null energy operator [155] and a special case of the operator $\mathbb{E}_{\Delta,J}$ described above with $\Delta = d$ and $J = 2$.[26] In particular, in the limit $r \to 0$, this operator is equivalent to the averaged null energy operator.

Causality in CFT implies that the four-point function obeys certain analyticity properties [58, 79, 92, 93]. For generic CFTs in $d \geq 3$, these analyticity conditions dictate that the averaged null energy operator must be non-negative [79]. However, for holographic CFTs, causality leads to stronger constraints. In particular, causality

[26] We are using the following convention for points $x \in \mathbb{R}^{1,d-1}$ in CFT_d:

$$x = (t, x^1, \vec{x}) \equiv (u, v, \vec{x}) \ , \qquad \text{where,} \qquad u = t - x^1 \ , \qquad v = t + x^1 \ . \tag{3.53}$$

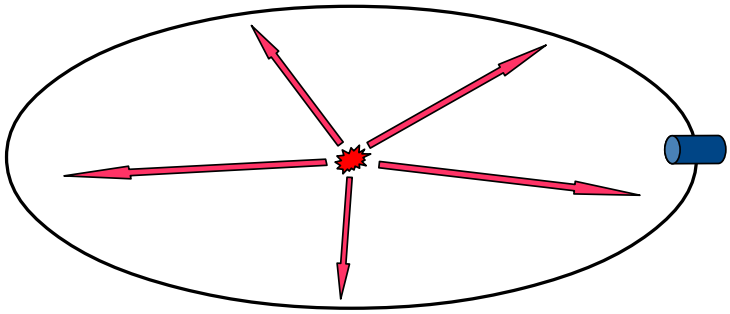

Figure 3.6: Holographic null energy condition (HNEC): A holographic CFT is prepared in an excited state $|\Psi\rangle$ by inserting an operator O near the origin and an instrument which is shown in blue, measures the holographic null energy $\mathcal{E}_r$ far away from the excitation.

of CFT four-point functions in the Regge limit implies that the expectation value of the holographic null energy operator is positive in a subspace of the total Hilbert space of holographic CFTs [155, 157]:

$$\mathcal{E}(\rho) \equiv \lim_{B\to\infty} \langle\Psi|\mathcal{E}_{\sqrt{\rho}B}(B)|\Psi\rangle \geq 0 \ , \tag{3.54}$$

where, $0 < \rho < 1$. The class of states $|\Psi\rangle$ are created by inserting an arbitrary operator O near the origin

$$|\Psi\rangle = \int dy^1 d^{d-2}\vec{y}\, \epsilon.O(-i\delta, y^1, \vec{y})|0\rangle \ , \qquad \langle\Psi| = \int dy^1 d^{d-2}\vec{y}\, \langle 0|\epsilon^*.O(i\delta, y^1, \vec{y}) \ , \tag{3.55}$$

where, ϵ is the polarization of the operator O with

$$\epsilon.O \equiv \epsilon_{\mu\nu\ldots} O^{\mu\nu\ldots} \tag{3.56}$$

and $\delta > 0$. The state $|\Psi\rangle$ is equivalent to the Hofman-Maldacena state of the original conformal collider [56] which was created by acting local operators, smeared with Gaussian wave-packets, on the CFT vacuum.

The HNEC is practically a conformal collider experiment for holographic CFTs (in $d \geq 3$) in which the CFT is prepared in an excited state $|\Psi\rangle$ by inserting an

operator O near the origin and an instrument measures $\mathcal{E}(\rho)$ far away from the excitation, as shown in figure 3.6. Then, causality implies that the measured value $\mathcal{E}(\rho)$ must be non-negative for large-N CFTs with a sparse spectrum. Next, creating the state $|\Psi\rangle$ by inserting the higher spin operator X_J, we show that the inequality (3.54) leads to surprising equalities among various OPE coefficients that appear in $\langle X_J X_J T\rangle$.

3.3.2 $D > 4$

We will use the HNEC to derive bounds on higher spin single trace primary operators in $d \geq 4$ (or AdS_D with $D \geq 5$). We will explicitly show that spin 3 and 4 operators are completely ruled out and then argue that the same must be true even for $J > 4$. The case of $D = 4$ is more subtle and will be discussed separately.

Spin-3 Operators

Let us start with an operator X_J with $J = 3$ which does not violate the chaos growth bound because it has $\mathbb{Z}_2$ or some other symmetry which sets $\langle OOX_{J=3}\rangle = 0$ for all O. Consequently, this operator does not contribute as an exchange operator in any four-point function in the Regge limit and the leading contribution to the Regge four-point function still comes from the exchange of spin-2 single trace (stress tensor) and double trace operators. Therefore, the HNEC is still valid and we can use it with states created by smeared $X_{J=3}$ to derive constraints on $\langle X_{J=3}X_{J=3}T\rangle$.

The CFT three-point function $\langle X_{J=3}X_{J=3}T\rangle$, is completely fixed by conformal symmetry up to a finite number of OPE coefficients (see appendix B.4). After imposing permutation symmetry and conservation equation, the three-point function

$\langle X_{J=3} X_{J=3} T\rangle$ has 9 independent OPE coefficients. We now compute the expectation value of the holographic null energy operator $\mathcal{E}(\rho)$ in states created by smeared $X_{J=3}$:

$$|\Psi\rangle = \int dy^1 d^{d-2}\vec{y}\, \epsilon^{\mu_1}\epsilon^{\mu_2}\epsilon^{\mu_3} X_{\mu_1\mu_2\mu_3}(-i\delta, y^1, \vec{y})|0\rangle \ , \tag{3.57}$$

where, ϵ^μ is a null polarization vector:

$$\epsilon^\mu = (-i\xi, -i, \vec{\varepsilon}_\perp) \ , \tag{3.58}$$

with $\xi = \pm 1$ and $\vec{\varepsilon}_\perp{}^2 = 0$.[27] Following the procedure outlined in [157], we can compute $\mathcal{E}(\rho)$ in state (3.57). The result has the following form

$$\mathcal{E}(\rho) = \frac{1}{(1-\rho)^{d+3}} \sum_{n=0}^{\infty} I_\xi^{(n)}(\lambda^2)(1-\rho)^n \ , \tag{3.59}$$

where, $I_\xi^{(n)}(\lambda^2)$ are polynomials in λ^2 which in general have terms up to order λ^6, where

$$\lambda^2 = \frac{1}{2}\vec{\varepsilon}_\perp \cdot \vec{\varepsilon}^*_\perp \geq 0 \ . \tag{3.60}$$

Given our choice of polarization, different powers of λ^2 correspond to independent spinning structures and decomposition of $SO(d-1,1)^3$ to representations under $SO(d-2)$. Therefore positivity of $\mathcal{E}(\rho)$ implies that the coefficients of each power of λ^2 must individually satisfy positivity, for $\xi = +1$ as well as $\xi = -1$. Now, applying the HNEC order by order in the limit $\rho \to 1$, the inequalities lead to 9 equalities among the 9 OPE coefficients. We find that the 9 OPE coefficients cannot be consistently chosen to satisfy these equalities. Hence, causality implies that

$$\langle X_{J=3} X_{J=3} T\rangle = 0 \ . \tag{3.61}$$

Moreover, the Ward identity relates C_{X_3}, coefficient of the two-point function $\langle X_{J=3} X_{J=3}\rangle$ (see eq B.28), to a particular linear combination of the OPE coefficients

[27] Note that in $d = 3$ this choice of polarization vector does not work. In this case, one needs to use a general polarization tensor to derive constraints.

$C_{i,j,k}$ and hence the two-point function $\langle X_{J=3} X_{J=3}\rangle$ must vanish as well. This implies that we cannot have individual spin-3 single trace primary operators in the spectrum. The detail of the calculation are rather long and not very illuminating, so we relegate them to appendix B.5.

Spin-4 Operators

We can perform a similar analysis with a spin-4 operator which leads to the same conclusion, however, the details are little different. The three-point function $\langle X_{J=4} X_{J=4} T\rangle$, after imposing permutation symmetry and conservation equation, has 12 independent OPE coefficients (see appendix B.6). But the HNEC leads to stronger constraints as we increase the spin of X and these 12 OPE coefficients cannot be consistently chosen to satisfy all the positivity constraints. In fact, as we will show, it is easier to rule out spin-4 operators using the HNEC than spin-3 operators.

We again perform a conformal collider experiment for holographic CFTs (in $d \geq 3$) in which the CFT is prepared in an excited state

$$|\Psi\rangle = \int dy^1 d^{d-2}\vec{y}\, \epsilon^{\mu_1}\epsilon^{\mu_2}\epsilon^{\mu_3}\epsilon^{\mu_4} X_{\mu_1\mu_2\mu_3\mu_4}(-i\delta, y^1, \vec{y})|0\rangle \ , \tag{3.62}$$

where, ϵ^μ is the null polarization vector (3.58). The expectation value of the holographic null energy operator $\mathcal{E}(\rho)$ in states created by smeared $X_{J=4}$ can be computed using methods used in [157]

$$\mathcal{E}(\rho) = \frac{1}{(1-\rho)^{d+5}} \sum_{n=0}^{\infty} \tilde{I}_\xi^{(n)}(\lambda)(1-\rho)^n \ , \tag{3.63}$$

where, $\tilde{I}_\xi^{(n)}(\lambda^2)$ are polynomials in λ^2 (3.60) with terms up to λ^8 in general. Causality implies that different powers of λ^2 must satisfy positivity individually, for $\xi = +1$

as well as $\xi = -1$. We find that the 12 OPE coefficients cannot be consistently chosen to satisfy all the positivity constraints implying (see appendix B.6)

$$\langle X_{J=4} X_{J=4} T \rangle = 0 \ . \tag{3.64}$$

Consequently, the Ward identity dictates that the two-point function of $X_{J=4}$ must vanish as well. This rules out single trace spin-4 operators with scaling dimensions below Δ_{gap} in the spectrum of a holographic CFT. As shown in the appendix B.6, we ruled out spin-4 operators even without considering $\mathcal{E}_{\xi=-1}(\rho)$. This is because as we increase the spin of X, the number of constraint equations increases faster than the number of independent OPE coefficients. This is also apparent from the fact that for spin-3, we had to go to order $\frac{1}{(1-\rho)^{d-2}}$ to derive all constraints. Whereas, for spin-4, the full set of constraints were obtained at the order $\frac{1}{(1-\rho)^{d-1}}$.

Spin $J > 4$

For operators with spin $J \geq 5$, the argument is exactly the same. In fact, it is easier to rule them out because the HNEC leads to stronger constraints at higher spins. For example, for $J = 1$, there are 3 independent OPE coefficients but the HNEC yields 2 linear relations among them. Consequently, the three-point function $\langle X_{J=1} X_{J=1} T \rangle$ is fixed up to one coefficient. The same is true for $J = 2$ – there are 6 independent OPE coefficients and 5 constraints from the HNEC. Furthermore, in both of these cases, constraint equations ensure that the expectation value of the holographic null energy operator behaves exactly like that of the scalars: $\mathcal{E}(\rho) \sim \frac{1}{(1-\rho)^{d-3}}$ for $d \geq 4$. In fact, this is true for all low spin operators of holographic CFTs.

The HNEC barely rules out operators with $J = 3$. There are 9 independent OPE coefficients. Using the positivity conditions all the way up to order $\frac{1}{(1-\rho)^{d-2}}$

for $\xi = \pm 1$, we showed that the OPE coefficients cannot be consistently chosen to satisfy all the positivity constraints. Whereas, the HNEC rules out $J = 4$ operators quite comfortably. We only needed to consider positivity conditions up to order $\frac{1}{(1-\rho)^{d-1}}$ and only for $\xi = +1$ to rule them out. The same pattern persists even for operators with spins $J \geq 5$ so we will not repeat our argument for each spin. Instead, we present a general discussion about the structure of $\mathcal{E}(\rho)$ at each order in the limit $\rho \to 1$ for general Δ and J (in $d \geq 4$ dimensions). This enables us to count the number of constraint equations at each order. A simple counting immediately suggests that a non-vanishing $\langle X_J X_J T \rangle$ cannot be consistent with the HNEC even for spins higher than 4. By studying various examples with specific values of J, Δ and d, we have explicitly checked that our simple counting argument is indeed true.

The three point function $\langle X_J X_J T \rangle$ has $5 + 6(J-1)$ OPE coefficients to begin with, however not all of them are independent. Permutation symmetry implies that only $4J$ OPE coefficients can be independent. In addition, conservation of the stress-tensor operator T imposes J additional constraints among the remaining $4J$ OPE coefficients. Therefore, the three-point function $\langle X_J X_J T \rangle$ is fixed by conformal invariance up to $3J$ truly independent OPE coefficients.[28] Furthermore, the Ward identity leads to a relation between these OPE coefficients and the coefficient of the two-point function C_{X_J}.

We again perform a conformal collider experiment for holographic CFTs (in $d \geq 4$) in which the CFT is prepared in an excited state created by smeared X_J. In the limit $\rho \to 1$, the leading contribution to $\mathcal{E}(\rho)$ goes as

$$\mathcal{E}(\rho) \sim \frac{1}{(1-\rho)^{d+2J-3}} \ , \tag{3.65}$$

[28]The number of independent OPE coefficients is different in $d = 3$.

where only a single structure contributes with an overall factor that depends on a specific linear combination of OPE coefficients. Just like before, the structure changes sign for different powers of λ^2 and hence in the 1st order, the HNEC produces only one constraint. It is clear from [155, 157] that the coefficient of the term $\mathcal{E}(\rho) \sim \frac{1}{(1-\rho)^{d-3}}$ is fixed by the Ward identity and hence automatically positive. On the other hand, the HNEC in general can lead to constraints up to the $2J$-th order, i.e. the order $\mathcal{E}(\rho) \sim \frac{1}{(1-\rho)^{d-2}}$. But for $J > 3$, one gets $3J$ independent constraints from the HNEC even before the $2J$-th order.

It is easier to rule out operators with higher and higher spins. A simple counting clearly shows why this is not at all surprising. First, let us assume that the HNEC rules out any operator with some particular spin $J = J_* > 2$. That means for spin J_* the HNEC generates $3J_*$ independent relations among the OPE coefficients. If we increase the spin by 1: $J = J_* + 1$, we get 3 more independent OPE coefficients. However, the $(2J_* + 1)$-th and $(2J_* + 2)$-th orders in $\mathcal{E}(\rho)$ produce new constraints and at each new order there can be $J_* + 1$ new equalities. Moreover, the λ^2 polynomials at each order now has a $\lambda^{2(J_*+1)}$ term with its own positivity condition – this means that there can be $2J_*$ additional equalities from the first $2J_*$ orders. Therefore, for spin $J_* + 1$, there are 3 new OPE coefficients, whereas there can be $2(2J_* + 1)$ new constraints among them. Of course, this is not exactly true because some of $2(2J_* + 1)$ constraints are not independent. However, for $J_* \geq 4$, the number of new constraints $2(2J_* + 1) \gg 3$ and hence this simple counting suggests that the HNEC must rule out operators with spin $J \geq 5$.

Let us now demonstrate that this simple counting argument is indeed correct. First, consider $J = 1$. This is the simplest possible case which was studied in [157]. For $J = 1$, there are 3 independent OPE coefficients. The number of constraints

(equality) from the HNEC at each order is given by $\{1,1\}$.[29] After imposing these constraints the expectation value of the holographic null energy operator goes as $\sim \frac{1}{(1-\rho)^{d-3}}$. Similarly, for $J=2$ the number of constraints from the HNEC at each order is given by {1,1,2,1} and the total number of constraints is still less than the number of independent OPE coefficients [157].

For $J=3$, the sequence is $\{1,1,2,2,2,1\}$ (see appendix B.5) and hence spin-3 operators were completely ruled out at the order $\frac{1}{(1-\rho)^{d-2}}$. If we increase the spin by 1, we find that the number of constraints from the HNEC at each order is $\{1,1,2,2,3,2,1,0\}$ (see appendix B.6). The zero at the end indicates that spin-4 operators were already ruled out at the order $\frac{1}{(1-\rho)^{d-1}}$. Our simple counting suggests that the number of zeroes should increase as we go to higher spins. Explicit computation agrees with this expectation. In particular, for $J=5$, there are 15 independent OPE coefficients and the number of constraints at each order is $\{1,1,3,3,5,2,0,0,0,0\}$. Therefore the spin-5 operators are ruled out at the order $\frac{1}{(1-\rho)^{d+2}}$. Similarly, for $J=6$, there are 18 independent OPE coefficients. Explicit calculation shows that the number of constraints at each order is $\{1,1,3,3,5,5,0,0,0,0,0,0\}$. Therefore, spin-6 operators can be ruled out even at the order $\frac{1}{(1-\rho)^{d+4}}$. All of these results imply that the presence of any single trace primary operator with spin $J>2$ is not compatible with causality.

3.3.3 $\mathbf{AdS_4/CFT_3}$

Similar to the $D=4$ case on the gravity side, CFTs in $d=3$ are special. Of course, large-N CFTs with a sparse spectrum in $(2+1)$-dimensions are still holographic

[29] The n-th element of the sequence $\{c_1,\cdots,c_n,\cdots,c_{2J}\}$ represents the number of independent constraints at the order n.

and the HNEC once again implies that higher spin single trace operators with $\Delta \ll \Delta_{gap}$ are ruled out. However, there are several aspects of the $d = 3$ CFTs which are different from the higher dimensional case.

First of all, in CFT_3 the three-point functions $\langle X_J X_J T\rangle$ have both parity even and parity odd structures for any J

$$\langle X_J X_J T\rangle = \langle X_J X_J T\rangle_+ + \langle X_J X_J T\rangle_- \ . \tag{3.66}$$

Furthermore, the number of independent parity even structures at $d = 3$ is different from the higher dimensional case. The general three-point function (B.30) implies that after imposing permutation symmetry and conservation equation, similar to the higher dimensional case $\langle X_J X_J T\rangle_+$ should contain $3J$ independent structures. However, for $d = 3$, not all of these structures are independent. In particular, this overcounting should be corrected by setting OPE coefficients $C_{1,1,k} = 0$ for $k \geq 1$ in (B.30) [117]. Therefore, in $d = 3$, the parity even part $\langle X_J X_J T\rangle_+$ has $2J + 1$ independent OPE coefficients. Whereas, the parity odd part $\langle X_J X_J T\rangle_-$ has $2J$ independent OPE coefficients. Note that this is exactly what is expected from interactions of gravitons with higher spin fields in 4d gravity.

There is another aspect of $d = 3$ which is different from the higher dimensional case. The choice of polarization (3.58) in $d = 3$ implies that $\vec{\varepsilon}_\perp = 0$ and hence the λ-trick does not work. However, the full set of bounds can be obtained by considering the full polarization tensor for X_J. This can be achieved by using the projection operator of [117] which makes the analysis more complicated. However the final conclusion remains unchanged.

Since we expect that the HNEC imposes stronger constraints as we increase the spin, it is sufficient to only rule out $X_{J=3}$. The steps are exactly the same but details are little different. After imposing permutation symmetry and conservation

equation, the three-point function $\langle X_{J=3} X_{J=3} T \rangle$ has 7 parity even and 6 parity odd independent OPE coefficients. We again compute the expectation value of the holographic null energy operator $\mathcal{E}(\rho)$ in states created by smeared $X_{J=3}$:

$$|\Psi\rangle = \int dy^1 dy^2 \, \epsilon^{\mu_1\mu_2\mu_3} X_{\mu_1\mu_2\mu_3}(-i\delta, y^1, y^2)|0\rangle \ , \tag{3.67}$$

where $\epsilon^{\mu_1\mu_2\mu_3}$ is the traceless symmetric polarization tensor. Using the techniques developed in [157], we now compute the expectation value of the holographic null energy operator $\mathcal{E}(\rho)$ in this state which can be schematically expressed in the following form

$$\mathcal{E}(\rho) = \sum_{n=1}^{6} \frac{j_n(\epsilon^{\mu_1\mu_2\mu_3}, C_{i,j,k})}{(1-\rho)^n} + j_0(\epsilon^{\mu_1\mu_2\mu_3}, C_{i,j,k}) \ln(1-\rho) + \cdots \ , \tag{3.68}$$

where $j_n(\epsilon^{\mu_1\mu_2\mu_3}, C_{i,j,k})$ are specific functions of the the polarization tensors and the OPE coefficients. The dots in the above expression represent terms that vanish in the limit $\rho \to 1$. The $\ln(1-\rho)$ term is unique to the 3d case and is a manifestation of soft graviton effects in the IR.

By applying the HNEC order by order in the limit $\rho \to 1$, we again find that the HNEC can only be satisfied for all polarizations if and only if all the OPE coefficients vanish. Consequently, the Ward identity implies that we cannot have individual spin-3 operators in the spectrum.[30] Moreover, a simple counting again suggests that the same is true even for $J > 3$. In $d = 3$, as we increase the spin by one, the number of parity even OPE coefficients increases by 2. However, now there are two more orders perturbatively in $(1-\rho)$ that generate new relations among the OPE coefficients. Each new order produces at least one new constraint suggesting that if the HNEC rules out parity even operators with some particular spin J, it will also rule out all parity even operators with spin $J+1$. In addition, it is

[30] As explained in appendix B.7 it is still possible to use the λ-trick to derive constraints in dimension $d = 3$. This implies that individual spin-4 single trace operators (at least the parity even part) are also ruled out.

straightforward to extend this argument to include parity odd structures, however, we will not do so in this paper.

3.3.4 Maldacena-Zhiboedov Theorem and Massless Higher Spin Fields

In this section we argued that in holographic CFTs, any higher spin single trace non-conserved primary operator violates causality. On the gravity side, this rules out any higher spin massive field with mass below the cut-off scale (for example the string scale). But what about massless higher spin fields? In asymptotically flat spacetime, this question has already been answered by the Weinberg-Witten/Porrati theorem [**?**, **?**]. The same statement can be proven in AdS by using the argument of this section but for conserved $X_J \equiv \mathcal{J}$. Conservation of $\mathcal{J}$ leads to additional relations among the OPE coefficients $C_{i,j,k}$'s in $\langle \mathcal{J}\mathcal{J}T\rangle$. Even before we impose these additional conservation relations, the HNEC implies $C_{i,j,k} = 0$ for $J > 2$, which is obviously consistent with these new relations from conservation. Hence, our argument is valid even for higher spin conserved current $\mathcal{J}$.

Causality of CFT four-point functions in the lightcone limit also rules out a finite number of conserved higher spin currents in any CFT [58]. This is a partial generalization of the Maldacena-Zhiboedov theorem [108], from $d = 3$ to higher dimensions. The argument which was used in [58] to rule out higher spin conserved current is not applicable here since $\mathcal{J}$ does not contribute to generic CFT four-point functions as exchange operators.[31] However, we can repeat the argument of [58] for a mixed correlator $\langle \mathcal{O}\mathcal{O}\mathcal{O}\mathcal{O}\rangle$ in the lightcone limit where, $\mathcal{O} \equiv \mathcal{T} + \mathcal{J}$. For this

[31] Let us recall that none of the operators are charged under $\mathcal{J}$ and hence one can tune $\langle \mathcal{J}OO\rangle = 0$ for any O. Consequently, $\mathcal{J}$ does not contribute as an exchange operator.

mixed correlator, $\mathcal{J}$ does contribute as an exchange operator in the lightcone limit. In particular, we can schematically write

$$\langle\mathcal{O}\mathcal{O}\mathcal{O}\mathcal{O}\rangle = \quad + \quad + \quad + \cdots \,, \tag{3.69}$$

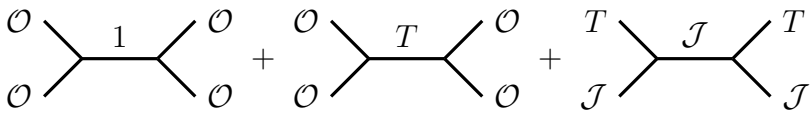

where each diagram represents a spinning conformal block and dots represent contributions suppressed by the lightcone limit. The argument of [58], now applied to the correlator $\langle\mathcal{O}\mathcal{O}\mathcal{O}\mathcal{O}\rangle$, implies that this correlator is causal if and only if the last term in (3.69) is identically zero. The $\mathcal{J}$-exchange conformal blocks, for $J > 2$, in the lightcone grow faster than allowed by causality. This necessarily requires that the three-point function $\langle\mathcal{J}\mathcal{J}T\rangle$ must vanish – which is sufficient to rule out $\mathcal{J}$ for $J > 2$. This generalizes the argument of [58] ruling out higher spin conserved currents even when none of the operators are charged under it. We should note that technically it might be plausible for the OPE coefficients to conspire in a non-trivial way such that a conserved current $\mathcal{J}$ cannot contribute as an exchange operator (for all polarizations of the external operators) but still has a non-vanishing $\langle\mathcal{J}\mathcal{J}T\rangle$. However, it is very unlikely that such a cancellation is possible since the three-point function $\langle\mathcal{J}\mathcal{J}T\rangle$ can only have three independent OPE coefficients. This unlikely scenario can be ruled out by explicit calculations.

The above argument is applicable only because $\mathcal{J}$ is conserved. However, one might expect that a similar argument in the Regge limit should rule out even non-conserved X_J for holographic CFTs. This is probably true but the argument is more subtle in the Regge limit because an infinite tower of double trace operators also contribute to the correlator $\langle\mathcal{O}\mathcal{O}\mathcal{O}\mathcal{O}\rangle$. Hence, one needs to smear all four operators appropriately, in a way similar to [152, 155], such that the double trace contributions are projected out. One might then use causality/chaos bounds to rule

out the three-point function $\langle X_J X_J T\rangle$. However, it is possible that the smearing procedure sets contributions from certain spinning structures in $\langle X_J X_J T\rangle$ to zero as well. In that case, this argument will not be sufficient. A proof along this line requires the computation of a completely smeared spinning Regge correlator which is technically challenging even in the holographic limit.

3.3.5 Comments

Small Deviation from the Holographic Conditions

Large-N CFTs with a sparse spectrum are indeed special because at low energies they exhibit gravity-like behavior. This immediately poses a question about the assumptions of large-N and sparse spectrum: how rigid are these conditions? In other words, do we still get a consistent CFT if we allow small deviations away from these conditions?

In this section, we answered a version of this question for the sparseness condition. The sparseness condition requires that any single trace primary operator with spin $J > 2$, must necessarily have dimension $\Delta \geq \Delta_{gap} \gg 1$. This condition ensures that the dual gravity theory has a low energy description given by Einstein gravity. However, we can imagine a small deviation from this condition by allowing a finite number of additional higher spin single trace primary operators X_J with $J > 2$ and scaling dimension $\Delta \ll \Delta_{\text{gap}}$. As we have shown in this section, these new operators violate the HNEC implying the resulting CFTs are acausal.

Minkowski vs AdS

It is rather apparent that the technical details of the flat spacetime argument and the AdS argument are very similar. For example, the number of independent structures for a particular spin is the same in both cases. In flat spacetime as well as in AdS, we start with inequalities which can be interpreted as some kind of time-delay. In addition, these inequalities when applied order by order, lead to equalities among various structures. These equalities eventually rule out higher spin particles. However, the AdS argument has one conceptual advantage, namely, it does not require any additional assumption about the exponentiation of the leading contribution. The CFT-based argument relies on the HNEC. The derivation of the HNEC utilized the causality of a CFT correlator which was designed to probe high energy scattering deep into the AdS bulk. It is therefore not a coincidence that the technical details of the AdS and the flat space arguments are so similar. Since the local high energy scattering is insensitive to the spacetime curvature, it is not very surprising that the bounds in flat space and in AdS are identical. This also suggests that the same bound should hold even in de Sitter.

Higher Spin Operators in Generic CFTs

The argument of this section does not rule out higher spin non-conserved operators in non-holographic CFTs. However, the HNEC in certain limits can be utilized to constrain interactions of higher spin operators even in generic CFTs. In particular, the limit $\rho \to 0$ in (3.54) corresponds to the lightcone limit and in this limit, the HNEC becomes the averaged null energy condition (ANEC). The proof of the ANEC [57, 79] implies that in the limit $\rho \to 0$, the inequality $\mathcal{E}(\rho) \geq 0$ must be true

for any interacting CFT in $d \geq 3$. Moreover in this limit, the HNEC is equivalent to the conformal collider setup of [56] which is known to yield optimal bounds. Therefore, the same computation performed in the limit $\rho \to 0$ can be used to derive non-trivial but weaker constraints on the three-point functions $\langle X_J X_J T \rangle$ which are true for any interacting CFT in $d \geq 3$. These constraints, even though easy to obtain from our calculations of $\mathcal{E}(\rho)$, are rather long and complicated and we will not transcribe them here.

Other Applications of the Regge OPE

In this note we specialized $\mathbb{E}_{\Delta,J}$ to the case of $\Delta = d$ and $J = 2$ to arrive at the HNEC operator in order to make use of the universality of the stress-tensor Regge trajectory in holographic theories. However $\mathbb{E}_{\Delta,J}$ more generally describes the contribution of any operator to the Regge OPE of identical scalar operators. It would be interesting to find the actual spectrum of these operators contributing to the Regge limit of the OPE in specific theories. It would also be worthwhile to try and understand the subleading contributions to the Regge OPE in holographic theories. Although these contributions are not universal, we expect that causality will impose constraints on these contributions as well.

We have explored the Regge limit of the OPE of two identical scalars. Generalization to other representations is straightforward as it only requires knowledge of the CFT three-point functions whose functional form is fixed by symmetry. Positivity of these generalized Regge OPE operators will likely lead to new constraints since they allow access to more general representations. Furthermore decomposition of the additional Lorentz indices under the little group will result on more constraint equations which need to be satisfied to preserve causality.

3.4 Restoring Causality

3.4.1 Make CFT Causal Again

In the previous section, we considered large-N CFTs in $d \geq 3$ dimensions with the property that the lightest single trace operator with spin $J > 2$ has dimension $\Delta \equiv \Delta_{\text{gap}} \gg 1$. These holographic conditions are equivalent to the statement that in the gravity side the low energy behavior is governed by the Einstein gravity. Moreover, Δ_{gap} corresponds to the scale of new physics Λ in the effective action in AdS (for example it can be the string scale M_s). In any sensible theory of quantum gravity it is expected that the Einstein-Hilbert action should receive higher derivative corrections which are suppressed by the scale Λ. On the CFT side, this translates into the fact that there is an infinite tower of higher spin operators with dimensions above the Δ_{gap}. All of these higher spin operators must appear as exchange operators in CFT four-point functions in order to restore causality at high energies [152]. Furthermore, in this paper we showed that the sparseness condition is very rigid and we are not allowed to add an additional higher spin operator X_J with spin $J > 2$ and $\Delta \ll \Delta_{\text{gap}}$ if causality is to be preserved. Let us consider adding an additional higher spin primary single trace operator X_J with dimension $\Delta = \Delta_0 \ll \Delta_{\text{gap}}$ (or on the gravity side a higher spin particle with mass $M_0 \ll \Lambda$) and ask whether it is possible to restore causality by adding one or more primary operators (or new particles) that cancel the causality violating contributions? In this section, we answer this question from the CFT side.

The bound obtained in the previous section from the HNEC is expected to be exact strictly in the limit $\Delta_{\text{gap}} \to \infty$. However, it is easy to see that the same

conclusion is true even when Δ_{gap} is large but finite, as long as $\Delta_0 \ll \Delta_{\text{gap}}$. In this case, one might expect that the OPE coefficients are no longer exactly zero but receive corrections $C_{i,j,k}/C_{X_J} \sim \frac{1}{\Delta_{\text{gap}}^a}$, where a is some positive number.[32] However, this is inconsistent with the Ward identity which requires that at least some of $C_{i,j,k}/C_{X_J} \sim \mathcal{O}(\infty)$. Therefore, even for large but finite Δ_{gap}, the operator X_J is ruled out as long as $\Delta_0 \ll \Delta_{\text{gap}}$. In addition, this also implies that if we want to add X_J, it will not be possible to save causality by changing the spectrum above Δ_{gap}. Let us add extra operators at dimensions $\sim \Delta'_{\text{gap}} \ll \Delta_{\text{gap}}$ in order to restore causality. Note that if $\Delta'_{\text{gap}} \gg \Delta_0$, then contributions of these extra operators are expected to be suppressed by Δ'_{gap} and hence we can again make the above argument. Therefore, contributions of these extra operators can be significant enough to restore causality if and only if $\Delta'_{\text{gap}} \sim \Delta_0$.

The above argument also implies that perturbative $1/N$ effects are not sufficient to save causality either. Any such correction must be suppressed by positive powers of $1/N$ and hence inconsistent with the Ward identity. This is also clear from the gravity side, both in flat space and in AdS. Causality requires that the tree level higher spin-higher spin-graviton amplitude must vanish. One might expect that loop effects can generate a non-vanishing amplitude without violating causality, however, these effects must be $1/N$ suppressed. Hence, this scenario is in tension with the universality of gravitational interactions dictated by the equivalence principle.

The behavior of four-point functions in the Regge limit makes it obvious that these extra operators at Δ'_{gap} must have spin $J \geq 2$ so that they can contribute significantly in the Regge limit to restore causality. Furthermore, causality imposes strong restrictions on what higher spin operators can be added at Δ'_{gap}. The

[32] C_{X_J} is the coefficient of the two-point function of X_J and $C_{i,j,k}$ are the OPE coefficients for $\langle X_J X_J T\rangle$ (see appendix B.4).

simplest possibility is to add a finite or infinite set of higher spin operators at Δ'_{gap} which do not contribute as exchange operators in any four-point functions. However, this scenario makes the causality problem even worse. The causality of the Regge four point functions still leads to the HNEC and one can rule out even an infinite set of such operators by applying the HNEC to individual higher spin operators. The only other possibility is to add a set of higher spin operators at Δ'_{gap} which do contribute as exchange operators in the four-point function $\langle X_J X_J \psi\psi\rangle$, where ψ is a heavy scalar operator. In this case2, the HNEC is no longer applicable and hence the argument of the previous section breaks down. However, a finite number of higher spin primaries ($J > 2$) that contribute as exchange operators violate chaos/causality bound [27, 152] and consequently this scenario necessarily requires an infinite tower of higher spin operators.[33] Therefore, the only way causality can be restored is to add an infinite tower of finely tuned higher spin primaries with $\Delta \sim \Delta'_{\text{gap}} \sim \Delta_0$. In other words, addition of a single higher spin operator with $\Delta = \Delta_0$ necessarily brings down the gap to Δ_0.

Let us note that the above argument did not require that this new tower of operators contribute to the TT OPE. For this reason, one might hope that it is possible to fine-tune the higher spin operators such that causality is restored and the gap is still at Δ_{gap} when considering states created by the stress tensor. However, this scenario is also not allowed as we explain next. In this case, one can still prove the HNEC starting from the Regge OPE of TT when both operators are smeared appropriately (see [157]). One can then repeat the argument of the previous section to rule out X_J, as well as the entire tower of operators at Δ'_{gap}.

[33] Note that the chaos bound does not directly rule out spin-2 exchange operators. Therefore, one might expect that the causality problem may be resolved by adding a finite number of spin-2 non-conserved single trace primaries. However, it was shown in [46] that non-conserved spin-2 primaries when contribute as exchange operators lead to additional causality violation and hence we will not consider this scenario.

Therefore, the only way the tower at $\Delta'_{\text{gap}} \sim \Delta_0$ can lead to a causal CFT is if they also contribute to the TT OPE. In particular, an infinite subset of all higher spin operators must appear in the OPE of the stress tensor (and all low spin operators)

$$TT \sim \sum_J X_J \ . \tag{3.70}$$

Let us end this section by summarizing in the gravity language. At the energy scale $E \ll \Lambda$, the dynamics of gravitons is completely determined by the Einstein-Hilbert action. If we wish to add even one higher spin elementary particle ($J > 2$) with mass $M_0 \ll \Lambda$, the only way for the theory to remain causal is if we also add an infinite tower of higher spin particles with mass $\sim M_0$. Causality also requires that an infinite subset of these new higher spin particles should be able to decay into two gravitons. As a result, the dynamics of graviton can now be approximated by the the Einstein-Hilbert action only in the energy scale $E \ll M_0$ and hence M_0 is the new cut-off even if we only consider external states created by gravitons.

3.4.2 Stringy Operators above the Gap

We concluded from both gravity and CFT arguments that finitely many higher spin fields with scaling dimensions $\Delta \ll \Delta_{gap}$ are inconsistent with causality even as external operators. We can ask how this result may be modified if we consider external operator X to be a heavy state above the gap, analogous to stringy states in classical string theory.

Let us consider the expectation value of the generalized HNEC operator (3.50) in the Hofman-Maldacena states created by a heavy single-trace higher spin operator

with spin l. Following [154] we parametrize the leading Regge trajectory as

$$j(\nu) = 2 - \frac{1}{\Delta_{gap}^2}\left(\frac{d^2}{4} + \nu^2\right) + \mathcal{O}\left(\frac{1}{\Delta_{gap}^4}\right) \ . \tag{3.71}$$

The external operator has the scaling dimension $\Delta_X \geq \Delta_{gap}$. Consequently, we cannot take the $\Delta_{gap} \to \infty$ limit as before. Instead we must take Δ_{gap} to be large but finite and keep track of terms that may grow in this limit. In the Regge limit $u \to \infty$, with $1 - \rho \gtrsim \frac{\log(u)}{\Delta_{gap}^2}$, we expect the leading trajectory to be nearly flat and integration over the spectral density (3.50) to be approximated by the stress-tensor contribution at $\nu = -i\frac{d}{2}$ up to $\frac{1}{\Delta_{\text{gap}}^2}$ corrections. This limit is similar to the discussion in section 5.5 in [153] for bounds on real part of phase shift for scattering in AdS. See also discussion about imaginary part of phase shift for AdS scattering in [153, 154, 156].

Therefore the operator with a positive expectation value is given by[34]

$$u\langle \mathbb{E}_{\Delta(J=2),2}(\rho)\rangle_X = u\sum_{i=0}^{2l} \frac{t^{(i)}}{(1-\rho)^{d-3+i}} + \cdots \ , \tag{3.72}$$

where the dots denote terms which are subleading in Δ_{gap}, $t^{(i)}$'s consist of certain combination of OPE coefficients and polarization tensors. The OPE coefficients $t^{(i)}$, are analytic continuation of original OPE coefficients. We have already seen that if the OPE coefficients do not grow with Δ_{gap}, the existence of the operator X is inconsistent with causality. One way in which causality may be restored, is to impose the following gap dependence on the OPE coefficients between heavy operators and the exchange operator[35]:

$$\frac{t^{(i)}}{t^{(0)}} \lesssim \frac{1}{\Delta_{gap}^i} \ . \tag{3.73}$$

[34] The second line follows from the fact that at large Δ_{gap} the saddle point is dominated by the stress-tensor. Here we have assumed that the OPE coefficients do not scale exponentially with increasing Δ_{gap} and hence will not affect the saddle-point.

[35] In fact, in the case of stress-tensor exchange, Ward identities forces at least one combination of OPE coefficients to grow with $\Delta_X \sim \Delta_{gap}$.

The dependence of OPE coefficients on Δ_{gap} is chosen in (3.73) such that higher negative powers of $1-\rho$ would be multiplied by higher powers of $\frac{1}{\Delta_{gap}}$ and consequently become more suppressed in the regime of validity of stress-tensor exchange. This means that we would not get the previous constraints by sending $\rho \to 1$ and as a result, there is no inconsistency with Ward identity or causality for higher spin operators above the gap.

Based on our CFT arguments, (3.73) is not fixed to be the unique choice which restores causality. However, this behaviour is very similar to how the scattering amplitude in classical string theory is consistent with causality. The high energy limit of scattering amplitudes in string theory are explored in [184–188]. In addition, generating functions of three point and four point amplitudes for strings on the leading Regge trajectory with arbitrary spin are constructed in [189, 190]. Here we focus on a high energy limit of a two to two scattering between closed higher spin strings and tachyons in bosonic string theory. Using the results of [189, 190], the string amplitude is given by the compact expression

$$M(s,t) = (\text{POL})\frac{\Gamma(-\frac{\alpha' s}{4})\Gamma(-\frac{\alpha' t}{4})\Gamma(-\frac{\alpha' u}{4})}{\Gamma(1+\frac{\alpha' s}{4})\Gamma(1+\frac{\alpha' t}{4})\Gamma(1+\frac{\alpha' u}{4})}\,, \tag{3.74}$$

where the Mandelstam variables satisfy $s+t+u = \frac{4}{\alpha'}(l-4)$ for closed strings. Here, (POL) represents the tensor structures and polynomials of different momenta. The Gamma functions poles in the numerator of (3.74) correspond to the exchange of infinitely many higher spin particles with even spins and the mass relation $m(J)^2 = \frac{2}{\alpha'}(J-2)$. In the Regge limit, $s \to \infty$ with t held fixed, the amplitude simplifies to

$$M(s,t) \approx (\text{POL})\frac{\Gamma(-\frac{\alpha' t}{4})}{\Gamma(1+\frac{\alpha' t}{4})}\left(-i\frac{s\alpha'}{4}\right)^{-2+\frac{\alpha' t}{2}}\,. \tag{3.75}$$

Note that the Mandelstam variable s plays the same role as u in the CFT analogue. Therefore, to make gravity the dominant force we can either take $\alpha' \to 0$ which

corresponds to $\Delta_{\text{gap}} \to \infty$ in the CFT, or take $t \to 0$ which in CFT language is the lightcone limit $\rho \to 0$. In both cases, the polarization part, (POL) becomes

$$\lim_{\alpha' \to 0 \text{ or } t \to 0} (\text{POL}) \propto s^4 \mathcal{E}_{1\mu_1\mu_2\cdots\mu_l} \mathcal{E}_3{}^{\mu_1\mu_2\cdots\mu_l} \ , \tag{3.76}$$

where powers of s are dictated by consistency with the gravity result in limits mentioned above. Note that the tensor structure in (3.76) is independent of the momenta and does not change sign even if we perform the eikonal experiment in this limit. Thus, in the limit that gravity is dominant, possible causality violating structures are also vanishing and there is no problem with causality. This happens naturally in string theory since there is only one scale α', controlling coefficients in tensor structures, interactions between particles and their masses. As a result, vertices or tensor structures which have higher powers of momentum $\vec{q}$ (analogous to powers of $\frac{1}{1-\rho}$ in CFT) should be accompanied with higher powers of $\sqrt{\alpha'}$ (analogous to powers of $\frac{1}{\Delta_{gap}}$) on dimensional grounds. See also [46, 191] for interesting details of eikonal experiment in string theory.

3.5 Cosmological Implications

The bound on higher spin particles has a natural application in inflation. The epoch of inflation is a quasi de Sitter expansion of the universe, immediately after the big bang. The primordial cosmological fluctuations produced during inflation naturally explains the observed temperature fluctuations of cosmic microwave background (CMB) and the large-scale structures of the universe. If higher spin particles were present during inflation, they would affect the behavior of primordial cosmological fluctuations. In particular, higher spin particles would produce distinct signatures on the three-point function of scalar perturbations in the squeezed limit. Hence,

the bound on higher spin particles imposes rather strong constraints on these three-point functions.

Consider one or more higher spin particles during inflation. The approximate de Sitter symmetry during inflation dictates that mass of any such particle, even before we impose our causality constraints, must satisfy the Higuchi bound [192, 193]

$$m^2 > J(J-1)H^2 \ , \tag{3.77}$$

where, H is the Hubble rate during inflation. Particles with masses that violate the Higuchi bound correspond to non-unitary representations in de Sitter space, so the Higuchi bound is analogous to the unitarity bound in CFT.[36] The bound on higher spin particles obtained in this paper are valid in flat and AdS spacetime. We will not attempt to derive similar bounds directly in de Sitter. Instead, we will adopt the point of view of [46, 161] and assume that the same bounds hold even in de Sitter spacetime. This is indeed a reasonable assumption since these bounds were obtained by studying local high energy scattering which is insensitive to the spacetime curvature. Therefore, in de Sitter spacetime in Einstein gravity, any additional elementary particle with spin $J > 2$ cannot have a mass $m \lesssim \Lambda$, where Λ is the scale of new physics in the original effective action. In any sensible low energy theory we must have $H \ll \Lambda$ and hence the causality bound is stronger than the Higuchi bound. Furthermore, the causality bound also implies that all elementary higher spin particles must belong to the principal series of unitary representation of the de Sitter isometry group.

Inflation naturally predicts that the scalar curvature perturbation ζ produced during inflation is nearly scale invariant and Gaussian. The momentum space

[36] We should note that certain discrete values of mass below the Higuchi bound are also allowed. See [194] for a nice review.

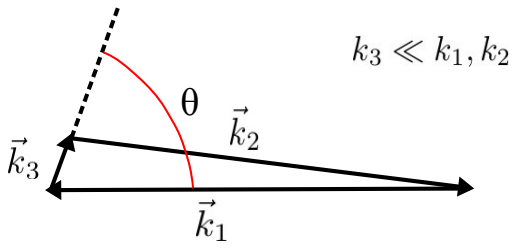

Figure 3.7: The squeezed limit of three-point functions.

three-point function of the scalar curvature perturbation $\langle\zeta(\vec{k}_1)\zeta(\vec{k}_2)\zeta(\vec{k}_3)\rangle$ is a good measure of the deviation from exact Gaussianity. Higher spin particles affect the three-point function of scalar perturbations in a unique way. In an inflating universe, the massive higher spin particles can be spontaneously created. It was shown in [160] that the spontaneous creation of higher spin particles produces characteristic signatures on the late time three-point function of scalar fluctuations. In particular, in the squeezed limit $k_1, k_2 \gg k_3$ (see figure 3.7), the late time scalar three-point function admits an expansion in spin of the new particles present during inflation:[37]

$$\frac{\langle\zeta(\vec{k}_1)\zeta(\vec{k}_2)\zeta(\vec{k}_3)\rangle}{\langle\zeta(\vec{k}_1)\zeta(-\vec{k}_1)\rangle\langle\zeta(\vec{k}_3)\zeta(-\vec{k}_3)\rangle} \sim \epsilon M_{Pl}^2 \sum_J \lambda_J^2 \; I_J\left(\frac{m_J}{H}, \frac{k_3}{k_1}\right) P_J(\cos\theta) \;, \tag{3.78}$$

where ϵ is one of the slow roll parameters and λ_J is the coupling between ζ and the higher spin particle with mass m_J and spin J. $P_J(\cos\theta)$ is the Legendre polynomial whose index is fixed by the spin of the particle and θ is the angle between vectors $\vec{k}_1$ and $\vec{k}_3$. The exact form of the function $I_J\left(\frac{m_J}{H}, \frac{k_3}{k_1}\right)$ can be found in [160]. The bound on higher spin particles from causality implies that $m_J \sim \Lambda \gg H$ for $J > 2$ and hence

$$I_J\left(\frac{m_J}{H}, \frac{k_3}{k_1}\right) \sim -\pi^2 e^{-\frac{2\pi\Lambda}{H}} \left(\frac{\Lambda}{H}\right)^{2J-3} \left(\frac{k_3}{k_1}\right)^{3/2} \mathrm{Re}\left[e^{\frac{i\pi}{4}} \left(\frac{k_3}{4k_1}\right)^{i\frac{\Lambda}{H}}\right] \;. \tag{3.79}$$

[37] For simplicity of notation, we are omitting the Dirac delta functions.

The oscillatory behavior of the above expression is a consequence of a quantum interference effect between two different processes [160]. Moreover, the above expression also implies that contributions of higher spins to the three-point function in the squeezed limit must be exponentially suppressed. The exponential suppression can be understood as the probability for the spontaneous production of massive higher spin particles in the principal series at de Sitter temperature $T_{dS} = H/2\pi$.

Now, if I_J with $J > 2$ is detected in future experiments, then the scale of new physics must be $\Lambda \sim H$. This necessarily requires the presence of not one but an infinite tower of higher spin particles with spins $J > 2$ and masses comparable to the Hubble scale. This scenario is very similar to string theory. Any detection of I_J with $J > 2$ can be interpreted as evidence in favor of string theory with the string scale comparable to the Hubble scale and a very weak coupling which explains small H/M_{pl}.

It is obvious from (3.78) that the effects of higher spin particles are always suppressed by the slow roll parameter and hence not observable in the near future. The derivation of (3.78) relied heavily on the approximate conformal invariance of the inflationary background. This approximate conformal invariance is also responsible for the slow roll suppression. However, if we allow for a large breaking of conformal invariance, the signatures of massive higher spin particles can be large enough to be detected by future experiments. In particular, using the framework of effective field theory of inflation it was shown in [195] that there are interesting scenarios in which higher spin particles contribute significantly to the scalar non-Gaussanity. Furthermore, it was shown in [195] that higher spin particles can also produce detectable as well as distinctive signatures on the scalar-scalar-graviton three-point function in the squeezed limit. Experimental exploration of this form

of non-Gaussanity through the measurement of the $\langle BTT \rangle$ correlator of CMB anisotropies can actually be a reality in the near future [195]. In fact, in the most optimistic scenario, the proposed CMB Stage IV experiments [196] will be sensitive enough to detect massive higher spin particles, providing indirect evidence in favor of a theory which is very similar to low scale string theory.

Acknowledgements

It is our pleasure to thank Tom Hartman for several helpful discussions as well as comments on a draft. We would also like to thank Nima Arkani-Hamed, Ibou Bah, Brando Bellazzini, James Bonifacio, Ted Jacobson, Marc Kamionkowski, David Kaplan, Jared Kaplan, Petr Kravchuk, David Meltzer, Joao Penedones, Eric Perlmutter, and David Simmons-Duffin for discussions. The work of NAJ and AT is supported by Simons Foundation grant 488643. SK is supported by the Simons Collaboration Grant on the Non-Perturbative Bootstrap. We are grateful to Caltech and the Simons Bootstrap Collaboration for hospitality and support during the Bootstrap 2018 workshop where part of this work was completed.

CHAPTER 4

FAST CONFORMAL BOOTSTRAP AND CONSTRAINTS ON 3D GRAVITY

Abstract[1]

The crossing equations of a conformal field theory can be systematically truncated to a finite, closed system of polynomial equations. In certain cases, solutions of the truncated equations place strict bounds on the space of all unitary CFTs. We describe the conditions under which this holds, and use the results to develop a fast algorithm for modular bootstrap in 2d CFT. We then apply it to compute spectral gaps to very high precision, find scaling dimensions for over a thousand operators, and extend the numerical bootstrap to the regime of large central charge, relevant to holography. This leads to new bounds on the spectrum of black holes in three-dimensional gravity. We provide numerical evidence that the asymptotic bound on the spectral gap from spinless modular bootstrap, at large central charge c, is $\Delta_1 \lesssim c/9.1$.

[1]This chapter is based on the paper [73].

4.1 Introduction

The conformal bootstrap is a rapidly growing array of techniques to solve strongly interacting quantum field theories. It had early success in two spacetime dimensions [197], and more recently has proved successful in higher dimensions [52]. An important impetus has been the development of numerical techniques to analyze the crossing equations, starting with the introduction of the functional bootstrap method in 2008 by Rattazzi, Rychkov, Tonni, and Vichi [198]. This method uses linear (or semidefinite [199]) programming to constrain solutions to the crossing equations, thereby carving out the allowed parameter space of unitary CFTs. It has also been used to solve individual CFTs, including the 3d critical Ising model [200, 201]. The method relies on finding extremal functionals, often numerically, which bound the space of CFTs, and in certain cases encode the spectrum of the target theory [202, 203].

Despite this exciting progress, the current numerical methods are in their infancy, and there are many potential areas for improvement, both technical and conceptual. For example, with semidefinite programming, there is no clear way to leverage analytic results, such as the spectrum at high spin, to improve the numerics [204]. This is a tantalizing hint that much more efficient algorithms are waiting to be discovered. Such algorithms, combined with powerful analytics, will be needed to address certain physics problems, such as solving theories with large global symmetries [205, 206], pushing bootstrap into the hydrodynamic regime [207, 208], or exploring the boundaries of quantum gravity by combining numerical bootstrap with AdS/CFT in the black hole regime.

In this paper, we develop a new algorithm for numerical bootstrap, and apply

it to 3d gravity. The method is based on solving truncated crossing equations. It builds on one of the extremal functional methods of El-Showk and Paulos [209], and is very similar in many respects, but differs in some important details that extend the reach by several orders of magnitude. In principle, these methods are general, but in practice, they are limited to a certain class of bootstrap problems, where one can easily generate approximate solutions to the truncated equations. We will show that this is possible for the modular bootstrap problem relevant to 3d gravity.

The modular bootstrap is a variant of the conformal bootstrap introduced by Hellerman to constrain the spectrum of 2d CFTs [72]. Hellerman used it to prove analytically that any theory of 3d gravity has a primary operator with scaling dimension $\Delta \lesssim c/6$. From a holographic point of view, this bound is perhaps weaker than expected, because all known theories of 3d gravity have BTZ black holes [210] starting at $\Delta \sim c/12$. The bound can be systematically improved by numerics, but the difficulty grows rapidly with c [211, 212]. Previous numerical calculations were effective only for $c \lesssim 100$ and did not reach the semiclassical regime — the bound had not converged in c, and it was not possible to estimate the asymptotics. A stronger bound is worth pursuing, because if it could be pushed down to the black hole threshold, then the numerics could also potentially be used to construct or rule out candidate theories of 3d gravity, or to suggest new analytic methods.

Using our algorithm, we extend the modular bootstrap up to $c \sim 1800$. This central charge appears to be in the semiclassical regime, where the bound has nearly converged, and we estimate the asymptotic bound to be $\Delta \lesssim c/9.1$. This estimate relies on an extrapolation in c, which appears to be reliable, but strictly

speaking it is impossible to rule out a stronger bound as $c \to \infty$. Our bound is not at the black hole threshold, so unfortunately cannot be used to construct candidate theories of 3d gravity or to address the questions above. We have not included the constraints from spin; it is possible that incorporating spin would lead to a stronger bound that saturates the black hole threshold.

The functional bootstrap is an expansion in derivatives, truncated at some order N_{deriv}. Our calculations are performed up to derivative order $N_{\text{deriv}} \sim 5000$. For a given c, this takes several CPU-hours on a standard laptop. It is impossible to make a direct comparison to existing methods, but a rough extrapolation suggests that semidefinite programming would require at least 10^7 CPU-hours to perform the same calculation. A basic version of our algorithm, sufficient for modular bootstrap, is straightforward to implement in Mathematica with a few dozen lines of code.

On the down side, our methods do not generalize in any obvious way to bootstrap problems with spin. This has (so far) prevented us from applying the algorithm to the spinning modular bootstrap, or to the 3d critical Ising model.

We begin with a review of the crossing equations and a summary of the truncation in section 4.2. We explain under what circumstances the truncated equations can be used to place general bounds. In section 4.3 we review the functional method, introduce a new method to optimize bootstrap functionals, and show that it is Lagrange dual to the truncation method. Section 4.4 describes the algorithm, and in section 4.5 it is applied to modular bootstrap and 3d gravity.

Comparing our results to semidefinite programming requires very accurate bounds. In a standalone appendix C.3, we describe a method to find high precision bounds with linear programming, which has some advantages over the standard

bisection method.

Although we have stressed the computational aspects, it seems likely that the truncated crossing equations can also be solving analytically in various limits — lightcone [43, 107], large N [42], short distance [213], etc. This could be used to derive analytic bounds, to jumpstart the numerics, or to develop variational methods that go to much higher orders. We consider it likely that with more refinement, numerical methods can be extended to functionals with millions of derivatives. Further discussion of the outlook, including the challenges presented by problems with spin, is in section 4.6.

4.2 Truncating the Primal Bootstrap

The functional bootstrap is an optimization problem, and as such, it has a *primal* and *dual* formulation. The primal bootstrap refers to the crossing equations themselves. The dual approach uses linear functionals. We will rely on both pictures, starting on the primal side. In this section and section 4.3, we consider a broad class of spinless bootstrap problems. We will specialize later to modular bootstrap.

4.2.1 Setup

Consider a crossing equation of the form

$$\sum_{\Delta,J} a_\Delta^J W_\Delta^J(z,\bar{z}) = 0 \tag{4.1}$$

where J is spin, and $W_{\Delta,J}$ is the difference of a conformal block and a crossed block,

$$W^J_\Delta(z,\bar{z}) = g_{\Delta,J}(z,\bar{z}) - g_{\Delta,J}(1-z,1-\bar{z}) \ . \tag{4.2}$$

Unitarity requires $a^J_\Delta > 0$, and places lower bounds on Δ. Here we use the notation of the correlator bootstrap, with z and $\bar{z}$ conformal cross ratios, but the equations apply also to modular bootstrap, by replacing $(z, 1-z) \to (\tau, -1/\tau)$ with τ the torus modulus.

Following [198], let us act on (4.1) by linear functionals

$$\mathcal{F} = \sum_{m=0}^{M} \sum_{\bar{m}=0}^{\bar{M}} \alpha_{m,\bar{m}} \left. \frac{\phi^m}{\phi z^m} \frac{\phi^{\bar{m}}}{\phi \bar{z}^{\bar{m}}} \right|_{z=\bar{z}=1/2} \ . \tag{4.3}$$

(The methods may also apply to more general bases; see discussion section.) Choose a set $\{\mathcal{F}_i\}_{i=1\ldots P}$ of P such functionals, and let

$$f^J_i(\Delta) \equiv \mathcal{F}_i[W^J_\Delta(z,\bar{z})] \ , \tag{4.4}$$

where for each J, the f^J_i are linearly independent. Applying $\mathcal{F}_i$ to the crossing equation (4.1) gives

$$\sum_{\Delta,J} a^J_\Delta f^J_i(\Delta) = 0 \ , \tag{4.5}$$

(assuming the $\mathcal{F}_i$ are sufficiently well behaved to bring the derivatives inside the sum). These are the *primal* bootstrap equations. There are P equations for an infinite number of parameters: the spectrum of (Δ, J) and the coefficients a^J_Δ. After absorbing a positive prefactor into the a^J_Δ, these equations are well approximated by polynomials [52].

We will restrict our attention to bootstrap problems without spin dependence. In this case we set $z = \bar{z}$ (or $\tau = -\bar{\tau}$ in the modular bootstrap), and drop the spin label J. This class of problems includes spinless modular bootstrap, 1d correlators, the $sl(2)$ subsector of correlator bootstrap in higher dimensions.

4.2.2 Truncation

Let us take P even, and truncate to $P/2+1$ states, including the identity term with $a_0 \equiv 1$, $\Delta_0 \equiv 0$. This results in the *truncated primal equations*:

$$\sum_{\mu=0}^{P/2} a_\mu f_i(\Delta_\mu) = 0 \ . \tag{4.6}$$

This is now a closed system of P polynomial equations for P unknowns.

This seems a rather brutal truncation of the crossing equations, so at this point, it is not clear that it is useful. Nonetheless we will show that, sometimes, solutions of (4.6) can be used to place bounds on the space of all unitary CFTs.

In the numerical bootstrap, the goal is to maximize some physical quantity, such as the first scaling dimension Δ_1, over all unitary solutions to the P equations (4.5). In practice, the optimal solution has a finite number of states in the sum. If it happens that the optimal solution has exactly $P/2+1$ states, then it can be found by solving the closed equations (4.6). We will show that this is the case for 2d modular bootstrap at zero angular potential.

This leads to our main analytic result:

> *In modular bootstrap, at any order P and central charge c, there is a solution to the truncated bootstrap equations* (4.6)*, with scalar gap $\Delta_1^{(c,P)}$, such that all unitary CFTs of central charge c have $\Delta_1 \leq \Delta_1^{(c,P)}$.*

It follows that general bounds on all unitary CFTs can be found by solving (4.6). To derive this, we will show that a solution to (4.6) can be used to build an extremal functional, identical to that obtained in the usual numerical bootstrap. Note that

this claim does not apply to all solutions of (4.6), but to one special solution, which must be carefully sought among many.

This is based on the same idea used for numerical bootstrap of 1d correlators in [209]. Other approaches to the correlator bootstrap using truncated crossing equations have also been discussed in [214–216].

4.2.3 Comments on Monotonicity

The largest dimension participating in (4.6), $\Delta_{P/2}$, grows with P. Therefore the truncation order P acts as a UV cutoff. Qualitatively, there is a parallel between changing $P \to P-2$ and a renormalization group transformation: As P is decreased, the effect of high-dimension operators must be absorbed into the low-dimension spectrum and OPE coefficients, in order to preserve the crossing equations. A corollary of the result stated above is monotonicity:

Under reducing the cutoff $P \to P-2$, the gap $\Delta_1^{(c,P)}$ is non-decreasing.

Roughly speaking, we can view a solution to (4.6) as a bootstrap version of an effective field theory, in the following sense. For $P \gg 1$, the low-lying operators Δ_μ are insensitive to the truncation, and take their physical values for the target CFT. For $\mu \sim P/2$, the operators of dimension Δ_μ are not true operators in the full-fledged CFT, but are effective operators in the cutoff theory, at least for the purposes of the crossing equation. Like the higher dimension operators in a Wilsonian effective Lagrangian, they parameterize all of the contributions from the UV, and very good approximations to the low energy physics can be obtained with a finite number of effective operators. This point of view is useful to keep in

mind when interpreting solutions to the truncated equations, because we should not expect operators with $\mu \sim P/2$ to have their physical scaling dimensions; they must also encode the effects of the UV states that are removed by the truncation. We will see this effect in the numerics.

4.3 Dual Bootstrap

In this section, we derive the claims of section 4.2, by relating the primal equations to the functional bootstrap. We will first recast the functional bootstrap as a nonlinear optimization problem, then dualize to the primal equations.

4.3.1 Review

The functional method [198] relies on the following observation. Consider the action of a linear functional on W_Δ,

$$f(\Delta) = \sum_{i=1}^{P} \alpha_i f_i(\Delta) \ . \tag{4.7}$$

The α_i parameterize the functional. If we find a functional that is positive on the vacuum, and on all dimensions above some gap,

$$f(0) > 0 \quad \text{and} \quad f(\Delta) > 0 \text{ for } \Delta > \Delta_1 \tag{4.8}$$

then every term in the sum (4.1) is positive for dimensions in this range. Therefore, to satisfy crossing, every unitary CFT must have an operator at or below Δ_1.

The strongest bounds come from minimizing Δ_1. For our purposes, a useful way to state the optimization procedure is as follows. Fix P, the gap Δ_1, and the

normalization condition $\alpha_P = 1$, and:[2]

$$\begin{aligned} &\text{maximize } f(0) \text{ over } \alpha_a \\ &\text{subject to } f(\Delta) \geq 0 \text{ for } \Delta \geq \Delta_1 \ . \end{aligned} \tag{4.9}$$

Here and below, the indices run over the ranges

$$\begin{aligned} a, b, c, \ldots &= 1 \ldots P-1 \ , \\ i, j, k, \ldots &= 1 \ldots P \ . \end{aligned} \tag{4.10}$$

(4.9) is a linear program with an infinite number of constraints, or can be recast as a semidefinite program [199]. If the constraints are feasible, and the objective $f(0)$ is positive at the maximum, then the initial choice of Δ_1 is ruled out. This procedure is repeated, for different values of Δ_1, until the theory is marginally excluded, *i.e.,* $f(0) = 0$ (to some desired precision). This is the edge of the exclusion region, and the optimal functional at this point is called the extremal functional. The *dual bootstrap* refers to the problem of finding the extremal functional.

4.3.2 Functionals parameterized by zeroes

The zeroes of the extremal functional correspond to solutions of the primal equations (4.5). This is a general fact of linear programs, which has been used to find the spectrum of various CFTs, including the critical Ising model in two [203] and three [201] dimensions.

In certain spinless bootstrap problems, including modular bootstrap, the extremal functional has a very simple pattern of zeroes. Empirically, for even P, there

[2]Generally, the optimum may occur either for $\alpha_P > 0$ or $\alpha_P < 0$. We choose the overall sign of the functionals such that it is always positive.

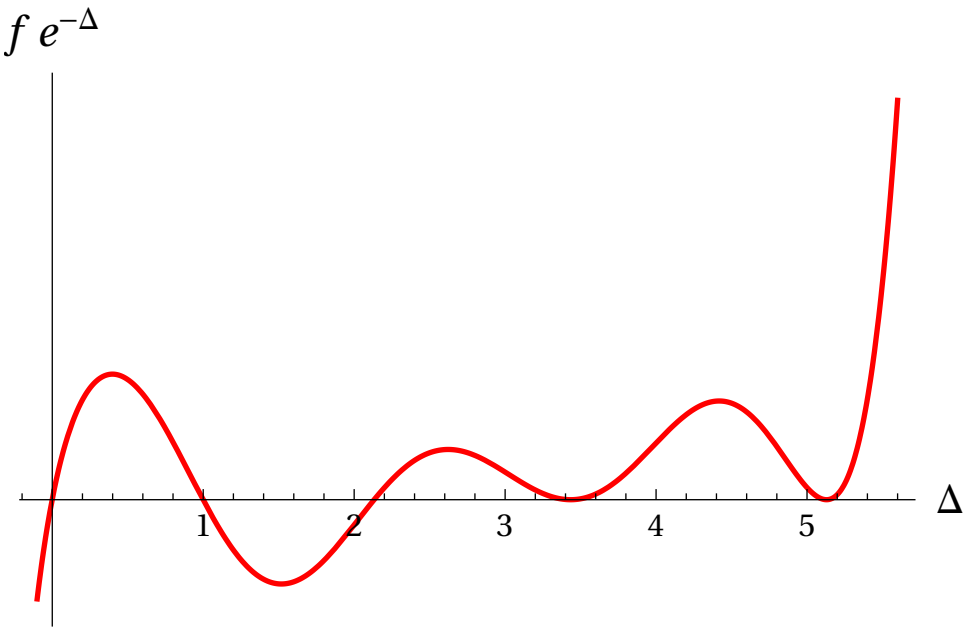

Figure 4.1: Example of an extremal functional for modular bootstrap, with $c = 12$ and truncation order $P = 6$. There are single zeroes at $\Delta_0 \approx 0$ and $\Delta_1 \approx 2.13$, and double zeroes at $\Delta_2 \approx 3.43$ and $\Delta_3 \approx 5.13$. The additional single zero near $\Delta \approx 1$ plays no role in the discussion. (The root near the origin is slightly shifted due to null state contributions described in section 4.4.1, but this too small to be visible in the plot.)

are single zeroes at $\Delta = 0$ and $\Delta = \Delta_1$, and double zeroes at $P/2 - 1$ additional states. An example is plotted in figure 4.1. This set of $P/2 + 1$ zeroes corresponds to a solution of the truncated primal equations (4.6).

We will make an ansatz for the functional by assuming that this pattern of zeroes continues at higher P. We will confirm *a posteriori* that this assumption holds for modular bootstrap, at least for all c and P that we consider.

Given this assumption about the pattern of zeroes, we now replace the linear optimization problem (4.9) by a nonlinear optimization. Choose a spectrum Δ_μ for

$\mu = 1 \ldots P/2$. From this spectrum, construct the unique functional obeying

$$f(\Delta_1) = 0 \ , \tag{4.11}$$
$$f(\Delta_\mu) = f'(\Delta_\mu) = 0 \quad (\mu = 2 \ldots P/2) \ .$$

This is $P-1$ linear equations for the $P-1$ variables α_a, so the solution is unique. In other words, we can view the functional as parameterized by its roots. Next, the linear optimization (4.9) is replaced by:

$$\text{maximize } f(0) \text{ over } \Delta_\mu, \text{ with } \alpha_a \text{ determined by } (4.11) \ . \tag{4.12}$$

The optimization step can also be eliminated altogether by solving directly for the extremal functional. This has $f(0) = 0$ and is an extremum with respect to Δ_μ. So we simply append to (4.11) the equations

$$f(0) = 0 \ , \qquad \frac{d}{d\Delta_\mu} f(0) = 0 \ , \tag{4.13}$$

where in the latter equation, $\mu = 2 \ldots P/2$, and the gradient is taken along solutions to (4.11). That is, $\alpha_a = \alpha_a(\Delta_\mu)$ as determined by (4.11).

This is now a closed system of equations for the extremal functional. There is no guarantee that the positivity conditions will be obeyed in this formulation, but this is easily checked after the functional has been constructed, and holds in the applications we will consider. A similar system of equations, but for the linear version of the problem and involving also the primal variables, appears in [209].

To summarize, we have formulated the problem of finding the extremal functional as $3P/2 - 1$ equations (4.11) and (4.13) for the $P/2$ dimensions Δ_μ and $P-1$ functional parameters α_a. In the derivative basis, the equations are polynomial (after absorbing a positive Δ-dependent factor into the coefficients a_μ).

This reduces the problem of finding the extremal functional to the problem of finding zeroes of a system of polynomial equations. The degree of the polynomials

grows with P, so this is non-trivial. Moreover, we have replaced a convex optimization by a non-convex root-finding problem, where there may be runaways and spurious solutions. In practice, these obstacles can be overcome if we can generate a good guess to use in the first step of Newton's method. We will describe how to do this for modular bootstrap in section 4.4.

4.3.3 Duality

As the nomenclature suggests, the truncated versions of the primal and dual bootstrap are, in fact, Lagrange duals. With our nonlinear formulation of the dual problem, this duality holds under the assumption that the double roots Δ_μ of the extremal functional have multiplicity exactly two – not higher.

The duality immediately proves the main results stated in section 4.2. In the dual bootstrap, monotonicity of the gap under changing P is obvious — if we allow a more general functional, the bound on Δ_1 can only get stronger. When translated into primal language, this monotonicity property becomes more surprising.

The duality that we describe is already very well known in the linear formulation of the problem. We will rederive it in terms of the nonlinear version above.

We will start with the dual bootstrap — *i.e.,* the problem of finding extremal functionals (4.12) — then dualize to the primal bootstrap (4.6). The constrained optimization (4.12) is equivalent to maximizing the Lagrangian

$$L = \alpha_i f_i(0) + a_\mu \alpha_i f_i(\Delta_\mu) + \lambda_\nu \alpha_i f_i'(\Delta_\nu) \tag{4.14}$$

over the independent variables α_a, Δ_μ and the Lagrange multipliers a_μ, λ_ν (with $\mu = 1 \dots P/2$, $\nu = 2 \dots P/2$.) Using the normalization condition $\alpha_P = 1$ and

rearranging terms,

$$L = E_P + \alpha_a E_a \tag{4.15}$$

with

$$E_i \equiv f_i(0) + a_\mu f_i(\Delta_\mu) + \lambda_\nu f_i'(\Delta_\nu) \ . \tag{4.16}$$

To dualize, we reinterpret this Lagrangian, viewing $\Delta_\mu, a_\mu, \lambda_\nu$ as independent variables, and α_a as a Lagrange multiplier. Assuming $f_i''(\Delta_\mu) \neq 0$ so that no roots have multiplicity higher than two, the equation of motion for Δ_μ imposes $\lambda_\nu = 0$. Therefore, the primal optimization problem is

$$\begin{aligned} &\text{maximize } f_P(0) + a_\mu f_P(\Delta_\mu) \text{ over } \ \Delta_\mu, a_\mu \\ &\text{subject to } f_a(0) + a_\mu f_a(\Delta_\mu) = 0 \ . \end{aligned} \tag{4.17}$$

These are the same sums as appear in the primal crossing equation (4.6), so the constraints consist of the first $P-1$ primal equations. Finally, let us also impose extremality, $f(0) = 0$, so the assumed gap is marginally excluded. This is equivalent to the Pth primal equation.

The conclusion is that the problem of finding the extremal functional is precisely dual to the problem of solving the P truncated crossing equations, (4.6), for the spectrum and coefficients. In appendix C.1, we derive the same statement by direct analysis of the extremal functional equations (4.11)-(4.13), and in the process, give a formula for the truncated OPE coefficients a_μ in terms of the extremal functional.

4.3.4 From primal solutions to extremal functionals

Given a solution to the primal equations (4.6) for some P, it is straightforward (and computationally trivial) to construct the dual extremal functional: Fix Δ_μ to

the primal values, and solve the linear equations (4.11) for the functional α_a. A consistency check is that this functional should vanish on the identity, $f(0) = 0$.

Once a candidate extremal functional has been obtained this way, it can be plotted to confirm the positivity conditions (4.8). If (4.8) is satisfied, then the functional implies rigorous bounds, so in the end, our bounds are not conditioned on any assumptions about the pattern of zeroes.

It is also guaranteed that the bounds we derive are optimal, in the sense that linear programming at the same value of P will always produce exactly the same bounds. It is impossible to derive a stronger bound (at a given P), because doing so would contradict the primal solution that we have found. In other words, the method we have described produces solutions which are primal-dual feasible, and therefore optimal.

4.4 Modular Bootstrap Algorithm

So far, our discussion has applied to a general class of spinless bootstrap problems, with a certain pattern of zeroes in the extremal functional. We now focus on the modular bootstrap exclusively. In this section we first review the (spinless) modular bootstrap [72, 211], then describe our algorithm in detail.

4.4.1 Setup

Consider the partition function of a 2d CFT at zero angular potential,

$$Z(\beta) = \sum_{\text{states}} e^{-2\pi\beta(\Delta - \frac{c}{12})} \tag{4.18}$$

$$= \sum_{\text{primaries}} \chi_\Delta(\beta) \tag{4.19}$$

with $\beta > 0$, and c the central charge. In the second line we have organized the sum into characters of the algebra, Virasoro $\times$ Virasoro.[3] Crossing symmetry in this context is modular invariance: $Z(\beta) = Z(1/\beta)$. It is convenient to define the reduced partition function

$$\hat{Z}(\beta) = |\eta(i\beta)|^2 |i\beta|^{1/2} Z(\beta) \tag{4.20}$$

$$= \sum_{\mu=0}^{\infty} \rho_\mu G_{\Delta_\mu}(\beta) \ . \tag{4.21}$$

where ρ_μ is the degeneracy of primaries with dimension Δ_μ. This function is also modular invariant, $\hat{Z}(\beta) = \hat{Z}(1/\beta)$. The vacuum is $\Delta_0 = 0$, $\rho_0 = 1$. The Dedekind η-functions cancel similar factors in χ_Δ, such that in (4.21), the blocks for non-vacuum states are

$$G_\Delta(\beta) = \beta^{1/2} \exp\left[-2\pi\beta(\Delta - \frac{c-1}{12})\right] \ , \tag{4.22}$$

and, for the vacuum,

$$G_0(\beta) = \beta^{1/2} e^{2\pi\beta\frac{c-1}{12}} (1 - e^{-2\pi\beta})^2 \ . \tag{4.23}$$

(The extra factors in the vacuum block are to account for the null state at level one, $L_{-1}|0\rangle = 0$.) The crossing equation (4.1) is

$$\sum_{\mu=0}^{\infty} \rho_\mu W_{\Delta_\mu}(\beta) = 0 \tag{4.24}$$

$$W_\Delta(\beta) \equiv G_\Delta(\beta) - G_\Delta(\frac{1}{\beta}) \ .$$

[3] $\chi_\Delta(\beta) \equiv \left(\chi^{Vir}_{\Delta/2}(i\beta)\right)^2$, with $\chi^{Vir}_h(\tau)$ the standard chiral Virasoro character.

We choose the basis of derivative functionals

$$\mathcal{F}_k = \frac{1}{2(2k-1)!}\left[\frac{1}{2}(1+\beta)^2\phi_\beta\right]^{2k-1}\frac{1+\beta}{2\sqrt{\beta}}\bigg|_{\beta=1} , \tag{4.25}$$

for $k = 1 \dots P$. This is a convenient basis because the resulting f_k are simply odd-index Laguerre polynomials, L_{2k-1}. Indeed, acting with $\mathcal{F}_k$ on the crossing equation (4.24) gives[4]

$$\sum_{\mu=0}^{\infty} a_\mu f_k(\Delta_\mu) = 0 , \tag{4.27}$$

where

$$a_\mu \equiv \rho_\mu e^{-2\pi\Delta_\mu} , \tag{4.28}$$

and, for $\Delta > 0$,

$$f_k(\Delta) = L_{2k-1}(4\pi x) , \quad x \equiv \Delta - \frac{c-1}{12} . \tag{4.29}$$

The vacuum state is different due to the extra factors in (4.23),

$$f_k(0) = L_{2k-1}(4\pi x_0) - 2e^{-2\pi}L_{2k-1}(4\pi(x_0+1)) + e^{-4\pi}L_{2k-1}(4\pi(x_0+2)) , \tag{4.30}$$

with $x_0 = -\frac{c-1}{12}$.

At this point, we have written the primal bootstrap equations in the same format as section 4.2. The truncated version, a closed system of P equations for P unknowns, is

$$\sum_{\mu=0}^{P/2} a_\mu f_k(\Delta_\mu) = 0 , \tag{4.31}$$

[4] *Derivation:* The generating function for Laguerre polynomials is

$$\sum_{p\geq 0} t^p L_p(2w)e^{-w} = (1-t)^{-1}\exp\left(-\frac{1+t}{1-t}w\right) \tag{4.26}$$

Therefore acting with $\frac{1}{p!}(\phi_t)^p|_{t=0}$ on the right-hand side gives $L_p(2w)e^{-w}$. With the identification $\beta = \frac{1+t}{1-t}$, this is the same as $\mathcal{F}_k[W_\Delta(\beta)]$. The even-index Laguerre's do not appear because the corresponding differential operator vanishes on the modular-odd function $W_\Delta(\beta)$.

4.4.2 Algorithm

We now turn to numerical algorithms based on the reformulation of the crossing problem described in sections 4.2-4.3. We focus on the simplest bootstrap question, which is to place an upper bound on the scalar gap Δ_1, given the central charge c. The algorithms can be modified to accommodate similar problems.

We can consider two main approaches:

- *Dual*: Solve the functional equations (4.11) and (4.13), for the spectrum and the functional.
- *Primal*: Solve the P truncated primal crossing equations, (4.6), for the spectrum and degeneracies.

Note that standard optimization methods for functional bootstrap require an additional scan over Δ_1. In our case, Δ_1 is a free parameter, so this step is not necessary.

For modular bootstrap, both the dual and primal algorithms are much faster than semidefinite programming. In the rest of this paper we will consider only the primal algorithm, which was somewhat faster in our preliminary testing, and conceptually simpler.

The purpose of the algorithm is to solve the equations (4.31) for some large value of P. The strategy is to start at small P, solve the equations by Newton's method, then gradually increase P, using the previous results to generate a good initial guess for Newton's method. The same strategy was used for 1d correlator bootstrap in [209] (specifically, our algorithm is similar to the 'upgrading + error

correction' method). Besides the differences between 1d correlator bootstrap and 2d modular bootstrap, our algorithm has two significant improvements: better numerical stability, and a more elaborate, more accurate method to guess the initial points. This will allows us to increase P in large increments.

For numerical stability, we first introduce normalization factors to rescale the $P \times P/2$ matrix $f_k(\Delta_\mu)$. Rewrite (4.31) as

$$\sum_{\mu=0}^{P/2} \tilde{a}_\mu \tilde{f}_k(\Delta_\mu) = 0 \ , \tag{4.32}$$

where

$$\tilde{a}_\mu = a_\mu |\max_k f_k(\Delta_\mu)| \tag{4.33}$$

$$\tilde{f}_k(\Delta_\mu) = \frac{f_k(\Delta_\mu)}{f_k(0)|\max_k f_k(\Delta_\mu)|} \ . \tag{4.34}$$

The matrix $\tilde{f}_k(\Delta_\mu)$ is scaled such that the vacuum column is all 1's, and every other column has an absolute maximum entry of ± 1.

We now apply Newton's method to the equations (4.32) for the P unknowns $(\tilde{a}_\mu, \Delta_\mu)$. The Laguerre polynomials, and their derivatives, are calculated by 3-term recurrence relations. This is faster and more numerically stable than direct evaluation. Our implementation of Newton's method is completely standard so we will not review it.

An important element in the algorithm is a guess generator, to provide the initial point in Newton's method. The method is largely insensitive to the initial guesses for $\tilde{a}_\mu$, so for these coefficients we always guess $\tilde{a}_\mu = 1$. Convergence is very sensitive to the starting Δ_μ, so these must be chosen carefully. We start by solving the equations for $P = 4, 6$. For these initial points, it is easy to find a good guess by hand (or using a linear/semidefinite optimizer such as SDPB [217]). Then we proceed upwards in P recursively, using previous results to generate a guess for Δ_μ.

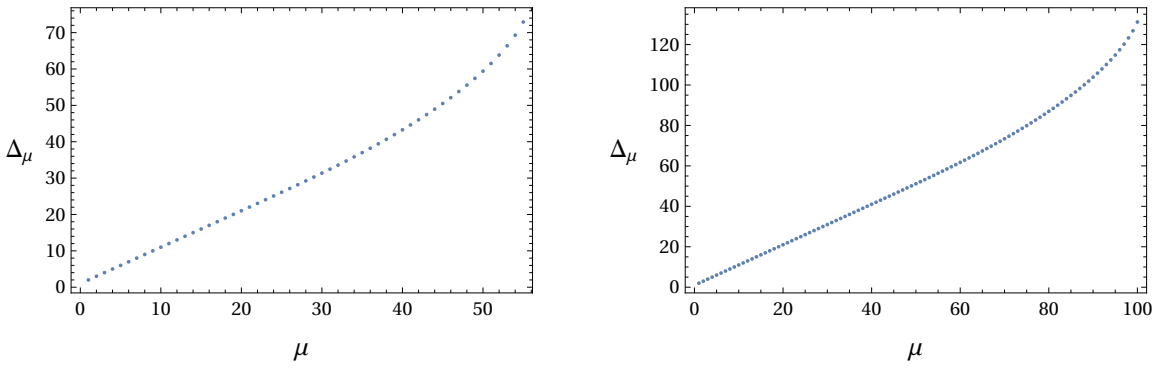

Figure 4.2: Spectrum of the $c = 12$ solution at truncation order $P = 110$ (left) and $P = 200$ (right). The horizontal axis is the state number, $\mu = 1, 2, \ldots, P/2$. Note that the curves are approximately the same shape. This observation is used to generate very accurate guesses for the initial point in Newton's method.

Our guess generator is based on the observation that the spectrum, at different values of P, is self-similar. That is, the curve Δ_μ as a (discrete) function of μ has almost exactly the same shape for all P, once P is large enough. This is illustrated by the plots in fig. 4.2, which are the exact spectra at $P = 110$ and $P = 200$ for the $c = 12$ modular bootstrap. The shapes in the two plots are almost identical; only the scaling of the axes and the state spacing differs. This motivates a guess where we rescale the lower-P spectrum, and re-sample at the appropriate points. This generates a good guess, and we use precisely this method for $P \lesssim 200$. However, we can do better, and take larger P-steps, by correcting for the fact that the spectrum is not quite self-similar. We do this by parameterizing the shape curve, fitting the parameters as functions of P, and extrapolating. The full algorithm is given in appendix C.2.

The resulting guesses are very accurate. For example, in the $c = 100$ modular bootstrap, using data from $P = 120, 122, 124, \ldots, 200$, the extrapolation to $P = 280$

produces a spectrum $\Delta_\mu^{\text{guess}}$ that differs from the exact spectrum by under one part in 10^3-10^5. Results at higher P are comparable. This means that we never need to run more than a handful of Newton steps to converge to an accurate spectrum.

This completes the algorithm. The only computationally expensive step is inverting the Jacobian in Newton's method, which scales roughly as P^3. The computations are performed in Mathematica with high precision arithmetic.

4.5 Modular Bootstrap Results

4.5.1 3d gravity and summary of existing bounds

Three-dimensional gravity in the semiclassical limit is holographically dual to a 2d CFT with a large central charge, $c \gg 1$. Quantum fields in the bulk, aside from the graviton, are dual to low-dimension operators in the CFT. It follows that the CFT should also have a sparse spectrum of low-dimension operators, in that the number of states below any fixed Δ_* should be finite as $c \to \infty$.

'Pure' 3d gravity, which consists only of the graviton plus black holes, would have no new primaries between the vacuum and black hole threshold. That is, $\Delta_1 \sim \frac{c}{12}$. It is unknown whether pure gravity exists as a quantum theory. A putative partition function was suggested by Witten [60], but explicit calculations by Maloney and Witten [67] gave a different answer that was incompatible with a holographic interpretation. It is possible that this calculation can be modified to produce a consistent quantum theory [66], but at this point, the realm of possibilities is poorly understood.

Even the simplest question is unanswered: What is the largest gap Δ_1 compatible with diffeomorphism invariance? Large diffeomorphisms in 3d gravity correspond to modular transformations in the dual CFT, so this is a question for the modular bootstrap.

The functional approach to modular bootstrap was initiated in [72], where, working analytically at $P = 2$, it was proved that $\Delta_1 \leq \frac{c}{6} + 0.474$. This is known as the Hellerman bound. At large c, the Hellerman bound is a factor of 2 above the black hole threshold. It has also been shown analytically that, for $\Delta \gtrsim \frac{c}{6}$, 2d CFTs with a large gap have the same entropy as BTZ black holes [49]. However, the range $\frac{c}{12} \leq \Delta \leq \frac{c}{6}$ remains enigmatic. This range certainly does not have a universal spectrum, even in holographic theories, but it is an open question whether there must be any states at all within this window.

Numerical evidence strongly suggests that the asymptotic bootstrap bound can be improved to somewhere between $c/12$ and $c/6$ [211, 212, 218]. (For related work, see [219–233]). For $c \lesssim 150$, numerical bounds are as strong as $\Delta_1 \lesssim c/8.2$. However, $c \sim 150$ is the largest central charge accessible to standard numerical methods, and at this value, it is clear that the bound has not yet converged. Results at larger c are needed to find the bound in the semiclassical, large-c limit.

The difficulty is that for large c, the bound on Δ_1 converges slowly with P, so large c requires large P. This is a general obstacle to bootstrapping quantum gravity in the regime $\Delta \sim c$, which presents a significant challenge to probing black hole physics with the bootstrap. (On the other hand, many interesting questions in AdS/CFT already arise for states with $\Delta \ll c$, and in these cases numerical bootstrap has been very successful.)

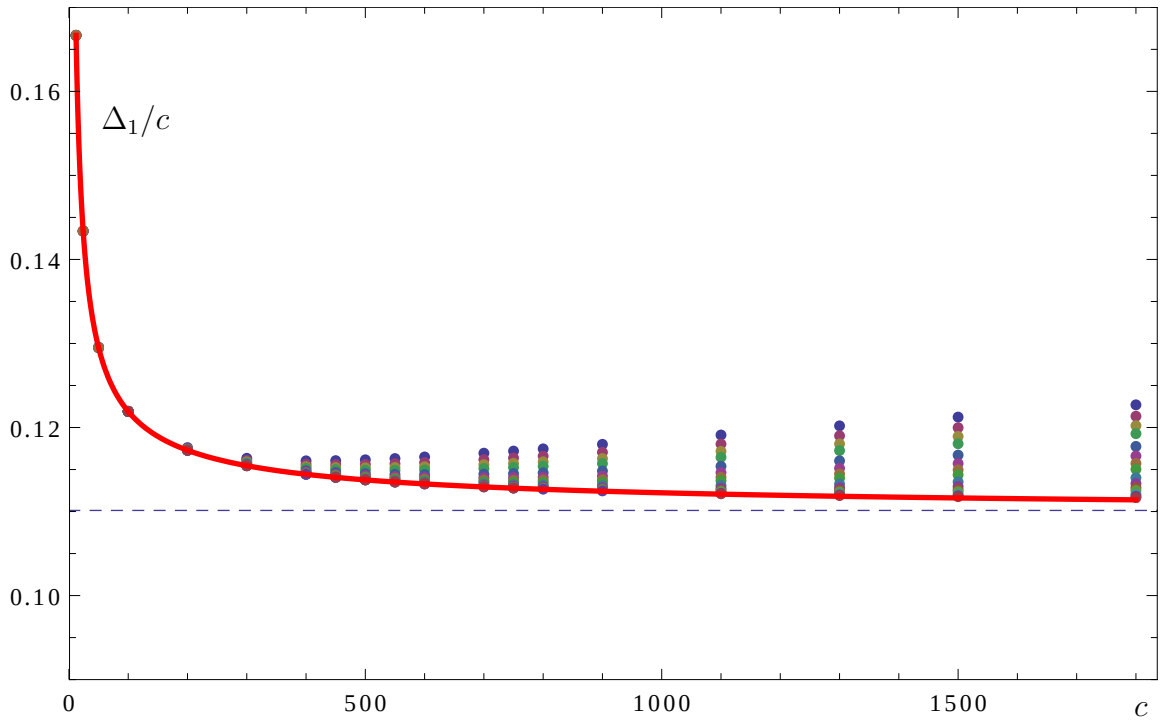

Figure 4.3: Upper bound on Δ_1/c, as a function of c. Dots are numerical data for truncation at $P = 270$, 310, 350, 390, 470, 550, 630, 710, 870, 1030, 1350, 1670, 1990, 2310, from top to bottom. The solid red line is the extrapolation to $P = \infty$. The dashed blue line is the asymptotic estimate at large c, 1/9.08.

The largest truncation order considered in the literature on modular bootstrap is $P = 92$ [212], using the semidefinite program solver SDPB [217]. We apply our algorithm up to $P \sim 2250$ (derivative order 4500). At small P, we have checked that our bounds agree exactly with those produced by SDPB.

4.5.2 Bound as a function of c

The upper bound on Δ_1/c is plotted in fig. 4.3. The dots are numerical data, and the solid line is the extrapolation to $P = \infty$ with an exponential fit, $\Delta_1(P) = \Delta_1^\infty + ae^{-bP}$.

Table 4.1: Fitting the bound as a function of c

Fitting Function	$1 - R^2_{\text{adj}}$	δ_{900}	δ_{1800}	Best fit A
$c/A + B_1$	10^{-7}	9×10^{-4}	3×10^{-3}	9.01
$c/A + B_1 + B_2/c$	10^{-9}	2×10^{-4}	9×10^{-4}	9.04
$c/A + B_1 + B_2 \log c$	6×10^{-11}	4×10^{-6}	2×10^{-5}	9.08

To estimate the asymptotic bound, we fit the data in the range $300 \leq c \leq 700$ to a function of c. In this range, the bound has converged very close to its $P \to \infty$ limit. The estimate depends on what function is used in the fit, but natural choices all give estimates clustered around the same value,

$$\Delta_1 \lesssim c/9.1 \ . \tag{4.35}$$

Of course this is not definitive, because we are working at finite c, but the errors in the fit are very small. Different choices of fitting function, together with the adjusted R^2 of the fit, are reported in table 4.1. We also give an error estimate δ_c, which is defined as the fractional error of our two extrapolations. For example, δ_{900} compares the extrapolation in c (which was found using data only from $c \leq 700$) to our actual data at $c = 900$, extrapolated up to $P = \infty$. The errors are smallest for the logarithmic fit,

$$\Delta_1^{\max} \approx \frac{c}{9.08} + 0.439 \log c - 0.896 \ . \tag{4.36}$$

The best strict (non-extrapolated) bound on Δ_1/c is $c = 1800, P = 2310$, for which $\Delta_1^{\max} = c/8.956$.

In addition to the gap, Δ_1, the method also provides a spectrum with over a thousand operators. As an example, the spectrum for $c = 500$, $P = 2310$ is plotted in fig. 4.4. As discussed in section 4.2.3, only the operators $\mu \ll P$ should be

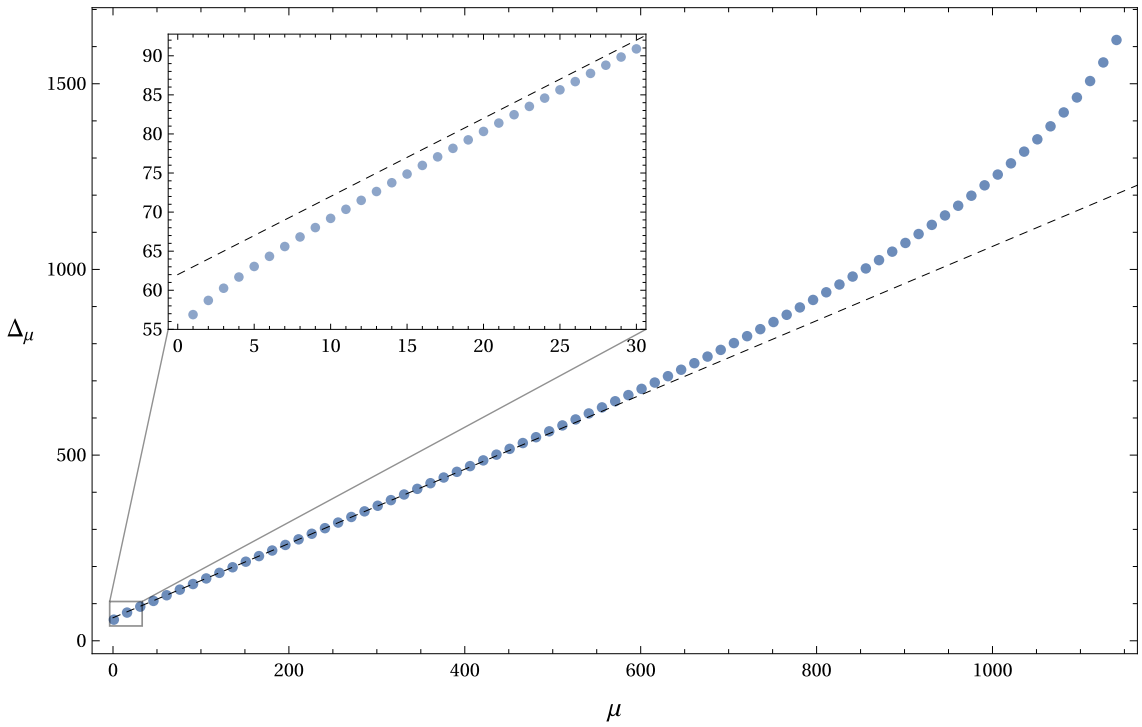

Figure 4.4: The numerical spectrum Δ_μ for $c = 500$ and $P = 2310$. In the larger plot we show every 15th scaling dimension to reduce clutter. The smaller inset figure shows the first 30 scaling dimensions with deviation away from linearity. In [1], the linear regime of the spectrum with $\Delta_\mu = \frac{c-4}{8} + \mu$ (dashed line) will be explained analytically.

trusted, but in practice, roughly the lower half of the spectrum with $\mu \lesssim P/4$ is converged.

4.5.3 $c = 12$ and the modular j-function

The case $c = 12$ is especially interesting, because the numerics appears to converge to a spectrum with integer scaling dimensions $\Delta_\mu = 2, 3, \ldots$, and integer degeneracies. (The case $c = 4$ has a similar story.) The bound on the gap at $c = 12$, obtained

with $P = 2000$ in a few hours of CPU time, is:

$$\Delta_1 < 2 + 1 \times 10^{-30} \qquad (c = 12,\ P = 2000)\ . \tag{4.37}$$

The numerical solution of the truncated crossing equations at $P = 2000$ is

$$\begin{aligned}\hat{Z} \approx q^{1/12}\beta^{1/2}\Big[&q^{-1}(1-q)^2 + (196882 + 2\times 10^{-24})q \\ &+ (21099994 + 4\times 10^{-22})q^2 + (821115567 + 3\times 10^{-20})q^3 + \cdots\Big]\end{aligned} \tag{4.38}$$

where $q \equiv e^{-2\pi\beta}$. The degeneracies converge to integers that suggest a link to the modular j-function. Indeed, reintroducing the η-functions removed in (4.20), this corresponds to

$$Z \approx j(\tau) - 744\ , \qquad \tau = i\beta\ . \tag{4.39}$$

This coincidence will be explained analytically in [1]. Note that we did not impose invariance under $\tau \to \tau + 1$, so it is surprising to find the j-function appearing.

4.5.4 Algorithm Benchmarks

Runtime is compared to semidefinite programming with SDPB (v1) [217] in fig. 4.5. Extrapolating the runtime of SDPB to large P may be unreliable, but naively fitting to a power law and setting $P = 2000$ gives the estimate $\sim 10^9$ s.

We can also compare to the extremal functional method of El-Showk and Paulos [209]. They solve a different problem (1d correlators) so it is not a direct comparison, but they report runtime of 45 minutes at $P = 150$. For modular bootstrap, our algorithm runs in seconds at the same P. The algorithm is very similar to that described in [209], so we do not know the exact origin of the speedup, but it presumably comes from some combination of improvements to numerical

stability, the guess generator described in section 4.4.2, or inherent differences in modular bootstrap.[5]

Our procedure is numerically stable, in the sense that round-off errors do not accumulate dramatically. This means that the same accuracy as semidefinite programming is achieved with much lower precision at intermediate steps. (This gives a significant speed-up, but is not the main factor.) For example, at $c = 12$, machine precision (16 decimal digits) is sufficient up to $P \sim 90$, and 60 digits is sufficient for $P \sim 2000$. Calculations at larger c require higher precision, because more terms participate significantly in the crossing equations. The data in fig. 4.3 was produced with a range of precisions from 16 to 500 digits, chosen to ensure that the matrix inversion step in Newton's method is well behaved.

4.6 Discussion

In summary, we have described a reformulation of the modular bootstrap equations, amenable to both analytic and numerical analysis. On the analytic side, the main logic was to show that (i) extremal functionals can be efficiently parameterized by their roots, and (ii) this is dual to solving the truncated crossing equations.

For modular bootstrap, our algorithm is orders of magnitude faster than semidefinite programming or any other previous method, extending the maximum truncation order from $P \sim 100$ to $P \sim 2500$. Other potential advantages include:

- It is numerically stable, so intermediate steps do not require very high

[5] It is also not clear to us whether the calculations in [209] were done using the primal equations alone, or the primal-dual formulation of the problem. We use only the primal equations.

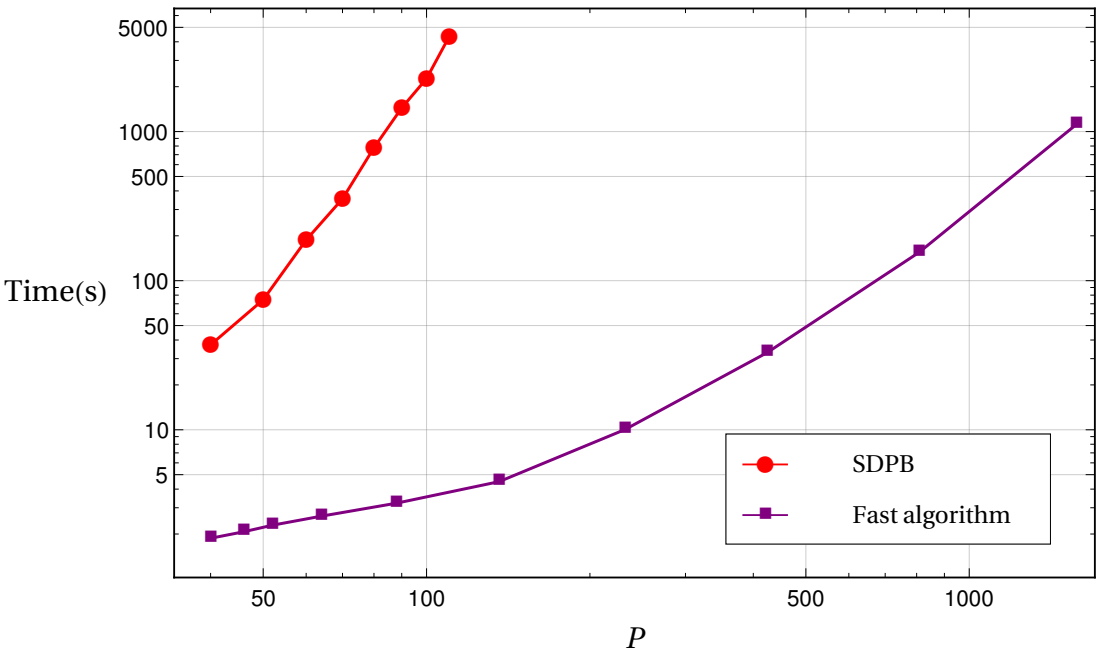

Figure 4.5: Runtime of SDPB and our Newton-based algorithm for modular bootstrap at c=12, vs the number of polynomials, P. Larger c requires more precision, so runtimes are somewhat longer.

precision.

- The method might apply to non-derivative or non-polynomial functionals. (One choice has been considered [234].) We restricted to derivative functionals only because in this basis, we have confirmed explicitly (in examples) the pattern of zeroes invoked in section 4.3. The method applies to any basis of functionals with a similar pattern of zeroes.

- The algorithm can be sped up significantly by hot starting, *i.e.,* inputting a guess for the spectrum of the target CFT. This means that analytic results can potentially be leveraged for faster numerics, similar to the way we used results at small P for faster convergence at large P.

- Although the strict bounds we derived apply only to unitary CFTs, the

truncated primal equations may also have solutions corresponding to non-unitary CFTs, with potential applications to weakly first order phase transitions [52, 235]. This would be similar to the approach taken in [214, 215].

- The truncated bootstrap equations (4.6) can be studied analytically. This may lend additional insights.

There is also a major drawback to our approach, at least in our current implementation. We considered only bootstrap problems without spin dependence. More generally, for example in the modular bootstrap with angular potential, or the correlator bootstrap of the 3d Ising model, there are more constraints on the extremal functional, labeled by J. This typically leads to a different pattern of zeros, not the simple pattern we observed here. In primal language, the problem is that with spin, the solution of the primal optimization problem at truncation order P typically does not have exactly $P/2+1$ states.[6]

This makes it impossible to truncate to a closed, primal-only problem, as we have done here. Instead one can write primal-dual equations for the extremal functional, involving $(\alpha_a, a_\mu, \Delta_\mu)$ simultaneously, as in [209]. In principle, we could use Newton's method to solve this enlarged problem, but in practice, we have not found any efficient way to generate initial guesses. The pattern of states does not change predictably as the truncation order is increased.

As described in the introduction, part of our motivation in this work was to push the numerical bootstrap to the point where it can be used to construct, or rule out, candidate theories of 3d gravity. However, our bound $\Delta_1 \lesssim c/9.1$ does not

[6]The simple pattern of zeros in the spinless modular bootstrap may be related to total positivity of the functionals, which was noted in [236]. Totally positive functionals lead to polynomials $f_i(\Delta)$ with interlacing roots [237]. This fact seems to give the polynomials the right shape to be able to produce one new double root with the addition of two new polynomials.

saturate the black hole threshold, so it appears that spinless modular bootstrap is not powerful enough to attack these problems. It might be possible with spinning modular bootstrap, but spin requires new methods.

Eventually, it may be possible to use numerics to settle longstanding questions in quantum gravity: Do all theories of quantum gravity require new states well below the Planck scale, such as strings or Kaluza-Klein modes (see e.g. [238]) ? Does quantum gravity in the ultraviolet rule out a swampland of effective theories in the infrared [239]? Is there a quantum theory of pure gravity in three dimensions [60]? Versions of all these questions, in anti-de Sitter, can be posed in terms of the space of solutions to the crossing equations. Of course it would be better to solve these problems analytically, but definitive numerical answers would be a good start.

Acknowledgments We are grateful to David Simmons-Duffin for discussions of semidefinite and simplex methods and to Dalimil Mazáč and Leonardo Rastelli for comments on the draft. We also thank other members of the Simons Bootstrap Collaboration, and the organizers of the bootstrap workshops at ICTS in 2017, and the Azores and Caltech in 2018, as well as the Aspen Center for Physics, where much of this work was done or inspired. This work is supported by Simons Foundation grant 488643.

CHAPTER 5

REPLICA WORMHOLES AND THE ENTROPY OF HAWKING RADIATION

Abstract[1]

The information paradox can be realized in anti-de Sitter spacetime joined to a Minkowski region. In this setting, we show that the large discrepancy between the von Neumann entropy as calculated by Hawking and the requirements of unitarity is fixed by including new saddles in the gravitational path integral. These saddles arise in the replica method as complexified wormholes connecting different copies of the black hole. As the replica number $n \to 1$, the presence of these wormholes leads to the island rule for the computation of the fine-grained gravitational entropy. We discuss these replica wormholes explicitly in two-dimensional Jackiw-Teitelboim gravity coupled to matter.

[1]This chapter is based on the paper [78].

Hawking famously noted that the process of black hole formation and evaporation seems to create entropy [240]. We can form a black hole from a pure state. The formation of the black hole horizon leaves an inaccessible region behind, and the entanglement of quantum fields across the horizon is responsible for the thermal nature of the Hawking radiation as well as its growing entropy.

A useful diagnostic for information loss is the fine-grained (von Neumann) entropy of the Hawking radiation, $S_R = -\operatorname{tr} \rho_R \log \rho_R$, where ρ_R is the density matrix of the radiation. This entropy initially increases, because the Hawking radiation is entangled with its partners in the black hole interior. But if the evaporation is unitary, then it must eventually fall back to zero following the Page curve [241, 242]. On the other hand, Hawking's calculation predicts an entropy that rises monotonically as the black hole evaporates.

Hawking's computation of the entropy seems straightforward. It can be done far from the black hole where the effects of quantum gravity are small, so it is unclear what could have gone wrong. An answer to this puzzle was recently proposed [243–245] (see also [246–258]). The proposal is that Hawking used the wrong formula for computing the entropy. As the theory is coupled to gravity, we should use the proper gravitational formula for entropy: the gravitational fine-grained entropy formula studied by Ryu and Takayanagi [28] and extended in [34, 259, 260], also allowing for spatially disconnected regions, called "islands," see figure 5.1. Even though the radiation lives in a region where the gravitational effects are small, the fact that we are describing a state in a theory of gravity implies that we should use the gravitational formula for the entropy, including the island rule.

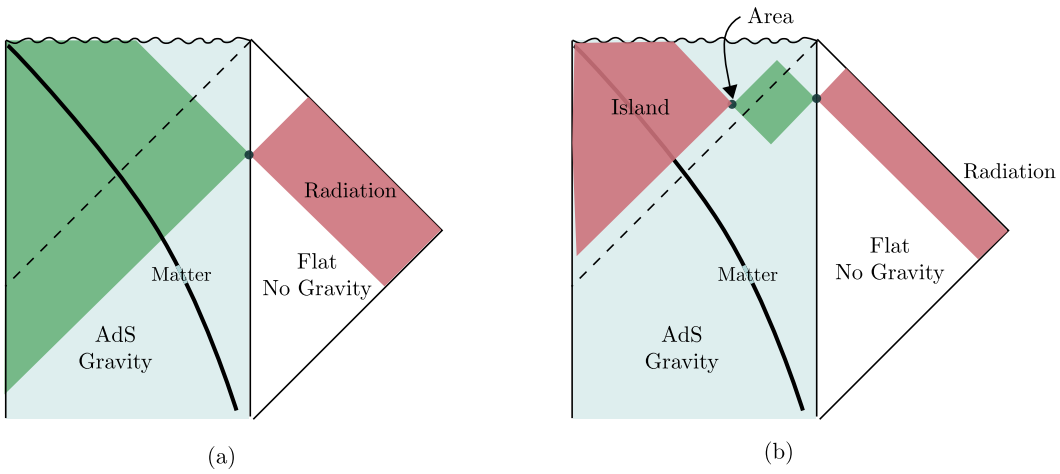

Figure 5.1: We display an evaporating black hole. The vertical line separates a region on the left where gravity is dynamical from a region on the right where we can approximate it as not being dynamical. The black hole is evaporating into this second region. In red we see the regions associated to the computation of the entropy of radiation and in green the regions computing the entropy of the black hole. (a) Early times. (b) Late times, where we have an island.

In this paper we consider a version of the information paradox formulated recently in [243, 244] (see also [261]) where a black hole hole in anti-de Sitter spacetime radiates into an attached Minkowski region. We show that the first principles computation of the fine-grained entropy using the gravitational path integral description receives large corrections from non-perturbative effects. The effects come from new saddles in the gravitational path integral — replica wormholes — that dominate over the standard Euclidean black hole saddle, and lead to a fine-grained entropy consistent with unitarity.

We will discuss the saddles explicitly only in some simple examples related to the information paradox for eternal black holes in two-dimensional Jackiw-Teitelboim (JT) gravity [262–264], reviewed below, but we can nonetheless compute the effect on the fine-grained entropy more generally. The same answer for the entropy was

obtained holographically in [245, 254, 255]. Our goal is to provide a direct, bulk derivation without using holography.

To summarize our approach briefly, we will revisit the calculation of the von Neumann entropy of radiation outside a black hole in AdS glued to flat space, using the replica method. We introduce n copies of the original black hole, analytically continue to non-integer n, and compute the von Neumann entropy as $S_R = -\phi_n \operatorname{tr}(\rho_R)^n|_{n=1}$. Since the theory is coupled to gravity, we must do the gravitational path integral to calculate $\operatorname{tr}(\rho_R)^n$. Under our assumptions about the matter content, this path integral is dominated by a saddlepoint. There is one obvious saddle, in which the geometry is n copies of the original black hole; this saddle leads to the standard Hawking result for the von Neumann entropy, *i.e.*, the entropy of quantum fields in a fixed curved spacetime, see figure 5.6(a).

There is, however, another class of saddles in which the different replicas are connected by a new geometry. These are the replica wormholes, see figure 5.6(b), 5.7. In the examples we consider, whenever the Hawking-like calculation leads to an entropy in tension with unitarity, the replica wormholes start to dominate the gravitational path integral, and resolve the tension.

Our use of the replica trick in a theory coupled to gravity closely parallels the derivation of the Ryu-Takayanagi formula and its generalizations [260, 265–267].

In the rest of the introduction we summarize the main idea in more detail.

Similar ideas are explored independently in a paper by Penington, Shenker, Stanford, and Yang [268].

5.0.1 The island rule for computing gravitational von Neumann entropies

We begin by reviewing the recent progress on the information paradox in AdS/CFT [243, 244].

The classic information paradox is difficult to study in AdS/CFT, because large black holes do not evaporate. Radiation bounces off the AdS boundary and falls back into the black hole. For this reason, until recently, most discussions of the information paradox in AdS/CFT have focused on exponentially small effects, such as the late-time behavior of boundary correlation functions [74, 269–271].

In contrast, the discrepancy in the Page curve is a large, $O(1/G_N)$, effect. This classic version of the information paradox can be embedded into AdS/CFT by coupling AdS to an auxiliary system that absorbs the radiation, allowing the black hole to evaporate [243, 244] (see also [246, 272, 273]). This is illustrated in fig. 5.1 in the case where the auxiliary system is half of Minkowski space, glued to the boundary of AdS. There is no gravity in the Minkowski region, where effectively $G_N \to 0$, but radiation into matter fields is allowed to pass through the interface.

In this setup, the Page curve of the black hole was calculated in [243, 244]. It is important to note that this calculation gives the Page curve of the black hole, not the radiation, which is where the paradox lies; we return to this momentarily. The entropy of the black hole is given by the generalized entropy of the quantum extremal surface (QES) [34], which is a quantum-corrected Ryu-Takayanagi (or Hubeny-Rangamani-Takayanagi) surface [28, 259]. According to the QES proposal,

the von Neumann entropy of the black hole is

$$S_B = \text{ext}_Q \left[\frac{\text{Area}(Q)}{4G_N} + S_{\text{matter}}(B) \right] \tag{5.1}$$

where Q is the quantum extremal surface, and B is the region between Q and the AdS boundary. S_{matter} denotes the von Neumann entropy of the quantum field theory (including perturbative gravitons) calculated in the fixed background geometry. The extremization is over the choice of surface Q. If there is more than one extremum, then Q is the surface with minimal entropy. For dilaton gravity in AdS_2, Q is a point, and its 'area' means the value of the dilaton.

The black hole Page curve is the function $S_B(t)$, where t is the time on the AdS boundary where B is anchored. It depends on time because the radiation can cross into the auxiliary system. It behaves as expected: it grows at early times, then eventually falls back to zero [243, 244]. A crucial element of this analysis is that at late times, the dominant quantum extremal surface sits near the black hole horizon, as in fig. 5.1.

This does not resolve the Hawking paradox, which involves the radiation entropy $S_{\text{matter}}(R)$, where R is a region outside the black hole containing the radiation that has come out. Clearly the problem is that neither R nor B includes the region I behind the horizon, called the island, see figure 5.1. The state of the quantum fields on $R \cup B$ is apparently not pure, and, apparently $S_R \neq S_B$. Only if we assume unitarity, or related holographic input such as entanglement wedge reconstruction [243], can we claim that the QES computes the entropy of the radiation. It does, however, tell us what to aim for in a unitary theory.

With this motivation, in [245], the evaporating black hole in Jackiw-Teitelboim (JT) gravity in AdS_2 was embedded into a holographic theory in one higher dimension. The AdS_2 black hole lives on a brane at the boundary of AdS_3,

similar to a Randall-Sundrum model [274, 275], with JT gravity on the brane (see also [249] for an analogous construction on an AdS_4 boundary of AdS_5). In this setup, [245] derived the QES prescription *for the radiation* using AdS_3 holography. It was found that the von Neumann entropy of the radiation in region R, computed holographically in AdS_3, agrees with the black hole entropy in (5.1). This led to the conjecture that in a system coupled to gravity, the ordinary calculation of von Neumann entropy should be supplemented by the contribution from "islands" according to the following rule:

$$S(\rho_R) = \text{ext}_Q \left[\frac{\text{Area}(Q)}{4G_N} + S(\tilde{\rho}_{I\cup R}) \right] , \tag{5.2}$$

up to subleading corrections. Here ρ_R is the density matrix of the region R in the full theory coupled to quantum gravity, and $\tilde{\rho}_{I\cup R}$ is the density matrix of the state prepared via the semi-classical path integral on the Euclidean black hole saddle. This is equal to (5.1), since the quantum fields are pure on the full Cauchy slice $I \cup B \cup R$. Thus the tension with unitarity is resolved within three-dimensional holography.

In this paper we explain how the surprising island rule (5.2) follows from the standard rules for computing gravitational fine-grained entropy, without appealing to higher dimensional holography.

5.0.2 Two dimensional eternal black holes and the information paradox

We consider an AdS_2 JT gravity theory coupled to a 2d CFT. This CFT also lives in non-gravitational Minkowski regions, and has transparent boundary conditions

at the AdS boundary. The dilaton goes to infinity at the AdS_2 boundary so it is consistent to freeze gravity on the outside [244, 273]. We will assume that the matter CFT has a large central charge $c \gg 1$, but we will not assume that it is holographic, as all our calculations are done directly in the 2d theory. For example it could be c free bosons. Taking the central charge large is to suppress the quantum fluctuations of the (boundary) graviton relative to the matter sector.

This simple model of an AdS_2 black hole glued to flat space can be directly applied to certain four dimensional black holes. For example, for the near extremal magnetically charged black holes discussed in [276], at low temperatures we can approximate the dynamics as an AdS_2 region joined to a flat space region, and the light fields come from effectively two dimensional fields moving in the radial and time direction that connect the two regions.

We will consider a simple initial state which is the thermofield double state for the black hole plus radiation. This state is prepared by a simple Euclidean path integral, see figure 5.2. The resulting Lorentzian geometry is shown in figure 5.3.

Despite its simplicity, this setup exhibits Hawking's information paradox, and the corresponding puzzle with the Page curve [241, 242]. To reach a paradox, we collect Hawking radiation in region R in figure 5.3. As a function of time, R moves upward on both sides of the Penrose diagram, so this is not a symmetry. Indeed, the von Neumann entropy of the radiation as calculated by Hawking, $S_{\text{matter}}(R(t))$, grows linearly with time, see fig. 5.5. The origin of this growth is the following. At $t = 0$ the radiation modes on the left are entangled with modes on the right. However, as time progresses some of these modes fall into the black holes, others are replaced by black hole modes, see figure 5.4.

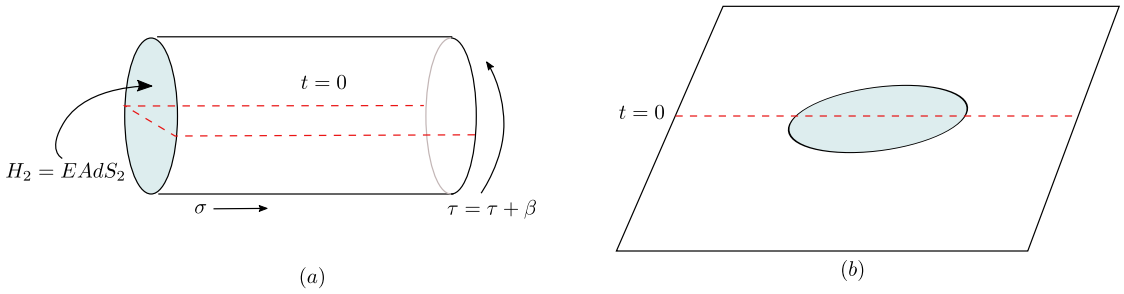

Figure 5.2: We prepare the combined thermofield double state of the black hole and radiation using a Euclidean path integral. These are two pictures for the combined geometry. In (b) we have represented the outside cylinder as the outside of the disk. By cutting along the red dotted line, we get our desired thermofield double initial state that we can then use for subsequent Lorentzian evolution (forwards or backwards in time) to get the diagram in figure 5.3.

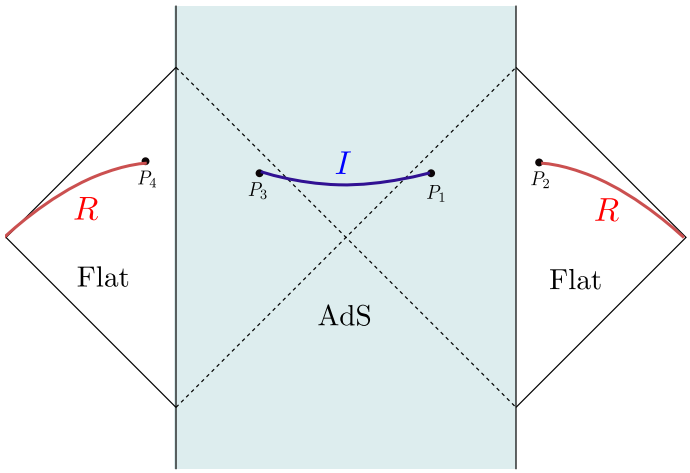

Figure 5.3: Eternal black hole in AdS_2, glued to Minkowski space on both sides. Hawking radiation is collected in region R, which has two disjoint components. Region I is the island. The shaded region is coupled to JT gravity.

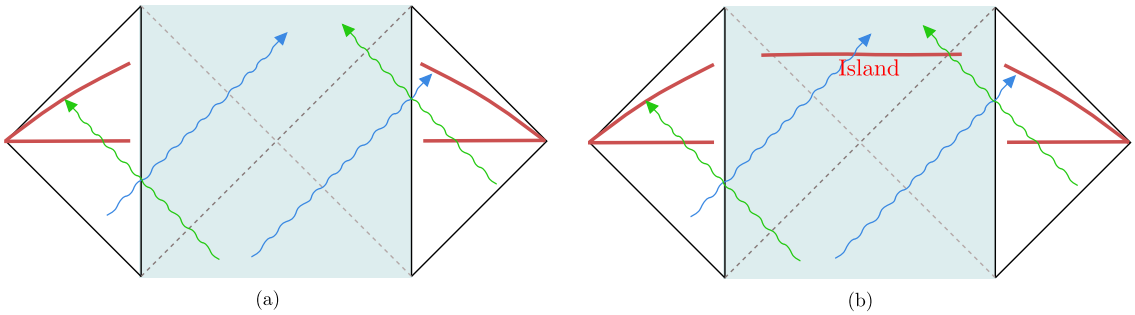

Figure 5.4: (a) Growing entropy for the radiation for an eternal black hole plus radiation in the thermofield double state. We draw two instants in time. The particles with the same color are entangled. They do not contribute to the entanglement of the radiation region (indicated in red) at $t = 0$ but they do contribute at a later value of t. (b) When the island is included the entanglement ceases to grow, because now both entangled modes mentioned above are included in $I \cup R$.

If this growth were to continue forever, it would become larger than the Bekenstein-Hawking entropies of the two black holes, and this is a contradiction. See a related discussion of the critically illuminated black hole in flat spacetime in [277].

In a unitary theory, $S_R(t)$ should saturate at around twice the Bekenstein-Hawking entropy of each black hole, see figure 5.5. This was confirmed using the island rule in [253].

5.0.3 Replica wormholes to the rescue

To reproduce the unitary answer directly from a gravity calculation, we will use the replica method to compute the von Neumann entropy of region R. The saddles relevant to the unitary Page curve will ultimately be complex solutions of

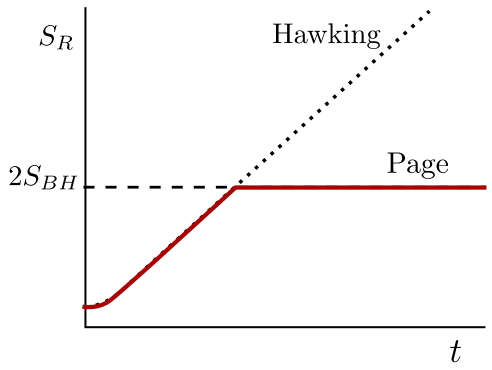

Figure 5.5: Page curve for the entropy of the radiation, for the model in fig. 5.3. The dotted line is the growing result given by the Hawking computation, and the entropy calculated from the other saddle is dashed. The minimum of the two is the Page curve for this model.

the gravitational equations. The idea is to do Euclidean computations and then analytically continue to Lorentzian signature.

Consider $n = 2$ replicas. The replica partition function $\mathrm{tr}(\rho_R)^2$ is computed by a Euclidean path integral on two copies of the Euclidean system, with the matter sector sewed together along the cuts on region R. Since we are doing a gravitational path integral, we do not specify the geometry in the gravity region; we only fix the boundary conditions at the edge. Gravity then fills in the geometry dynamically, see fig. 5.6.

We consider two different saddles with the correct boundary conditions. The first is the Hawking saddle, see figure 5.6(a). The corresponding von Neumann entropy is the usual answer, $S_{\mathrm{matter}}(R(t))$, which grows linearly forever. The second is the replica wormhole, which, as we will show, reproduces the entropy of the island rule, see figure 5.6(b). A replica wormhole with higher n is illustrated in fig. 5.7.

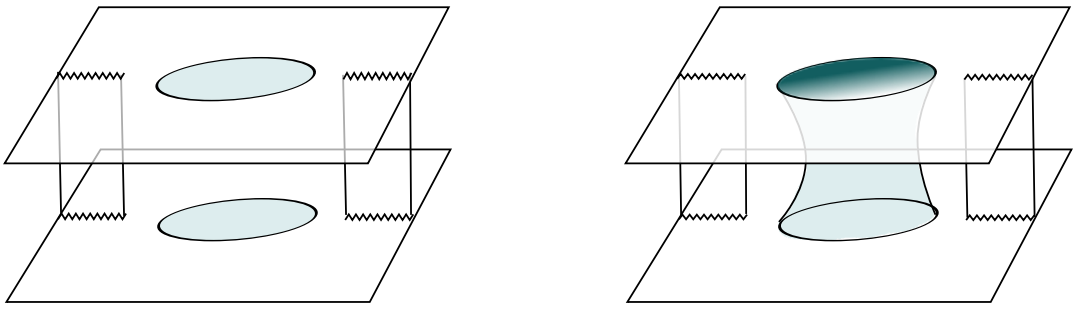

Figure 5.6: Two different saddlepoint contributions to the two-replica path integral in the presence of gravity in the shaded region. On the left the replicas are sewn together along the branch points, outside of the shaded region, as we would do in an ordinary quantum field theory calculation. These will give the standard QFT answer, as computed by Hawking, which can lead to a paradox. On the right we have a saddle where gravity dynamically glues together the shaded regions. This is the replica wormhole. In the examples considered in this paper, this saddle dominates in the relevant kinematics, leading to a Page curve consistent with unitarity.

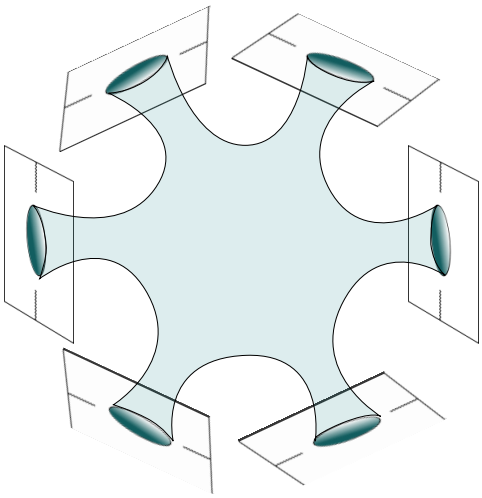

Figure 5.7: Topology of a replica wormhole with $n = 6$. The sheets are also glued together cyclically along the cuts in the matter region.

Replica wormholes have higher topology, so they are suppressed by factors of e^{-S_0} where S_0 is the genus-counting parameter of JT gravity. At late times, the contribution of the Hawking saddle is heavily suppressed by the kinematics, and this is what makes it possible for the replica wormhole to take over despite the topological suppression. Indeed, the n^{th} wormhole, see fig. 5.7, gives a partition function $Z_n \propto e^{S_0(2-n)}$ which leads to a $2S_0$ contribution to the entropy.

The wormhole topology has a saddle point at finite n. (We will not show this in general, but confirm it explicitly in certain limits; see below for details.) The equations that control this saddle point can be analytically continued to non-integer n, and used to define the replica limit $n \to 1$. To analyze this limit it is most convenient to assume replica symmetry and go to a quotient space which has a simpler topology but contains conical singularities and insertions of twist operators for the matter fields, see figure 5.9. In the limit $n \to 1$ both of these effects become very small and represent a small perturbation for the geometry, but they give a contribution to the entropy of precisely the same form as the gravitational generalized entropy for regions in the $n = 1$ solution. The boundaries of the regions are specified by the locations of the twist operators. The replica wormholes give rise to the island contributions to the entropy.

This paper is organized as follows.

In section 5.1.1 we review and slightly clarify the gravitational derivation of the quantum extremal surface presciption from the replica trick in a general theory [260, 265–267]. The slight improvement is that we show that the off shell action near $n \sim 1$ becomes the generalized entropy, so that the extremality condition follows directly from the extremization of the action. In section 5.1.2 we discuss some general aspects of replica manifolds for the case of JT gravity plus a CFT.

In section 5.2 we discuss the computation of the entropy for an interval that contains the degrees of freedom living at the AdS boundary. In this case the quantum extremal surface is slightly outside the horizon. We set up the discussion of the Renyi entropy computations for this case. We reduce the problem to an integro-differential equation for a single function $\theta(\tau)$ that relates the physical time τ to the AdS time θ. We solve this equation for $n \to 1$ recovering the quantum extremal surface result. We also solve the problem for relatively high temperatures but for any n.

In section 5.3 we discuss the special case of the zero temperature limit, and we comment on some features of the island in that case.

In section 5.4 we discuss aspects of the two intervals case, which is the one most relevant for the information problem for the eternal black hole.

In section 5.5 we make the connection to entanglement wedge reconstruction of the black hole interior.

We end in section 5.6 with conclusions and discussion.

5.1 The replica trick for the von Neumann entropy

The replica trick for computing the von Neumann entropy is based on the observation that the computation of $Tr[\rho^n]$ can be viewed as an observable in n copies of the original system [278]. In particular, for a quantum field theory the von Neumann entropy of some region can be computed by considering n copies of the original theory and choosing boundary conditions that connect the various copies inside the interval in a cyclic way, see e.g. [279] for a review. This can be viewed as the

insertion of a "twist operator" in the quantum field theory containing n copies of the original system. This unnormalized correlator of twist operators can also be viewed as the partition function of the theory on a topologically non-trivial manifold, $Z_n = Z[\widetilde{\mathcal{M}}_n] = \langle \mathcal{T}_1 \cdots \mathcal{T}_k \rangle$. Then the entropy can be computed by analytically continuing in n and setting

$$S = -\,\partial_n \left(\frac{\log Z_n}{n} \right) \Big|_{n=1} \tag{5.3}$$

We will now review the argument for how this is computed in theories of gravity. Then we will consider the specific case of the JT gravity theory.

5.1.1 The replicated action for $n \sim 1$ becomes the generalized entropy

In this section we review the ideas in [260, 265–267] for proving the holographic formula for the fine-grained entropy, or von Neumann entropy. We clarify why we get the generalized entropy when we evaluate the off shell gravity action near the $n = 1$ solution.

The replica trick involves a manifold $\widetilde{\mathcal{M}}_n$ which computes the n^{th} Renyi entropy. The geometry of this manifold is completely fixed in the non-gravitational region, where we define the regions whose entropies we are computing[2]. In the gravitational region we can consider any manifold, with any topology, which obeys the appropriate boundary conditions. The full action for the system is a sum of the gravitational action and the partition function for the quantum fields on the geometry $\widetilde{\mathcal{M}}_n$,

$$\frac{\log Z_n}{n} = -\frac{1}{n} I_{\text{grav}}[\widetilde{\mathcal{M}}_n] + \frac{1}{n} \log Z_{\text{mat}}[\widetilde{\mathcal{M}}_n] \,. \tag{5.4}$$

[2]If we only had the AdS theory, without an outside region, then the non-gravitational part should be viewed just as the boundary of AdS.

This is an effective action for the geometry and we will look for a classical solution of this combined action. In other words, the integral over geometries is evaluated as a saddle point. So the metric is classical, but the equations contain the quantum expectation value of the matter stress tensor on that geometry. Under the assumption of replica symmetry, we can instead consider another manifold $\mathcal{M}_n = \widetilde{\mathcal{M}}_n/Z_n$. This manifold can be viewed as one where n identical copies of the field theory are living. We have twist operators $\mathcal{T}_n$ at the endpoints of the intervals in the non-gravitational region. In the gravitational region we also have twist operators $\mathcal{T}_n$ at the fixed points of the Z_n action, where the manifold $\mathcal{M}_n$ has conical singularities with opening angle $2\pi/n$. Of course, at these points the covering manifold $\widetilde{\mathcal{M}}_n$ is smooth. It is convenient to translate the problem in (5.4) to a problem involving the manifold $\mathcal{M}_n$. We have n copies of the matter theory propagating on this manifold. In the gravitational region we can enforce the proper conical singularities in $\mathcal{M}_n$ by adding codimension-two "cosmic branes" of tension

$$4G_N T_n = 1 - \frac{1}{n}. \tag{5.5}$$

At these cosmic branes we also insert twist operators $\mathcal{T}_n$ for the n copies of the matter theory. In two dimensions these "cosmic branes" are simply points, while in four dimensions they are "cosmic strings." The positions of these cosmic branes are fixed by solving the Einstein equations. We then replace the gravitational part of the action in (5.4) by

$$\frac{1}{n} I_{\text{grav}}[\widetilde{\mathcal{M}}_n] = I_{\text{grav}}[\mathcal{M}_n] + T_n \int_{\Sigma_{d-2}} \sqrt{g}. \tag{5.6}$$

As opposed to [265], here we add the action of these cosmic branes explicity and we also integrate the Einstein term through the singularity, which includes a δ function for the curvature. These two extra terms cancel out so that we get the same final answer as in [265] where no contribution from the singularity was included. We

will see that the present prescription is more convenient[3].

In the part of the manifold where the metric is dynamical the position of these cosmic branes is fixed by the Einstein equations. Also, the reparametrization symmetry implies we cannot fix these points from the outside.

When $n = 1$ we have the manifold $\mathcal{M}_1 = \widetilde{\mathcal{M}}_1$, which is the original solution to the problem. It is a solution of the action $I_1^{\rm tot}$. In order to find the manifold $\mathcal{M}_n$ for $n \sim 1$ we need to add the cosmic branes. Then the action is

$$\left(\frac{I^{\rm tot}}{n}\right)_{n\to 1} = I_1 + \delta\left(\frac{I}{n}\right) \tag{5.7}$$

where δI contains extra terms that arise from two effects, both of which are of order $n-1$. The first comes from the tension of the cosmic brane (the second term in (5.6). The second comes from the insertion of the twist fields at the position of this cosmic brane. To evaluate the action perturbatively, we start from the solution $\mathcal{M}_1$, we add the cosmic brane and twist fields, and we also consider a small deformation of the geometry away from $\mathcal{M}_1$, where all these effects are of order $n-1$. Because the $\mathcal{M}_1$ geometry is a solution of the original action I_1 in (5.7), any small deformation of the geometry drops out of the action. For the extra term $\delta(I/n)$ in (5.7), we can consider the cosmic brane action and twist fields as living on the old geometry $\mathcal{M}_1$ since these extra terms are already of order $n-1$.

Then we conclude that the δI term is simply proportional to the generalized entropy

$$\delta\left(\frac{\log Z}{n}\right) = -\delta\left(\frac{I}{n}\right) = (1-n)S_{\rm gen}(w_i) = (1-n)\left[\frac{\rm Area}{4G_N} + S_{\rm matter}\right], \quad n\sim 1 \tag{5.8}$$

where we emphasized that it depends on the positions of the cosmic branes. We

[3]In theories with higher derivatives we would need to add extra terms in the action of the cosmic brane so that they just produce a conical singularity. These presumably lead to an off shell action of the form considered in [280] but we did not check this.

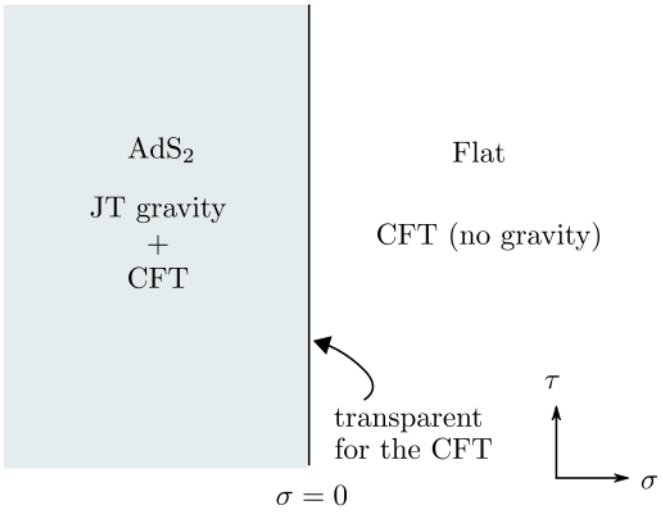

Figure 5.8: We consider nearly-AdS_2 gravity with a matter CFT. The same CFT lives in an exterior flat space with no gravity. We have transparent boundary conditions for the CFT.

should emphasize that (5.8) is the full off-shell action that we need to extremize to find the classical solution of I_n for $n \sim 1$. In this way, we obtain the quantum extremal surface prescription of [34], and also [28, 259]. Moreover, if we think of the cosmic strings as dynamical objects, then we can pair create them so as to form islands. This pair creation is possible in the gravity region where the tension is finite. In the region without gravity their tension is effectively infinite.

5.1.2 The two dimensional JT gravity theory plus a CFT

In this section we specify in more detail the theory under consideration. We have the Jackiw-Teitelboim gravity theory describing a nearly AdS_2 spacetime coupled to a matter theory that is a CFT. In addition, we have the same CFT living in an exterior flat and rigid geometry with no gravity. Since the interior and the

exterior involve the same CFT we can impose transparent boundary conditions at the boundary, see figure 5.8. In other words, we have the action

$$\log Z^{\text{tot}} = \frac{S_0}{4\pi}\left[\int_{\Sigma_2} R + \int_{\partial\Sigma_2} 2K\right] + \int_{\Sigma_2}\frac{\phi}{4\pi}(R+2) + \frac{\phi_b}{4\pi}\int_{\partial\Sigma_2} 2K + \log Z_{CFT}[g] \quad (5.9)$$

where the CFT action is defined over a geometry which is rigid in the exterior region and is dynamical in the interior region. We are setting $4G_N = 1$ so that the area terms in the entropies will be just given by the value of ϕ, $\frac{\text{Area}}{4G_N} = S_0 + \phi$.

In this theory, we want to consider the replica manifolds described above, see figure 5.7. Because we consider replica symmetric solutions, it is convenient to quotient by Z_n and discuss a single manifold with n copies of the matter theory on it. In other words, we go from the action (5.9) on $\widetilde{\mathcal{M}}_n$ to a problem on $\mathcal{M}_n = \widetilde{\mathcal{M}}_n/Z_n$. We find that this simplifies a bit the description of the manifold, see figure 5.9. Namely, the manifold $\mathcal{M}_n$ can be viewed as a disk with conical singularities and with twist operators for the matter theory inserted at these singularities. These are the cosmic branes discussed in section 5.1.1. The final gravitational action is as in (5.9) but with an additional factor of n and extra terms that produce the conical singularities

$$-\frac{1}{n}I_{\text{grav}} = \frac{S_0}{4\pi}\left[\int_{\Sigma_2} R + \int_{\partial\Sigma_2} 2K\right] + \int_{\Sigma_2}\frac{\phi}{4\pi}(R+2) + \frac{\phi_b}{4\pi}\int_{\partial\Sigma_2} 2K - (1-\frac{1}{n})\sum_i [S_0 + \phi(w_i)] \quad (5.10)$$

where w_i are the positions of the conical singularities, or cosmic branes (which are just instantons or -1 branes). We can consider (5.10) as a new gravity theory and add n copies of the CFT. In addition, we put twist fields at the positions w_i of the cosmic branes. It might look like we are breaking reparametrization invariance when when add these terms. Reparametrization symmetry is restored because w_i are dynamical variables which can be anywhere on the manifold and will be fixed by the equations of motion.

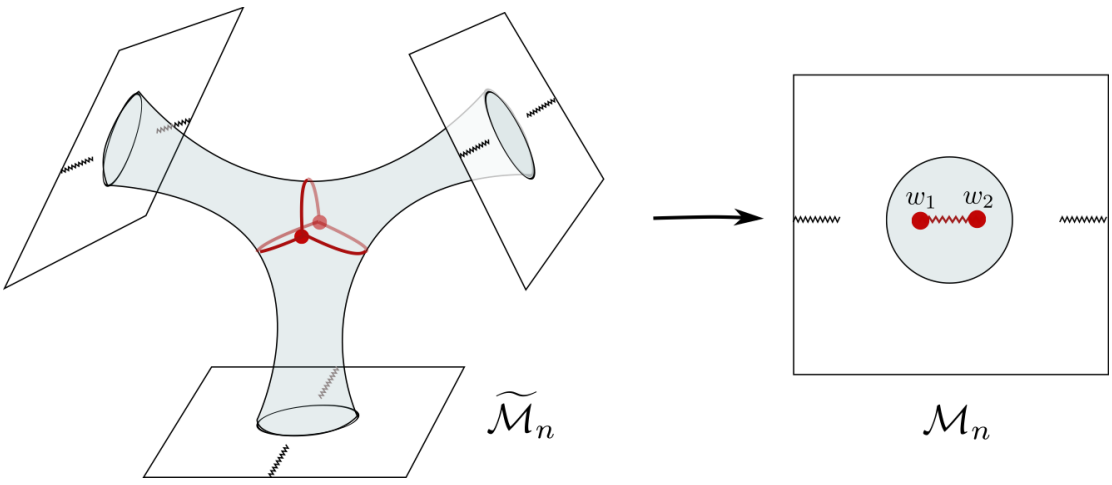

Figure 5.9: Here we display the replica manifold, $\widetilde{\mathcal{M}}_3$, and also the manifold $\mathcal{M}_3 = \widetilde{\mathcal{M}}_3/Z_3$ which has the topology of the disk with conical singularities at two points w_1 and w_2 which corresponds to the fixed points of the Z_3 action on $\widetilde{\mathcal{M}}_3$. We parametrize this disk in terms of the holomorphic coordinate w. The exterior regions of $\widetilde{\mathcal{M}}_n$ are also glued together cyclically along the cuts.

We treat the CFT as a quantum theory and evaluate its partition function. Then we solve the classical equations for the metric and dilaton inserting the quantum expectation value of the stress tensor. This approximation is particularly appropriate when the central charge is large $c \gg 1$. So we imagine that we are in that regime for the simple euclidean solutions we discuss here. The approximation can also be justified in other regimes where the entanglement entropy of matter is large for kinematical reasons. However, this description is *not* correct when we need to include the quantum aspects of gravity. That computation should be done in the original manifold and the fact that the fluctuations can break the replica symmetry is important.

We can define an interior complex coordinate w where the metric for the

manifold $\mathcal{M}_n$ in the gravitational region is

$$ds^2 = e^{2\rho} dw d\bar{w} \ , \qquad \text{with} \ \ |w| \leq 1 \, . \tag{5.11}$$

The boundary of AdS_2 is at $|w| = 1$, or $w = e^{i\theta}$. (5.11) is a constant curvature metric on the disk $|w| \leq 1$ with conical singularities at certain values w_i with opening angle $2\pi/n$. This type of metric is enforced by the dilaton equation of motion in (5.10)

$$-4\partial_w \partial_{\bar{w}} \rho + e^{2\rho} = 2\pi(1 - \frac{1}{n}) \sum_i \delta^2(w - w_i) \tag{5.12}$$

On this space we have n copies of the CFT and we have twist fields inserted at the conical singularities. Notice that once we impose this equation, the contributions in (5.10) from the delta functions in the curvature cancel against the explicit cosmic brane action terms, as we anticipated in section 5.1.1.

This metric should be joined to the flat space outside. We consider a finite temperature configuration where $\tau \sim \tau + 2\pi$. For general temperatures, all we need to do is to rescale $\phi_r \to 2\pi\phi_r/\beta$. In other words, the only dimensionful scale is ϕ_r, so the only dependence on the temperature for dimensionless quantities is through ϕ_r/β. We define the coordinate $v = e^y$. So the physical half cylinder $\sigma \geq 0$ corresponds to $|v| \geq 1$. At the boundary we have that $w = e^{i\theta(\tau)}$, $v = e^{i\tau}$. Unfortunately, we cannot extend this to a holomorphic map in the interior of the disk. However, we can find another coordinate z such that there are holomorphic maps from $|w| \leq 1$ and $|v| \geq 1$ to the coordinate z, see figure 5.10.

In other words, it is possible to find two functions G and F such that

$$\begin{aligned} z &= G(w) \ , \quad \text{for} \quad |w| \leq 1 \\ z &= F(v) \ , \quad \text{for} \quad |v| \geq 1 \end{aligned}$$

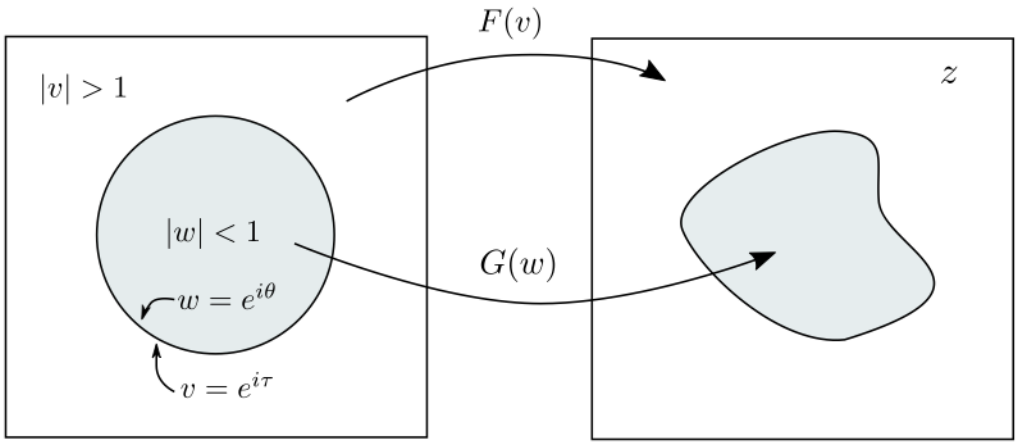

Figure 5.10: The conformal welding problem. We are given two disks, one parametrized by $|w| \leq 1$ and another by $|v| \geq 1$ with their boundaries glued in terms of a given function $\theta(\tau)$ where $w = e^{i\theta}$ and $v = e^{i\tau}$. Then we need to find holomorphic maps of each disk to a region of the complex z plane so that they are compatible at the boundary. The functions F and G are only required to be holomorphic inside their respective disks.

$$G(e^{i\theta(\tau)}) = F(e^{i\tau}) \,, \quad \text{for} \quad |w| = |v| = 1 \,. \tag{5.13}$$

The functions F and G are holomorphic in their respective domains (they do not have to be holomorphic at the boundary). The problem of finding F and G given $\theta(\tau)$ is called the "conformal welding problem," see [281] for a nice discussion.[4] F and G end up depending non-locally on $\theta(\tau)$ and they map the inside and outside disks to the inside and outside of some irregular region in the complex plane, see figure 5.10. In our problem, $\theta(\tau)$ arises as the reparametrization mode, or "boundary graviton" of the nearly-AdS_2 gravity theory [273, 282, 283].

When $n = 1$, we have a trivial stress tensor in the z plane. We then insert the twist operators in the outside region, and also in the inside region. We are free

[4]We thank L. Iliesiu and Z. Yang for discussions on this problem, and A. Lupsasca for pointing out the connection to [281].

to insert as many conical singularities and twist fields in the inside as we want. This amounts to considering various numbers of islands in the gravity region. We will only discuss cases with one or two inside insertions in the subsequent sections. This gives us a non-trivial stress tensor $T_{zz}(z)$ and $T_{\bar{z}\bar{z}}(\bar{z})$. We can then compute the physical stress tensor that will appear in the equation of motion using the conformal anomaly,

$$T_{yy} = \left(\frac{dF(e^{iy})}{dy}\right)^2 T_{zz} - \frac{c}{24\pi}\{F(e^{iy}), y\} \tag{5.14}$$

and a similar expression for $T_{\bar{y}\bar{y}}$. The expression for the physical stress tensor in the w plane involves the function G and also a conformal anomaly contribution from ρ in the metric (5.11).

Let us now turn to the problem of writing the equations of motion for the boundary reparametrization mode. Naively we are tempted to write the action just as $\{e^{i\theta}, \tau\}$. This would be correct if there were no conical singularities in the interior. However, the presence of those conical singularities implies that the metric (5.11) has small deviations compared to the metric of a standard hyperbolic disk

$$ds^2 = e^{2\rho} dw d\bar{w} \ , \qquad e^{2\rho} = \frac{4}{(1-|w|^2)^2} e^{2\delta\rho} \tag{5.15}$$

where $\delta\rho$ goes as

$$\delta\rho \sim -\frac{(1-|w|)^2}{3} U(\theta) \ , \qquad \text{as} \quad |w| \to 1 \, . \tag{5.16}$$

The function U depends on the positions of the conical singularities and therefore also on the moduli of the Riemann surface. This then implies that the Schwarzian term, and the full equation of motion can now be written as

$$\frac{\phi_r}{2\pi}\frac{d}{d\tau}\left[\{e^{i\theta}, \tau\} + U(\theta)\theta'^2\right] = i(T_{yy} - T_{\bar{y}\bar{y}}) = T_{\tau\sigma} \, . \tag{5.17}$$

The term in brackets is proportional to the energy. This equation relates the change in energy to the energy flux from the flat space region. Here the flux of energy

on the right hand side is that of one copy, or the flux of the n copies divided by n. The action can be derived from the extrinsic curvature term in the same way that was discussed in [273, 282, 283], see appendix D.1, where we also discuss the explicit derivation of the equation of motion (5.17).

There are also equations that result from varying the moduli of the Riemann surface, or the positions of the conical singularities. They have the form

$$-(1-\frac{1}{n})\partial_w\phi(w_i)+\partial_{w_i}\left(\frac{\log Z_n^{\rm mat}}{n}\right)=0\,, \tag{5.18}$$

where we used that the w_i dependence of the gravitational part of the action comes only from the last term in (5.10).

In the $n\to 1$ limit we can replace the $n=1$ value for the dilaton in (5.18). Similarly the value of $\log Z_n^{\rm mat}/n$ near $n=1$ involves the matter entropy. Therefore (5.18) reduces to the condition on the extremization of the generalized entropy, as we discussed in general above.

For general n, we need to compute the dilaton by solving its equations of motion in order to write (5.18). This can be done using the expression for the stress tensor in the interior of the disk. We have not attempted to simplify it further. However, we should note that for the particular case of one interval, discussed in section 5.2, there is only one point and there are no moduli for the Riemann surface. Therefore this equation is redundant and in fact, it is contained in (5.17) as will be discussed in section 5.2.

Next we apply this general discussion to the calculation of the entropy of various subregions of the flat space CFT. The goal is to understand how configurations of the gravity region contribute to the entropy of those CFT regions.

5.2 Single interval at finite temperature

We begin with the simple case of a single interval that contains one of the AdS_2 boundaries, as shown in figure 5.11(a). This is the interval $B \equiv [0, b]$.

To compute the entropy of this region we must consider the Euclidean path integral that evaluates the trace of powers of the density matrix $\text{Tr}\,[\rho_B^n]$. This is given by the path integral on n copies of the theory identified across the region B, as shown in figure 5.11. The crucial point is that the presence of the branch point on the unit circle, which is where the asymptotic AdS boundary lives, elongates this circle by a factor of n. The Euclidean gravity configurations we must consider are all smooth manifolds with a single boundary that is identified with this elongated AdS boundary.

The simplest configuration to consider will be that with the topology of a disk. All other higher genus manifolds will be subleading since each extra handle will come with a cost of e^{-S_0}. Filling out the gravity region has the effect of extending the identification across the different sheets into the gravity region, which ends on some point "$-a$" in figure 5.11. The location of the point "$-a$" will be dynamically determined by the saddle point of the path integral.

We will now construct replica wormholes explicitly for a single interval in the eternal black hole in AdS_2. The Lorentzian and Euclidean geometries are shown in figure 5.12. We will first review of the result of the QES calculation [253], then proceed to derive it from replica wormholes.

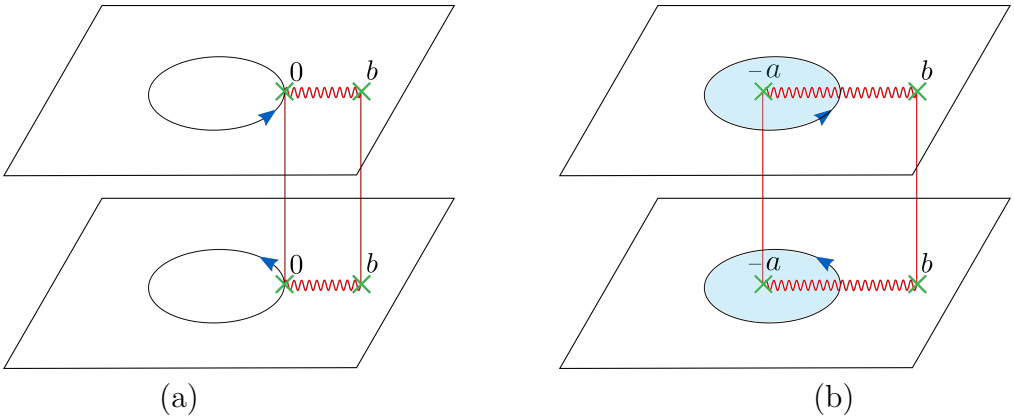

Figure 5.11: (a) We have a flat space field theory on the exterior of the disk. The disk is hollow in this picture, and will be filled in with gravitational configurations subject to the boundary conditions on the unit circle. This boundary is connected into a single long circle n times longer than the original one. This is indicated by the blue arrow which tells you how to go around the cut. (b) The disk is filled in with a gravitational configuration with the topology of a disk which ends on the elongated unit circle. This configuration can be represented by adding a branch point inside. Note that the local geometry at the branch point "$-a$" is completely smooth.

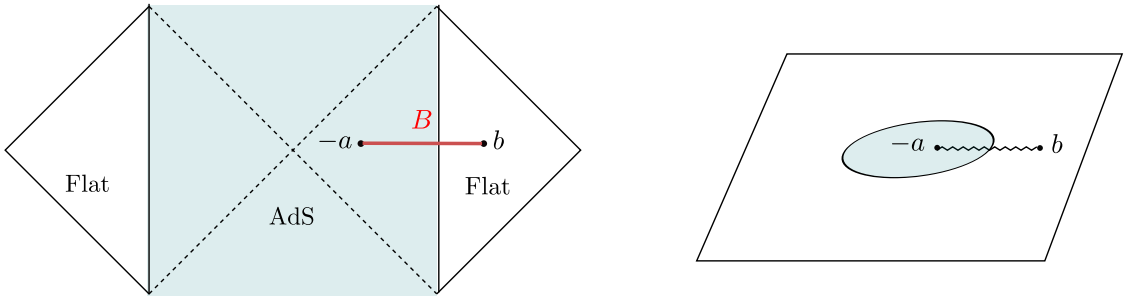

Figure 5.12: The single interval configuration in Lorentzian signature (left) and in Euclidean signature (right).

5.2.1 Geometry of the black hole

The metric of eternal black hole, glued to flat space on both sides, is

$$ds^2_{\rm in} = \frac{4\pi^2}{\beta^2}\frac{dyd\bar{y}}{\sinh^2\frac{\pi}{\beta}(y+\bar{y})}, \qquad ds^2_{\rm out} = \frac{1}{\epsilon^2}dyd\bar{y}\ , \tag{5.19}$$

$$y = \sigma + i\tau, \qquad \bar{y} = \sigma - i\tau\ , \qquad \tau = \tau + \beta\ . \tag{5.20}$$

The subscript 'in' refers to the gravity zone, and 'out' refers to the matter zone[5]. The interface is along the circle $\sigma = -\epsilon$. Lorenztian time t is $\tau = -it$. The welding maps of figure 5.10 are trivial and we have

$$z = v = w = e^{2\pi y/\beta}\ , \qquad y = \frac{\beta}{2\pi}\log w\ . \tag{5.22}$$

The Euclidean solution is therefore the w-plane with gravity inside the unit disk, $|w| < 1 - \frac{2\pi\epsilon}{\beta}$. The metric is

$$ds^2_{\rm in} = \frac{4dwd\bar{w}}{(1-|w|^2)^2}, \qquad ds^2_{\rm out} = \frac{\beta^2}{4\pi^2\epsilon^2}\frac{dwd\bar{w}}{|w|^2}\ . \tag{5.23}$$

The dilaton, which is defined only on the inside region, is rotationally invariant on the w-plane,

$$\phi = \frac{2\pi\phi_r}{\beta}\frac{1+|w|^2}{1-|w|^2} = -\frac{2\pi\phi_r}{\beta}\frac{1}{\tanh\frac{2\pi\sigma}{\beta}}\ . \tag{5.24}$$

with $\phi = \phi_r/\epsilon$ at the boundary. In what follows, we will usually set $\epsilon = 0$, and rescale the exterior coordinate by ϵ so that $ds^2_{out} = dyd\bar{y}$.

[5]The Poincare coordinates are $x = \tanh\frac{\pi y}{\beta}$, $ds^2_{\rm in} = 4dxd\bar{x}/(x+\bar{x})^2$. The Schwarzschild coordinates are

$$y = \frac{\beta}{2\pi}\log\frac{r}{\sqrt{r(r+4\pi/\beta)}} + i\tau\ , \qquad ds^2_{in} = r(r+\frac{4\pi}{\beta})d\tau^2 + \frac{dr^2}{r(r+\frac{4\pi}{\beta})}\ . \tag{5.21}$$

5.2.2 Quantum extremal surface

We now review the computation of the entropy of the region $B = [0, b]$ which includes the AdS_2 boundary, see figure 5.11. In gravity this will involve an interval $[-a, b]$, with $a, b > 0$, see figure 5.12.

The generalized entropy of the region $[-a, b]$ is

$$S_{\text{gen}} = S_0 + \phi(-a) + S_{\text{CFT}}([-a, b]) \ . \tag{5.25}$$

The entanglement entropy of a CFT on the interval $[w_1, w_2]$ in the metric $ds^2 = \Omega^{-2} dw d\bar{w}$ is

$$S_{\text{CFT}}(w_1, w_2) = \frac{c}{6} \log \left(\frac{|w_1 - w_2|^2}{\epsilon_{1,UV} \epsilon_{2,UV} \Omega(w_1, \bar{w}_1) \Omega(w_2, \bar{w}_2)} \right) \ . \tag{5.26}$$

Using the map $w = e^{2\pi y/\beta}$ and the conformal factors in (5.23) this becomes

$$S_{\text{CFT}}([-a, b]) = \frac{c}{6} \log \left(\frac{2\beta \sinh^2 \left(\frac{\pi}{\beta}(a+b) \right)}{\epsilon_{a,UV} \epsilon_{b,UV} \pi \sinh \left(\frac{2\pi a}{\beta} \right)} \right) \tag{5.27}$$

Then, using the dilaton in (5.24), (5.25) becomes

$$S_{\text{gen}}([-a, b]) = S_0 + \frac{2\pi\phi_r}{\beta} \frac{1}{\tanh \left(\frac{2\pi a}{\beta} \right)} + \frac{c}{6} \log \left(\frac{2\beta \sinh^2 \left(\frac{\pi}{\beta}(a+b) \right)}{\pi \epsilon \sinh \left(\frac{2\pi a}{\beta} \right)} \right) \ . \tag{5.28}$$

The UV divergence $\epsilon_{a,UV}$ was absorbed into S_0 and we dropped the outside one at point b. The quantum extremal surface is defined by extremizing S_{gen} over a

$$\partial_a S_{\text{gen}} = 0 \quad \rightarrow \qquad \sinh \left(\frac{2\pi a}{\beta} \right) = \frac{12\pi\phi_r}{\beta c} \frac{\sinh \left(\frac{\pi}{\beta}(b+a) \right)}{\sinh \left(\frac{\pi}{\beta}(a-b) \right)} \tag{5.29}$$

This is a cubic equation for $e^{2\pi a/\beta}$. For $b \gtrsim \frac{\beta}{2\pi}$ and $\phi_r/(\beta c) \gtrsim 1$, the solution is

$$a \approx b + \frac{\beta}{2\pi} \log \left(\frac{24\pi\phi_r}{\beta c} \right) \ , \qquad \text{or} \qquad e^{-\frac{2\pi a}{\beta}} \approx \frac{\beta c}{24\pi\phi_r} e^{-\frac{2\pi b}{\beta}} \tag{5.30}$$

Since we've restricted to one side of the black hole in this calculation, the configuration is invariant under translations in the Schwarzschild t direction. Therefore the

general extremal surface at $t \neq 0$ is related by a time translation; for an interval that starts at t_b and $\sigma_b = b$, the other endpoint is at $t_a = t_b$ and $\sigma_a = -a$, with a as in (5.29).

5.2.3 Setting up the replica geometries

We will do the replica calculation in Euclidean signature, with a, b real. We set $\beta = 2\pi$, and reintroduce it later by dimensional analysis.

The replica wormhole that we seek is an n-fold cover of the Euclidean black hole, branched at the points a and b, see figure (5.12). This manifold will have a nontrivial gluing at the unit circle (unlike the black hole itself), so it is more convenient to introduce different coordinates on the inside and outside. We use w, with $|w| < 1$, for the inside and $v = e^y$, with $|v| > 1$ for the outside. The gluing function is $\theta(\tau)$, with $w = e^{i\theta}$, $v = e^{i\tau}$, as in (5.13). We write the branch points as

$$w = A = e^{-a} , \qquad v = B = e^{b} . \tag{5.31}$$

The Schwarzian equation is simplest in a different coordinate,

$$\widetilde{w} = \left(\frac{w - A}{1 - Aw}\right)^{1/n} . \tag{5.32}$$

This coordinate uniformizes n copies of the unit disk, so here we have the standard hyperbolic metric,

$$ds^2_{in} = \frac{4|d\tilde{w}|^2}{(1 - |\tilde{w}|^2)^2} . \tag{5.33}$$

Defining $\tilde{w} = e^{i\tilde{\theta}}$ at the boundary, the Schwarzian equation is

$$\frac{\phi_r}{2\pi}\phi_\tau\{e^{i\tilde{\theta}}, \tau\} = i(T_{yy}(i\tau) - T_{\bar{y}\bar{y}}(-i\tau)) . \tag{5.34}$$

We can now return to the w-disk using the Schwarzian composition identity

$$\{e^{i\tilde{\theta}},\tau\} = \{e^{i\theta},\tau\} + \frac{1}{2}\left(1-\frac{1}{n^2}\right)R(\theta)\ , \tag{5.35}$$

with

$$R(\theta) = -\frac{(1-A^2)^2(\partial_\tau\theta)^2}{|1-Ae^{i\theta}|^4}\ . \tag{5.36}$$

This puts the equation of motion (5.34) into exactly the form of equation (5.17), which we have just derived by a slightly different route. In appendix D.1 we show that they are equivalent.

The stress tensor appearing on the right-hand side of (5.34) is obtained through the conformal welding. That is, we define the z coordinate by the map G on the inside and F on the outside as in (5.13). These maps each have an ambiguity under $SL(2,C)$ transformations of z, which we may use to map the twist operator at $w=A$ to $z=0$, and the twist operator at $v=B$ to $z=\infty$. We further discuss the symmetries of the conformal welding problem in appendix D.2.

The z-coordinate covers the full plane holomorphically. It has twist points at the origin and at infinity, which can be removed by the standard mapping, $\tilde{z}=z^{1/n}$. On the $\tilde{z}$ plane, the stress tensor vanishes, so on the z-plane,

$$T_{zz}(z) = -\frac{c}{24\pi}\{z^{1/n},z\} = -\frac{c}{48\pi}\left(1-\frac{1}{n^2}\right)\frac{1}{z^2}\ . \tag{5.37}$$

Finally the stress tensor T_{yy} comes from inverting the conformal welding map to return to the v-plane, and using $v=e^y$:

$$T_{yy}(y) = e^{2y}\left[F'(v)^2T_{zz} - \frac{c}{24\pi}\{F,v\}\right] - \frac{1}{2}\ . \tag{5.38}$$

Putting it all together, the equation of motion (5.34) is

$$\frac{24\pi\phi_r}{c\beta}\phi_\tau\left[\{e^{i\theta(\tau)},\tau\} + \frac{1}{2}(1-\frac{1}{n^2})R(\theta(\tau))\right] = ie^{2i\tau}\left[-\frac{1}{2}(1-\frac{1}{n^2})\frac{F'(e^{i\tau})^2}{F(e^{i\tau})^2} - \{F,e^{i\tau}\}\right] + cc \tag{5.39}$$

This equation originated on the smooth replica manifold $\widetilde{\mathcal{M}}_n$, but has now been written entirely on the quotient manifold $\mathcal{M}_n = \widetilde{\mathcal{M}}_n/\mathbf{Z}_n$. We have restored the nontrivial temperature dependence[6]. In particular, note that $\theta(\tau+2\pi) = \theta+2\pi$. The $\tau \to -\tau$ symmetry of the insertions allows us to choose a function $\theta(\tau) = -\theta(-\tau)$ which will automatically obey $\theta(0) = 0$, $\theta''(0) = 0$. In addition, we should then impose $\theta(\pi) = \pi$ and $\theta''(\pi) = 0$. The problem now is such that n appears as a continuous parameter and there is no difficulty in analytically continuing in n.

This is our final answer for the equation of motion at finite n. It is quite complicated, because the welding map F depends implicitly on the gluing function $\theta(\tau)$. We will solve it in two limits: $\beta \to 0$ at any n, and $n \to 1$ at any β.

5.2.4 Replica solution as $n \to 1$

We will now show that the equation of motion (5.39) reproduces the equation for the quantum extremal surface.

We start with the solution for $n = 1$. In this case the welding problem is trivial and we can set $w = v$ everywhere. It is convenient to set

$$z = F(v) = \frac{v - A}{B - v} = G(w) \ , \qquad w = v \tag{5.40}$$

At $n = 1$ any choice of A can do. Different choices of A can be related by an $SL(2, R)$ transformation that acts on w. It will be convenient for us to choose A so that when we go to $n \sim 1$, it corresponds to the position of the conical singularity.

We now go near $n \sim 1$ and expand

$$e^{i\theta} = e^{i\tau} + e^{i\tau} i\delta\theta(\tau) \ , \tag{5.41}$$

[6]The trivial temperature dependence is restored by $\tau \to \frac{2\pi}{\beta}\tau_{phys}$, with τ_{phys} the physical Euclidean time with period β.

where $\delta\theta$ is of order $n-1$. We aim to solve (5.39) for $\delta\theta$. The first step is to find the welding map perturbatively in $(n-1)$. In appendix D.2, we show that

$$e^{2i\tau}\{F, e^{i\tau}\} = -\delta\{e^{i\theta}, \tau\}_- = -(\delta\theta''' + \delta\theta')_- \tag{5.42}$$

where we used

$$\delta\{e^{i\theta}, \tau\} \equiv \{e^{i\tau + i\delta\theta}, \tau\} - \{e^{i\tau}, \tau\} = \delta\theta''' + \delta\theta' \tag{5.43}$$

The minus subscript indicates that this is projected onto negative-frequency modes. This can be written neatly using the Hilbert transform, H, which is defined by the action $\mathrm{H}\cdot e^{im\tau} = -\mathrm{sgn}(m)e^{im\tau}$ (and $\mathrm{H}\cdot 1 = 0$). Then

$$e^{2i\tau}\{F, e^{i\tau}\} = -\frac{1}{2}(1+\mathrm{H})(\delta\theta''' + \delta\theta'). \tag{5.44}$$

Wherever else F appears in (5.39), it is multiplied by $(n-1)$, so there we can set $F = \frac{v-A}{B-v}$, as in (5.40). Therefore the equation of motion for the perturbation is

$$\phi_\tau(\delta\theta''' + \delta\theta') + \frac{ic}{12\phi_r}\mathrm{H}\cdot(\delta\theta''' + \delta\theta') = (n-1)\left[\frac{c}{12\phi_r}\mathcal{F} - \phi_\tau R(\tau)\right] \tag{5.45}$$

where

$$\mathcal{F} = -i\frac{e^{2i\tau}(A-B)^2}{(e^{i\tau}-A)^2(e^{i\tau}-B)^2} + cc\ . \tag{5.46}$$

Equation (5.45) is nonlocal, due to the Hilbert transform. We can solve it by expanding both sides in a Fourier series. The important observation is that, due to the structure of derivatives in each term of the left hand side of (5.45), the terms with Fourier modes of the form $e^{ik\tau}$ for $k = 0, \pm 1$ are automatically zero in the left hand side. Therefore, in order to solve this equation, we must impose the same condition on the right-hand side. The $k = 1$ mode requires

$$\int_0^{2\pi} d\tau e^{-i\tau}\left(\frac{c}{12\phi_r}\mathcal{F} - \phi_\tau R(\tau)\right) = 0\ . \tag{5.47}$$

Doing the integrals, this gives the condition

$$\frac{c}{6\phi_r}\frac{\sinh\frac{a-b}{2}}{\sinh\frac{b+a}{2}} = \frac{1}{\sinh a}\ . \tag{5.48}$$

This matches the equation for the quantum extremal surface (5.29) that came from the derivative of the generalized entropy. The term with $k = 0$ is automatically zero in the right hand side, as $\partial_\tau R$ is explicitly a total derivative and $\int_0^{2\pi} d\tau \mathcal{F} = 0$.

Thus we have reproduced the QES directly from the equations of motion. Once the QES condition is imposed, it is straightforward to solve for the rest of the the Fourier modes of $\delta\theta$ to confirm that there is indeed a solution.

The Hilbert transform that appeared in the equations of motion (5.45) has a natural interpretation in Lorentzian signature as the term responsible for dissipation of an evaporating black hole into Hawking radiation. This is elaborated upon in appendix D.3.

5.2.5 Entropy

To calculate the entropy, we must evaluate the action to leading order in $n - 1$. By the general arguments of section 5.1.1, this will reproduce the generalized entropy in the bulk. Here we will check this explicitly.

The gravitational action (5.10) in terms of the Schwarzian is

$$-I_{\text{grav}} = S_0 + \frac{\phi_r}{2\pi} n \int_0^{2\pi} d\tau \left(\{e^{i\theta}, \tau\} + \frac{1}{2}(1 - \frac{1}{n^2}) R(\theta) \right) . \tag{5.49}$$

The first term is $-S_0$ times the Euler characteristic of the replica wormholes, $\chi = 1$ in this case. After normalizing, the contribution to $-\log \text{ Tr } (\rho_R)^n$ for $n \approx 1$ is

$$-I_{\text{grav}}(n) + nI_{\text{grav}}(1) \approx (1-n)S_0 + (n-1)\frac{\phi_r}{2\pi}\int_0^{2\pi} d\tau R(\tau) + (n-1)\frac{\phi_r}{2\pi}\int_0^{2\pi} d\tau \phi_n \{e^{i\theta}, \tau\} . \tag{5.50}$$

The first two terms give the area term in the generalized entropy. The second term

is the dilaton at the branch point,

$$\frac{\phi_r}{2\pi}\int_0^{2\pi} d\tau R(\tau) = -\frac{\phi_r}{\tanh a} \tag{5.51}$$

The leading term in the matter action is the von Neumann entropy of the CFT,[7] plus a contribution from an order $(n-1)$ change in the metric

$$\log Z_n^{\rm mat} - n \log Z_1^{\rm mat} = -(n-1) S_{\rm bulk}([-a,b]) + \delta_g \log Z_M \ . \tag{5.52}$$

The matter action is evaluating on the manifold with the dynamical twist point in the gravity region, so the bulk entropy includes the island, I. By the equation of motion at $n=1$, the last term in (5.50) cancels the last term in (5.52), leading to

$$\log\ {\rm Tr}\ (\rho_B)^n \approx (1-n) S_{\rm gen}([-a,b]) \quad \to \quad S([0,b]) = S_{\rm gen}([-a,b]) \ . \tag{5.53}$$

as predicted by the general arguments reviewed in section 5.1.1 [267].

5.2.6 High-temperature limit

For general n is is convenient to write the equation as follows. The problem has an $SL(2,R)$ gauge symmetry that acts on w and A. We can use it to gauge fix $A=0$. Then the equation (5.39) becomes

$$\phi_\tau \{e^{i\theta(\tau)/n}, \tau\} = \kappa i e^{2i\tau}\left[-\frac{1}{2}(1-\frac{1}{n^2})\frac{F'(e^{i\tau})^2}{F(e^{i\tau})^2} - \{F, e^{i\tau}\}\right] + cc \tag{5.54}$$

Where we introduced

$$\kappa \equiv \frac{c\beta}{24\pi\phi_r} \tag{5.55}$$

This is proportional to the ratio of c and the near extremal entropy of the black hole $S - S_0$. When this parameter is small, the equations simplify. This essentially

[7] This is derived in the standard way, for example by integrating the CFT Ward identity for $\phi_b \log Z_M$ [284].

corresponds to weak gravitational coupling. In this section we will study the equations for small $\kappa \ll 1$.

To leading order, we can ignore the effects of welding and set $F = G$ with

$$F(v) = \frac{v}{B - v} , \qquad G(w) = \frac{w}{B - w} \tag{5.56}$$

This eliminates all the effects of welding, so the equation of motion is a completely explicit differential equation for $\theta(\tau)$. We expand

$$\theta(\tau) = \tau + \delta\theta(\tau) , \tag{5.57}$$

with $\delta\theta$ of order κ. The equation (5.54) is

$$\phi_\tau \left(\delta\theta''' + \frac{1}{n^2}\delta\theta' \right) = \frac{\kappa}{2}(1 - \frac{1}{n^2})\mathcal{F} \tag{5.58}$$

with

$$\mathcal{F} = -i \left(1 - \frac{e^{i\tau}}{B} \right)^{-2} + cc . \tag{5.59}$$

We can expand this in a power series. The constant Fourier mode is absent in the right hand side of (5.58). After solving (5.58) in Fourier space we get

$$\delta\theta = -i\frac{\kappa}{2}(1 - \frac{1}{n^2}) \sum_{m=1}^{\infty} \frac{(m+1)}{m^2(m^2 - \frac{1}{n^2})} \frac{e^{im\tau}}{B^m} + c.c. \tag{5.60}$$

This is the solution to this order. Inserting this into the action we can compute the Renyi entropies. We can go to higher orders by solving the conformal welding problem for $\theta = \tau + \delta\theta$, as explained in [281], computing the flux to next order, and solving again the Schwarzian equation to find the next approximation for $\theta(\tau)$. In this way we can systematically go to any order we want.

As a check of (5.60), we can consider the $n \to 1$ limit. In this case all Fourier coefficients of (5.60) go to zero except $m = \pm 1$ so that we get

$$\delta\theta = -i\frac{\kappa}{B}(e^{i\tau} - e^{-i\tau}) \tag{5.61}$$

In order to compare with the results of the quantum extremal surface calculation we should recall that we have gauge fixed A to be zero. Indeed the final solution (5.61) looks like an infinitesimal $SL(2,R)$ transformation of the $\theta = \tau$ solution. This is precisely what results from the transformation

$$e^{i\theta} \sim e^{i\tau}(1 + i\delta\theta) \sim \frac{e^{i\tau} - A}{1 - Ae^{i\tau}} \sim e^{i\tau}(1 - Ae^{-i\tau} + Ae^{i\tau}) \ , \qquad A \sim \frac{\kappa}{B} \ll 1 \quad (5.62)$$

for small A as in (5.30). This shows that the finite-n solution at high temperatures has the right $n \to 1$ limit.

5.3 Single interval at zero temperature

There is a very simple version of the information paradox at zero temperature [253]. Consider the region R in fig. 5.13. Ignoring gravity, the von Neumann entropy of the quantum fields on this region is infrared divergent. This is the Hawking-like calculation of the entropy using quantum field theory on a fixed background.

The state of the quantum fields on a full Cauchy slice is pure. However, the AdS_2 region is supposed to be a quantum system with S_0 states. This is a contradiction, because it is impossible for the finite states in the AdS_2 region to purify the IR-divergent entropy of region R. The UV divergence is not relevant to this issue because it is purified by CFT modes very close to the endpoint.

This is resolved by including an island, as in fig. 5.13 [253]. We will describe briefly how this is reproduced from a replica wormhole. This doesn't require any new calculations because we can take the limit $\beta \to \infty$ in the finite temperature result. The pictures, however, are slightly different, because the replica geometries degenerate in this limit and the topology changes.

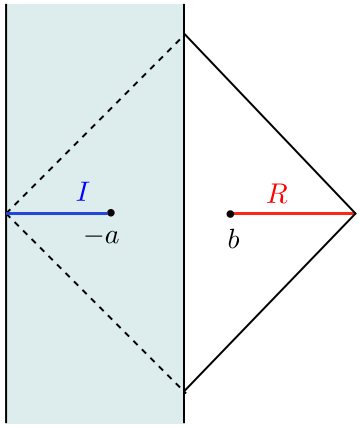

Figure 5.13: An information puzzle at zero temperature, with AdS_2 on the left and flat space on the right. The naive calculation of matter entropy in region R is infrared-divergent, but this cannot be purified by quantum gravity in AdS_2. This is resolved by including the island, I.

5.3.1 Quantum extremal surface

The metric and dilaton for the zero-temperature solution are

$$ds^2_{in} = \frac{4dyd\bar{y}}{(y+\bar{y})^2} , \qquad \phi = -\frac{2\phi_r}{y+\bar{y}} , \qquad y = \sigma + i\tau \tag{5.63}$$

with $\sigma < 0$. As before we glue it to flat space $dyd\bar{y}$ at $\sigma = 0$. The region R and the island I are the intervals

$$I: \quad y \in (-\infty, -a], \qquad R: \quad y \in [b, \infty) \tag{5.64}$$

at $t = 0$. The generalized entropy, including the island, is

$$S_{\text{gen}}(I \cup R) = \frac{\phi_r}{a} + \frac{c}{6}\log\frac{(a+b)^2}{a} . \tag{5.65}$$

Setting $\phi_a S_{\text{gen}} = 0$ gives the position of the QES,

$$a = \frac{1}{2}(k + b + \sqrt{b^2 + 6bk + k^2}) , \quad k \equiv \frac{6\phi_r}{c} . \tag{5.66}$$

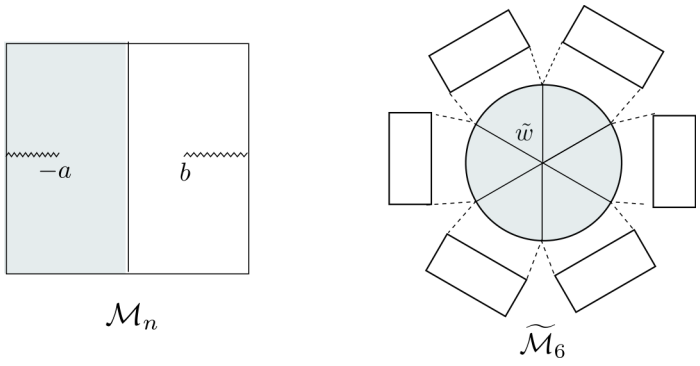

Figure 5.14: Replica wormhole at zero temperature. On the right, the disk is glued to n copies of the half-plane, as indicated by the dashed lines.

5.3.2 Replica wormholes at zero temperature

The replica partition function $\text{Tr}\ (\rho_A)^n$ is given by the path integral in fig. 5.14. The boundary condition for the gravity region is n copies of the real line. The Hawking saddle fills in the gravity region with n independent copies of $\mathbb{H}_2$. The replica wormhole, shown in the figure, fills in the gravity region with a single copy of $\mathbb{H}_2$. To see all n sheets of the gravity region, we go to the uniformizing coordinate

$$\widetilde{w} = \left(\frac{a+y}{a-y}\right)^{1/n} . \tag{5.67}$$

This maps the full gravity region to a single hyperbolic disk, $|\widetilde{w}| < 1$. This disk is a wormhole connecting n copies of flat space. The n^{th} copy is glued to the segment with $\arg \widetilde{w} \in [-\frac{\pi}{n}, \frac{\pi}{n}]$.

The equation of motion, and the answer for the position of the QES, is found by taking $\beta \to \infty$ in the results of section 5.2. This of course agrees with (5.66). (It is also possible to solve this problem directly at zero temperature, but we found it easier to treat the welding problem at finite temperature where the gluing is compact. In the end, the welding effects drop out in the determination of the

position of the QES, as we saw below (5.45).)

5.4 Two intervals in the eternal black hole

We now turn to the information paradox in the eternal black hole [253], described in the introduction and pictured in fig. 5.3. In the late-time regime relevant to the information paradox, the generalized entropy, including the island, is simply twice the answer for a single interval. We would like to understand how this is reproduced from wormholes. This is essentially just putting together the general discussion of section 5.1 with the single-interval results of section 5.2, so we will be brief. We will only discuss the saddles near $n = 1$; it would be nice to have a more complete understanding of the finite-n wormholes in this setup.

5.4.1 Review of the QES

We set $\beta = 2\pi$. The points in fig. 5.3 have (σ, t) coordinates

$$P_1 = (-a, t_a) \ , \quad P_2 = (b, t_b) \ , \quad P_3 = (-a, -t_a + i\pi) \ , \quad P_4 = (b, -t_b + i\pi) \ . \tag{5.68}$$

The radiation region is

$$R = [P_4, \infty_L) \cup [P_2, \infty_R) \ , \tag{5.69}$$

and the island is

$$I = [P_3, P_1] \ . \tag{5.70}$$

The CFT state is pure on the full Cauchy slice, so

$$S_{\rm CFT}(I \cup R) = S_{\rm CFT}([P_4, P_3] \cup [P_1, P_2]) \ . \tag{5.71}$$

This entropy is non-universal; it depends on the CFT. In the theory of c free Dirac fermions [285], the entanglement entropy of the region

$$[x_1, x_2] \cup [x_3, x_4] \ , \tag{5.72}$$

with metric $ds^2 = \Omega^{-2} dx d\bar{x}$, is

$$S_{\text{fermions}} = \frac{c}{6} \log \left[\frac{|x_{21} x_{32} x_{43} x_{41}|^2}{|x_{31} x_{42}|^2 \Omega_1 \Omega_2 \Omega_3 \Omega_4} \right] \ . \tag{5.73}$$

where we dropped the UV divergences. With our kinematics and conformal factors, this gives

$$S_{\text{fermions}}(I \cup R) = \frac{c}{3} \log \left[\frac{2 \cosh t_a \cosh t_b \, |\cosh(t_a - t_b) - \cosh(a+b)|}{\sinh a \cosh(\frac{a+b-t_a-t_b}{2}) \cosh(\frac{a+b+t_a+t_b}{2})} \right] \tag{5.74}$$

In a general CFT, the two-interval entanglement entropy is a function of the conformal cross-ratios $(z, \bar{z})$ which agrees with (5.74) in the OPE limits $z \to 0$ and $z \to 1$. For concreteness we will do the calculations for the free fermion, but the regime of interest for the information paradox will turn out to be universal.

The generalized entropy, including the island, is

$$S_{\text{gen}}(I \cup R) = 2S_0 + \frac{2\phi_r}{\tanh a} + S_{\text{fermions}}(I \cup R) \ , \tag{5.75}$$

Without an island, the entropy is the CFT entropy on the complement of R, the interval $[P_4, P_2]$, which is

$$S_{\text{gen}}^{\text{no island}} = S_{\text{fermions}}(R) = \frac{c}{3} \log (2 \cosh t_b) \tag{5.76}$$

At $t = 0$,

$$S_{\text{gen}}^{\text{island}} = 2S_0 + \frac{2\phi_r}{\tanh a} + \frac{c}{3} \log \left(\frac{4 \tanh^2 \frac{a+b}{2}}{\sinh a} \right) \ . \tag{5.77}$$

The extremality condition $\phi_a S_{\text{gen}}^{\text{island}} = 0$ at $t_a = t_b = 0$ gives

$$\frac{6\phi_r}{c} \sinh(a+b) = 2 \sinh^2 a - \sinh a \cosh a \sinh(a+b) \ . \tag{5.78}$$

Whether this has a real-valued solution depends on the parameters b and ϕ_r/c. For example, if $b = 0$, then it has a real solution minimizing $S_{\text{gen}}^{\text{island}}$ when ϕ_r/c is small, but not otherwise.

At late times, the extremality condition $\phi_a S_{\text{gen}}^{\text{island}} = 0$ always has a real solution. The true entropy, according to the QES prescription, is

$$S(R) = \min\left\{S_{\text{gen}}^{\text{no island}}, S_{\text{gen}}^{\text{island}}\right\} . \tag{5.79}$$

The island always exists and dominates the entropy at late times, because the non-island entropy grows linearly with t, see fig. 5.5. This solution is in the OPE limit where we can approximate the entanglement entropy by twice the single-interval answer,

$$S_{\text{matter}}(I \cup R) \approx 2S_{\text{matter}}([P_1, P_2]) = \frac{c}{3}\log\left(\frac{2|\cosh(a+b) - \cosh(t_a - t_b)|}{\sinh a}\right) . \tag{5.80}$$

and the QES condition sets $t_a = t_b$.

5.4.2 Replica wormholes

We would like to discuss some aspects of the wormhole solutions that lead to the island prescription.

For general n these are wormholes which have the topology shown in figures 5.6(b), 5.7. Already from these figures we can derive the S_0-dependent contribution (5.9) since it involves only the topology of the manifold. The replica wormhole that involves nontrivial connections, see figure (5.7), has the topology of a sphere with n holes. This gives a contribution going like $Z_n \propto e^{S_0(2-n)}$ and a contribution of $2S_0 = (1 - n\partial_n)\log Z_n|_{n=1}$ for the von Neumann entropy. This is good, since the

island contribution indeed had such a term (5.77).

It is useful to assume replica symmetry and view the Riemann surface as arising from a single disk with n copies of the matter theory and with pairs of twist operators that connect all these n copies in a cyclic fashion, see figure 5.9. In order to find the full answer, we need to solve the equations (5.17) (5.18). The important point is that, at this stage, we have that n appears purely as a parameter and we can analytically continue the equations in n. We have not managed to solve the equations for finite n. But let us discuss some properties we expect. In the limit of large $c\beta/\phi_r$, it is likely that solutions exist in Euclidean signature.[8] We can put points P_1 and P_4 at $v = \pm Be^{\pm i\varphi}$. Once this solution is found, we can analytically continue $\varphi \to -it$ to generate the Lorentzian solution. That Lorenzian solution at late times t is expected to to exist even for low values of $c\beta/\phi_r$. In principle, it should be possible, and probably easier, to analyze directly the late-times Lorentzian equation. In fact, we expect that there should be a way to relate the single interval solution to the two interval solution in this regime. The intuitive reason is that at late times the distance between the two horizons is increasing and so the distance between the two cosmic branes is increasing. We have an external source cosmic brane outside the gravitational region, at the tip of region R. The cosmic brane has some tension, as well as a twist operator on it. For the Hawking saddle, the one without the replica wormholes, the twist operators, and the topological line operators[9] that connect them, generate a contribution that grows linearly in time, due to the behavior of Renyi entropies for the matter quantum field theory, as well as the fact that the wormhole length grows with time. At late times the topological line operator can break by pair producing cosmic branes, with their twist operators.

[8]For low values of $c\beta/\phi_r$ we have already seen, in (5.78), that near $n \sim 1$ the solutions can be complex.

[9]These topological line operators exchange the n copies in a cyclic way. They are represented by red lines in figure 5.9(b).

The cost of creating a pair of cosmic branes is finite in the gravitational region, because the dilaton is finite. This cost would be infinite in the non-gravitational region. But once the external cosmic brane is screened by the cosmic brane that appeared in the gravity region we expect to have two approximately independent single interval problems. The reason is that the distance between the left and right sides is growing with time. This is somewhat analogous to two point charges that generate a two dimensional electric field. As one separates the charges it might be convenient to create a pair of charges that screens the electric field. For this it is important that the charges one creates have finite mass.

In the $n \to 1$ limit we can analyze the solution and we get the generalized entropy. This is not too surprising since the arguments in [267] say that this should always work. Here the non-trivial input is the ansatz for the configuration of intervals which follows from the structure of the Riemann surfaces. As discussed in section 5.1.1, the effective action reduces to the action of certain cosmic branes which are manifestly very light in the $n \to 1$ limit. So in this case, the argument of the previous paragraph can be explicitly checked and one indeed obtains that we get the sum over the two single interval problems [253].

5.4.3 Purity of the total state

One can take the perspective that our model is defined via a quantum theory living on the flat space region including its boundary endpoints. The global pure state we consider should be a pure state of this region, and a natural question is whether this is captured in the gravity description. Replica wormholes do indeed capture this feature.

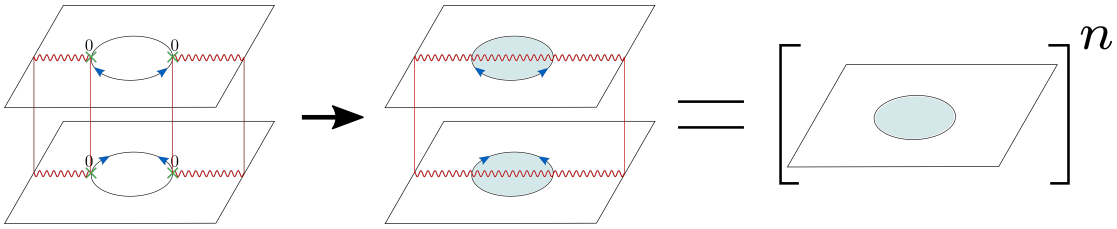

Figure 5.15: The computation of the entropy of the entire flat space regions including the boundary points. The dominant gravitational saddle connects consecutive sheets. This factorizes into n separate sheets and produces a vanishing entropy consistent with the purity of the flat space region union the endpoints. The blue arrows indicate how the unit circle is identified across the cut.

The computation of the entropy of this region is given by evaluating the path integral on the manifold shown in figure 5.15. The branch cuts split the entire flat space region including its boundaries, identifying one half of one sheet with the other half of the next sheet. The most obvious gravitational saddle is the one that connects these consecutive sheets and thereby naturally extending the branch cut through the entire gravity region. A simple rearranging of these sheets shows that this contribution to the Renyi entropy factorizes. This disconnected saddle satisfies $Z_n = Z_1^n$, and evaluating the on shell action on this configuration will give vanishing entropy since

$$\text{Tr } \rho^n = \frac{Z_n}{Z_1^n} = 1\,. \tag{5.81}$$

This saddle clearly dominates over all other configurations.

Since the different sheets are not coupled at all in the flat space region, it's plausible that this disconnected saddle is the only saddle that exists. Other off-shell contributions can indeed exist, but we speculate they should give a vanishing contribution in a model with a definite Hamiltonian with no averaging.

5.5 Comments on reconstructing the interior

The island contribution to the entropy of a flat space region R indicates there is a dictionary between the island I and R in the sense of entanglement wedge reconstruction in AdS/CFT. We could discuss this in general but for concreteness consider the two interval case discussed in the previous section. Let's take the state at late times such that the entropy of R has plateaued and its entropy receives a contribution from the island as shown in figure 5.16.

The first step to establishing a dictionary is to define a subspace of states which have the same "entanglement wedge" or island. This defines what we will call the code subspace $\mathcal{H}_{code}$, which we imagine can be prepared via the Euclidean path integral with possible operator insertions. By having the same island we mean that the leading saddle points in the Renyi computations are only modified perturbatively. This naturally puts restrictions on the size of the allowed code subspace for which the statements of this section hold, see for example [286, 287].

We assume that the full Hilbert space of our model is that of the two flat space regions including their boundary, which we write as $\mathcal{H}_{\text{Left}} \otimes \mathcal{H}_{\text{Right}}$. The region R that we are considering is a tensor factor of this Hilbert space, where we can write

$$\mathcal{H}_{\text{Left}} \otimes \mathcal{H}_{\text{Right}} = \mathcal{H}_R \otimes \mathcal{H}_{\bar{R}} \tag{5.82}$$

where $\bar{R}$ is the complement of the region R in the flat space region including the boundary points.

The code subspace $\mathcal{H}_{code}$ is a subspace of $\mathcal{H}_{\text{Left}} \otimes \mathcal{H}_{\text{Right}}$. However, the code subspace also has a simpler description in terms of the combined description of gravity plus the flat space region as that of effective field theory on a Cauchy slice

of the full spacetime. This is the description where the state is prepared using the semi-classical saddle via the Euclidean black hole solution. The code subspace should be thought of as isomorphic to this. Therefore, the code subspace admits the decomposition[10]

$$\mathcal{H}_{code} \cong \mathcal{H}_R \otimes \mathcal{H}_D \otimes \mathcal{H}_I \tag{5.83}$$

where the region D is the complement of $R \cup I$ on the Cauchy slice. The decomposition is shown in figure 5.16. It is within this effective description that for any state in the code subspace $|i\rangle \in \mathcal{H}_{code}$, we have

$$S(\rho_R^i) = S(\tilde{\rho}_{RI}^i) + \frac{\text{Area}[\partial I]}{4G_N} \tag{5.84}$$

where ρ_R^i is what you get by tracing out $\bar{R}$ in the full quantum description $\mathcal{H}_{\text{Left}} \otimes \mathcal{H}_{\text{Right}}$, and $\tilde{\rho}_{RI}^i$ is the density matrix obtained by tracing out the complement of RI in the semi-classical description consisting of quantum fields on a classical geometry.

The validity of the island formula (for a fixed island) within the code subspace implies the equivalence of the relative entropy in the exact state and the semi-classical state:

$$S_{\text{Rel}}(\rho_R|\sigma_R) = S_{\text{Rel}}(\tilde{\rho}_{RI}|\tilde{\sigma}_{RI}) \tag{5.85}$$

A similar observation in the context of AdS/CFT [30] was key in proving entanglement wedge reconstruction [32] using the quantum error correction interpretation of the duality [29]. The same line of argument can be applied here to establish the dictionary. In particular, one can show that for any operator $\mathcal{O}_I$ (and it's Hermitian conjugate) acting within the $\mathcal{H}_{code}$ and supported on the Island one can find an

[10]This should be understood as approximate up to usual issues of the non-factorizability of continuum QFT.

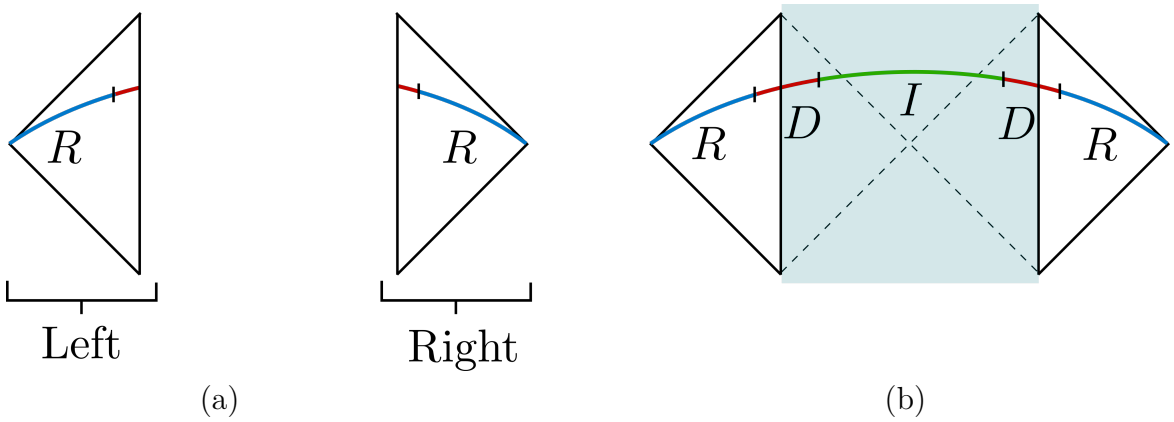

(a) (b)

Figure 5.16: (a) The full Hilbert space is the product Hilbert space of the entire left and right flat space regions including the boundary points. The region R we are interested in is a union of two subregions in the two flat space regions. (b) The effective state used in the island prescription is the semi-classical state defined on the Cauchy slice of the full system. R is the same region in the flat space region whose exact entropy we are computing, I is the Island, and D is the complement of the two.

operator supported on R such that:

$$\mathcal{O}_I|i\rangle = \mathcal{O}_R|i\rangle \tag{5.86}$$

$$\mathcal{O}_I^\dagger|i\rangle = \mathcal{O}_R^\dagger|i\rangle \tag{5.87}$$

The operator $\mathcal{O}_R$ is given by a complicated operator on R involving the matrix elements of $\mathcal{O}_I$ within the code subspace.

In summary, we are using the fine grained entropy formula to understand how the interior is encoded in the full Hilbert space. The relative entropy equality (5.85) tells us that distinguishable states in the interior (the island) are also distinguishable in the radiation, within the full exact quantum description.

5.6 Discussion

In this paper, we have exhibited non-perturbative effects that dramatically reduce the late time von Neumann entropy of quantum fields outside a black hole.

The computation of the Renyi entropies corresponds to the expectation value of a swap or cyclic permutation operator in n copies of the theory. Systems with very high entropy have very small, exponentially small, expectation values for this observable. This means that non-perturbative effects can compete with the naive answers. In particular, the Hawking-like computation of the Renyi entropies of radiation corresponds to a computation on the leading gravitational background. A growing entropy corresponds to an exponentially decreasing Renyi entropy or expectation value for the cyclic permutation operator. It decreases exponentially as time progresses. For this reason, we need to pay attention to other geometries, with other topologies. These other topologies give exponentially small effects, but they do not continue decreasing with time for long times. Said in this way, the effects are vaguely similar to the ones discussed for corrections of other exponentially small effects [74, 269–271]. Though the Renyi entropies are small, the von Neumann entropy is large and the new series of saddles gives rise to a constant von Neumann entropy at late times. More precisely, we can think of the computation of the Renyi entropies in the two interval case as an insertion of a pair of external cosmic branes in the non-gravitational region. As time progresses these are separated further and further through the wormhole. Eventually the dominant contribution is one where a pair of cosmic branes is created in the gravitational region that "screen" the external ones, giving an entropy which is the same as that of two copies of the single interval entropy.

These other topologies are present as subleading saddles also at short times (perhaps as complex saddles) where we can analyze them using Euclidean methods and then analytically continue. We have only done this analytic continuation for the von Neumann entropies, not the Renyi entropies. It would be interesting to do it more explicitly for the Renyi entropies.

There have been discussions on whether small corrections to the density matrix, of order $e^{-S_{BH}}$, could or could not restore unitarity. These results suggest that they interfere constructively to give rise to the right expression for the entropy.

This is evidence that including nonperturbative gravitational effects can indeed lead to results compatible with unitarity. However, we emphasize that this is not a full microscopic resolution of the information paradox. We have not given a gravitational description for the S-matrix describing how infalling matter escapes into the radiation. In this sense, these results are on a footing similar to the Bekenstein-Hawking calculation of the entropy, which uses a Euclidean path integral to compute the right answer but does not give an explicit Hilbert space picture for what it is counting. In contrast, the Strominger-Vafa computation of the entropy [71] gives us an explicit Hilbert space, but not a detailed description of the microstates in the gravity variables. Something similar can be said of the CFT description in AdS/CFT. Hopefully these results will be useful for providing a more explicit map.

It is amusing to note that wormholes were initially thought to destroy information [288–290]. But more recently the work of [270,271], as well as the present discussion, and [268], suggests that the opposite is true. Wormholes are important for producing results that are compatible with unitarity. For earlier work in this direction see also [291,292].

We assumed that $c \gg 1$ as a blanket justification for analyzing the equations classically. However, even for small $c \sim 1$, the basic picture for the Page curve can be justified. The basic point is simple. First consider the single interval computation. In that case for $c \sim 1$ we see that the correction to the black hole solution is very small, for all the Renyi entropies. In other words, we find that A is small, and we can probably not distinguish such a small value of A from zero but that does not matter, the geometries and the entropies are basically those of a black hole. Now when we go to two intervals, and we consider the late time situation, then all that really matters is that we can do an OPE-like expansion of the twist operator insertions. The important observation is that the twist operator insertions in the interior of the black hole are very far from each other. This is the fact that the wormhole is getting longer [293, 294]. Then the solution becomes similar to two non-interacting copies of the single interval solution. The fact that c is small only implies that we will have to wait longer for the island solution to dominate. We just have to wait a time of order the entropy, $t \propto \beta(S - S_0)/c$ for it to dominate.

In [270], it was argued that pure JT gravity should be interpreted in terms of an average over Hamiltonians. In addition, higher genus corrections were precisely matched. This has raised the question of whether the corrections we are discussing in this paper crucially involve an average over Hamiltonians, or whether they would also apply to a system which has a definite Hamiltonian. Though JT gravity plus a CFT probably does not define a complete quantum gravity theory, it seems likely that well defined theories could be approximated by JT gravity plus a CFT. For example, we could imagine an AdS/CFT example that involves an extremal black hole such that it also has a CFT on its geometry. All we need is this low energy description, the theory might have lots of other massive fields which will not drastically participate in the discussion. They might lead to additional saddles,

but it seems that they will not correct the saddles we have been discussing. And we have the seen that the saddles we discussed already give an answer consistent with unitarity, at least for the entropy. In contrast with [270], we are not doing the full path integral, we are simply using a saddle point approximation, so the JT gravity plus CFT only needs to be valid around these saddles.

As we mentioned in the introduction, the setup in this paper can be viewed as an approximation to some magnetically charged near extremal four dimensional black holes [276]. But one could analyze more general asymptotically flat black holes and wonder how to define either exactly or approximately the various entropies involved. In particular, to have a sharp definition of the entropy of radiation it seems important to go to null infinity.

Another interesting question is whether we can give a Lorentzian interpretation to the modification of the density matrix implied by the existence of replica wormholes.

It has been pointed out that a black hole as seen from outside looks like a system obeying the laws of hydrodynamics. For this reason, it is sometimes thought that gravity is just an approximation that intrinsically loses information. Here we see that if we include the black hole interior, and we do a more complete gravity computation, we can get results compatible with unitarity. The fact that gravity is more than dissipative hydrodynamics is already contained in the Ryu-Takayanagi formula for the fine grained entropy, which shows that the geometry of the interior can discriminate between pure and mixed states for a black hole.

Acknowledgments We are grateful to Tarek Anous, Raphael Bousso, Kanato

Goto, Daniel Harlow, Luca Iliesiu, Alexei Kitaev, Alexandru Lupsasca, Raghu Mahajan, Alexei Milekhin, Shiraz Minwalla, Geoff Penington, Steve Shenker, Julian Sonner, Douglas Stanford, Andrew Strominger, Sandip Trivedi and Zhenbin Yang for helpful discussions of this and related work. AA and TH thank the organizers of the workshop *Quantum Information In Quantum Gravity* at UC Davis, August 2019, and AA, TH, and JM thank the organizers of the workshop *Quantum Gravity in the Lab* at Google X, November 2019. A.A. is supported by funds from the Ministry of Presidential Affairs, UAE. The work of ES is supported by the Simons Foundation as part of the Simons Collaboration on the Nonperturbative Bootstrap. The work of TH and AT is supported by DOE grant DE-SC0020397. J.M. is supported in part by U.S. Department of Energy grant DE-SC0009988 and by the Simons Foundation grant 385600.

APPENDIX A

CHAPTER 2 OF APPENDIX

A.1 Rotation of three-point functions

In this appendix, we will derive equation (2.66). Let us start with the three-point function $\langle\overline{O(y=\delta)}\,\mathcal{E}_s\,O(y=\delta)\rangle$, where $O(y=\delta)$ is some arbitrary operator

$$O(y=\delta)=\sum_n c_n\;\varepsilon^n.\mathcal{O}^n(y=\delta)\;,\qquad \overline{O(y=\delta)}=\sum_n c_n^*\;\overline{\varepsilon}^n.\mathcal{O}^{n\dagger}(y=-\delta)\;. \tag{A.1}$$

$\mathcal{O}^n$'s are (not necessarily a primary) operators with any spin and $\mathcal{E}_s$ is defined in equation (2.62). $\overline{\varepsilon}$ is defined in the usual way $\overline{\varepsilon}^{\mu\nu\cdots}=(-1)^P(\varepsilon^{\mu\nu\cdots})^*$, where P is the total number of t and y indices. Let us now look at one of the terms of this three point function: $\langle\overline{\varepsilon}_1.\mathcal{O}_1^\dagger(-i\epsilon,-\delta)\;\mathcal{E}_s\;\varepsilon_2.\mathcal{O}_2(i\epsilon,\delta)\rangle$. Before performing the u-integral, this three point function, in general has the following branch cut structure:

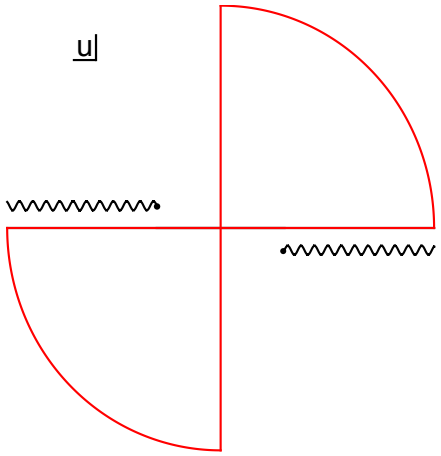

(A.2)

Now, using the integration contour shown in red in the above figure, one can show that

$$\langle\overline{\varepsilon}_1.\mathcal{O}_1^\dagger(-i\epsilon,-\delta)\mathcal{E}_s\;\varepsilon_2.\mathcal{O}_2(i\epsilon,\delta)\rangle=i\langle\overline{\varepsilon}_1.\mathcal{O}_1^\dagger(0,-\delta)\int_{-\infty}^{\infty}du X_{uuu\cdots u}(iu)\;\varepsilon_2.\mathcal{O}_2(0,\delta)\rangle\;. \tag{A.3}$$

There is no ambiguity in the right hand side correlator and hence the $i\epsilon$ has been removed. Let us now look at the three point function $\langle \bar{\varepsilon}_1.\mathcal{O}_1^\dagger(0,-\delta)X_{uuu\cdots u}(iu)\ \varepsilon_2.\mathcal{O}_2(0,\delta)\rangle$. This three-point function can be obtained by starting with some appropriate correlator in the Euclidean space: $(x_0, x_1, \vec{x})$ and performing an analytic continuation $x_0 = it, x_1 = y$. On the other hand, we can start with the same Euclidean correlator and perform a different analytic continuation: $x_1 = it, x_0 = y$ to obtain a different Lorentzian correlator. Hence, these two Lorentzian correlators should be related to each other. More explicitly, one can show that

$$\begin{aligned}&\langle \bar{\varepsilon}_1.\mathcal{O}_1^\dagger(y=-\delta)X_{uuu\cdots u}(iu)\ \varepsilon_2.\mathcal{O}_2(y=\delta)\rangle \\ &\qquad = i^s\langle \tilde{\varepsilon}_1^*.\mathcal{O}_1^\dagger(t=i\delta)X_{uuu\cdots u}(-u)\ \tilde{\varepsilon}_2.\mathcal{O}_2(t=-i\delta)\rangle\ , \end{aligned} \tag{A.4}$$

where,

$$\tilde{\varepsilon}^{\mu\nu\ldots} = \left(\Lambda^\mu_\alpha\Lambda^\nu_\beta\ldots\right)\varepsilon^{\alpha\beta\ldots}\ , \qquad \Lambda^\mu_\alpha = \begin{pmatrix} 0 & -i & 0 \\ -i & 0 & 0 \\ 0 & 0 & \mathbb{1} \end{pmatrix}\ . \tag{A.5}$$

Therefore, finally we can write,

$$\langle \bar{\varepsilon}_1.\mathcal{O}_1^\dagger(y=-\delta)\mathcal{E}_s\ \varepsilon_2.\mathcal{O}_2(y=\delta)\rangle = i^{s+1}\langle \tilde{\varepsilon}_1^*.\mathcal{O}_1^\dagger(t=i\delta)\mathcal{E}_s\ \tilde{\varepsilon}_2.\mathcal{O}_2(t=-i\delta)\rangle\ . \tag{A.6}$$

A.2 Normalized three point function for $\langle JXJ\rangle$

Here we write the matrix **A** and two point function of states we used in the paper explicitly. The three point function involving two same operators with spin one and another operator with spin 4 is given by

$$\langle J(x_1,\varepsilon_1)X(x_2,\varepsilon_2)J(x_3,\varepsilon_3)\rangle = \frac{1}{(x_{12}^2)^{\frac{\Delta_X}{2}+2}(x_{23}^2)^{\frac{\Delta_X}{2}+2}(x_{31}^2)^{\Delta_J+\frac{\Delta_X}{2}-1}}\{\alpha_1 V_1 V_3 V_2^4 + \alpha_2 V_2^3(V_3 H_{12} + H_{23} V_1) + \alpha_3 V_2^2 H_{12} H_{23} + \alpha_4 V_2^4 H_{13}\} \tag{A.7}$$

In which conformal building blocks are expressed by

$$\begin{aligned} H_{ij} &= -2x_{ij}\cdot\varepsilon_j x_{ij}\cdot\varepsilon_i + x_{ij}^2\varepsilon_i\cdot\varepsilon_j \\ V_i \equiv V_{i,jk} &= \frac{1}{x_{jk}^2}(x_{ij}^2 x_{ik}\cdot\varepsilon_i - x_{ik}^2 x_{ij}\cdot\varepsilon_i) \end{aligned} \tag{A.8}$$

For state defined in 2.54 expectation value of spin 4 operator X is given by

$$\begin{aligned} & c_{\psi\psi X}\langle\varepsilon^*\cdot J|\int_\infty^\infty du X_{uuuu}(0,u)|\varepsilon\cdot J\rangle = \\ & (Vol)c_{\psi\psi X}\frac{2^{\Delta_X-4\Delta_J-3}\pi^{\frac{5}{2}}\Gamma(2\Delta_J)\Gamma(\frac{3+\Delta_X}{2})}{\delta^{2\Delta_J}\Gamma(3+\Delta_J-\frac{\Delta_X}{2})\Gamma(3+\frac{\Delta_X}{2})\Gamma(1+\Delta_J+\frac{\Delta_X}{2})}\times \\ & \{|\varepsilon^+|^2(4+\Delta_X)(2\Delta_J+\Delta_X)(\Delta_X+2\Delta_J-2)(\Delta_X+2\Delta_J)(2\alpha_4-\alpha_1) \\ & +|\varepsilon^-|^2(4(4+2\Delta_J-\Delta_X)(12-\Delta_X^2+2\Delta_J(4+\Delta_X))\alpha_2+ \\ & 2(4+\Delta_X)(-2-2\Delta_J+\Delta_X)((8+4\Delta_J-2\Delta_X)\alpha_3+(\Delta_X-2\Delta_J)\alpha_4) \\ & -(96+16\Delta_J(4+\Delta_J)+4\Delta_J(1+\Delta_J)\Delta_X-2(3+2\Delta_J)\Delta_X^2+\Delta_X^3)\alpha_1)+ \\ & 2(\varepsilon^+\varepsilon^{-*}+\varepsilon^-\varepsilon^{+*})(2\Delta_J+\Delta_X)((16+4\Delta_X-\Delta_X^2+2\Delta_J(2+\Delta_X))\alpha_1 \\ & -2(4+2\Delta_J-\Delta_X)(2+\Delta_X)\alpha_2-4(4+\Delta_X)\alpha_4) \\ & +|\varepsilon^\perp|^2(4+\Delta_X)(2\Delta_J+\Delta_X)(\alpha_1+(2+2\Delta_J-\Delta_X))\alpha_4\} \end{aligned} \tag{A.9}$$

By imposing unitarity $\Delta_J \geq d-1$ and the convexity condition for the twist of a spin-4 operator $d-2 \leq \Delta_X - 4 \leq 2(d-2)$ [107] (in $d=4$), all gamma functions are positive.

The volume term in three point function is canceled out by the same factor in the two point function, which is always positive:

$$\langle \varepsilon^* \cdot J | \varepsilon \cdot J \rangle =$$
$$(Vol)\ \frac{2^{3-2\Delta_J} c_J \Gamma(\Delta_1 - \frac{3}{2})}{\delta^{2\Delta_J - 3}\Gamma(1+\Delta_J)} \{(|\varepsilon^+|^2 + |\varepsilon^-|^2)(2\Delta_J - 4) - 2(\varepsilon^+ \varepsilon^{-*} + \varepsilon^- \varepsilon^{+*}) + |\varepsilon^\perp|^2(\Delta_J - 1)\} \tag{A.10}$$

A.3 Free scalars

In this appendix, we show that the inequality $\mathcal{E}_s = \int du X_{uuu\cdots u} \geq 0$ holds also for free scalar fields, with $s \geq 2$ an even spin. For $s = 2$, this is the ANEC, proved for free scalars in [**?**, 87]. The OPE methods in the body of the paper do not immediately apply, because the expansion in twist has an infinite number of contributions already at leading order. Instead we will follow the derivation of the ANEC in [87].

The all-null components of the conserved, symmetric, traceless spin-s current in the theory of a free scalar takes the form

$$X_{u\cdots u} = \sum_{i=0}^{s} a_i^s :(\phi_u)^i \phi (\phi_u)^{s-i} \phi: \tag{A.11}$$

where a_i^s are known coefficients. (The explicit formula is equation (4.99) in [295] but will not be needed.) Therefore after integration by parts, the generalization of the averaged null energy, up to an overall constant, is

$$\mathcal{E}_s \sim \int du\ :(\phi_u)^{s/2} \phi (\phi_u)^{s/2} \phi:\ . \tag{A.12}$$

The overall coefficient does not matter, since we only need to show that $\mathcal{E}_s$ has a definite sign – if it is non-positive, we can defined $X \to -X$ to make it non-negative.

Classically, (A.12) is obviously sign-definite because the integrand is positive, but quantum mechanically this is true only after doing the integral. To proceed, we use the standard mode expansion for the scalar field operator $\phi = \int d^{d-1}\vec{k}[u_{\vec{k}}a_{\vec{k}} + h.c.]$ with $u_{\vec{k}} \sim e^{-ikx}$ to write the integrand of (A.12) as

$$\int d^{d-1}\vec{k} \int d^{d-1}\vec{k}' \Big[2(-ik_u)^{s/2}(ik'_u)^{s/2} u_{\vec{k}} u^*_{\vec{k}'} a^\dagger_{\vec{k}'} a_{\vec{k}} + (-ik_u)^{s/2}(-ik'_u)^{s/2} u_{\vec{k}} a_{\vec{k}} u_{\vec{k}'} a_{\vec{k}'} + (ik_u)^{s/2}(ik'_u)^{s/2} u^*_{\vec{k}} a^\dagger_{\vec{k}} u^*_{\vec{k}'} a^\dagger_{\vec{k}'} \Big] \tag{A.13}$$

The first term is obviously a non-negative operator, since it is $\int d^{d-1}\vec{k} u_{\vec{k}} a_{\vec{k}}$ times its Hermitian conjugate. The other terms can be negative (for example in squeezed states), but disappear upon integrating over the null ray in (A.12), leaving only non-negative contributions. See [87] for details of these integrals, as well a careful demonstration that exchanging the order of the u-integral and k-integrals is justified in states with a finite number of particles and finite energy.

APPENDIX B

CHAPTER 3 OF APPENDIX

B.1 Transverse Polarizations

We construct the transverse polarization tensors used in section 3.2 explicitly. These polarization tensors have only component in transverse directions $x - y$ so they can be used in $D \geq 4$. Let us define

$$x^+ = x + iy \ , \qquad x^- = x - iy \ . \tag{B.1}$$

Let us consider following basis vectors

$$\begin{aligned} e^+ &= \frac{1}{\sqrt{2}}(\partial_x - i\partial_y) \ , \qquad e_- = \frac{1}{\sqrt{2}}(\partial_x + i\partial_y) \ , \\ e^{+\mu}\partial_{b^\mu} &= \frac{1}{\sqrt{2}}\partial_{b^+} \ , \qquad e^{-\mu}\partial_{b^\mu} = \frac{1}{\sqrt{2}}\partial_{b^-} \ , \end{aligned} \tag{B.2}$$

where both of them are null vector. Also we have $e^+ \cdot e^- = 1$. Hence they can be used for constructing the transverse traceless polarization tensor $e^{\mu_1\mu_2\cdots\mu_s}$:

$$e^{(+)\mu_1\mu_2\cdots\mu_s} = e^{+\mu_1}e^{+\mu_2}\cdots e^{+\mu_s} \ , \qquad e^{(-)\mu_1\mu_2\cdots\mu_s} = e^{-\mu_1}e^{-\mu_2}\cdots e^{-\mu_s}. \tag{B.3}$$

These polarization tensors are not orthogonal to each other. They can be made orthogonal by taking the following linear combinations

$$\begin{aligned} e^{\oplus\mu_1\mu_2\cdots\mu_s} &= \frac{1}{\sqrt{2}}\left(e^{(+)\mu_1\mu_2\cdots\mu_s} + e^{(-)\mu_1\mu_2\cdots\mu_s}\right) \ , \\ e^{\otimes\mu_1\mu_2\cdots\mu_s} &= \frac{i}{\sqrt{2}}\left(e^{(+)\mu_1\mu_2\cdots\mu_s} - e^{(-)\mu_1\mu_2\cdots\mu_s}\right) \ , \end{aligned} \tag{B.4}$$

where they satisfy

$$\begin{aligned} &e^{\oplus\mu_1\mu_2\cdots\mu_s}e^{\otimes}{}_{\mu_1\mu_2\cdots\mu_s} = 0 \ , \qquad e^{\oplus\mu_1\mu_2\cdots\mu_s}e^{\oplus}{}_{\mu_1\mu_2\cdots\mu_s} = e^{\otimes\mu_1\mu_2\cdots\mu_s}e^{\otimes}{}_{\mu_1\mu_2\cdots\mu_s} = 1 \ , \\ &e^{\oplus\mu_1\mu_2\cdots\mu_s}\ e^{\oplus}_{\mu_1\mu_2\cdots\mu_s\mu_{s+1}\cdots\mu_{s+j}} = \frac{1}{\sqrt{2}}e^{\oplus}{}_{\mu_{s+1}\mu_{s+2}\cdots\mu_{s+j}} \ , \\ &e^{\otimes\mu_1\mu_2\cdots\mu_s}\ e^{\otimes}_{\mu_1\mu_2\cdots\mu_s\mu_{s+1}\cdots\mu_{s+j}} = \frac{1}{\sqrt{2}}e^{\oplus}{}_{\mu_{s+1}\mu_{s+2}\cdots\mu_{s+j}} \ , \end{aligned} \tag{B.5}$$

where s and j are positive numbers.

B.2 Phase Shift Computations

A Lemma

In order to get the bounds in the transverse plane, we can use a trick that will be used many times in this appendix. After plugging the polarization tensors for particles, we always find the following equation

$$I = e^{\mu_1\mu_2\cdots\mu_i\mu_{i+1}\cdots\mu_J} e_{\mu_1\mu_2\cdots\mu_i}{}^{\nu_{i+1}\nu_{i+2}\cdots\nu_{J'}} \partial_{b^{\mu_{i+1}}}\cdots\partial_{b^{\mu_J}}\partial_{b^{\nu_{i+1}}}\cdots\partial_{b^{\nu_{J'}}}\frac{1}{b^{D-4}}\ . \qquad \text{(B.6)}$$

We would like to show that sign of I alternates by choosing different directions for $\vec{b}$ in the transverse plane.

Let us first consider $J \neq J'$, $J' = J + K$. We specify x^+, x^- to be two arbitrary directions in the transverse plane and the direction of the impact parameter $\vec{b}$ is picked in the same plane spanned by x^+, x^-. By using $e = e^{\oplus}$ we find

$$\begin{aligned} I =& 2^{-1+J+K/2}\left(\partial_{b^+}^K + \partial_{b^-}^K\right)(\partial_{b^+}\partial_{b^-})^J\frac{1}{b^{D-4}} \\ =& 2^{J+K/2}(-1)^K\left[\left(\frac{D-4}{2}\right)_J\right]^2\left(\frac{D-4}{2}+J\right)_K\frac{\cos(K\theta)}{b^{D-4+2J+K}} \end{aligned} \qquad \text{(B.7)}$$

where $(a)_b \equiv \frac{\Gamma(a+b)}{\Gamma(a)}$ and θ is the angle between the vector $\vec{b}$ and the x-axis, where $x = \frac{1}{\sqrt{2}}(x^+ + x^-)$. This implies that rotating $\vec{b}$ with respect to x-axis changes the sign of I for $K \neq 0$.

If $K = 0$, both $e^{\oplus}$ and $e^{\otimes}$ yield the same sign for I, and we need to use polarizations having components in other transverse directions, therefore the following argument could not be applied to $D = 4$. For $D \geq 5$, we can separate another transverse coordinate z from x^+, x^- and after taking derivative we place the impact parameter $\vec{b}$ in x, y, z plane. These coordinates are enough for getting the bounds and we do not have to consider other transverse directions in for $D \geq 6$. Again by plugging $e = e^{\oplus}$, we find

$$I = 2^{-1+J} \frac{\cos(\theta)^{2J}}{b^{D-4+2J}} \left(\frac{\Gamma(\frac{D-4}{2} + J)}{\Gamma(\frac{D-4}{2})} \right)^2 {}_2F_1\left(-J, -J, \frac{D-4}{2}, -\tan(\theta)^2 \right) , \qquad \text{(B.8)}$$

where θ is the angle between $\hat{z}$ and $\vec{b}$. For any integer value of J and D, the hypergeometric function in (B.8) is a polynomial in its variable, changing sign for both even and odd J.

Diagonal Element Between $\mathcal{E}_J$

We set $\mathcal{E}^{(3)^{\mu_1\mu_2\cdots\mu_J}} = z_{3T}^{\mu_1} z_{3T}^{\mu_1} \cdots z_{3T}^{\mu_J}, \mathcal{E}^{(1)^{\mu_1\mu_2\cdots\mu_J}} = z_{1T}^{\mu_1} z_{1T}^{\mu_1} \cdots z_{1T}^{\mu_J}$ and send $e^{\mu_1} e^{\mu_2} \cdots e^{\mu_J} \to e^{\mu_1\mu_2\cdots\mu_J}$. We also need to impose $e_3^{\mu_1\mu_2\cdots\mu_J} = (e_1^{\mu_1\mu_2\cdots\mu_J})^\dagger$ to have positivity. With this choice of polarization, only $\mathcal{A}_1, \cdots, \mathcal{A}_{J+1}$ contribute to phase shift and we write down the contribution of each vertex to the phase shift. Let us define $\tilde{\delta}(s, \vec{b}) = \frac{\pi^{D/2-2}}{\Gamma(\frac{D-4}{2}) G_N s} \delta(s, \vec{b})$,

$$\tilde{\delta}(s, \vec{b})\Big|_{\mathcal{A}_i} = (-1)^{(i-1)} a_i e^{\mu_1\cdots\mu_{i-1}\mu_i\mu_{i+1}\cdots\mu_J} e^{\nu_1\cdots\nu_{i-1}}{}_{\mu_i\mu_{i+1}\cdots\mu_J} \partial_{b^{\mu_1}} \cdots \partial_{b^{\mu_{i-1}}} \partial_{b^{\nu_1}} \cdots \partial_{b^{\nu_{i-1}}} \frac{1}{|b|^{D-4}}. \qquad \text{(B.9)}$$

In the small impact parameter limit, the term with the most negative powers of b dominates over other terms. As explained in the lemma B.2, choosing different

direction for $\vec{b}$ for $D \geq 5$ changes the sign for each of these terms. Therefore by applying the argument successively, we find

$$a_i = 0 \qquad 2 \leq i \leq J+1. \tag{B.10}$$

Note that for a_1, there is no derivative and hence rotating direction of $\vec{b}$ does not change the sign of this term. Choosing e to be either $e^{\otimes}$ or $e^{\oplus}$ we find for $\mathcal{A}_1$ a manifestly positive contribution

$$\tilde{\delta}(s,\vec{b})^{\oplus}\Big|_{\mathcal{A}_1} = \tilde{\delta}(s,\vec{b})^{\otimes}\Big|_{\mathcal{A}_1} = \frac{a_1}{|b|^{D-4}} \ . \tag{B.11}$$

$\mathcal{E}_{J-1}$

We again set $\mathcal{E}^{(3)\mu_1\mu_2\cdots\mu_J} = \mathcal{E}^{(1)\mu_1\mu_2\cdots\mu_J} = \varepsilon_L^{(\mu_1}\varepsilon_T^{\mu_2}\varepsilon_T^{\mu_2}\cdots\varepsilon_T^{\mu_J)}$. In this case all the remaining vertices contribute to the phase shift and each vertex contribution is as follows

$$\begin{aligned}\tilde{\delta}(s,\vec{b})\Big|_{\mathcal{A}_{2J+1+K}} =& \frac{2(-1)^{i-1}}{m^2J^2}(a_{2J+1+K} - (J-K)a_{J+K+1}) \\ & \times e^{\mu_1\cdots\mu_i\mu_{i+1}\cdots\mu_J}e^{\nu_1\cdots\nu_i}{}_{\mu_{i+1}\cdots\mu_J}\partial_{b^{\mu_1}}\cdots\partial_{b^{\mu_i}}\partial_{b^{\nu_1}}\cdots\partial_{b^{\nu_i}}\frac{1}{|b|^{D-4}} \ ,\end{aligned} \tag{B.12}$$

which by taking b small and using the trick discussed in B.2 yields

$$a_{2J+1+K} = (J-K)a_{J+K+1} \qquad 2 \leq K \leq J-1 \ . \tag{B.13}$$

While at the $\frac{1}{b^{D-2}}$ order, $\mathcal{A}_1$ contributes and we find

$$a_{2J+2} - (J-1)a_{J+2} = -a_1\frac{J(J-1)}{2} \ . \tag{B.14}$$

Off-diagonal Components of $\mathcal{E}_J$ and $\mathcal{E}_{J-1}$

In order to impose constraints on $\mathcal{A}_{J+2}, \mathcal{A}_{J+3}, \cdots \mathcal{A}_{2J+1}$, we use $\mathcal{E}^{(1)} = \mathcal{E}_J$, $\mathcal{E}^{(3)} = \mathcal{E}_{J-1}$. Subsequently, we find the contribution due to each of remaining vertices

$$\tilde{\delta}(s,\vec{b})\Big|_{\mathcal{A}_{J+1+i}} = \frac{2(-1)^i}{Jm} a_{J+1+i} e^{\mu_1\cdots\mu_i\mu_{i+1}\cdots\mu_J} e^{\nu_2\cdots\nu_i}{}_{\mu_{i+1}\cdots\mu_J} \partial_{b^{\mu_1}}\cdots\partial_{b^{\mu_i}}\partial_{b^{\nu_2}}\cdots\partial_{b^{\nu_i}} \frac{1}{|b|^{D-4}} \tag{B.15}$$

impling that $a_{J+1+i} = 0$. Using the diagonal elements in $\mathcal{E}_{J-1}$ we find

$$a_{J+1+i} = 0 \qquad i = 2, \cdots, J, \tag{B.16}$$

$$a_{2J+1+i} = 0 \qquad i = 2, \cdots, J-1. \tag{B.17}$$

However the contribution from $\mathcal{A}_1$ is given by

$$\tilde{\delta}(s,\vec{b})\Big|_{\mathcal{A}_1} = \frac{2(-i)}{m} a_1 e^{\mu_1\mu_2\cdots\mu_{J-1}\mu_J} e_{\mu_1\mu_2\cdots\mu_{J-1}} \partial_{b^{\mu_J}} \frac{1}{|b|^{D-4}} \ . \tag{B.18}$$

Therefore, we find $a_{J+2} = J\ a_1\ ,\ a_{2J+2} = \frac{J(J-1)}{2} a_1$. This proves (3.26).

Diagonal Elements of $\mathcal{E}_{J-2}$

For constraining a_1 we used the diagonal elements in $\mathcal{E}_{J-2}$ for both particles. Computing C_{JJ2} after imposing all the other constraints, we find for $J \geq 4$

$$\tilde{\delta}(s,\vec{b}) = a_1 \frac{3(J-2)(J-3)}{m^4 J(J-1)} \left(\frac{D+2J-6}{D+2J-5}\right)^2 e^{\mu_1\mu_2\mu_3\cdots\mu_{J-2}} e_{\mu_3\cdots\mu_{J-2}}{}^{\nu_1\nu_2} \partial_{b^{\mu_1}}\partial_{b^{\mu_2}}\partial_{b^{\nu_1}}\partial_{b^{\nu_2}} \frac{1}{|b|^{D-4}} \tag{B.19}$$

and hence $a_1 = 0$ due to the trick used in B.2. The equation B.19 is valid for $J \geq 4$. For $J = 3$, we used interference between $\mathcal{E}^{(1)} = \mathcal{E}_0$ and $\mathcal{E}^{(3)} = \mathcal{E}_3$ to set $a_1 = 0$.

Bounds for $D = 4$

Positivity of the phase shift (3.36) leads to the following constraints in $D = 4$:

$$\begin{aligned}
&\bar{a}_n = 0 \ , \qquad n = 1, \cdots, 2J \ , \\
&\frac{a_{n+1}}{a_n} = \frac{(n-J)(n+J-1)}{n(2n-1)} \frac{1}{m^2} \ , \qquad n = 1, \cdots, J \ , \\
&\frac{a_{J+n+2}}{a_{J+n+1}} = \frac{n^2 - J^2}{n(2n+1)} \frac{1}{m^2} \ , \qquad n = 1, \cdots, J-1 \ ,
\end{aligned} \tag{B.20}$$

with $a_{J+2} = J a_1$.

B.3 Parity Violating Interactions in $D = 5$

Only in $D = 4$ and 5, the massive higher spin particles can interact with gravity in a way that violates parity. We already discussed the case of $D = 4$. Let us now discuss the parity odd interactions in $D = 5$. Unlike $D = 4$, only massive particles are allowed to couple to gravity in a way that does not preserve parity. In order to list all possible parity odd vertices for the interaction $J - J - 2$, we introduce the following parity odd building block:

$$\mathcal{B} = \epsilon^{\mu_1 \mu_2 \mu_3 \mu_4 \mu_5} z_{1;\mu_1} z_{3;\mu_2} z_{\mu_3} q_{\mu_4} p_{3;\mu_5} \ . \tag{B.21}$$

The most general form of parity odd on-shell three-point amplitude can then be constructed using this building block. In particular, we can write two distinct sets

of vertices. The first set contains J independent structures:

$$\begin{aligned}
\mathcal{A}_1^{odd} &= \mathcal{B}(z\cdot p_3)(z_1\cdot z_3)^{J-1}\ , \\
\mathcal{A}_2^{odd} &= \mathcal{B}(z\cdot p_3)(z_1\cdot z_3)^{J-2}(z_3\cdot q)(z_1\cdot q)\ , \\
&\vdots \\
\mathcal{A}_J^{odd} &= \mathcal{B}(z\cdot p_3)(z_3\cdot q)^{J-1}(z_1\cdot q)^{J-1}\ .
\end{aligned} \tag{B.22}$$

While the second set contains $J-1$ independent structures:

$$\begin{aligned}
\mathcal{A}_{J+1}^{odd} &= \mathcal{B}((z\cdot z_3)(z_1\cdot q)-(z\cdot z_1)(z_3\cdot q))(z_1\cdot z_3)^{J-2}, \\
\mathcal{A}_{J+2}^{odd} &= \mathcal{B}((z\cdot z_3)(z_1\cdot q)-(z\cdot z_1)(z_3\cdot q))(z_1\cdot z_3)^{J-3}(z_3\cdot q)(z_1\cdot q), \\
&\vdots \\
\mathcal{A}_{2J-1}^{odd} &= \mathcal{B}((z\cdot z_3)(z_1\cdot q)-(z\cdot z_1)(z_3\cdot q))(z_3\cdot q)^{J-2}(z_1\cdot q)^{J-2}\ .
\end{aligned} \tag{B.23}$$

The most general form of the parity violating three-point amplitude is given by

$$C_{JJ2} = \sqrt{32\pi G_N}\sum_{n=1}^{2J-1}\bar{a}_n\mathcal{A}_n^{odd}\ . \tag{B.24}$$

Bounds on parity violating interactions can be obtained by using a simple null polarization vector

$$\epsilon^\mu(p_1) = i\epsilon_L^\mu(p_1) - i\epsilon_{T,\hat{x}}^\mu(p_1) + \sqrt{2}\epsilon_{T,\hat{y}}^\mu(p_1)\ , \qquad \epsilon^\mu(p_3) = -i\epsilon_L^\mu(p_3) + i\epsilon_{T,\hat{x}}^\mu(p_3) + \sqrt{2}\epsilon_{T,\hat{y}}^\mu(p_3)\ , \tag{B.25}$$

where the transverse and longitudinal vectors are defined in (3.16). The vectors $\hat{x}$ and $\hat{y}$ are given by $\hat{x} = (0,0,1,0,0)$ and $\hat{y} = (0,0,0,1,0)$. Positivity of the phase shift for this polarization leads to

$$\bar{a}_n = 0\ , \qquad n = 1,\cdots,2J-1 \tag{B.26}$$

for any spin J. Note that this bound holds even for $J = 1$ and 2.

B.4 Correlators of Higher Spin Operators in CFT

Let us first define the building blocks

$$H_{ij} \equiv x_{ij}^2 \varepsilon_i \cdot \varepsilon_j - 2(x_{ij} \cdot \varepsilon_i)(x_{ij} \cdot \varepsilon_j), \qquad V_{i,jk} \equiv \frac{x_{ij}^2 x_{ik} \cdot \varepsilon_i - x_{ik}^2 x_{ij} \cdot \varepsilon_i}{x_{jk}^2} \ , \quad \text{(B.27)}$$

where, $x_{ij}^\mu = (x_i - x_j)^\mu$.

Two-point function

$$\langle \varepsilon_1 . X_J(x_1) \varepsilon_2 . X_J(x_2) \rangle = C_{X_J} \frac{H_{12}^J}{x_{12}^{2(\Delta+J)}} \ , \quad \text{(B.28)}$$

where, Δ is the dimension of the operator X_J and C_{X_J} is a positive constant. ε_1 and ε_2 are null polarization vectors contracted with the indices of X_J in the following way

$$(\varepsilon^\mu \varepsilon^\nu \cdots) \, X_{\mu\nu\ldots} \equiv \varepsilon . X \ . \quad \text{(B.29)}$$

Three-point Function

Let us now discuss the three-point function $\langle \varepsilon_1 . X_J(x_1) \varepsilon_2 . X_J(x_2) \varepsilon_3 . T(x_3) \rangle$:

$$\langle \varepsilon_1 . X_J(x_1) \varepsilon_2 . X_J(x_2) \varepsilon_3 . T(x_3) \rangle$$
$$= \sum_{\{n_{23}, n_{13}, n_{12}\}} C_{n_{23}, n_{13}, n_{12}} \frac{V_{1,23}^{J-n_{12}-n_{13}} V_{2,13}^{J-n_{12}-n_{23}} V_{3,12}^{2-n_{13}-n_{23}} H_{12}^{n_{12}} H_{13}^{n_{13}} H_{23}^{n_{23}}}{x_{12}^{(2h-d-2)} x_{13}^{(d+2)} x_{23}^{(d+2)}}, \quad \text{(B.30)}$$

where $C_{n_{23},n_{13},n_{12}}$ are OPE coefficients and $h \equiv \Delta + J$. In the above expression all of the polarization vectors are null, however polarizations $\varepsilon^\mu \varepsilon^\nu \cdots$ can be converted into an arbitrary polarization tensor $\varepsilon^{\mu\nu\ldots}$ by using projection operators from [117].

The sum in (B.30) is over all triplets of non-negative integers $\{n_{23}, n_{13}, n_{12}\}$ satisfying

$$J - n_{12} - n_{13} \geq 0 \ , \qquad J - n_{12} - n_{23} \geq 0 \ , \qquad 2 - n_{13} - n_{23} \geq 0 \ . \tag{B.31}$$

To begin with, there are $5 + 6(J-1)$ OPE coefficients $C_{n_{23},n_{13},n_{12}}$, however, not all of them are independent. The three-point function (B.30) must be symmetric with respect to the exchange $(x_1, \varepsilon_1) \leftrightarrow (x_2, \varepsilon_2)$ which implies that only $4J$ OPE coefficients can be independent in general. Moreover, conservation of the stress-tensor operator T will impose additional restrictions on the remaining OPE coefficients $C_{n_{23},n_{13},n_{12}}$.

Conservation Equation

Relations between the OPE coefficients from conservation of the stress-tensor operator T can be obtained by imposing the vanishing of $\frac{\partial}{\partial x^\mu}\langle T(x)\cdots\rangle$ up to contact terms. For $\langle X_J X_J T\rangle$, the conservation equation leads to J additional constraint amongst the remaining $4J$ OPE coefficients. Therefore, the three-point function $\langle X_J X_J T\rangle$ is fixed by conformal invariance up to $3J$ independent OPE coefficients. Furthermore, the Ward identity leads to a relation between these OPE coefficients and the coefficient of the two-point function C_{X_J}.

B.5 Details of Spin-3 Calculation in $D > 4$

Constraints from Conservation Equation

Conservation equation leads to 3 relations among the OPE coefficients

$$C_{0,0,0} = -\frac{1}{3}\left(d^2+4d\right)C_{0,2,0} - \frac{1}{6}\left(-d^2-4d+12\right)C_{1,1,0} + 2C_{0,1,0}, \tag{B.32}$$

$$C_{0,0,1} = -\frac{1}{2}\left(d^2+2d\right)C_{0,2,1} - \frac{1}{4}\left(-d^2-2d+8\right)C_{1,1,1} - \frac{3}{2}dC_{0,2,0} - \frac{1}{2}(2-d)C_{1,1,0} + 2C_{0,1,1}, \tag{B.33}$$

$$C_{0,0,2} = -\frac{1}{2}\left(4-d^2\right)C_{1,1,2} - 2dC_{0,2,1} - \frac{1}{2}(2-d)C_{1,1,1} + 2C_{0,1,2}\ . \tag{B.34}$$

Deriving Constraints from the HNEC

Let us first start with $\xi = +1$. In the limit $\rho \to 1$, the leading contribution to $\mathcal{E}(\rho)$ goes as $(1-\rho)^{-(d+3)}$, in particular

$$\mathcal{E}_+(\rho) = \frac{d(-4+d^2) - 18d(2+d)\lambda^2 + 72(2+d)\lambda^4 - 48\lambda^6}{(1-\rho)^{d+3}}t_1 + \cdots \tag{B.35}$$

up to some overall positive coefficient. t_1 in the above expression is a particular linear combination of all the OPE coefficients. Positivity of coefficients of each powers of λ^2 leads to the constraint

$$t_1 = 0. \tag{B.36}$$

After imposing this constraint, the next leading term becomes

$$\mathcal{E}_+(\rho) = \frac{(d-2)d - 12d\lambda^2 + 24\lambda^4}{(1-\rho)^{d+2}}t_2 + \cdots, \tag{B.37}$$

where, t_2 is another linear combination of all the OPE coefficients. Positivity now implies

$$t_2 = 0 \ . \tag{B.38}$$

After imposing both these constraints the next leading contribution can be written in terms of two new linear combinations t_3 and t_4 of OPE coefficients:

$$\mathcal{E}_+(\rho) = \frac{t_3 - (a_3 t_3 + a_4 t_4)\lambda^2 + t_4\lambda^4 - (b_3 t_3 + b_4 t_4)\lambda^6}{(1-\rho)^{d+1}} + \cdots \ , \tag{B.39}$$

where, a_3, a_4, b_3, b_4 are numerical factors shown later in this appendix. The exact values of these numerical factors are not important, but note that $a_3, a_4, b_4 > 0$ for $d > 3$. Positivity of coefficients of λ^0 and λ^4 imply that $t_3, t_4 \geq 0$. Then, positivity of coefficients of λ^2 dictates that

$$t_3 = t_4 = 0 \ . \tag{B.40}$$

After imposing these constraints, we get something very similar

$$\mathcal{E}_+(\rho) = \frac{t_5 - (a_5 t_5 + a_6 t_6)\lambda^2 + t_6\lambda^4}{(1-\rho)^{d}} + \cdots \ , \tag{B.41}$$

where, t_5 and t_6 are two new linear combinations of OPE coefficients and a_5, a_6 are positive numerical factors shown at the end of this appendix. Note that there is no λ^6 term in this order. However, positivity of coefficients of λ^0, λ^2 and λ^4 still produces two equalities:

$$t_5 = t_6 = 0 \ . \tag{B.42}$$

Repeating the same procedure for the next order, we obtain

$$\mathcal{E}_+(\rho) = \frac{t_7 - (a_7 t_7 + a_8 t_8)\lambda^2 + t_8\lambda^4 - (b_7 t_7 + b_8 t_8)\lambda^6}{(1-\rho)^{d-1}} + \cdots \ , \tag{B.43}$$

where, a and b coefficients are shown at the end of this appendix. A similar argument in $d \geq 4$ leads to constraints

$$t_7 = t_8 = 0 \ . \tag{B.44}$$

After imposing all these constraints, finally we obtain

$$\mathcal{E}_+(\rho) = \frac{t_9}{(1-\rho)^{d-2}}\left(1 + \frac{4\Delta\lambda^2}{-d+2\Delta-2} + \frac{4\Delta(\Delta+1)\lambda^4}{(d-2\Delta)(d-2\Delta+2)}\right) , \tag{B.45}$$

where, coefficients of λ^0, λ^2 and λ^4 are now all positive. Hence, the holographic null energy condition now leads to $t_9 \geq 0$. We can now choose $\xi = -1$ and calculate $\mathcal{E}_-(\rho)$. After imposing $t_i = 0$ for $i = 1, \cdots, 8$, we get

$$\mathcal{E}_-(\rho) = -\frac{t_9}{(1-\rho)^{d-2}}\left(1 + \frac{4\Delta\lambda^2}{-d+2\Delta-2} + \frac{4\Delta(\Delta+1)\lambda^4}{(d-2\Delta)(d-2\Delta+2)}\right) \tag{B.46}$$

and hence $t_9 \leq 0$. Therefore, combining both these inequalities, we finally get

$$t_9 = 0 \ . \tag{B.47}$$

From the definitions of t_i's it is apparent that $t_1, \cdots, t_9$ are independent linear combinations of the OPE coefficients. Therefore, irrespective of their exact structures, $\{t_1, \cdots, t_9\}$ forms a complete basis in the space of OPE coefficients. As a consequence, the constraints $t_1, \cdots, t_9 = 0$ necessarily require that all OPE coefficients $C_{i,j,k}$ must vanish.

a and b Coefficients

a and b coefficients are given by

$$a_3 = \frac{2d(13\Delta+9) - 8(\Delta+3)}{(d-2)(d(4\Delta+3) - 2(\Delta+2))} , \qquad b_3 = -\frac{16\Delta}{(d-2)d(d(4\Delta+3) - 2(\Delta+2))} ,$$

$$a_4 = \frac{(d-3)d(\Delta+1)}{8d\Delta + 6d - 4\Delta - 8} , \qquad b_4 = \frac{4\Delta+2}{4d\Delta + 3d - 2\Delta - 4} ,$$

$$a_5 = \frac{6(\Delta-1)}{(d-2)(2\Delta-1)} , \qquad a_6 = \frac{(d-3)\Delta}{2(2\Delta-1)} ,$$

$$a_7 = \frac{2d^2(2\Delta(\Delta+1)(\Delta+2) - 3) - 4d(\Delta(\Delta+2)(7\Delta+1) - 3) + 48(\Delta+1)\Delta^2}{(d-2)(d-2\Delta)\left(2(d-5)\Delta^2 + 4(d-1)\Delta - 3d + 6\right)} ,$$

$$b_7 = -\frac{8\Delta^2(\Delta+1)}{(d-2)(d-2\Delta)\left(2(d-5)\Delta^2 + 4(d-1)\Delta - 3d + 6\right)} ,$$

$$a_8 = \frac{(d-3)(\Delta-1)(d-2(\Delta+1))}{2(d-5)\Delta^2 + 4(d-1)\Delta - 3d + 6} , \qquad b_8 = \frac{2\left(2\Delta^2 + \Delta - 1\right)}{2(d-5)\Delta^2 + 4(d-1)\Delta - 3d + 6} .$$

t-basis in $d = 4$

For the purpose of illustration, let us transcribe $t_1, \cdots, t_9$ for $d = 4$. We will not show the general d expressions because the exact structures of $t_1, \cdots, t_9$ are not important. The fact that $t_1, \cdots, t_9$ are independent linear combinations of $C_{i,j,k}$ is sufficient to rule out the existence of spin-3 operators.

$$
\begin{aligned}
t_1 = &-\frac{5\pi^{7/2}4^{1-\Delta}\Gamma\left(\Delta-\frac{1}{2}\right)}{\Delta\left(\Delta^2-1\right)\Gamma(\Delta+4)}\{-(2\Delta+5)((\Delta+5)((\Delta+5)\Delta+28)\Delta+168)C_{0,1,0}+24(2\Delta+5)((\Delta+5)\Delta+10)C_{0,1,1}\\
&+\Delta(2(((((\Delta+17)\Delta+119)\Delta+471)\Delta+1044)\Delta+1156)C_{0,2,0}-24(((3\Delta+34)\Delta+121)\Delta+170)C_{0,2,1}\\
&-\Delta(((((\Delta+13)\Delta+91)\Delta+379)\Delta+964)C_{1,1,0}-12((3\Delta+26)\Delta+103)C_{1,1,1}+864C_{1,1,2})-576C_{0,1,2}\\
&-8(173C_{1,1,0}-300C_{1,1,1}+468C_{1,1,2}))+864C_{0,0,3}-48(30C_{0,1,2}-17C_{0,2,0}+22C_{0,2,1}+18C_{1,1,0}-39C_{1,1,1}+114C_{1,1,2})\}\,,\\
t_2 = &\frac{5\pi^{7/2}2^{1-2\Delta}(2\Delta-3)\Gamma\left(\Delta-\frac{3}{2}\right)}{3(\Delta-1)\Delta\left(3\Delta^4+26\Delta^3+103\Delta^2+200\Delta+156\right)\Gamma(\Delta+3)}\{-6\Delta^9C_{0,2,0}+3\Delta^9C_{1,1,0}-102\Delta^8C_{0,2,0}\\
&+45\Delta^8C_{1,1,0}-828\Delta^7C_{0,2,0}+334\Delta^7C_{1,1,0}+72\Delta^6C_{0,1,1}-4156\Delta^6C_{0,2,0}-288\Delta^6C_{0,2,1}+1562\Delta^6C_{1,1,0}\\
&+864\Delta^5C_{0,1,1}-14446\Delta^5C_{0,2,0}-432\Delta^5C_{0,2,1}+5067\Delta^5C_{1,1,0}-2592\Delta^5C_{1,1,2}+4584\Delta^4C_{0,1,1}-2592\Delta^4C_{0,1,2}\\
&-36662\Delta^4C_{0,2,0}+9888\Delta^4C_{0,2,1}+11773\Delta^4C_{1,1,0}-21600\Delta^4C_{1,1,2}+13632\Delta^3C_{0,1,1}-18432\Delta^3C_{0,1,2}\\
&-67616\Delta^3C_{0,2,0}+55920\Delta^3C_{0,2,1}+19292\Delta^3C_{1,1,0}-79200\Delta^3C_{1,1,2}+24816\Delta^2C_{0,1,1}-53856\Delta^2C_{0,1,2}\\
&-85464\Delta^2C_{0,2,0}+129408\Delta^2C_{0,2,1}+21108\Delta^2C_{1,1,0}-156960\Delta^2C_{1,1,2}+1728\left(3\Delta^3+15\Delta^2+35\Delta+30\right)C_{0,0,3}\\
&+\left(3\Delta^8+40\Delta^7+236\Delta^6+762\Delta^5+1393\Delta^4+1190\Delta^3-720\Delta^2-3024\Delta-1728\right)C_{0,1,0}+27072\Delta C_{0,1,1}\\
&-77760\Delta C_{0,1,2}-67392\Delta C_{0,2,0}+157824\Delta C_{0,2,1}+13968\Delta C_{1,1,0}-184896\Delta C_{1,1,2}+12096C_{0,1,1}-41472C_{0,1,2}\\
&-25920C_{0,2,0}+86400C_{0,2,1}+4320C_{1,1,0}-103680C_{1,1,2}\}\,,
\end{aligned}
$$

$$t_3 = \frac{-\pi^{7/2}4^{-\Delta}(2\Delta-3)\Gamma\left(\Delta-\frac{3}{2}\right)}{3(\Delta-1)\left(3\Delta^9+51\Delta^8+414\Delta^7+2078\Delta^6+7223\Delta^5+18331\Delta^4+33808\Delta^3+42732\Delta^2+33696\Delta+12960\right)\Gamma(\Delta+2))}$$
$$\times\{1728(18\Delta^7+177\Delta^6+831\Delta^5+2334\Delta^4+4645\Delta^3+6783\Delta^2+5732\Delta+1680)C_{0,0,3}+(3\Delta^{12}+42\Delta^{11}+219\Delta^{10}$$
$$+206\Delta^9-3651\Delta^8-24138\Delta^7-81903\Delta^6-183990\Delta^5-316308\Delta^4-452936\Delta^3-445512\Delta^2-140544\Delta+126144)C_{0,1,0}$$
$$-2(3\Delta^{12}C_{1,1,0}+42\Delta^{11}C_{1,1,0}+432\Delta^{10}C_{0,2,1}+285\Delta^{10}C_{1,1,0}+720\Delta^9C_{0,2,1}+1448\Delta^9C_{1,1,0}+5184\Delta^9C_{1,1,2}$$
$$-31608\Delta^8C_{0,2,1}+6519\Delta^8C_{1,1,0}+62208\Delta^8C_{1,1,2}-264672\Delta^7C_{0,2,1}+24066\Delta^7C_{1,1,0}+340416\Delta^7C_{1,1,2}$$
$$-1033008\Delta^6C_{0,2,1}+67035\Delta^6C_{1,1,0}+1107648\Delta^6C_{1,1,2}-2495520\Delta^5C_{0,2,1}+140208\Delta^5C_{1,1,0}+2474496\Delta^5C_{1,1,2}$$
$$-4233192\Delta^4C_{0,2,1}+220446\Delta^4C_{1,1,0}+4206816\Delta^4C_{1,1,2}-5473296\Delta^3C_{0,2,1}+264508\Delta^3C_{1,1,0}+5894208\Delta^3C_{1,1,2}$$
$$-5511264\Delta^2C_{0,2,1}+234480\Delta^2C_{1,1,0}+6862752\Delta^2C_{1,1,2}+432(15\Delta^8+172\Delta^7+888\Delta^6+2690\Delta^5+5447\Delta^4$$
$$+8078\Delta^3+7918\Delta^2+3304\Delta-624)C_{0,1,2}-12(9\Delta^{10}+141\Delta^9+1011\Delta^8+4350\Delta^7+12601\Delta^6+26427\Delta^5+43243\Delta^4$$
$$+58314\Delta^3+53728\Delta^2+15312\Delta-14112)C_{0,1,1}-3664512\Delta C_{0,2,1}+129600\Delta C_{1,1,0}+5173632\Delta C_{1,1,2}-967680C_{0,2,1}$$
$$+34560C_{1,1,0}+1347840C_{1,1,2})\}\,,$$

$$t_4 = \frac{\pi^{7/2}4^{-\Delta}(2\Delta-3)\Gamma\left(\Delta-\frac{3}{2}\right)}{3(\Delta-1)\Delta\left(3\Delta^9+51\Delta^8+414\Delta^7+2078\Delta^6+7223\Delta^5+18331\Delta^4+33808\Delta^3+42732\Delta^2+33696\Delta+12960\right)\Gamma(\Delta+2)}$$
$$\times\{-1728\Delta\left(9\Delta^7+105\Delta^6+550\Delta^5+1797\Delta^4+4019\Delta^3+5976\Delta^2+4704\Delta+1152\right)C_{0,0,3}$$
$$-2(-144(33\Delta^9+482\Delta^8+3220\Delta^7+13428\Delta^6+39443\Delta^5+84574\Delta^4+129300\Delta^3+133632\Delta^2+88992\Delta+31104)C_{0,1,2}$$
$$+12(15\Delta^{11}+300\Delta^{10}+2836\Delta^9+16806\Delta^8+70033\Delta^7+217146\Delta^6+511924\Delta^5+913140\Delta^4+1197048\Delta^3+1090080\Delta^2+634176\Delta$$
$$+186624)C_{0,1,1}+\Delta(-288(9\Delta^9+135\Delta^8+902\Delta^7+3736\Delta^6+10842\Delta^5+22703\Delta^4+33325\Delta^3+32796\Delta^2+17496\Delta+1728)C_{1,1,2}$$
$$-24(30\Delta^{10}+411\Delta^9+2444\Delta^8+8520\Delta^7+19136\Delta^6+25089\Delta^5+1406\Delta^4-65772\Delta^3-129792\Delta^2-107712\Delta-27648)C_{0,2,1}$$
$$+(9\Delta^{12}+166\Delta^{11}+1543\Delta^{10}+9146\Delta^9+38267\Delta^8+119030\Delta^7+280469\Delta^6+495754\Delta^5+634144\Delta^4+536256\Delta^3$$
$$+238752\Delta^2-41472)C_{1,1,0}))+(9\Delta^{13}+208\Delta^{12}+2517\Delta^{11}+20148\Delta^{10}+116751\Delta^9+511632\Delta^8+1737543\Delta^7$$
$$+4628948\Delta^6+9669660\Delta^5+15584136\Delta^4+18714816\Delta^3+15761088\Delta^2+8439552\Delta+2239488)C_{0,1,0}\}\,,$$

$$t_5 = \frac{\pi^{7/2}4^{-\Delta}(2\Delta-3)\Gamma\left(\Delta-\frac{3}{2}\right)}{3(9\Delta^6+87\Delta^5+370\Delta^4+951\Delta^3+1667\Delta^2+1980\Delta+1008)\Gamma(\Delta+1)}\{(15\Delta^8+125\Delta^7+636\Delta^6+2162\Delta^5+5397\Delta^4$$
$$+9413\Delta^3+12150\Delta^2+10062\Delta+4212)C_{0,1,0}-2(15\Delta^8C_{1,1,0}+80\Delta^7C_{1,1,0}+258\Delta^6C_{1,1,0}+583\Delta^5C_{1,1,0}$$
$$+2592\Delta^5C_{1,1,2}+1130\Delta^4C_{1,1,0}+9936\Delta^4C_{1,1,2}+1317\Delta^3C_{1,1,0}+12096\Delta^3C_{1,1,2}+1333\Delta^2C_{1,1,0}-6480\Delta^2C_{1,1,2}$$
$$+6(9\Delta^6+84\Delta^5+400\Delta^4+988\Delta^3+1387\Delta^2+1036\Delta+384)C_{0,1,1}-12(18\Delta^6+285\Delta^5+1136\Delta^4+1817\Delta^3+752\Delta^2$$
$$-400\Delta-168)C_{0,2,1}+252\Delta C_{1,1,0}-6912\Delta C_{1,1,2}-720C_{1,1,0}+8208C_{1,1,2})\}\,,$$

$$t_6 = \frac{-\pi^{7/2}2^{1-2\Delta}(\Delta+1)(2\Delta-3)\Gamma\left(\Delta-\frac{3}{2}\right)}{(\Delta-1)\left(9\Delta^6+87\Delta^5+370\Delta^4+951\Delta^3+1667\Delta^2+1980\Delta+1008\right)\Gamma(\Delta+1)}\{(3\Delta^8+28\Delta^7+160\Delta^6+603\Delta^5$$
$$+1622\Delta^4+3005\Delta^3+4191\Delta^2+3564\Delta+1296)C_{0,1,0}-2(3\Delta^8C_{1,1,0}+19\Delta^7C_{1,1,0}+73\Delta^6C_{1,1,0}+173\Delta^5C_{1,1,0}$$
$$+327\Delta^4C_{1,1,0}-864\Delta^4C_{1,1,2}+354\Delta^3C_{1,1,0}-2016\Delta^3C_{1,1,2}+263\Delta^2C_{1,1,0}-4320\Delta^2C_{1,1,2}-12(6\Delta^4+47\Delta^3$$
$$+104\Delta^2+131\Delta+72)\Delta^2C_{0,2,1}+6(3\Delta^6+28\Delta^5+112\Delta^4+244\Delta^3+393\Delta^2+372\Delta+144)C_{0,1,1}$$
$$+12\Delta C_{1,1,0}-576\Delta C_{1,1,2}-144C_{1,1,0}+3456C_{1,1,2})\}\,,$$

$$t_7 = \frac{\pi^{7/2}4^{-\Delta-1}\left(2\Delta^2-7\Delta+6\right)\Gamma\left(\Delta-\frac{3}{2}\right)}{9\left(3\Delta^6+8\Delta^5+16\Delta^4+15\Delta^3+11\Delta^2+\Delta-9\right)\Gamma(\Delta)}\{\left(15\Delta^6+64\Delta^5-4\Delta^4-130\Delta^3+244\Delta^2+270\Delta+243\right)C_{0,1,0}$$

$$t_9 = \frac{\pi^{7/2}4^{-2\Delta-3}C_{0,1,0}}{63\,(\Delta^2-\Delta-1)\,\Gamma(\Delta+4)^2}\{24\sqrt{\pi}(\Delta+2)(\Delta+3)(16\Delta^{12}+112\Delta^{11}+802\Delta^{10}+2041\Delta^9-3583\Delta^8-27783\Delta^7$$
$$-97848\Delta^6-361565\Delta^5-1046943\Delta^4-1943909\Delta^3-2130484\Delta^2-1182496\Delta-72840)\Gamma(2\Delta-2)$$
$$-\frac{4^{\Delta}\Gamma\left(\Delta-\frac{1}{2}\right)\Gamma(\Delta+4)}{\Delta\,(\Delta^2-1)}(48\Delta^{12}+560\Delta^{11}+2182\Delta^{10}+2763\Delta^9-7389\Delta^8-69237\Delta^7-307656\Delta^6$$
$$-1103735\Delta^5-3121789\Delta^4-5823663\Delta^3-6399516\Delta^2-3547488\Delta-218520)\}\ .$$

B.6 Details of Spin-4 Calculation in $D > 4$

Constraints From Conservation Equation

Conservation equation leads to 4 relations among the OPE coefficients of $\langle X_{J=4}X_{J=4}T\rangle$:

$$\tilde{C}_{0,0,0} = \frac{1}{8}\left((d-2)(d+8)\tilde{C}_{1,1,0} - 2d(d+6)\tilde{C}_{0,2,0}\right) + 2\tilde{C}_{0,1,0}\ ,$$
$$\tilde{C}_{0,0,1} = \frac{1}{6}\left(-8d\tilde{C}_{0,2,0} - 2d(d+4)\tilde{C}_{0,2,1} + (d-2)\left((d+6)\tilde{C}_{1,1,1} + 3\tilde{C}_{1,1,0}\right) + 12\tilde{C}_{0,1,1}\right)\ ,$$
$$\tilde{C}_{0,0,2} = \frac{1}{4}\left(-6d\tilde{C}_{0,2,1} - 2d(d+2)\tilde{C}_{0,2,2} + (d-2)\left((d+4)\tilde{C}_{1,1,2} + 2\tilde{C}_{1,1,1}\right) + 8\tilde{C}_{0,1,2}\right)\ ,$$
$$\tilde{C}_{0,0,3} = \frac{1}{2}\left(-4d\tilde{C}_{0,2,2} + (d-2)\left((d+2)\tilde{C}_{1,1,3} + \tilde{C}_{1,1,2}\right) + 4\tilde{C}_{0,1,3}\right)\ .$$

Deriving Constraints from the HNEC

The full expression for $\mathcal{E}(\rho)$ is long and not very illuminating, so we will not transcribe it here. Instead we introduce a new basis $\{\tau_1, \cdots, \tau_{12}\}$ in the space of OPE coefficients $\tilde{C}_{i,j,k}$ and use this new basis to derive constraints. The exact structures of $\tau_1, \cdots, \tau_{12}$ are not important because the fact that $\tau_1, \cdots, \tau_{12}$ are

independent linear combinations of $\tilde{C}_{i,j,k}$ is sufficient to rule out the existence of spin-4 operators.

We again start with $\xi = +1$, however, for spin-4, this will be sufficient to rule them out completely. In the limit $\rho \to 1$, the leading contribution to $\mathcal{E}(\rho)$ goes as $(1-\rho)^{-(d+5)}$, in particular

$$\mathcal{E}_+(\rho) = \frac{\tau_1}{(d-2)d(d+2)(d+4)(1-\rho)^{(d+5)}} \left((d-2)d(d+2)(d+4)\right.$$
$$\left. -32d(d+2)(d+4)\lambda^2 + 288(d+2)(d+4)\lambda^4 - 768(d+4)\lambda^6 + 384\lambda^8\right) + \cdots \ . \tag{B.48}$$

Positivity of coefficients of each powers of λ^2 leads to the constraint

$$\tilde{t}_1 = 0 \ . \tag{B.49}$$

After imposing this constraint, the next leading term becomes

$$\mathcal{E}_+(\rho) = \frac{\tilde{t}_2}{(1-\rho)^{d+4}} \left(1 - \frac{24\lambda^2}{d-2} + \frac{144\lambda^4}{(d-2)d} - \frac{192\lambda^6}{d(d^2-4)}\right) + \cdots \ , \tag{B.50}$$

where, positivity now implies

$$\tilde{t}_2 = 0 \ . \tag{B.51}$$

After imposing both these constraints the next leading contribution behaves similar to the spin-3 case:

$$\mathcal{E}_+(\rho) = \frac{\tilde{t}_3 - (\tilde{a}_3\tilde{t}_3 + \tilde{a}_4\tilde{t}_4)\lambda^2 + \tilde{t}_4\lambda^4 + (\tilde{b}_3\tilde{t}_3 + \tilde{b}_4\tilde{t}_4)\lambda^6 + (\tilde{c}_3\tilde{t}_3 + \tilde{c}_4\tilde{t}_4)\lambda^8}{(1-\rho)^{d+3}} + \cdots \ , \tag{B.52}$$

where, $\tilde{a}_3, \tilde{a}_4, \tilde{b}_3, \tilde{b}_4, \tilde{c}_3, \tilde{c}_4$ are numerical factors given later in this appendix. Note that $\tilde{a}_3, \tilde{a}_4 > 0$ and hence positivity of coefficients of λ^0, λ^2 and λ^4 imply that

$$\tilde{t}_3 = \tilde{t}_4 = 0 \ . \tag{B.53}$$

The next order contribution has an identical structure:

$$\mathcal{E}_+(\rho) = \frac{\tau_5 - (\alpha_5\tau_5 + \alpha_6\tau_6)\lambda^2 + \tau_6\lambda^4 + (\beta_5\tau_5 + \beta_6\tau_6)\lambda^6}{(1-\rho)^{d+2}} + \cdots \ , \tag{B.54}$$

with $\alpha_5, \alpha_6 > 0$, implying

$$\tau_5 = \tau_6 = 0 \ . \tag{B.55}$$

So far, everything is very similar to the spin-3 case. But the next order contribution is somewhat different. In the next order, there are three independent structures

$$\mathcal{E}_+(\rho) = \frac{\tau_7 - (\alpha_7\tau_7 + \alpha_8\tau_8 + \alpha_9\tau_9)\lambda^2 + \tau_8\lambda^4 + \tau_9\lambda^6 + (\beta_7\tau_7 + \beta_8\tau_8 + \beta_9\tau_9)\lambda^8}{(1-\rho)^{d+1}} + \cdots \ , \tag{B.56}$$

where, $\alpha_7, \alpha_8, \alpha_9 > 0$. Positivity now leads to three constraints

$$\tau_7 = \tau_8 = \tau_9 = 0 \ . \tag{B.57}$$

However, after imposing these constraints, in the next order we get only two new structures mainly because a lot of contributions vanish after imposing the previous constraints. In particular, we obtain

$$\mathcal{E}_+(\rho) = \frac{\tau_{10} - (\alpha_{10}\tau_{10} + \alpha_{11}\tau_{11})\lambda^2 + \tau_{11}\lambda^4 - (\beta_{10}\tau_{10} + \beta_{11}\tau_{11})\lambda^6}{(1-\rho)^{d}} + \cdots \tag{B.58}$$

with either $\alpha_{10}, \alpha_{11} > 0$ or $\beta_{10}, \beta_{11} > 0$ which again implies

$$\tau_{10} = \tau_{11} = 0 \ . \tag{B.59}$$

Finally, in the next order we get

$$\mathcal{E}_+(\rho) = \frac{\tilde{t}_{12}}{(1-\rho)^{d-1}} \left(1 + \tilde{a}_{12}\lambda^2 + \tilde{b}_{12}\lambda^4 - \tilde{c}_{12}\lambda^6\right) + \cdots \ , \tag{B.60}$$

where, $\tilde{a}_{12}, \tilde{b}_{12}, \tilde{c}_{12} > 0$ as shown later in this appendix. Note that unlike the spin-3 case, signs of coefficients of different powers of λ^2 switch sign. Therefore, we can conclude that

$$\tilde{t}_{12} = 0 \ . \tag{B.61}$$

$\{\tilde{t}_1, \cdots, \tilde{t}_{12}\}$ forms a complete basis in the space of OPE coefficients and hence the constraints $\tilde{t}_1, \cdots, \tilde{t}_{12} = 0$ necessarily require that all OPE coefficients $\tilde{C}_{i,j,k}$ must vanish implying

$$\langle X_{J=4} X_{J=4} T \rangle = 0 \ . \tag{B.62}$$

$\tilde{a}$, $\tilde{b}$ and $\tilde{c}$ Coefficients

$\tilde{a}$, $\tilde{b}$ and $\tilde{c}$ coefficients are given by

$$\tilde{a}_3 = \frac{2(d(41\Delta+73)-4(\Delta+11))}{(d-2)(d(6\Delta+11)-4(\Delta+3))} \ , \qquad \tilde{a}_4 = \frac{(d-3)d(\Delta+2)}{3(d(6\Delta+11)-4(\Delta+3))} \ ,$$
$$\tilde{b}_3 = \frac{48(d(27\Delta+43)+52\Delta+60)}{d\left(d^2-4\right)(d(6\Delta+11)-4(\Delta+3))} \ , \quad \tilde{b}_4 = -\frac{8(d(3\Delta+5)+5\Delta+6)}{(d+2)(d(6\Delta+11)-4(\Delta+3))} \ ,$$
$$\tilde{c}_3 = -\frac{192(5\Delta+7)}{d\left(d^2-4\right)(d(6\Delta+11)-4(\Delta+3))} \ , \quad \tilde{c}_4 = \frac{8(2\Delta+3)}{(d+2)(d(6\Delta+11)-4(\Delta+3))} \ ,$$
$$\tilde{a}_5 = \frac{d(38\Delta+24)-4(\Delta+8)}{(d-2)(d(4\Delta+3)-2(\Delta+2))} \ , \qquad \tilde{a}_6 = \frac{(d-3)d(\Delta+1)}{3(d(4\Delta+3)-2(\Delta+2))} \ ,$$
$$\tilde{b}_5 = \frac{144\Delta}{(d-2)d(d(4\Delta+3)-2(\Delta+2))} \ , \qquad \tilde{b}_6 = \frac{8\Delta+4}{-4d\Delta-3d+2\Delta+4} \ ,$$
$$\tilde{a}_7 = \frac{12(3d+1)(\Delta-1)(2\Delta+1)}{(d-2)\left(d\left(13\Delta^2-3\right)+\Delta^2-1\right)} \ , \tilde{b}_7 = \frac{24\Delta\left(\Delta^2-1\right)}{d\left(d^2-3d+2\right)(\Delta+2)\left(d\left(13\Delta^2-3\right)+\Delta^2-1\right)} \ ,$$
$$\tilde{a}_8 = \frac{(d-3)d\Delta(2\Delta+1)}{d\left(13\Delta^2-3\right)+\Delta^2-1} \ , \qquad \tilde{b}_8 = \frac{2\left(-4\Delta^3-4\Delta^2+\Delta+1\right)}{(d-1)(\Delta+2)\left(d\left(13\Delta^2-3\right)+\Delta^2-1\right)} \ ,$$
$$\tilde{a}_9 = \frac{(d-3)^2 d\Delta(\Delta+1)}{4\left(d\left(13\Delta^2-3\right)+\Delta^2-1\right)} \ , \quad \tilde{b}_9 = -\frac{(2\Delta+1)(d(7\Delta(\Delta+1)-5)-\Delta(\Delta+1))}{(d-1)(\Delta+2)\left(d\left(13\Delta^2-3\right)+\Delta^2-1\right)} \ ,$$
$$\tilde{a}_{10} = -\frac{2\left(-((d-9)d+26)\Delta^3-6((d-7)d+4)\Delta^2-(d-1)(11d+2)\Delta+6(d-2)(d+1)\right)}{(d-2)(d-2\Delta)(d(\Delta(\Delta+4)-3)-\Delta(7\Delta+4)+6)} \ ,$$
$$\tilde{b}_{10} = -\frac{24\Delta(\Delta+1)(\Delta+2)}{(d-2)(d-2\Delta)\left(d\left(\Delta^2+4\Delta-3\right)-7\Delta^2-4\Delta+6\right)} \ ,$$
$$\tilde{a}_{11} = \frac{(d-3)(\Delta-1)(d-2(\Delta+1))}{2(d(\Delta(\Delta+4)-3)-\Delta(7\Delta+4)+6)} \ , \quad \tilde{b}_{11} = \frac{2(\Delta+2)(2\Delta-1)}{d\left(\Delta^2+4\Delta-3\right)-7\Delta^2-4\Delta+6} \ ,$$
$$\tilde{a}_{12} = \frac{2\left(2(5-2d)\Delta^2-3d\Delta+d+2\right)}{(d-2)(2\Delta-1)(d-2\Delta+2)} \ , \quad b_{12} = \frac{4\Delta(d(\Delta+3)(2\Delta+1)-2(\Delta(4\Delta+5)+3))}{(d-2)(2\Delta-1)(d-2\Delta)(d-2\Delta+2)} \ ,$$
$$\tilde{c}_{12} = \frac{8\Delta(\Delta+1)^2}{(d-2)(2\Delta-1)(d-2\Delta)(d-2\Delta+2)} \ .$$

B.7 Details of CFT$_3$ calculations

In this appendix, we discuss the details of the the parity even structures for spin 3 operators in $d = 3$. The full expression for $\mathcal{E}(\rho)$ is rather long and not very illuminating, so we will not transcribe it here. Following the logic of the higher d case, we introduce a new basis $\{t_1, \cdots, t_7\}$ in the space of OPE coefficients $C_{i,j,k}$ and use this new basis to derive constraints.

In the limit $\rho \to 1$, the leading parity even contribution to $\mathcal{E}(\rho)$ goes as $(1-\rho)^{-6}$, in particular

$$\mathcal{E}(\rho) = \frac{j_6(\epsilon^{\mu_1\mu_2\mu_3})}{(1-\rho)^6} t_1 + \cdots \ , \tag{B.63}$$

where, $j_6(\epsilon^{\mu_1\mu_2\mu_3})$ is a specific function of the traceless symmetric polarization tensor. $j_6(\epsilon^{\mu_1\mu_2\mu_3})$ has the property that

$$\begin{aligned} j_6(\epsilon^{\mu_1\mu_2\mu_3}) &\sim \epsilon^{000}\epsilon^{000*} \geq 0 \qquad \text{for} \qquad \epsilon^{\mu_1\mu_2 2} = 0 \ , \\ j_6(\epsilon^{\mu_1\mu_2\mu_3}) &\sim -\epsilon^{222}\epsilon^{222*} \leq 0 \qquad \text{for} \qquad \epsilon^{\mu_1\mu_2 0} = 0 \ . \end{aligned} \tag{B.64}$$

Therefore, the HNEC implies that

$$t_1 = 0 \ . \tag{B.65}$$

After imposing this constraint, the next leading term becomes

$$\mathcal{E}(\rho) = \frac{j_5(\epsilon^{\mu_1\mu_2\mu_3})}{(1-\rho)^5} t_2 + \cdots \ , \tag{B.66}$$

where, $j_5(\epsilon^{\mu_1\mu_2\mu_3})$ is another function which has the property that

$$j_5(\epsilon^{\mu_1\mu_2\mu_3}) \sim \text{Re}\left[\epsilon^{000}\left(\epsilon^{001} + \epsilon^{010} + \epsilon^{100}\right)^*\right] \qquad \text{for} \qquad \epsilon^{\mu_1\mu_2 2} = 0 \tag{B.67}$$

which changes sign as $\epsilon^{001} \to -\epsilon^{001}$ implying

$$t_2 = 0 \ . \tag{B.68}$$

The next order term has two structures:

$$\mathcal{E}(\rho) = \frac{j_4(\epsilon^{\mu_1\mu_2\mu_3})}{(1-\rho)^4} t_3 + \frac{\tilde{j}_4(\epsilon^{\mu_1\mu_2\mu_3})}{(1-\rho)^4} t_4 + \cdots \ , \tag{B.69}$$

where, j_4 and $\tilde{j}_4$ are specific functions of the polarization tensors. Now, applying the HNEC for the following set of polarizations:

$$\begin{aligned} &(a)\ \epsilon^{000} = \epsilon^{011} = \epsilon^{101} = \epsilon^{110} = 1 \ , \\ &(b)\ \epsilon^{012} = 1 \ , \\ &(c)\ \epsilon^{222} = -\epsilon^{211} = -\epsilon^{121} = -\epsilon^{112} = 1 \ , \\ &(d)\ \epsilon^{000} = \epsilon^{220} = \epsilon^{202} = \epsilon^{022} = 1 \end{aligned} \tag{B.70}$$

we find that both t_3 and t_4 must vanish. After imposing these constraints, the next order term also has two structures:

$$\mathcal{E}(\rho) = \frac{j_3(\epsilon^{\mu_1\mu_2\mu_3})}{(1-\rho)^3} t_5 + \frac{\tilde{j}_3(\epsilon^{\mu_1\mu_2\mu_3})}{(1-\rho)^3} t_6 + \cdots \ , \tag{B.71}$$

where, again we will not transcribe j_5 and $\tilde{j}_5$ for simplicity. Now, applying the HNEC for the following set of polarizations:

$$\begin{aligned} &(a)\ \epsilon^{2\mu\nu} = 0 \ , \\ &(b)\ \epsilon^{012} = \pm 1 \ , \qquad \epsilon^{222} = -\epsilon^{211} = -\epsilon^{121} = -\epsilon^{112} = 1 \end{aligned} \tag{B.72}$$

we get

$$t_5 = t_6 = 0 \ . \tag{B.73}$$

After imposing all these constraints, we finally obtain

$$\mathcal{E}(\rho) = \frac{j_2(\epsilon^{\mu_1\mu_2\mu_3})}{(1-\rho)^2} t_7 + \cdots \ . \tag{B.74}$$

We repeat the same procedure by choosing $(a)\ \epsilon^{0\mu\nu} = 0$ and $(b)\ \epsilon^{2\mu\nu} = 0$ that lead to the final constraint

$$t_7 = 0 \ . \tag{B.75}$$

Since, $\{t_1, \cdots, t_7\}$ forms a complete basis in the space of OPE coefficients, the constraints $t_1, \cdots, t_7 = 0$ necessarily require that all OPE coefficients $C_{i,j,k}$ must vanish. It is interesting to note that the same set of constraints can also be obtained by using the λ-trick. We can first impose $C_{1,1,k} = 0$ and then use the polarization (3.58) to derive constraints in general dimension d. Then taking the limit $d \to 3$ leads to the correct set of constraints at each order.

APPENDIX C

CHAPTER 4 OF APPENDIX

C.1 Direct derivation of optimization duality

In this section, we re-derive the duality of section 4.3.3 by direct analysis of the extrema of the functional optimization (4.12). This is useful in practice for translating between dual and primal solutions. Denote

$$f_{i\mu} \equiv f_i(\Delta_\mu) \ , \quad f'_{i\mu} \equiv f'_i(\Delta_\mu), \quad f''_{i\mu} \equiv f''_i(\Delta_\mu) \tag{C.1}$$

and form the block matrix

$$V_{i\beta} = [f_{i\mu} \ \ f'_{i\nu}] \tag{C.2}$$

where $i = 1 \dots P$, $\mu = 1 \dots P/2$, $\nu = 2 \dots P/2$, and $\beta = 1 \dots P-1$. The roots (4.11), using (4.7), impose

$$\alpha_i V_{i\beta} = \alpha_a V_{a\beta} + V_{P\beta} = 0 \ , \tag{C.3}$$

where we have used the normalization condition $\alpha_P = 1$. Therefore, given Δ_μ, the functional with the correct zeroes is

$$\alpha_a = -V_{P\beta} V^{-1}_{\beta a} \ , \tag{C.4}$$

where V^{-1} denotes the inverse of the square submatrix $V_{a\beta}$ (recall a is restricted to the range $1 \dots P-1$). The functional evaluated on the identity term is

$$f(0) = \alpha_i f_i(0) = f_P(0) - V_{P\beta} V^{-1}_{\beta a} f_a(0) \ . \tag{C.5}$$

According to (4.12), we seek to maximize this over Δ_μ. Ultimately we are interested in a maximum with $f(0) = 0$, so we can assume the maximum is actually obtained,

and therefore occurs at a critical point. The gradient, with $\partial_\mu \equiv \frac{d}{d\Delta_\mu}$, is

$$\partial_\mu f(0) = -(\partial_\mu V_{P\beta}) V^{-1}_{\beta a} f_a(0) + V_{P\beta} V^{-1}_{\beta b} (\partial_\mu V_{b\gamma}) V^{-1}_{\gamma a} f_a(0) \tag{C.6}$$

$$= -\alpha_i (\partial_\mu V_{i\beta}) V^{-1}_{\beta a} f_a(0) \tag{C.7}$$

$$= -\alpha_i f'_{i\mu} V^{-1}_{\mu a} f_a(0) - \alpha_i f''_{i\mu} V^{-1}_{\mu+P/2-1,a} f_a(0) \tag{C.8}$$

$$= -\alpha_i f''_{i\mu} V^{-1}_{\mu+P/2-1,a} f_a(0) \tag{C.9}$$

Here $\mu = 2 \dots P/2$ is not summed. The first line uses the matrix identity $\partial X^{-1} = -X^{-1} \partial X X^{-1}$; the second line repackages the two terms into $i = 1 \dots P$; the third line uses (C.2); and the last line follows from (C.3).

Therefore we have two options: $f''_{i\mu} = 0$, so some Δ_μ is actually a triple rather than double root, or

$$V^{-1}_{\beta a} f_a(0) = 0 \qquad (\beta = P/2 + 1 \dots P - 1) \tag{C.10}$$

We assume the latter, so that no roots have multiplicity higher than two. To understand the resulting constraint, define $c_\beta = V^{-1}_{\beta a} f_a(0)$. (C.10) states that the vector c_β takes the block form

$$c_\beta = [-a_\mu \;\; 0_\nu] \; , \tag{C.11}$$

where $\mu = 1 \dots P/2$ and 0_ν is a vector of $P/2 - 1$ zeros. Inverting gives

$$f_a(0) = -a_\mu f_{a\mu} \; . \tag{C.12}$$

Therefore, letting $a_0 = 1$ and $\Delta_0 = 0$, we have

$$\sum_{\mu=0}^{P/2} a_\mu f_a(\Delta_\mu) = 0 \; . \tag{C.13}$$

This is precisely the first $P-1$ equations of the primal bootstrap, (4.6), with a_μ the OPE coefficient. Now let us impose extremality, *i.e.,* that we are at the boundary

of the excluded parameter space. That is, we let Δ_1 be an independent variable and impose

$$0 = f(0) = \alpha_a f_a(0) + f_P(0) = -V_{P\beta} V^{-1}_{\beta a} f_a(0) + f_P(0) = -V_{P\beta} c_\beta + f_P(0) = V_{P\mu} a_\mu + f_P(0) \,. \tag{C.14}$$

This is the Pth equation of (4.6).

Therefore, the solution of (4.12), at extremality, is equivalent to a solution of the P primal bootstrap equations (4.6) (assuming no roots of multiplicity greater than two). We have also shown that, given the extremal functional, the OPE coefficients in the truncated primal solution are

$$a_\mu = -V^{-1}_{\mu a} f_a(0) \,. \tag{C.15}$$

C.2 Generating guesses for Newton's method

The logic of our guess generator is described in section 4.4.2. We fit to the curves in fig. 4.2, extrapolate in P to generate a new curve, then sample at the appropriate discrete points. In this appendix we describe the complete algorithm. The choice of parameters and fitting functions that we use is ad hoc, but produces good results.

Suppose we have already found the spectrum for various truncations $P = P_A$, $A = 1, \ldots, K-1$. Denote these spectra by $\Delta^{P_A}_\mu$. Define $\Delta^{P_A}(x)$ to be the continuous function that numerically interpolates this spectrum at integer x, *i.e.,*

$$\Delta^{P_A}(\mu) = \Delta^{P_A}_\mu \quad \text{for} \quad \mu = 1, 2, \ldots, P_A/2 \,. \tag{C.16}$$

We use a degree-22 Hermite interpolation (in Mathematica: `Interpolation[..., InterpolationOrder->22]`). Now suppose we want to guess the spectrum at

truncation order P_K. Let

$$F_\mu^{P_A} = \Delta^{P_A}\left(\frac{\mu P_A}{P_K}\right) . \tag{C.17}$$

This is defined at discrete P_A. Fit this this, as a function of P_A, to the continuous function

$$F_\mu(y) = a_1 + a_2 y + a_3 \log(y) + a_4 \log(y)^2 + a_5 \log(y)^3 . \tag{C.18}$$

The parameters a_i are chosen such that $F_\mu(P_A) \approx F_\mu^{P_A}$, with least-squares fitting. Finally, our guess for the spectrum at $P = P_K$ is

$$\Delta_\mu^{\text{guess}} = F_\mu(P_K) . \tag{C.19}$$

C.3 High precision bounds with linear programming

In this appendix we describe a simple method to find high-precision bounds on the gap, Δ_1, with linear programming. This is used when we compare our results to SDPB, but it is more general. For example, it is faster than the usual method to find bounds on the 3d Ising model (the 'kink' in [200]), if the bounds are needed to high accuracy.

The standard method is to run a program solver such as SDPB in feasibility mode, to rule in or out each gap Δ_1, and to zoom in on the optimal Δ_1 using bisection. Instead, we run the linear program (4.9). Call the objective at the optimum $M(\Delta_1)$. To find the optimal bound, *i.e.,* the gap Δ_1 which is marginally excluded, we use the secant method to solve $M(\Delta_1) = 0$.

In the first few steps, this method is slower, because the program solver takes longer to solve an optimization problem than a feasibility problem. But the secant

method converges exponentially faster than bisection, so for high accuracy bounds on Δ_1, this method is faster.

APPENDIX D

CHAPTER 5 OF APPENDIX

D.1 Derivation of the gravitational action

In this appendix we derive the action that leads to the equation of motion (5.17).

We start with the expansion of the metric near the boundary (5.15) (5.16)

$$ds^2 = \frac{4dwd\bar{w}}{(1-|w|^2)^2}\left(1-\frac{2}{3}(1-|w|)^2U(\theta)+\cdots\right). \tag{D.1}$$

We now write in terms of the variables $w = e^{-\gamma}e^{i\theta}$ and expand it in powers of γ as

$$ds^2 = \frac{d\theta^2}{\gamma^2}+\frac{d\gamma^2}{\gamma^2}-\frac{2}{3}d\theta^2U(\theta)\,. \tag{D.2}$$

We now equate this to $ds = \frac{d\tau}{\epsilon}$, we set $\theta = \theta(\tau)$ and solve for γ in a power series

$$\gamma = \epsilon\theta'\left[1+\epsilon^2\left(\frac{1}{2}\frac{\theta''^2}{\theta'^2}-\frac{1}{3}U(\theta)\theta'^2\right)+\cdots\right]. \tag{D.3}$$

We can now compute the tangent vector to the curve t^μ and the normal vector n^μ and compute the extrinsic curvature from

$$K = t^\mu t^\nu \nabla_\mu n_\nu = 1+\epsilon^2\left[\{\theta,\tau\}+\left(\frac{1}{2}+U(\theta)\right)\theta'^2\right]. \tag{D.4}$$

Up to the purely topological term, the gravitational action (5.10) reduces to the extrinsic curvature term

$$-I_{\text{grav}} = \frac{1}{4\pi}\frac{\phi_r}{\epsilon}\int\frac{d\tau}{\epsilon}2K = \frac{2\phi_r}{4\pi\epsilon^2}\int d\tau+\frac{\phi_r}{2\pi}\int d\tau\left[\{\theta(\tau),\tau\}+\left(\frac{1}{2}+U(\theta)\right)\theta'^2\right]+o(\epsilon)\,. \tag{D.5}$$

The first term is a purely local divergence that can be viewed as the correction to the vacuum energy. We should also remark that we can always choose a coordinate x where the metric locally looks like the standard Poincare coordinates.

In those coordinates the action is simply $\{x, \tau\}$. However, we will have a nontrivial identification for x as we move from $\tau \to \tau + 2\pi$. Here we simplified the boundary condition, it is just $\theta = \theta + 2\pi$, but we complicated a bit the action. Notice that we can think of $U(\theta)$ as a stress tensor, the change of coordinates is basically the same that we use to transform this stress tensor to zero. In other words, $x(\theta)$ is a function which obeys $\{x, \theta\} = \frac{1}{2} + U(\theta)$.

The conserved energy of the system is given by

$$E = \frac{\phi_r}{2\pi}\left[\{\theta(\tau), \tau\} + \left(\frac{1}{2} + U(\theta)\right)\theta'^2\right]. \tag{D.6}$$

We now compute $U(\theta)$ for the case when we put a conical defect at point A in the w plane. We have the metric (5.33) and the change of coordinates (5.32) which imply that

$$\begin{aligned} ds^2 &= \left|\frac{d\tilde{w}}{dw}\right|^2 \frac{4|dw|^2}{(1-|\tilde{w}|^2)^2} \\ &= \frac{4|dw|^2}{(1-|w|^2)^2}\left[1 - \frac{2}{3}(1-|w|)^2 U(\theta) + \cdots\right], \quad \text{as} \quad |w| \to 1 \end{aligned} \tag{D.7}$$

with

$$U(\theta) = -\frac{1}{2}\left(1 - \frac{1}{n^2}\right)\frac{(1-A^2)^2}{(e^{i\theta}-A)^2(e^{-i\theta}-A)^2}, \tag{D.8}$$

which leads to the same action as (5.36)

We now would like to derive the equations of motion for this action. In particular, we would like to see that as $\theta \to \theta + \delta\theta$ we get the right equations of motion. The change in gravitational action is simple, we just have

$$-\delta I_{\text{grav}} = -\frac{\phi_r}{2\pi}\int d\tau \frac{\left[\{\theta(\tau), \tau\} + (\frac{1}{2} + U(\theta))\theta'^2\right]'}{\theta'}\,\delta\theta\,. \tag{D.9}$$

Now, let us do the variation of the CFT part. Imagine that we choose locally complex coordinates so that

$$\log w = s + i\theta \tag{D.10}$$

We also have the outside coordinates $y = \sigma + i\tau$ and we can locally think of the relation between the two in terms of $\log w = i\theta(-iy)$. Now imagine that we do a small change $\theta(\tau) \to \theta + \delta\theta$ with $\delta\theta$ with compact support. This would change the relation between the two sides. However, let us imagine we instead keep the relation fixed, set by $\theta(\tau)$ and we redefine the outside coordinate by an infinitesimal reparametrization, $\tilde{y} = y + \zeta^y$ in such a way that the relation between the new variables is the same as the old one

$$\log w = i\theta(-i\tilde{y}) = i\theta(-iy) + i\delta\theta(-iy) = i\theta(-iy) + \theta'(-iy)\zeta^y \qquad \to \qquad \zeta^y = i\frac{\delta\theta}{\theta'} \tag{D.11}$$

and we have the complex conjugate expression for $\zeta^{\bar{y}}$. We can then extend this reparametrization in a non-holomorphic way in the region outside, defining

$$\tilde{\zeta}^y = i\frac{\delta\theta(-iy)}{\theta'(-iy)}h(\sigma)\ , \qquad \tilde{\zeta}^{\bar{y}} = -i\frac{\delta\theta(i\bar{y})}{\theta'(i\bar{y})}h(\sigma) \tag{D.12}$$

where $h(\sigma)$ is one for $\sigma = 0$ and quickly goes to zero at σ increases. An example is $h(\sigma) = \theta(\sigma_0 - \sigma)$ for a small σ_0. This change of coordinates is equivalent to a change in metric

$$ds^2 = dyd\bar{y} = d\tilde{y}d\bar{\tilde{y}} - 2\partial_\alpha\zeta^\beta d\tilde{y}^\alpha d\tilde{y}^\beta\ , \qquad \delta g_{\alpha\beta} = -2\partial_{(\alpha}\zeta_{\beta)} \tag{D.13}$$

This differs from the original metric by some terms that are localized near the point where we are doing the variation. The relation between $\log w$ and the $\tilde{y}$ variable was the same as it was before we did the variation, due to our choice of $\tilde{y}$ variable in (D.11). Furthermore, far from the region where we are doing the variation, both variables coincide. Thus, the only thing we are doing is locally changing the metric of the outside region. Using the definition of the stress tensor, $T_{\alpha\beta} = -\frac{2}{\sqrt{g}}\frac{\delta}{\delta g^{\alpha\beta}}\log Z$, we get

$$\delta \log \hat{Z}_M \quad = \quad -\frac{1}{2}\int d\varphi d\sigma (T_{yy}\delta g^{yy} + T_{\bar{y}\bar{y}}\delta g^{\bar{y}\bar{y}})$$

$$= \quad -2\int d\varphi d\sigma (T_{yy}\partial_{\bar{y}}\zeta^{y} + T_{\bar{y}\bar{y}}\partial_{y}\zeta^{\bar{y}})\,, \tag{D.14}$$

where we used that the background metric is flat and that the trace of the stress tensor is zero. We now use evaluate the derivatives

$$\partial_{\bar{y}}\zeta^{y} = \frac{i}{2}\frac{\delta\theta(-iy)}{\theta'(-iy)}h'(\sigma)\;, \qquad \partial_{y}\zeta^{\bar{y}} = -\frac{i}{2}\frac{\delta\theta(i\bar{y})}{\theta'(i\bar{y})}h'(\sigma)\;, \qquad h' = -\delta(\sigma-\sigma^{0})\,. \tag{D.15}$$

Here we used that the arguments of $\delta\theta$ and θ' are holomorphic or antiholomorphic, so the derivative receives only a contribution from h, which is just a delta function. Inserting this into (D.14), integrating over σ, and taking $\sigma^{0}\to 0$, we get

$$\delta \log \hat{Z}_{M} = i\int d\tau (T_{yy} - T_{\bar{y}\bar{y}})\frac{\delta\theta}{\theta'}\,. \tag{D.16}$$

Using (D.9) we get the appropriate equation (5.17) after cancelling the $1/\theta'$ factor from both sides.

D.2 Linearized solution to the welding problem

Let us start with a discussion of the symmetries of the welding problem (5.13). First we can imagine doing $SL(2,C)$ transformations of the z plane. These move around the point at infinity, and we would need to allow a pole in the functions F or G. If we fix that $F(\infty)=\infty$, then we can then impose that the functions are holomorphic everywhere, with no poles, and this group is reduced to just translations, scalings and rotations of the plane z. None of these transformations change the data for the welding problem which is $\theta(\tau)$. In addition, we have two $SL(2,R)$ transformations, one acting on w and one acting on v, both preserving the circles $|w|=1$ and $|v|=1$. These change the data of the welding problem by an $SL(2,R)$ transformation of $e^{i\theta}$ or $e^{i\tau}$ respectively. They map a solution of a welding problem with $\theta(\tau)$ to a

solution of a different welding problem given by the transformed function. In our combined gravity plus CFT problem, we are integrating over $\theta(\tau)$, so we can look for symmetries that change $\theta(\tau)$. It turns out that the $SL(2,R)_v$ that acts on the v plane is *not* a symmetry. It changes the Schwarzian action, for example. On the other hand, the $SL(2,R)_w$ is actually a gauge symmetry, when we also act with the $SL(2,R)$ transformation on the possible locations, w_i, of the conical singularities.

Consider a plane with coordinate w inside the unit disk, and v outside, as in fig. 5.10. The plane is glued along the unit circle with a gluing function $\theta(\tau)$, where $w = e^{i\theta}$ and $v = e^{i\tau}$. The solution to the welding problem is a pair of functions

$$z = G(w) \qquad \text{(inside)} \tag{D.17}$$

$$z = F(v) \qquad \text{(outside)} \tag{D.18}$$

where G is holomorphic inside the disk, and F is holomorphic outside the disk. In this appendix we will solve for F, G perturbatively, assuming the gluing is close to the identity, $\theta(\tau) = \tau + \delta\theta(\tau)$. Here we are considering $\delta\theta(\tau)$ to be a fixed input to the problem of finding F and G.

Expand in Fourier modes,

$$\theta(\tau) = \tau + \sum_{m=-\infty}^{\infty} c_m e^{im\tau} \ , \quad G(w) = w + \sum_{J=0}^{\infty} g_J w^J \ , \quad F(v) = v + \sum_{J=-\infty}^{2} f_J v^J \ . \tag{D.19}$$

Here c_m, d_1^J, and d_2^J are considered small. There is an SL(2) ambiguity in the zeroth order solution, which we have gauge-fixed to set these maps to the identity. (Note that this is different from the choice in the main text around eqn (5.56).) The matching condition on the unit circle is

$$G(e^{i\theta(\tau)}) = F(e^{i\theta}) \ . \tag{D.20}$$

At the linearized level, this sets

$$f_{J+1} = ic_J \qquad (J \leq -2) \tag{D.21}$$

$$g_{J+1} = -ic_J \qquad (J \geq 2) \tag{D.22}$$

and

$$ic_{-1} = f_2 - g_2 \ , \quad ic_0 = f_1 - g_1 \ , \quad ic_1 = f_2 - g_2 \ . \tag{D.23}$$

There an ambiguity by a small $SL(2,C)$ action on the z plane. We can fix it by setting $G(0) = 0$, $F(v) = v$+constant, as $v \to \infty$. This amounts to three complex conditions that set

$$g_0 = f_2 = f_1 = 0 \tag{D.24}$$

This now implies that we get a unique solution for the remaining coefficients in terms of the c_m

$$f_l = ic_{J-1}, \quad \text{for} \ \ J \leq 0 \ ; \qquad\qquad g_J = -ic_{J-1} \ , \quad \text{for} \quad J > 0 \ . \tag{D.25}$$

From here we can calculate

$$v^2\{F, v\} = \sum_{J=-\infty}^{-2} J(J^2-1)ic_J v^J \ . \tag{D.26}$$

Comparing to $\{w, \tau\} = \{e^{i\theta}, \tau\}$ gives the relation used in the main text,

$$e^{2i\tau}\{F, v\} = -\delta\{w, \tau\}_- = -(\delta\theta''' + \delta\theta')_- \ . \tag{D.27}$$

D.3 The equation of motion in Lorentzian signature

The Hilbert transform appearing in the equation of motion (5.45) has a nice interpretation in Lorentzian signature. It is responsible for the dissipation of energy

into the thermal bath outside. This makes contact with the Schwarzian equation for black hole evaporation studied in [244, 273].

In this appendix we set $n = 1$, but allow for CFT operators inserted in the non-gravitational region. The perturbative Schwarzian equation in Euclidean signature is

$$\phi_\tau S + i\kappa \mathrm{H} \cdot S = i\kappa \mathcal{F} \tag{D.28}$$

where $S = \delta\{e^{i\theta}, \tau\}$ and

$$\mathcal{F} = T_{yy}(i\tau) - T_{yy}(-i\tau) \ . \tag{D.29}$$

We separate this into positive and negative frequencies on the Euclidean τ-circle,

$$\phi_\tau S_+ - i\kappa S_+ = i\kappa \mathcal{F}_+ \tag{D.30}$$

$$\phi_\tau S_- + i\kappa S_- = i\kappa \mathcal{F}_- \ . \tag{D.31}$$

Here the '+' terms include only the non-negative powers of e^y, and the '$-$' terms have the negative powers. Now continuing to Lorentzian signature with $\tau = it$, this becomes

$$\phi_t S_\pm \pm \kappa S_\pm = -\kappa \mathcal{F}_\pm \tag{D.32}$$

This is the Lorentzian equation of motion. As an example, consider a state with two scalar operators $\mathcal{O}(y_1)\mathcal{O}(y_2)$ inserted at

$$y_1 = L + i\delta, \qquad y_2 = \bar{y}_1 = L - i\delta \ , \tag{D.33}$$

with $0 < \delta \ll L$. This creates a shockwave that falls into the AdS region at time $t \approx L$. The state is time-symmetric, so there is also a shockwave exiting the AdS region at $t \approx -L$. The stress tensor is

$$T_{yy}(y) = -\frac{h_O}{2\pi} \frac{v^2 (v_1 - v_2)^2}{(v - v_1)^2 (v - v_2)^2} \ , \tag{D.34}$$

with $v = e^y$. The projections onto positive and negative Euclidean frequencies are

$$\mathcal{F}_+ = -\frac{h_O}{2\pi}\frac{v^2(v_1-v_2)^2}{(v-v_1)^2(v-v_2)^2} \ , \qquad \mathcal{F}_- = \frac{h_O}{2\pi}\frac{v^2(v_1-v_2)^2}{(1-v_1v)^2(1-v_1v)^2} \ . \tag{D.35}$$

In Lorentzian signature this becomes

$$\mathcal{F}_+ = \frac{h_O \sin^2\delta}{2\pi(\cos\delta - \cosh(L+t))^2} \tag{D.36}$$

$$\mathcal{F}_- = -\frac{h_O \sin^2\delta}{2\pi(\cos\delta - \cosh(L-t))^2} \tag{D.37}$$

As $\delta \to 0$, these vanishes away from the singularities, leading to

$$\phi_t S_+ + \kappa S_+ = -\kappa E_O \delta(t+L) \tag{D.38}$$

$$\phi_t S_- - \kappa S_- = \kappa E_O \delta(t-L) \ , \tag{D.39}$$

where $E_O = h_O/\delta$. The delta functions are the shockwaves exiting and entering the AdS region. The signs here, and in particular the extra minus sign from the Hilbert transform, ensure that there is a sensible solution for the Schwarzian, which is time-symmetric and goes to zero as $t \to \pm\infty$. The solution is

$$S_+ = \Theta(-t-L)\kappa E_0 e^{\kappa(t+L)} \ , \qquad S_- = \Theta(t-L)\kappa E_0 e^{\kappa(L-t)} \ . \tag{D.40}$$

For $t > 0$, this is essentially the same solution as the evaporating black hole in [244], which had a shockwave produced by a joining quench rather than an operator insertion.

BIBLIOGRAPHY

[1] T. Hartman, D. Mazac and L. Rastelli, Sphere Packing and Quantum Gravity, JHEP **12**, 048, 2019, [arXiv:1905.01319 [hep-th]].

[2] LIGO Scientific, Virgo, Fermi-GBM, INTEGRAL collaboration, B. Abbott et al., Gravitational Waves and Gamma-rays from a Binary Neutron Star Merger: GW170817 and GRB 170817A, Astrophys. J. **848**, L13, 2017, [arXiv:1710.05834 [astro-ph.HE]].

[3] J. D. Bekenstein, Black holes and the second law, Lettere al Nuovo Cimento (1971-1985) **4**, 737–740, 1972.

[4] J. M. Bardeen, B. Carter and S. Hawking, The Four laws of black hole mechanics, Commun. Math. Phys. **31**, 161–170, 1973.

[5] S. W. Hawking, Gravitational radiation from colliding black holes, Phys. Rev. Lett. **26**, 1344–1346, 1971.

[6] R. PENROSE and R. M. FLOYD, Extraction of rotational energy from a black hole, Nature Physical Science **229**, 177–179, 1971.

[7] J. M. Maldacena, The Large N limit of superconformal field theories and supergravity, Int. J. Theor. Phys. **38**, 1113–1133, 1999, [arXiv:hep-th/9711200].

[8] G. 't Hooft, Dimensional reduction in quantum gravity, Conf. Proc. C **930308**, 284–296, 1993, [arXiv:gr-qc/9310026].

[9] L. Susskind, The World as a hologram, J. Math. Phys. **36**, 6377–6396, 1995, [arXiv:hep-th/9409089].

[10] E. Witten, Anti-de Sitter space and holography, Adv. Theor. Math. Phys. **2**, 253–291, 1998, [arXiv:hep-th/9802150].

[11] E. Witten, Anti-de Sitter space, thermal phase transition, and confinement in gauge theories, Adv. Theor. Math. Phys. **2**, 505–532, 1998, [arXiv:hep-th/9803131].

[12] S. Gubser, I. R. Klebanov and A. M. Polyakov, Gauge theory correlators from noncritical string theory, Phys. Lett. B **428**, 105–114, 1998, [arXiv:hep-th/9802109].

[13] T. Banks, M. R. Douglas, G. T. Horowitz and E. J. Martinec, AdS dynamics from conformal field theory, 1998, [arXiv:hep-th/9808016 [hep-th]].

[14] N. Beisert et al., Review of AdS/CFT Integrability: An Overview, Lett. Math. Phys. **99**, 3–32, 2012, [arXiv:1012.3982 [hep-th]].

[15] S. S. Gubser and A. Karch, From gauge-string duality to strong interactions:a pedestrian's guide, Annual Review of Nuclear and Particle Science **59**, 145–168, 2009, [https://doi.org/10.1146/annurev.nucl.010909.083602].

[16] J. Casalderrey-Solana, H. Liu, D. Mateos, K. Rajagopal and U. A. Wiedemann, *Gauge/String Duality, Hot QCD and Heavy Ion Collisions*. Cambridge University Press, 2014, 10.1017/CBO9781139136747.

[17] S. A. Hartnoll, Lectures on holographic methods for condensed matter physics, Classical and Quantum Gravity **26**, 224002, 2009.

[18] K. Skenderis, Lecture notes on holographic renormalization, Class. Quant. Grav. **19**, 5849–5876, 2002, [arXiv:hep-th/0209067].

[19] P. K. Kovtun, D. T. Son and A. O. Starinets, Viscosity in strongly interacting quantum field theories from black hole physics, Phys. Rev. Lett. **94**, 111601, 2005.

[20] V. E. Hubeny, S. Minwalla and M. Rangamani, The fluid/gravity correspondence, in *Theoretical Advanced Study Institute in Elementary Particle Physics: String theory and its Applications: From meV to the Planck Scale*, pp. 348–383, 2012. [arXiv:1107.5780 [hep-th]].

[21] V. E. Hubeny, The fluid/gravity correspondence: a new perspective on the membrane paradigm, Classical and Quantum Gravity **28**, 114007, 2011.

[22] P. M. Chesler, H. Liu and A. Adams, Holographic vortex liquids and superfluid turbulence, Science **341**, 368–372, 2013, [https://science.sciencemag.org/content/341/6144/368.full.pdf].

[23] B. Swingle, Entanglement renormalization and holography, Phys. Rev. D **86**, 065007, 2012.

[24] M. Van Raamsdonk, Comments on quantum gravity and entanglement, 2009, [arXiv:0907.2939 [hep-th]].

[25] L. Susskind, Butterflies on the Stretched Horizon, 2013, [arXiv:1311.7379 [hep-th]].

[26] S. de Haro, S. N. Solodukhin and K. Skenderis, Holographic reconstruction of space-time and renormalization in the AdS / CFT correspondence, Commun. Math. Phys. **217**, 595–622, 2001, [arXiv:hep-th/0002230].

[27] J. Maldacena, S. H. Shenker and D. Stanford, A bound on chaos, JHEP **08**, 106, 2016, [arXiv:1503.01409 [hep-th]].

[28] S. Ryu and T. Takayanagi, Holographic derivation of entanglement entropy from AdS/CFT, Phys. Rev. Lett. **96**, 181602, 2006, [arXiv:hep-th/0603001 [hep-th]].

[29] A. Almheiri, X. Dong and D. Harlow, Bulk Locality and Quantum Error Correction in AdS/CFT, JHEP **04**, 163, 2015, [arXiv:1411.7041 [hep-th]].

[30] D. L. Jafferis, A. Lewkowycz, J. Maldacena and S. J. Suh, Relative entropy equals bulk relative entropy, JHEP **06**, 004, 2016, [arXiv:1512.06431 [hep-th]].

[31] A. Hamilton, D. N. Kabat, G. Lifschytz and D. A. Lowe, Holographic representation of local bulk operators, Phys. Rev. D **74**, 066009, 2006, [arXiv:hep-th/0606141].

[32] X. Dong, D. Harlow and A. C. Wall, Reconstruction of Bulk Operators within the Entanglement Wedge in Gauge-Gravity Duality, Phys. Rev. Lett. **117**, 021601, 2016, [arXiv:1601.05416 [hep-th]].

[33] F. Pastawski, B. Yoshida, D. Harlow and J. Preskill, Holographic quantum error-correcting codes: Toy models for the bulk/boundary correspondence, JHEP **06**, 149, 2015, [arXiv:1503.06237 [hep-th]].

[34] N. Engelhardt and A. C. Wall, Quantum Extremal Surfaces: Holographic Entanglement Entropy beyond the Classical Regime, JHEP **01**, 073, 2015, [arXiv:1408.3203 [hep-th]].

[35] A. Almheiri, D. Marolf, J. Polchinski and J. Sully, Black Holes: Complementarity or Firewalls?, JHEP **02**, 062, 2013, [arXiv:1207.3123 [hep-th]].

[36] A. Almheiri, D. Marolf, J. Polchinski, D. Stanford and J. Sully, An Apologia for Firewalls, JHEP **09**, 018, 2013, [arXiv:1304.6483 [hep-th]].

[37] J. Maldacena and L. Susskind, Cool horizons for entangled black holes, Fortschritte der Physik **61**, 781–811, 2013, [https://onlinelibrary.wiley.com/doi/pdf/10.1002/prop.201300020].

[38] E. D'Hoker and D. Z. Freedman, General scalar exchange in AdS(d+1), Nucl. Phys. B **550**, 261–288, 1999, [arXiv:hep-th/9811257].

[39] D. Z. Freedman, S. D. Mathur, A. Matusis and L. Rastelli, Comments on 4 point functions in the CFT / AdS correspondence, Phys. Lett. B **452**, 61–68, 1999, [arXiv:hep-th/9808006].

[40] H. Liu, Scattering in anti-de Sitter space and operator product expansion, Phys. Rev. D **60**, 106005, 1999, [arXiv:hep-th/9811152].

[41] L. Cornalba, M. S. Costa, J. Penedones and R. Schiappa, Eikonal Approximation in AdS/CFT: From Shock Waves to Four-Point Functions, JHEP **08**, 019, 2007, [arXiv:hep-th/0611122].

[42] I. Heemskerk, J. Penedones, J. Polchinski and J. Sully, Holography from Conformal Field Theory, JHEP **10**, 079, 2009, [arXiv:0907.0151 [hep-th]].

[43] A. Fitzpatrick, J. Kaplan, D. Poland and D. Simmons-Duffin, The Analytic Bootstrap and AdS Superhorizon Locality, JHEP **12**, 004, 2013, [arXiv:1212.3616 [hep-th]].

[44] A. Fitzpatrick, J. Kaplan and M. T. Walters, Universality of Long-Distance AdS Physics from the CFT Bootstrap, JHEP **08**, 145, 2014, [arXiv:1403.6829 [hep-th]].

[45] L. F. Alday, A. Bissi and T. Lukowski, Lessons from crossing symmetry at large N, JHEP **06**, 074, 2015, [arXiv:1410.4717 [hep-th]].

[46] X. O. Camanho, J. D. Edelstein, J. Maldacena and A. Zhiboedov, Causality Constraints on Corrections to the Graviton Three-Point Coupling, JHEP **02**, 020, 2016, [arXiv:1407.5597 [hep-th]].

[47] J. Maldacena, D. Simmons-Duffin and A. Zhiboedov, Looking for a bulk point, JHEP **01**, 013, 2017, [arXiv:1509.03612 [hep-th]].

[48] L. F. Alday and A. Bissi, Unitarity and positivity constraints for CFT at large central charge, JHEP **07**, 044, 2017, [arXiv:1606.09593 [hep-th]].

[49] T. Hartman, C. A. Keller and B. Stoica, Universal Spectrum of 2d Conformal Field Theory in the Large c Limit, JHEP **09**, 118, 2014, [arXiv:1405.5137 [hep-th]].

[50] T. Hartman, Entanglement Entropy at Large Central Charge, 2013, [arXiv:1303.6955 [hep-th]].

[51] J. L. Cardy, Operator content of two-dimensional conformally invariant theories, Nuclear Physics B **270**, 186 – 204, 1986.

[52] D. Poland, S. Rychkov and A. Vichi, The Conformal Bootstrap: Theory, Numerical Techniques, and Applications, Rev. Mod. Phys. **91**, 015002, 2019, [arXiv:1805.04405 [hep-th]].

[53] D. Poland and D. Simmons-Duffin, The conformal bootstrap, Nature Phys. **12**, 535–539, 2016.

[54] N. Arkani-Hamed, L. Motl, A. Nicolis and C. Vafa, The String landscape, black holes and gravity as the weakest force, JHEP **06**, 060, 2007, [arXiv:hep-th/0601001 [hep-th]].

[55] N. Graham and K. D. Olum, Achronal averaged null energy condition, Phys. Rev. D **76**, 064001, 2007, [arXiv:0705.3193 [gr-qc]].

[56] D. M. Hofman and J. Maldacena, Conformal collider physics: Energy and charge correlations, JHEP **05**, 012, 2008, [arXiv:0803.1467 [hep-th]].

[57] T. Faulkner, R. G. Leigh, O. Parrikar and H. Wang, Modular Hamiltonians for Deformed Half-Spaces and the Averaged Null Energy Condition, JHEP **09**, 038, 2016, [arXiv:1605.08072 [hep-th]].

[58] T. Hartman, S. Jain and S. Kundu, Causality Constraints in Conformal Field Theory, JHEP **05**, 099, 2016, [arXiv:1509.00014 [hep-th]].

[59] W. R. Kelly and A. C. Wall, Holographic proof of the averaged null energy condition, Phys. Rev. D **90**, 106003, 2014, [arXiv:1408.3566 [gr-qc]].

[60] E. Witten, Three-Dimensional Gravity Revisited, 2007, [arXiv:0706.3359 [hep-th]].

[61] R. Dijkgraaf, J. M. Maldacena, G. W. Moore and E. P. Verlinde, A Black hole Farey tail, 2000, [arXiv:hep-th/0005003].

[62] J. Maldacena and A. Strominger, AdS3 black holes and a stringy exclusion principle, Journal of High Energy Physics **1998**, 005–005, 1998.

[63] D. Friedan and C. A. Keller, Constraints on 2d cft partition functions, Journal of High Energy Physics **2013**, 180, 2013.

[64] M. Bañados, C. Teitelboim and J. Zanelli, Black hole in three-dimensional spacetime, Phys. Rev. Lett. **69**, 1849–1851, 1992.

[65] J. D. Brown and M. Henneaux, Central charges in the canonical realization of asymptotic symmetries: An example from three dimensional gravity, Communications in Mathematical Physics **104**, 207–226, 1986.

[66] C. A. Keller and A. Maloney, Poincare Series, 3D Gravity and CFT Spectroscopy, JHEP **02**, 080, 2015, [arXiv:1407.6008 [hep-th]].

[67] A. Maloney and E. Witten, Quantum Gravity Partition Functions in Three Dimensions, JHEP **02**, 029, 2010, [arXiv:0712.0155 [hep-th]].

[68] S. Collier, A. Maloney, H. Maxfield and I. Tsiares, Universal Dynamics of Heavy Operators in CFT_2, 2019, [arXiv:1912.00222 [hep-th]].

[69] S. Giombi, A. Maloney and X. Yin, One-loop Partition Functions of 3D Gravity, JHEP **08**, 007, 2008, [arXiv:0804.1773 [hep-th]].

[70] S. Collier, Y. Gobeil, H. Maxfield and E. Perlmutter, Quantum Regge Trajectories and the Virasoro Analytic Bootstrap, JHEP **05**, 212, 2019, [arXiv:1811.05710 [hep-th]].

[71] A. Strominger and C. Vafa, Microscopic origin of the Bekenstein-Hawking entropy, Phys. Lett. **B379**, 99–104, 1996, [arXiv:hep-th/9601029 [hep-th]].

[72] S. Hellerman, A Universal Inequality for CFT and Quantum Gravity, JHEP **08**, 130, 2011, [arXiv:0902.2790 [hep-th]].

[73] N. Afkhami-Jeddi, T. Hartman and A. Tajdini, Fast Conformal Bootstrap and Constraints on 3d Gravity, JHEP **05**, 087, 2019, [arXiv:1903.06272 [hep-th]].

[74] J. M. Maldacena, Eternal black holes in anti-de Sitter, JHEP **04**, 021, 2003, [arXiv:hep-th/0106112 [hep-th]].

[75] T. Anous, T. Hartman, A. Rovai and J. Sonner, Black Hole Collapse in the 1/c Expansion, JHEP **07**, 123, 2016, [arXiv:1603.04856 [hep-th]].

[76] T. Anous, T. Hartman, A. Rovai and J. Sonner, From Conformal Blocks to Path Integrals in the Vaidya Geometry, JHEP **09**, 009, 2017, [arXiv:1706.02668 [hep-th]].

[77] A. L. Fitzpatrick, J. Kaplan, D. Li and J. Wang, On information loss in AdS_3/CFT_2, JHEP **05**, 109, 2016, [arXiv:1603.08925 [hep-th]].

[78] A. Almheiri, T. Hartman, J. Maldacena, E. Shaghoulian and A. Tajdini, Replica Wormholes and the Entropy of Hawking Radiation, 2019, [arXiv:1911.12333 [hep-th]].

[79] T. Hartman, S. Kundu and A. Tajdini, Averaged Null Energy Condition from Causality, JHEP **07**, 066, 2017, [arXiv:1610.05308 [hep-th]].

[80] A. Borde, Geodesic focusing, energy conditions and singularities, Class. Quant. Grav. **4**, 343–356, 1987.

[81] T. A. Roman, Quantum stress-energy tensors and the weak energy condition, Phys. Rev. D **33**, 3526–3533, 1986.

[82] T. Roman, On the 'Averaged Weak Energy Condition' and Penrose's Singularity Theorem, Phys. Rev. D **37**, 546–548, 1988.

[83] V. Frolov and I. Novikov, eds., *Black hole physics: Basic concepts and new developments*, vol. 96. 1998, 10.1007/978-94-011-5139-9.

[84] M. Morris, K. Thorne and U. Yurtsever, Wormholes, Time Machines, and the Weak Energy Condition, Phys. Rev. Lett. **61**, 1446–1449, 1988.

[85] J. L. Friedman, K. Schleich and D. M. Witt, Topological censorship, Phys. Rev. Lett. **71**, 1486–1489, 1993.

[86] A. C. Wall, Proving the Achronal Averaged Null Energy Condition from the Generalized Second Law, Phys. Rev. D **81**, 024038, 2010, [arXiv:0910.5751 [gr-qc]].

[87] G. Klinkhammer, Averaged energy conditions for free scalar fields in flat space-times, Phys. Rev. D **43**, 2542–2548, 1991.

[88] R. Wald and U. Yurtsever, General proof of the averaged null energy condition for a massless scalar field in two-dimensional curved spacetime, Phys. Rev. D **44**, 403–416, 1991.

[89] A. Folacci, Averaged null energy condition for electromagnetism in Minkowski space-time, Phys. Rev. D **46**, 2726–2729, 1992.

[90] R. Verch, The Averaged Null energy condition for general quantum field theories in two-dimensions, J. Math. Phys. **41**, 206–217, 2000, [arXiv:math-ph/9904036].

[91] R. Bousso, Z. Fisher, J. Koeller, S. Leichenauer and A. C. Wall, Proof of the Quantum Null Energy Condition, Phys. Rev. D **93**, 024017, 2016, [arXiv:1509.02542 [hep-th]].

[92] T. Hartman, S. Jain and S. Kundu, A New Spin on Causality Constraints, JHEP **10**, 141, 2016, [arXiv:1601.07904 [hep-th]].

[93] D. M. Hofman, D. Li, D. Meltzer, D. Poland and F. Rejon-Barrera, A Proof of the Conformal Collider Bounds, JHEP **06**, 111, 2016, [arXiv:1603.03771 [hep-th]].

[94] S. Gao and R. M. Wald, Theorems on gravitational time delay and related issues, Class. Quant. Grav. **17**, 4999–5008, 2000, [arXiv:gr-qc/0007021].

[95] S. Dubovsky, T. Gregoire, A. Nicolis and R. Rattazzi, Null energy condition and superluminal propagation, JHEP **03**, 025, 2006, [arXiv:hep-th/0512260].

[96] N. Engelhardt and S. Fischetti, The Gravity Dual of Boundary Causality, Class. Quant. Grav. **33**, 175004, 2016, [arXiv:1604.03944 [hep-th]].

[97] J. Cardy, Quantum Quenches to a Critical Point in One Dimension: some further results, J. Stat. Mech. **1602**, 023103, 2016, [arXiv:1507.07266 [cond-mat.stat-mech]].

[98] A. Allais and E. Tonni, Holographic evolution of the mutual information, JHEP **01**, 102, 2012, [arXiv:1110.1607 [hep-th]].

[99] A. C. Wall, Maximin Surfaces, and the Strong Subadditivity of the Covariant Holographic Entanglement Entropy, Class. Quant. Grav. **31**, 225007, 2014, [arXiv:1211.3494 [hep-th]].

[100] R. Bousso, Z. Fisher, S. Leichenauer and A. C. Wall, Quantum focusing conjecture, Phys. Rev. D **93**, 064044, 2016, [arXiv:1506.02669 [hep-th]].

[101] J. Koeller and S. Leichenauer, Holographic Proof of the Quantum Null Energy Condition, Phys. Rev. D **94**, 024026, 2016, [arXiv:1512.06109 [hep-th]].

[102] R. C. Myers and A. Sinha, Seeing a c-theorem with holography, Phys. Rev. D **82**, 046006, 2010, [arXiv:1006.1263 [hep-th]].

[103] D. L. Jafferis, I. R. Klebanov, S. S. Pufu and B. R. Safdi, Towards the F-Theorem: N=2 Field Theories on the Three-Sphere, JHEP **06**, 102, 2011, [arXiv:1103.1181 [hep-th]].

[104] H. Casini and M. Huerta, On the RG running of the entanglement entropy of a circle, Phys. Rev. D **85**, 125016, 2012, [arXiv:1202.5650 [hep-th]].

[105] Z. Komargodski and A. Schwimmer, On Renormalization Group Flows in Four Dimensions, JHEP **12**, 099, 2011, [arXiv:1107.3987 [hep-th]].

[106] R. Haag, *Local quantum physics: Fields, particles, algebras*. 1992.

[107] Z. Komargodski and A. Zhiboedov, Convexity and Liberation at Large Spin, JHEP **11**, 140, 2013, [arXiv:1212.4103 [hep-th]].

[108] J. Maldacena and A. Zhiboedov, Constraining Conformal Field Theories with A Higher Spin Symmetry, J. Phys. A **46**, 214011, 2013, [arXiv:1112.1016 [hep-th]].

[109] D. M. Hofman, Higher Derivative Gravity, Causality and Positivity of Energy in a UV complete QFT, Nucl. Phys. B **823**, 174–194, 2009, [arXiv:0907.1625 [hep-th]].

[110] R. Bousso, H. Casini, Z. Fisher and J. Maldacena, Entropy on a null surface for interacting quantum field theories and the Bousso bound, Phys. Rev. D **91**, 084030, 2015, [arXiv:1406.4545 [hep-th]].

[111] H. Osborn and A. Petkou, Implications of conformal invariance in field theories for general dimensions, Annals Phys. **231**, 311–362, 1994, [arXiv:hep-th/9307010].

[112] B. Czech, L. Lamprou, S. McCandlish, B. Mosk and J. Sully, A Stereoscopic Look into the Bulk, JHEP **07**, 129, 2016, [arXiv:1604.03110 [hep-th]].

[113] H. Casini, Wedge reflection positivity, J. Phys. A **44**, 435202, 2011, [arXiv:1009.3832 [hep-th]].

[114] A. Adams, N. Arkani-Hamed, S. Dubovsky, A. Nicolis and R. Rattazzi, Causality, analyticity and an IR obstruction to UV completion, JHEP **10**, 014, 2006, [arXiv:hep-th/0602178].

[115] D. Chowdhury, S. Raju, S. Sachdev, A. Singh and P. Strack, Multipoint correlators of conformal field theories: implications for quantum critical transport, Phys. Rev. B **87**, 085138, 2013, [arXiv:1210.5247 [cond-mat.str-el]].

[116] Z. Komargodski, M. Kulaxizi, A. Parnachev and A. Zhiboedov, Conformal Field Theories and Deep Inelastic Scattering, Phys. Rev. D **95**, 065011, 2017, [arXiv:1601.05453 [hep-th]].

[117] M. S. Costa, J. Penedones, D. Poland and S. Rychkov, Spinning Conformal Correlators, JHEP **11**, 071, 2011, [arXiv:1107.3554 [hep-th]].

[118] N. Afkhami-Jeddi and T. Hartman, unpublished, .

[119] N. Afkhami-Jeddi, S. Kundu and A. Tajdini, A Bound on Massive Higher Spin Particles, JHEP **04**, 056, 2019, [arXiv:1811.01952 [hep-th]].

[120] S. Weinberg, Photons and gravitons in s-matrix theory: Derivation of charge conservation and equality of gravitational and inertial mass, Phys. Rev. **135**, B1049–B1056, 1964.

[121] S. Weinberg and E. Witten, Limits on massless particles, Physics Letters B **96**, 59 – 62, 1980.

[122] M. Porrati, Universal limits on massless high-spin particles, Phys. Rev. D **78**, 065016, 2008.

[123] N. Arkani-Hamed, T.-C. Huang and Y.-t. Huang, Scattering Amplitudes For All Masses and Spins, 2017, [arXiv:1709.04891 [hep-th]].

[124] S.Weinberg, *Lectures On Elementary Particles and Quantum Field Theory, edited by S. Deser*. MIT Press, 1970.

[125] S. Ferrara, M. Porrati and V. L. Telegdi, $g = 2$ as the natural value of the tree-level gyromagnetic ratio of elementary particles, Phys. Rev. D **46**, 3529–3537, 1992.

[126] M. Porrati, Massive spin 5/2 fields coupled to gravity: Tree level unitarity versus the equivalence principle, Phys. Lett. B **304**, 77–80, 1993, [arXiv:gr-qc/9301012].

[127] A. Cucchieri, M. Porrati and S. Deser, Tree level unitarity constraints on the gravitational couplings of higher spin massive fields, Phys. Rev. D **51**, 4543–4549, 1995, [arXiv:hep-th/9408073].

[128] M. Vasiliev, Higher spin gauge theories in various dimensions, Fortsch. Phys. **52**, 702–717, 2004, [arXiv:hep-th/0401177].

[129] X. Bekaert, S. Cnockaert, C. Iazeolla and M. Vasiliev, Nonlinear higher spin theories in various dimensions, in *1st Solvay Workshop on Higher Spin Gauge Theories*, pp. 132–197, 2004. [arXiv:hep-th/0503128].

[130] M. T. Grisaru and H. Pendleton, Soft Spin 3/2 Fermions Require Gravity and Supersymmetry, Phys. Lett. B **67**, 323–326, 1977.

[131] M. T. Grisaru, H. N. Pendleton and P. van Nieuwenhuizen, Supergravity and the s matrix, Phys. Rev. D **15**, 996–1006, 1977.

[132] F. Loebbert, The Weinberg-Witten theorem on massless particles: An Essay, Annalen Phys. **17**, 803–829, 2008.

[133] C. Aragone and S. Deser, Consistency Problems of Hypergravity, Phys. Lett. B **86**, 161–163, 1979.

[134] F. A. Berends, J. W. van Holten, B. de Wit and P. van Nieuwenhuizen, On spin-5/2gauge fields, Journal of Physics A: Mathematical and General **13**, 1643–1649, 1980.

[135] C. Aragone and H. La Roche, Massless Second Order Tetradic Spin 3 Fields and Higher Helicity Bosons, Nuovo Cim. A **72**, 149, 1982.

[136] R. Metsaev, Cubic interaction vertices of massive and massless higher spin fields, Nucl. Phys. B **759**, 147–201, 2006, [arXiv:hep-th/0512342].

[137] N. Boulanger and S. Leclercq, Consistent couplings between spin-2 and spin-3 massless fields, JHEP **11**, 034, 2006, [arXiv:hep-th/0609221].

[138] N. Boulanger, S. Leclercq and P. Sundell, On The Uniqueness of Minimal Coupling in Higher-Spin Gauge Theory, JHEP **08**, 056, 2008, [arXiv:0805.2764 [hep-th]].

[139] L. Cornalba, M. S. Costa, J. Penedones and R. Schiappa, Eikonal Approximation in AdS/CFT: Conformal Partial Waves and Finite N Four-Point Functions, Nucl. Phys. B **767**, 327–351, 2007, [arXiv:hep-th/0611123].

[140] L. Cornalba, M. S. Costa and J. Penedones, Eikonal approximation in AdS/CFT: Resumming the gravitational loop expansion, JHEP **09**, 037, 2007, [arXiv:0707.0120 [hep-th]].

[141] G. Mack, D-dimensional conformal field theories with anomalous dimensions as dual resonance models, 2009.

[142] G. Mack, D-independent representation of Conformal Field Theories in D dimensions via transformation to auxiliary Dual Resonance Models. Scalar amplitudes, 2009, [arXiv:0907.2407 [hep-th]].

[143] A. Fitzpatrick, E. Katz, D. Poland and D. Simmons-Duffin, Effective Conformal Theory and the Flat-Space Limit of AdS, JHEP **07**, 023, 2011, [arXiv:1007.2412 [hep-th]].

[144] I. Heemskerk and J. Sully, More Holography from Conformal Field Theory, JHEP **09**, 099, 2010, [arXiv:1006.0976 [hep-th]].

[145] A. Fitzpatrick and J. Kaplan, Analyticity and the Holographic S-Matrix, JHEP **10**, 127, 2012, [arXiv:1111.6972 [hep-th]].

[146] A. Fitzpatrick, J. Kaplan, J. Penedones, S. Raju and B. C. van Rees, A Natural Language for AdS/CFT Correlators, JHEP **11**, 095, 2011, [arXiv:1107.1499 [hep-th]].

[147] S. El-Showk and K. Papadodimas, Emergent Spacetime and Holographic CFTs, JHEP **10**, 106, 2012, [arXiv:1101.4163 [hep-th]].

[148] A. Fitzpatrick and J. Kaplan, AdS Field Theory from Conformal Field Theory, JHEP **02**, 054, 2013, [arXiv:1208.0337 [hep-th]].

[149] V. GonÃğalves, J. Penedones and E. Trevisani, Factorization of Mellin amplitudes, JHEP **10**, 040, 2015, [arXiv:1410.4185 [hep-th]].

[150] E. Hijano, P. Kraus, E. Perlmutter and R. Snively, Witten Diagrams Revisited: The AdS Geometry of Conformal Blocks, JHEP **01**, 146, 2016, [arXiv:1508.00501 [hep-th]].

[151] S. Caron-Huot, Analyticity in Spin in Conformal Theories, JHEP **09**, 078, 2017, [arXiv:1703.00278 [hep-th]].

[152] N. Afkhami-Jeddi, T. Hartman, S. Kundu and A. Tajdini, Einstein gravity 3-point functions from conformal field theory, JHEP **12**, 049, 2017, [arXiv:1610.09378 [hep-th]].

[153] M. Kulaxizi, A. Parnachev and A. Zhiboedov, Bulk Phase Shift, CFT Regge Limit and Einstein Gravity, JHEP **06**, 121, 2018, [arXiv:1705.02934 [hep-th]].

[154] M. S. Costa, T. Hansen and J. Penedones, Bounds for OPE coefficients on the Regge trajectory, JHEP **10**, 197, 2017, [arXiv:1707.07689 [hep-th]].

[155] N. Afkhami-Jeddi, T. Hartman, S. Kundu and A. Tajdini, Shockwaves from the Operator Product Expansion, JHEP **03**, 201, 2019, [arXiv:1709.03597 [hep-th]].

[156] D. Meltzer and E. Perlmutter, Beyond $a = c$: gravitational couplings to matter and the stress tensor OPE, JHEP **07**, 157, 2018, [arXiv:1712.04861 [hep-th]].

[157] N. Afkhami-Jeddi, S. Kundu and A. Tajdini, A Conformal Collider for Holographic CFTs, JHEP **10**, 156, 2018, [arXiv:1805.07393 [hep-th]].

[158] N. Boulanger, D. Ponomarev, E. Skvortsov and M. Taronna, On the uniqueness of higher-spin symmetries in AdS and CFT, Int. J. Mod. Phys. A **28**, 1350162, 2013, [arXiv:1305.5180 [hep-th]].

[159] V. Alba and K. Diab, Constraining conformal field theories with a higher spin symmetry in $d > 3$ dimensions, JHEP **03**, 044, 2016, [arXiv:1510.02535 [hep-th]].

[160] N. Arkani-Hamed and J. Maldacena, Cosmological Collider Physics, 2015, [arXiv:1503.08043 [hep-th]].

[161] C. Cordova, J. Maldacena and G. J. Turiaci, Bounds on OPE Coefficients from Interference Effects in the Conformal Collider, JHEP **11**, 032, 2017, [arXiv:1710.03199 [hep-th]].

[162] K. Hinterbichler, A. Joyce and R. A. Rosen, Eikonal scattering and asymptotic superluminality of massless higher spin fields, Phys. Rev. D **97**, 125019, 2018, [arXiv:1712.10021 [hep-th]].

[163] J. Bonifacio, K. Hinterbichler, A. Joyce and R. A. Rosen, Massive and massless spin-2 scattering and asymptotic superluminality, Journal of High Energy Physics **2018**, 75, 2018.

[164] M. Lévy and J. Sucher, Eikonal approximation in quantum field theory, Phys. Rev. **186**, 1656–1670, 1969.

[165] X. O. Camanho, G. Lucena GÃşmez and R. Rahman, Causality Constraints on Massive Gravity, Phys. Rev. D **96**, 084007, 2017, [arXiv:1610.02033 [hep-th]].

[166] J. D. Edelstein, G. Giribet, C. Gomez, E. Kilicarslan, M. Leoni and B. Tekin, Causality in 3D Massive Gravity Theories, Phys. Rev. D **95**, 104016, 2017, [arXiv:1602.03376 [hep-th]].

[167] G. 't Hooft, Graviton Dominance in Ultrahigh-Energy Scattering, Phys. Lett. B **198**, 61–63, 1987.

[168] I. I. Shapiro, Fourth test of general relativity, Phys. Rev. Lett. **13**, 789–791, 1964.

[169] G. Tiktopoulos and S. Treiman, Relativistic eikonal approximation, Phys. Rev. D **3**, 1037–1040, 1971.

[170] H. Cheng and T. Wu, *EXPANDING PROTONS: SCATTERING AT HIGH-ENERGIES*. 1987.

[171] D. N. Kabat, Validity of the Eikonal approximation, Comments Nucl. Part. Phys. **20**, 325–335, 1992, [arXiv:hep-th/9204103].

[172] L. Singh and C. Hagen, Lagrangian formulation for arbitrary spin. 1. The boson case, Phys. Rev. D **9**, 898–909, 1974.

[173] L. Singh and C. Hagen, Lagrangian formulation for arbitrary spin. 2. The fermion case, Phys. Rev. D **9**, 910–920, 1974.

[174] Y. Zinoviev, On massive high spin particles in AdS, 2001, [arXiv:hep-th/0108192].

[175] J. Bonifacio and K. Hinterbichler, Universal bound on the strong coupling scale of a gravitationally coupled massive spin-2 particle, Phys. Rev. D **98**, 085006, 2018, [arXiv:1806.10607 [hep-th]].

[176] R. Rahman, Interacting massive higher spin fields, other thesis, 2009.

[177] M. S. Costa, V. Goncalves and J. Penedones, Conformal Regge theory, JHEP **12**, 091, 2012, [arXiv:1209.4355 [hep-th]].

[178] P. Kravchuk and D. Simmons-Duffin, Light-ray operators in conformal field theory, JHEP **11**, 102, 2018, [arXiv:1805.00098 [hep-th]].

[179] S. Ferrara, A. Grillo, G. Parisi and R. Gatto, The shadow operator formalism for conformal algebra. Vacuum expectation values and operator products, Lett. Nuovo Cim. **4S2**, 115–120, 1972.

[180] D. Simmons-Duffin, Projectors, Shadows, and Conformal Blocks, JHEP **04**, 146, 2014, [arXiv:1204.3894 [hep-th]].

[181] F. Dolan and H. Osborn, Conformal four point functions and the operator product expansion, Nucl. Phys. B **599**, 459–496, 2001, [arXiv:hep-th/0011040].

[182] J. de Boer, F. M. Haehl, M. P. Heller and R. C. Myers, Entanglement, holography and causal diamonds, JHEP **08**, 162, 2016, [arXiv:1606.03307 [hep-th]].

[183] R. C. Brower, J. Polchinski, M. J. Strassler and C.-I. Tan, The Pomeron and gauge/string duality, JHEP **12**, 005, 2007, [arXiv:hep-th/0603115].

[184] D. Amati, M. Ciafaloni and G. Veneziano, Planckian scattering beyond the semiclassical approximation, Physics Letters B **289**, 87 – 91, 1992.

[185] D. Amati, M. Ciafaloni and G. Veneziano, Can spacetime be probed below the string size?, Physics Letters B **216**, 41 – 47, 1989.

[186] D. Amati, M. Ciafaloni and G. Veneziano, Classical and Quantum Gravity Effects from Planckian Energy Superstring Collisions, Int. J. Mod. Phys. A **3**, 1615–1661, 1988.

[187] D. Amati, M. Ciafaloni and G. Veneziano, Superstring Collisions at Planckian Energies, Phys. Lett. B **197**, 81, 1987.

[188] D. Amati, M. Ciafaloni and G. Veneziano, Effective action and all-order gravitational eikonal at planckian energies, Nuclear Physics B **403**, 707 – 724, 1993.

[189] M. Taronna, Higher Spins and String Interactions, other thesis, 2010.

[190] A. Sagnotti and M. Taronna, String Lessons for Higher-Spin Interactions, Nucl. Phys. B **842**, 299–361, 2011, [arXiv:1006.5242 [hep-th]].

[191] G. D'Appollonio, P. Di Vecchia, R. Russo and G. Veneziano, Regge behavior saves String Theory from causality violations, JHEP **05**, 144, 2015, [arXiv:1502.01254 [hep-th]].

[192] A. Higuchi, Forbidden Mass Range for Spin-2 Field Theory in De Sitter Space-time, Nucl. Phys. B **282**, 397–436, 1987.

[193] S. Deser and A. Waldron, Partial masslessness of higher spins in (A)dS, Nucl. Phys. B **607**, 577–604, 2001, [arXiv:hep-th/0103198].

[194] D. Baumann, Primordial Cosmology, PoS **TASI2017**, 009, 2018, [arXiv:1807.03098 [hep-th]].

[195] H. Lee, D. Baumann and G. L. Pimentel, Non-Gaussianity as a Particle Detector, JHEP **12**, 040, 2016, [arXiv:1607.03735 [hep-th]].

[196] Topical Conveners: K.N. Abazajian, J.E. Carlstrom, A.T. Lee collaboration, K. Abazajian et al., Neutrino Physics from the Cosmic Microwave Background and Large Scale Structure, Astropart. Phys. **63**, 66–80, 2015, [arXiv:1309.5383 [astro-ph.CO]].

[197] A. A. Belavin, A. M. Polyakov and A. B. Zamolodchikov, Infinite Conformal Symmetry in Two-Dimensional Quantum Field Theory, Nucl. Phys. **B241**, 333–380, 1984.

[198] R. Rattazzi, V. S. Rychkov, E. Tonni and A. Vichi, Bounding scalar operator dimensions in 4D CFT, JHEP **12**, 031, 2008, [arXiv:0807.0004 [hep-th]].

[199] D. Poland, D. Simmons-Duffin and A. Vichi, Carving Out the Space of 4D CFTs, JHEP **05**, 110, 2012, [arXiv:1109.5176 [hep-th]].

[200] S. El-Showk, M. F. Paulos, D. Poland, S. Rychkov, D. Simmons-Duffin and A. Vichi, Solving the 3D Ising Model with the Conformal Bootstrap, Phys. Rev. **D86**, 025022, 2012, [arXiv:1203.6064 [hep-th]].

[201] S. El-Showk, M. F. Paulos, D. Poland, S. Rychkov, D. Simmons-Duffin and A. Vichi, Solving the 3d Ising Model with the Conformal Bootstrap II. c-Minimization and Precise Critical Exponents, J. Stat. Phys. **157**, 869, 2014, [arXiv:1403.4545 [hep-th]].

[202] D. Poland and D. Simmons-Duffin, Bounds on 4D Conformal and Superconformal Field Theories, JHEP **05**, 017, 2011, [arXiv:1009.2087 [hep-th]].

[203] S. El-Showk and M. F. Paulos, Bootstrapping Conformal Field Theories with the Extremal Functional Method, Phys. Rev. Lett. **111**, 241601, 2013, [arXiv:1211.2810 [hep-th]].

[204] D. Simmons-Duffin, The Lightcone Bootstrap and the Spectrum of the 3d Ising CFT, JHEP **03**, 086, 2017, [arXiv:1612.08471 [hep-th]].

[205] F. Kos, D. Poland, D. Simmons-Duffin and A. Vichi, Precision Islands in the Ising and $O(N)$ Models, JHEP **08**, 036, 2016, [arXiv:1603.04436 [hep-th]].

[206] S. M. Chester and S. S. Pufu, Towards bootstrapping QED_3, JHEP **08**, 019, 2016, [arXiv:1601.03476 [hep-th]].

[207] L. Iliesiu, M. Kolo?lu, R. Mahajan, E. Perlmutter and D. Simmons-Duffin, The Conformal Bootstrap at Finite Temperature, JHEP **10**, 070, 2018, [arXiv:1802.10266 [hep-th]].

[208] L. V. Delacretaz, T. Hartman, S. A. Hartnoll and A. Lewkowycz, Thermalization, Viscosity and the Averaged Null Energy Condition, JHEP **10**, 028, 2018, [arXiv:1805.04194 [hep-th]].

[209] S. El-Showk and M. F. Paulos, Extremal bootstrapping: go with the flow, JHEP **03**, 148, 2018, [arXiv:1605.08087 [hep-th]].

[210] M. Banados, C. Teitelboim and J. Zanelli, The Black hole in three-dimensional space-time, Phys. Rev. Lett. **69**, 1849–1851, 1992, [arXiv:hep-th/9204099 [hep-th]].

[211] D. Friedan and C. A. Keller, Constraints on 2d CFT partition functions, JHEP **10**, 180, 2013, [arXiv:1307.6562 [hep-th]].

[212] S. Collier, Y.-H. Lin and X. Yin, Modular Bootstrap Revisited, JHEP **09**, 061, 2018, [arXiv:1608.06241 [hep-th]].

[213] B. Mukhametzhanov and A. Zhiboedov, Analytic Euclidean Bootstrap, 2018, [arXiv:1808.03212 [hep-th]].

[214] F. Gliozzi, More constraining conformal bootstrap, Phys. Rev. Lett. **111**, 161602, 2013, [arXiv:1307.3111 [hep-th]].

[215] F. Gliozzi and A. Rago, Critical exponents of the 3d Ising and related models from Conformal Bootstrap, JHEP **10**, 042, 2014, [arXiv:1403.6003 [hep-th]].

[216] W. Li, New method for the conformal bootstrap with OPE truncations, 2017, [arXiv:1711.09075 [hep-th]].

[217] D. Simmons-Duffin, A Semidefinite Program Solver for the Conformal Bootstrap, JHEP **06**, 174, 2015, [arXiv:1502.02033 [hep-th]].

[218] J. D. Qualls and A. D. Shapere, Bounds on Operator Dimensions in 2D Conformal Field Theories, JHEP **05**, 091, 2014, [arXiv:1312.0038 [hep-th]].

[219] S. Hellerman and C. Schmidt-Colinet, Bounds for State Degeneracies in 2D Conformal Field Theory, JHEP **08**, 127, 2011, [arXiv:1007.0756 [hep-th]].

[220] C. A. Keller and H. Ooguri, Modular Constraints on Calabi-Yau Compactifications, Commun. Math. Phys. **324**, 107–127, 2013, [arXiv:1209.4649 [hep-th]].

[221] C.-M. Chang and Y.-H. Lin, Bootstrapping 2D CFTs in the Semiclassical Limit, JHEP **08**, 056, 2016, [arXiv:1510.02464 [hep-th]].

[222] E. Shaghoulian, Modular forms and a generalized Cardy formula in higher dimensions, Phys. Rev. **D93**, 126005, 2016, [arXiv:1508.02728 [hep-th]].

[223] H. Kim, P. Kravchuk and H. Ooguri, Reflections on Conformal Spectra, JHEP **04**, 184, 2016, [arXiv:1510.08772 [hep-th]].

[224] N. Benjamin, E. Dyer, A. L. Fitzpatrick and S. Kachru, Universal Bounds on Charged States in 2d CFT and 3d Gravity, JHEP **08**, 041, 2016, [arXiv:1603.09745 [hep-th]].

[225] D. Das, S. Datta and S. Pal, Charged structure constants from modularity, JHEP **11**, 183, 2017, [arXiv:1706.04612 [hep-th]].

[226] M. Cho, S. Collier and X. Yin, Genus Two Modular Bootstrap, 2017, [arXiv:1705.05865 [hep-th]].

[227] E. Dyer, A. L. Fitzpatrick and Y. Xin, Constraints on Flavored 2d CFT Partition Functions, JHEP **02**, 148, 2018, [arXiv:1709.01533 [hep-th]].

[228] L. Apolo, Bounds on CFTs with $\mathcal{W}_3$ algebras and AdS_3 higher spin theories, Phys. Rev. **D96**, 086003, 2017, [arXiv:1705.10402 [hep-th]].

[229] N. Afkhami-Jeddi, K. Colville, T. Hartman, A. Maloney and E. Perlmutter, Constraints on higher spin CFT_2, JHEP **05**, 092, 2018, [arXiv:1707.07717 [hep-th]].

[230] J.-B. Bae, S. Lee and J. Song, Modular Constraints on Conformal Field Theories with Currents, JHEP **12**, 045, 2017, [arXiv:1708.08815 [hep-th]].

[231] S. Collier, P. Kravchuk, Y.-H. Lin and X. Yin, Bootstrapping the Spectral Function: On the Uniqueness of Liouville and the Universality of BTZ, JHEP **09**, 150, 2018, [arXiv:1702.00423 [hep-th]].

[232] J.-B. Bae, S. Lee and J. Song, Modular Constraints on Superconformal Field Theories, JHEP **01**, 209, 2019, [arXiv:1811.00976 [hep-th]].

[233] T. Anous, R. Mahajan and E. Shaghoulian, Parity and the modular bootstrap, SciPost Phys. **5**, 022, 2018, [arXiv:1803.04938 [hep-th]].

[234] A. Castedo Echeverri, B. von Harling and M. Serone, The Effective Bootstrap, JHEP **09**, 097, 2016, [arXiv:1606.02771 [hep-th]].

[235] V. Gorbenko, S. Rychkov and B. Zan, Walking, Weak first-order transitions, and Complex CFTs, JHEP **10**, 108, 2018, [arXiv:1807.11512 [hep-th]].

[236] N. Arkani-Hamed, Y.-T. Huang and S.-H. Shao, On the Positive Geometry of Conformal Field Theory, 2018, [arXiv:1812.07739 [hep-th]].

[237] A. Pinkus, Spectral properties of totally positive kernels and matrices, in *Total positivity and its applications*, pp. 477–511. Springer, 1996.

[238] A. Belin, C. A. Keller and A. Maloney, String Universality for Permutation Orbifolds, Phys. Rev. **D91**, 106005, 2015, [arXiv:1412.7159 [hep-th]].

[239] C. Vafa, The String landscape and the swampland, 2005, [arXiv:hep-th/0509212 [hep-th]].

[240] S. W. Hawking, Breakdown of Predictability in Gravitational Collapse, Phys. Rev. **D14**, 2460–2473, 1976.

[241] D. N. Page, Information in black hole radiation, Phys. Rev. Lett. **71**, 3743–3746, 1993, [arXiv:hep-th/9306083 [hep-th]].

[242] D. N. Page, Time Dependence of Hawking Radiation Entropy, JCAP **1309**, 028, 2013, [arXiv:1301.4995 [hep-th]].

[243] G. Penington, Entanglement Wedge Reconstruction and the Information Paradox, 2019, [arXiv:1905.08255 [hep-th]].

[244] A. Almheiri, N. Engelhardt, D. Marolf and H. Maxfield, The entropy of bulk quantum fields and the entanglement wedge of an evaporating black hole, 2019, [arXiv:1905.08762 [hep-th]].

[245] A. Almheiri, R. Mahajan, J. Maldacena and Y. Zhao, The Page curve of Hawking radiation from semiclassical geometry, 2019, [arXiv:1908.10996 [hep-th]].

[246] T. G. Mertens, Towards Black Hole Evaporation in Jackiw-Teitelboim Gravity, JHEP **07**, 097, 2019, [arXiv:1903.10485 [hep-th]].

[247] C. Akers, A. Levine and S. Leichenauer, Large Breakdowns of Entanglement Wedge Reconstruction, 2019, [arXiv:1908.03975 [hep-th]].

[248] U. Moitra, S. K. Sake, S. P. Trivedi and V. Vishal, Jackiw-Teitelboim Model

Coupled to Conformal Matter in the Semi-Classical Limit, 2019, [arXiv:1908.08523 [hep-th]].

[249] A. Almheiri, R. Mahajan and J. E. Santos, Entanglement islands in higher dimensions, 2019, [arXiv:1911.09666 [hep-th]].

[250] Z. Fu and D. Marolf, Bag-of-gold spacetimes, Euclidean wormholes, and inflation from domain walls in AdS/CFT, JHEP **11**, 040, 2019, [arXiv:1909.02505 [hep-th]].

[251] P. Zhang, Evaporation dynamics of the Sachdev-Ye-Kitaev model, 2019, [arXiv:1909.10637 [cond-mat.str-el]].

[252] C. Akers, N. Engelhardt and D. Harlow, Simple holographic models of black hole evaporation, 2019, [arXiv:1910.00972 [hep-th]].

[253] A. Almheiri, R. Mahajan and J. Maldacena, Islands outside the horizon, 2019, [arXiv:1910.11077 [hep-th]].

[254] M. Rozali, J. Sully, M. Van Raamsdonk, C. Waddell and D. Wakeham, Information radiation in BCFT models of black holes, 2019, [arXiv:1910.12836 [hep-th]].

[255] H. Z. Chen, Z. Fisher, J. Hernandez, R. C. Myers and S.-M. Ruan, Information Flow in Black Hole Evaporation, 2019, [arXiv:1911.03402 [hep-th]].

[256] R. Bousso and M. Tomasevic, Unitarity From a Smooth Horizon?, 2019, [arXiv:1911.06305 [hep-th]].

[257] D. L. Jafferis and D. K. Kolchmeyer, Entanglement Entropy in Jackiw-Teitelboim Gravity, 2019, [arXiv:1911.10663 [hep-th]].

[258] A. Blommaert, T. G. Mertens and H. Verschelde, Eigenbranes in Jackiw-Teitelboim gravity, 2019, [arXiv:1911.11603 [hep-th]].

[259] V. E. Hubeny, M. Rangamani and T. Takayanagi, A Covariant holographic entanglement entropy proposal, JHEP **07**, 062, 2007, [arXiv:0705.0016 [hep-th]].

[260] T. Faulkner, A. Lewkowycz and J. Maldacena, Quantum corrections to holographic entanglement entropy, JHEP **11**, 074, 2013, [arXiv:1307.2892 [hep-th]].

[261] S. D. Mathur, What is the dual of two entangled CFTs?, 2014, [arXiv:1402.6378 [hep-th]].

[262] R. Jackiw, Lower Dimensional Gravity, Nucl. Phys. **B252**, 343–356, 1985.

[263] C. Teitelboim, Gravitation and Hamiltonian Structure in Two Space-Time Dimensions, Phys. Lett. **B126**, 41–45, 1983.

[264] A. Almheiri and J. Polchinski, Models of AdS_2 backreaction and holography, JHEP **11**, 014, 2015, [arXiv:1402.6334 [hep-th]].

[265] A. Lewkowycz and J. Maldacena, Generalized gravitational entropy, JHEP **08**, 090, 2013, [arXiv:1304.4926 [hep-th]].

[266] X. Dong, A. Lewkowycz and M. Rangamani, Deriving covariant holographic entanglement, JHEP **11**, 028, 2016, [arXiv:1607.07506 [hep-th]].

[267] X. Dong and A. Lewkowycz, Entropy, Extremality, Euclidean Variations, and the Equations of Motion, JHEP **01**, 081, 2018, [arXiv:1705.08453 [hep-th]].

[268] G. Penington, S. Shenker, D. Stanford and Z. Yang, To appear together with this paper, .

[269] P. Saad, S. H. Shenker and D. Stanford, A semiclassical ramp in SYK and in gravity, 2018, [arXiv:1806.06840 [hep-th]].

[270] P. Saad, S. H. Shenker and D. Stanford, JT gravity as a matrix integral, 2019, [arXiv:1903.11115 [hep-th]].

[271] P. Saad, Late Time Correlation Functions, Baby Universes, and ETH in JT Gravity, 2019, [arXiv:1910.10311 [hep-th]].

[272] J. V. Rocha, Evaporation of large black holes in AdS: Coupling to the evaporon, JHEP **08**, 075, 2008, [arXiv:0804.0055 [hep-th]].

[273] J. Engelsoy, T. G. Mertens and H. Verlinde, An investigation of AdS_2 backreaction and holography, JHEP **07**, 139, 2016, [arXiv:1606.03438 [hep-th]].

[274] L. Randall and R. Sundrum, An Alternative to compactification, Phys. Rev. Lett. **83**, 4690–4693, 1999, [arXiv:hep-th/9906064 [hep-th]].

[275] A. Karch and L. Randall, Locally localized gravity, JHEP **05**, 008, 2001, [arXiv:hep-th/0011156 [hep-th]].

[276] J. Maldacena, A. Milekhin and F. Popov, Traversable wormholes in four dimensions, 2018, [arXiv:1807.04726 [hep-th]].

[277] T. M. Fiola, J. Preskill, A. Strominger and S. P. Trivedi, Black hole thermodynamics and information loss in two-dimensions, Phys. Rev. **D50**, 3987–4014, 1994, [arXiv:hep-th/9403137 [hep-th]].

[278] C. G. Callan, Jr. and F. Wilczek, On geometric entropy, Phys. Lett. **B333**, 55–61, 1994, [arXiv:hep-th/9401072 [hep-th]].

[279] H. Casini and M. Huerta, Entanglement entropy in free quantum field theory, J. Phys. **A42**, 504007, 2009, [arXiv:0905.2562 [hep-th]].

[280] X. Dong, Holographic Entanglement Entropy for General Higher Derivative Gravity, JHEP **01**, 044, 2014, [arXiv:1310.5713 [hep-th]].

[281] E. Sharon and D. Mumford, 2D-Shape Analysis Using Conformal Mapping, International Journal of Computer Vision **70**, 55, 2006.

[282] K. Jensen, Chaos and hydrodynamics near AdS_2, 2016, [arXiv:1605.06098 [hep-th]].

[283] J. Maldacena, D. Stanford and Z. Yang, Conformal symmetry and its breaking in two dimensional Nearly Anti-de-Sitter space, PTEP **2016**, 12C104, 2016, [arXiv:1606.01857 [hep-th]].

[284] P. Calabrese and J. L. Cardy, Entanglement entropy and quantum field theory, J. Stat. Mech. **0406**, P06002, 2004, [arXiv:hep-th/0405152 [hep-th]].

[285] H. Casini, C. D. Fosco and M. Huerta, Entanglement and alpha entropies for a massive Dirac field in two dimensions, J. Stat. Mech. **0507**, P07007, 2005, [arXiv:cond-mat/0505563 [cond-mat]].

[286] P. Hayden and G. Penington, Learning the Alpha-bits of Black Holes, 2018, [arXiv:1807.06041 [hep-th]].

[287] P. Hayden and G. Penington, Approximate quantum error correction revisited: Introducing the alpha-bit, 2017.

[288] S. W. Hawking, Quantum Coherence Down the Wormhole, Phys. Lett. **B195**, 337, 1987.

[289] G. V. Lavrelashvili, V. A. Rubakov and P. G. Tinyakov, Disruption of Quantum Coherence upon a Change in Spatial Topology in Quantum Gravity, JETP Lett. **46**, 167–169, 1987.

[290] S. B. Giddings and A. Strominger, Axion Induced Topology Change in Quantum Gravity and String Theory, Nucl. Phys. **B306**, 890–907, 1988.

[291] S. R. Coleman, Black Holes as Red Herrings: Topological Fluctuations and the Loss of Quantum Coherence, Nucl. Phys. **B307**, 867–882, 1988.

[292] J. Polchinski and A. Strominger, A Possible resolution of the black hole information puzzle, Phys. Rev. **D50**, 7403–7409, 1994, [arXiv:hep-th/9407008 [hep-th]].

[293] T. Hartman and J. Maldacena, Time Evolution of Entanglement Entropy from Black Hole Interiors, JHEP **05**, 014, 2013, [arXiv:1303.1080 [hep-th]].

[294] L. Susskind, Entanglement is not enough, Fortsch. Phys. **64**, 49–71, 2016, [arXiv:1411.0690 [hep-th]].

[295] S. Giombi and X. Yin, Higher Spin Gauge Theory and Holography: The Three-Point Functions, JHEP **09**, 115, 2010, [arXiv:0912.3462 [hep-th]].